

**INHIBITION OF MICROBIAL  
 $\beta$ -GLUCURONIDASE BY NATURAL ZEOLITES  
AND THEIR EFFECTS ON CANCER PREVENTION  
IN HUMAN INTESTINAL SYSTEM**

**A Thesis Report Submitted to  
the Graduate School of Engineering and Sciences of  
İzmir Institute of Technology  
in Partial Fulfillment of the Requirements for the Degree of**

**DOCTOR OF PHILOSOPHY**

**in Chemical Engineering**

**by  
Dilek DEMİRBÜKER KAVAK**

**December 2010  
İZMİR**

We approve the thesis of **Dilek DEMİR BÜKER KAVAK**

---

**Prof. Dr. Semra ÜLKÜ**  
Supervisor

---

**Prof. Dr. Serdar ÖZÇELİK**  
Co-Supervisor

---

**Prof. Dr. Meral SAKIZLI**  
Committee Member

---

**Assoc. Prof. Dr. Fehime ÖZKAN**  
Committee Member

---

**Assoc. Prof. Dr. Oğuz BAYRAKTAR**  
Committee Member

---

**Assist. Prof. Dr. Gülşah ŞANLI**  
Committee Member

21 December 2010

---

**Prof. Dr. Mehmet POLAT**

Head of the Department of  
Chemical Engineering

---

**Prof. Dr. Durmuş Ali DEMİR**

Dean of the Graduate School of  
Engineering and Sciences

## ACKNOWLEDGEMENTS

I would like to express my sincere gratitude to my advisor, Dr. Semra Ülkü for her guidance, support and encouragement in all steps of this study. I am also grateful to Dr. Serdar Özçelik for his valuable suggestions and recommendations during experimental planning and progression of this study. I would like to thank to Dr. Fehime Özkan, Dr. Gülşah Şanlı, Dr. Meral Sakızlı for their valuable suggestions in committee. I thank to Dr. Oguz Bayraktar for his suggestions in committee as well as for all of his supports in Biochemical Engineering Research Laboratories. I am also thankful to State Planning Organization of Turkey for their financial supports to this project.

I wish to express my gratitude to specialists Dane Rusçuklu and Özgür Y. Çakmak for their friendly nature and helping me in cell culture experiments. I am also thankful to my friends Yasemin E. Kaya, Hasan Demir and Didem Berkün for their friendship.

Last, but most certainly not least, I wish to express my unending gratitude to my husband Özer Kavak, to my parents and sister, for their love, understanding, patience and encouragements.

## ABSTRACT

### INHIBITION OF MICROBIAL $\beta$ -GLUCURONIDASE BY NATURAL ZEOLITES AND THEIR EFFECTS ON CANCER PREVENTION IN HUMAN INTESTINAL SYSTEM

Bacterial  $\beta$ -glucuronidase (GUS) enzyme has an important role in the production of reactive metabolites related to some diseases and cancer development. In this thesis, health promoting role of clinoptilolite rich zeolite mineral was proposed to act as a potential inhibitor and as adsorbant of GUS and also to have cytotoxic effect towards cancer cells. Therefore inhibition and adsorption mechanism of GUS by clinoptilolite rich mineral and its cytotoxicity towards cancer cells were investigated. Additionally, another potential inhibitor; casein and their interactions with GUS and clinoptilolite rich mineral were revealed. Results showed that GUS activity was inhibited by either casein or clinoptilolite rich mineral and both of them acted as mixed type inhibitors. Additionally, it was found that clinoptilolite rich mineral was a potential adsorbent for GUS. Results showed that removal percentages of proteins were 9.4-54.4 % and 36.5-77.3 % for GUS and casein, respectively and depended on their initial concentrations. Equilibrium studies showed that both adsorptions were exothermic and physical and kinetic models implied that external fluid film or skin resistance, and intraparticle diffusion might be effective for GUS and casein adsorption, respectively. In cytotoxicity tests, clinoptilolite rich mineral (25mg/ml) inhibited approximately 50 % of the Caco-2 cell proliferation. This high inhibition was not observed for MCF-7 cells where inhibition was found to be 20-30 %. Flow cytometric results for both cell lines indicated that total apoptosis percentage in overall population was low compared to control sample. This result was also confirmed by cell cycle analyses.

## ÖZET

### MİKROBİYAL $\beta$ -GLUKURONİDAZ ENZİMİNİN DOĞAL ZEOLİTLERLE İNHİBİSYONU VE İNSAN BAĞIRSAK SİSTEMİNDEKİ KANSER ÖNLEYİCİ ETKİLERİ

Bakteriyal  $\beta$ -glucuronidaz enzimi (GUS) bazı hastalıklara ve kansere neden olan metabolitlerin üretiminde önemli bir role sahiptir. Bu tezde, klinoptilolitçe zengin doğal zeolit mineralinin sağlık üzerine olumlu etkisinin, GUS enziminin aktivitesini azaltması, onu adsorplaması ve kanser hücrelerine sitotoksik etki göstermesinden kaynaklandığı ileri sürülmektedir. Bu sebeple, GUS enziminin doğal zeolit ile olan inhibisyon ve adsorpsiyon mekanizmaları ve zeolitin kanser hücrelerine karşı sitotoksik etkisi incelenmiştir. Diğer potansiyel inhibitör olan kazein ve onun GUS ve zeolitle olan etkileşimleri de irdelenmiştir. Çalışmalarda zeolit ve kazeinin GUS enziminin aktivitesi baskıladıkları bulunmuş ve her iki inhibitöründe karışık tip inhibitör olarak davrandıkları gösterilmiştir. Bunun yanında doğal zeolitin GUS enzimi için potansiyel bir adsorbent olabileceği bulunmuştur. GUS enzimi ve kazein için giderim yüzdeleri ortamdaki ilk konsantrasyonlarına bağlı olarak değişmekle beraber sırasıyla .4-54.4% ve 36.5-77.3%'dir. Denge çalışmalarında her iki adsorpsiyonun ekzotermik ve fiziksel mekanizmayla gerçekleştiği bulunmuş, kinetik modellerle de GUS için tane yüzeyi ve tane içi kütle taşınımının, kazein için ise tane içi kütle taşınımının adsorpsiyonda etkili olabileceği gösterilmiştir. Sitotoksisite testlerinde ise zeolitin (25mg/ml) Caco-2 hücrelerinin üremesini % 50 düzeyinde azalttığı bulunmuştur. MCF-7 hücrelerinde ise bu oranda bir azaltıcı etki tespit edilememiş, oran % 20-30 civarında kalmıştır. Akım sitometri uygulamaları sonucunda, tüm popülasyondaki apoptotik hücre yüzdesi, kontrol hücrelerine kıyasla düşük bulunmuş, bu sonuç hücre döngüsü analizleriyle de doğrulanmıştır.

# TABLE OF CONTENTS

LIST OF FIGURES.....	x
LIST OF TABLES.....	xv
CHAPTER 1. INTRODUCTION.....	1
CHAPTER 2. INTESTINAL SYSTEM AND B-GLUCURONIDASE ENZYME.....	4
2.1. Human Intestinal System.....	4
2.1.1. Small Intestine.....	5
2.1.2. Digestion in Small Intestine and Importance of Liver and Bile.....	5
2.1.3. Large Intestine.....	6
2.2. Role of Microbial Flora in Human Intestinal System.....	7
2.2.1. Influence of Diet on Intestinal Microflora and Health.....	8
2.2.2. Bacterial Enzymes Associated with Cancer.....	9
2.3. $\beta$ -Glucuronidase.....	11
2.3.1. Structure and Function.....	11
2.3.2. Clinical Importance of GUS.....	13
2.3.2.1. Glucuronidation.....	14
2.3.2.2. $\beta$ -Glucuronidase in Drug Release and Prodrug Applications in Cancer Therapy.....	15
2.4. Inhibition of $\beta$ -Glucuronidase.....	16
2.4.1. Equilibrium Approach.....	18
2.4.2. Steady State Approach.....	20
2.4.3. Types of Inhibition.....	21
CHAPTER 3. ZEOLITES.....	26
3.1. Structure.....	26
3.2. Fundamental Properties.....	28
3.3. Zeolites for Protein Adsorption.....	30
3.3.1. Adsorption Phenomena.....	32
3.3.2. Adsorption Kinetics.....	34
3.3.2.1. External Mass Transfer.....	37
3.3.2.2. Macropore Diffusion.....	41
3.3.2.3. Micropore Diffusion.....	43

3.3.2.4. Adsorption Reaction Models.....	48
3.3.3. Adsorption Equilibrium and Adsorption Isotherms.....	58
3.4. Zeolites in Industrial Applications.....	61
3.5. Zeolites in Biomedical Applications.....	62
3.6. Natural Zeolites as Adjuvants in Cancer Therapy.....	65
CHAPTER 4. CASEIN.....	68
4.1. Structure.....	68
4.2. Casein Micelle.....	70
4.3. Casein and Health.....	71
4.3.1. Casein as a Nutritive and Immunomodulatory Compound.....	71
4.3.2. Antioxidative Property of Casein.....	73
4.3.3. Casein as Enzyme Inhibitor.....	75
CHAPTER 5. MATERIALS AND METHODS.....	77
5.1. Materials.....	77
5.2. Methods.....	78
5.2.1. Sample Preparation and Characterization.....	78
5.2.2. Enzymatic Studies.....	82
5.2.3. Zeolite, <i>E.coli</i> and Casein Interaction Experiments.....	83
5.2.4. Adsorption Experiments.....	85
5.3. Control of the Behaviour of Inhibitors in SIF Conditions.....	88
5.3.1. Zeolite-Cancer Cell Interaction Experiments.....	89
CHAPTER 6. RESULTS OF CHARACTERIZATION STUDIES.....	93
6.1. Simulated Digestion Studies.....	101
6.1.1. Effect of Zeolite on UV Absorption Spectra of Digestion Media 102	
6.2. Characterization Results for Simulated Digestion.....	105
CHAPTER 7. RESULTS OF INTERACTION STUDIES FOR B- GLUCURONIDASE, ZEOLITE AND CASEIN.....	121
7.1. Preliminary Results of the Interactions.....	122
7.2. GUS Inhibition Studies and Application of the Michaelis Menten Approach for Zeolite and Casein Inhibitors.....	128
7.3. Adsorption of $\beta$ -Glucuronidase and Casein onto Zeolite.....	131
7.3.1. Adsorption Kinetics.....	132

7.3.2. Adsorption Isotherms .....	147
7.3.3. Thermodynamic Parameters.....	149
7.3.4. Adsorption Mechanism .....	154
7.4. Behaviour of Inhibitors in SIF Conditions.....	171
7.4.1. Stability of Casein in SIF .....	171
7.4.2. Effect of Zeolite on pH and Ion Concentration of SIF.....	172
7.4.3. Antioxidant Activity of Casein .....	175
7.4.4. Effect of Zeolite Treatment on Charge and Size of Casein .....	178
7.4.5. Effect of Zeolite on UV and Fluorescence Spectra of Casein .....	180
7.4.6. Effect of Zeolite on Thermal Behaviour of Casein.....	182
7.4.7. Effect of Zeolite on FTIR Spectra of Casein .....	185
7.4.8. Effect of Zeolite on Surface Morphology of Casein.....	188
7.5. Interactions of Inhibitors with <i>E.coli</i> .....	193
7.5.1. Effect of Zeolite on <i>E.coli</i> Growth.....	193
7.5.2. Effect of Casein on <i>E.coli</i> Growth.....	195

## CHAPTER 8. RESULTS OF INTERACTION STUDIES OF ZEOLITES AND

CANCER CELLS .....	198
8.1. Antioxidant Activity of Zeolite.....	198
8.2. Zeolite and Caco-2 Cell (Human Epithelial Colorectal Adenocarcinoma Cell) Interactions.....	200
8.2.1. Effect of Zeolite Treatment Time on Caco-2 Cell Growth .....	203
8.2.2. Effect of Zeolite Concentrations on Caco-2 Cell Growth.....	205
8.3. Interactions of Zeolite with Cell Growth Media.....	206
8.3.1. Effect of Zeolite Treatment on pH and Conductivity of Cell Media .....	206
8.3.2. Effect of Zeolite Treatment on Elementary Concentrations in Cell Culture Media .....	209
8.3.3. FTIR Results of Cell Culture Media Treated Zeolite.....	211
8.4. Effect of Zeolite on GUS Activities of Caco-2 and MCF-7 Cancer Cells.....	212
8.5. Effect of Digested and Undigested Zeolite Samples on Cancer Cell Lines .....	215
8.5.1. Changes in pH, Conductivity Values and Color of Cancer Cell Culture Media .....	215
8.5.2. Cytotoxicity Tests for Caco-2 Cells Using Digested and Non- digested Zeolite Samples with Different Doses .....	217
8.5.3. Cytotoxicity Tests for MCF-7 Cells Using Digested and Non-	



digested Zeolite Samples with Different Doses .....	219
8.6. Cell Cycle Analysis and Apoptosis Results.....	222
CHAPTER 9. CONCLUSION .....	229
REFERENCES .....	232
APPENDICES	
APPENDIX A. COMPLEMENTARY ANALYZES.....	251
APPENDIX B. ANALYZES OF ADSORPTION DATA .....	261
APPENDIX C. ANALYZES WITH FLOW CYTOMETRY .....	264
APPENDIX D. GOVERNING EQUATIONS FOR ENZYME INHIBITION MODELS .....	277

## LIST OF FIGURES

<b>Figure</b>	<b>Page</b>
Figure 2.1. Catalyzed reaction for GUS .....	12
Figure 2.2. Changes in the internal energy of a system undergoing a chemical reaction from substrate S to product P.....	17
Figure 3.1. The secondary building units recognized in zeolite framework.....	27
Figure 3.2. Concentration gradients in adsorption process.....	35
Figure 3.3. Zeolite applications. ....	62
Figure 3.4. Growth rate of melanoma B16 treated with 150 mg micronized zeolite .....	66
Figure 3.5. Effect of the medium pretreated with 0.5, 5.0, and 50.0 mg/ml MZ.....	66
Figure 3.6. Binding of 3H-8-OH-DPAT to 5-HT1A receptors in the mouse brain.....	67
Figure 4.1. The structure of casein micelle in the sub-micelles model showing the protruding C-terminal parts of $\kappa$ -casein.....	71
Figure 4.2. Functions of bioactive peptides from caseins.....	73
Figure 4.3. Superoxide radical formation for different forms of casein. ....	74
Figure 5.1. Preparation of the digested samples and following characterization steps. ....	80
Figure 6.1. Scanning electron micrographs zeolite samples.....	93
Figure 6.2. Particle size distribution for Z1. ....	94
Figure 6.3. Particle size distribution for Z2. ....	95
Figure 6.4. Particle size distribution for CR. ....	95
Figure 6.5. TGA curves for Z1, Z2 and CR.....	96
Figure 6.6. Pore size distribution for the Z1 sample.....	97
Figure 6.7. Pore size distribution for the Z2 sample.....	98
Figure 6.8. Pore size distribution for the CR sample.....	98
Figure 6.9. XRD patterns of natural zeolite Z1 .....	99
Figure 6.10. XRD patterns of natural zeolite Z2. ....	99
Figure 6.11. XRD patterns of natural zeolite CR. ....	99
Figure 6.12. XRD patterns of referance natural zeolite Idaho.....	100
Figure 6.13. Infrared spectra of zeolite samples Z1,Z2 and CR.....	100
Figure 6.14. SEM images of zeolite samples.....	101
Figure 6.15. Comparison of UV spectra (240-300nm) of gastric fluids.....	102

Figure 6.16. UV spectra of gastric (M) and intestinal digested (D) fluid.....	104
Figure 6.17. UV spectra of gastric and digestion fluid.....	104
Figure 6.18. XRD patterns of natural zeolites. ....	106
Figure 6.19. Infrared spectra of Z1 after different treatments.. ....	108
Figure 6.20. Infrared spectra of Z2 after different treatments. ....	109
Figure 6.21. 400-1400 $\text{cm}^{-1}$ range showing the characteristic bands for Z1 .....	110
Figure 6.22. 400-1400 $\text{cm}^{-1}$ range showing the characteristic bands for Z2 .....	110
Figure 6.23. IR spectrum of simulated intestinal digestion fluid powders. ....	111
Figure 6.24. IR spectrum of simulated intestinal digestion fluid powders. ....	112
Figure 6.25. ATR-FTIR spectrum of simulated digestion fluid powders.....	113
Figure 6.26. Elementary composition change in Z1 .....	114
Figure 6.27. Elementary composition change in Z2.....	114
Figure 6.28. SEM images of Zeolite 1.....	116
Figure 6.29. SEM images of Zeolite 2.....	116
Figure 6.30. SEM images of alkali-treated ZSM-5. ....	117
Figure 6.31. Scanning electron microscopy microphotographs Ferrierite.....	117
Figure 6.32. SEM images of digested powder with 5000x magnification .....	118
Figure 6.33. SEM images of digested powder 5000x magnification.....	118
Figure 6.34. SEM images of digested powder 100x magnification.....	119
Figure 6.35. SEM images of digested powder 100x magnification a) without zeolite treatment b) treated with Z2.....	119
Figure 7.1. Change in relative fluorescent units (RFU) by time.....	122
Figure 7.2. Kinetic absorbance change of GUS.....	123
Figure 7.3. Kinetic change in UV absorption spectra of GUS .....	124
Figure 7.4. UV absorption spectra of enzyme incubations with different inhibitors....	125
Figure 7.5. FTIR spectra of zeolite .....	126
Figure 7.6. SEM image of zeolite .....	127
Figure 7.7. Double reciprocal plots for GUS enzyme:E and GUS enzyme incubated with casein inhibitor:I(C).....	130
Figure 7.8. Double reciprocal plot for GUS enzyme:E and GUS enzyme incubated with zeolite inhibitor:I(Z). ....	130
Figure 7.9. Comparison of the uptake curves for the digested and non digested (control) zeolite .....	133
Figure 7.10. Uptake curves for GUS adsorption onto zeolite.....	134

Figure 7.11. Uptake curves for casein adsorption onto zeolite.....	134
Figure 7.12. Uptake curves representing the reduction in the free GUS concentration.....	135
Figure 7.13. Uptake curves representing the reduction in the free casein concentration.....	136
Figure 7.14. Effect of solid liquid ratio on adsorption kinetics of GUS by zeolite .....	136
Figure 7.15. Effect of solid liquid ratio on adsorbed amounts of GUS at the end of 150 minutes.....	137
Figure 7.16. Effect of solid liquid ratio on adsorption kinetics of casein by zeolite ....	137
Figure 7.17. Effect of shaking rate on adsorption kinetics of GUS by zeolite .....	138
Figure 7.18. Effect of shaking rate on casein adsorption onto zeolite.....	138
Figure 7.19. Effect of pH on adsorption kinetics of GUS by zeolite.....	139
Figure 7.20. Variations in the zeta potential of zeolite (5mg/ml) in adsorption solutions .....	140
Figure 7.21. Charge distribution of GUS at pH 5.5.....	141
Figure 7.22. Charge distribution of GUS at pH 6.8.....	142
Figure 7.23. Charge distribution of GUS at pH 8.....	142
Figure 7.24. Size distribution of GUS at different pH values.....	143
Figure 7.25. Variation in activity of GUS (relative fluorescence unit:RFU) with pH.....	143
Figure 7.26. Effect of particle size on adsorption kinetics of GUS by zeolite .....	145
Figure 7.27. Effect of particle size on casein adsorption onto zeolite .....	145
Figure 7.28. Effect of temperature on adsorption kinetics of GUS by zeolite .....	146
Figure 7.29. Effect of temperature on adsorption kinetics of casein by zeolite .....	146
Figure 7.30. Adsorption isotherms for GUS.....	147
Figure 7.31. Adsorption Isotherms for casein.....	148
Figure 7.32. Van't Hoff's plot from Langmuir isotherm constants.....	149
Figure 7.33. Eyring plot of $\ln(k/T)$ vs $1/T$ for the adsorption of casein onto zeolite....	151
Figure 7.34. Arrhenius plot of $\ln k_2$ vs $1/T$ for the adsorption of GUS onto zeolite.....	153
Figure 7.35. Arrhenius plot of $\ln k_d$ vs $1/T$ for the adsorption of casein onto zeolite....	153
Figure 7.36. SEM image of zeolite sample and size of the macropore. ....	155
Figure 7.37. Representative plot used for the calculation of $k_f$ . ....	156
Figure 7.38. Representative plot used for the calculation of $k_d$ .....	158
Figure 7.39. Intraparticle diffusion plot for the adsorption of GUS onto zeolite ( $C_i$ :	

20-100 µg GUS/ml, 37°C, 150 rpm, S/L:5mg/ml, pH 6.8, particle size: 45-75µm).....	159
Figure 7.40. Intraparticle diffusion plot for the adsorption of GUS onto zeolite (Ci: 150-500 µg GUS/ml, 37°C, 150 rpm, S/L:5mg/ml, pH 6.8, particle size: 45-75µm).....	159
Figure 7.41. Intraparticle diffusion plot for the adsorption of casein onto zeolite (Ci: 0.06-0.41 mg /ml, 37°C, 150 rpm, S/L:5mg/ml, pH 6.8, particle size: 45- 75µm).....	160
Figure 7.42. Intraparticle diffusion plot for the adsorption of casein onto zeolite (Ci: 0.7-1.25 mg /ml, 37°C, 150 rpm, S/L:5mg/ml, pH 6.8, particle size: 45- 75µm).....	160
Figure 7.43. Representative plot used for the calculation of $D_p$ .....	161
Figure 7.44. Representative plot used for the calculation of $k_1$ .....	163
Figure 7.45. Representative plot used for the calculation of $k_2$ .....	164
Figure 7.46. Stability change of casein for 30h incubation time .....	172
Figure 7.47. Stability change of casein for 7h incubation time .....	172
Figure 7.48. pH changes in SIF incubated with zeolite .....	173
Figure 7.49. Change in $[Ca^{2+}]$ , $[Na^+]$ , $[Mg^{2+}]$ , $[K^+]$ in SIF.....	174
Figure 7.50. Radical inhibition capacity of casein at different concentrations.....	175
Figure 7.51. Antioxidant activity change in inhibition %.....	177
Figure 7.52. Protein content in SIF and their antioxidant capacity .....	177
Figure 7.53. Fluorescence emission spectra of casein (1.5 mg/ml) in SIF at pH 6.8. ..	181
Figure 7.54. UV Absorption spectra of casein (1.5 mg/ml) in SIF at pH 6.8.....	182
Figure 7.55. DSC thermograms of casein in SIF .....	183
Figure 7.56. IR spectra of zeolite.....	185
Figure 7.57. Standard protein FTIR spectra .....	186
Figure 7.58. IR spectrum of casein powder (untreated). .....	187
Figure 7.59. IR spectrum of casein .....	187
Figure 7.60. SEM images of casein samples. a) Casein powder (Untreated); b) Solubilized casein in SIF at initial. ....	188
Figure 7.61. Casein after 4h incubation in SIF (without zeolite) b) Casein after 4h incubation in SIF with zeolite .....	189
Figure 7.62. SEM images of zeolite samples. a) Zeolite after incubated 4h in SIF with casein b) Zeolite (casein free;control). ....	190

Figure 7.63. SEM images of casein powder .....	191
Figure 7.64. Fluorescent limination under UV light.....	193
Figure 7.5. Effect of different zeolite concentrations on growth (%) of <i>E.coli</i> .....	194
Figure 7.66. Changes of OD of <i>E.coli</i> with respect to time at various casein concentrations added to growth media .....	195
Figure 7.67. Logarithmic growth rate of <i>E.coli</i> at various concentration of the casein .....	196
Figure 7.68. Specific growth rate curve as a function of casein concentration .....	197
Figure 8.1. Effect of zeolite concentration on antioxidant activity. ....	199
Figure 8.2. Effect of zeolite concentration on inhibition % of ABTS <sup>+</sup> . ....	199
Figure 8.3. Images of Caco-2 cell under microscope.(a)View of Caco-2 cells on an optical microscope at 100% confluency, (b) Size of the cells.....	200
Figure 8.4. Confocal microscopy images of fine zeolite particles with the Caco-2. ....	202
Figure 8.5. Effect of the medium pretreated with 75mg/ml zeolite on the growth of Caco-2 cell line. ....	203
Figure 8.6. Change in absorbance values in XTT assay for the samples including non-treated (control) growth media. ....	204
Figure 8.7. Change in absorbance values in XTT assay for the samples including 75mg/ml zeolite treated growth media. ....	204
Figure 8.8. Change in cell growth (%) using 18h and 24h zeolite treated growth media.....	206
Figure 8.9. Color change in zeolite treated media after storage at +4°C for 21 days in the sample order of 25, 50, 75 (mg/ml) zeolite and 18(pink)- 24h(yellow) treatment respectively. ....	208
Figure 8.10. FTIR spectra of cell growth media treated with zeolite: 18h treated; 24h treated; untreated (control).....	212
Figure 8.11. Viability histograms of two types of cancer cell lines after zeolite treatment .....	213
Figure 8.12. GUS activity histograms of cancer cells in terms of relative fluorescence unit (RFU) per µg total protein of cell lysates.....	214
Figure 8.13. Color of cancer cell growth media treated with digested and non- digested zeolite samples with different doses.....	217
Figure 8.14. Cell proliferation % for Caco-2 cell treated with Zeolite 1.....	218
Figure 8.15. Cell proliferation % for Caco-2 cell treated with digested Zeolite 1 .....	218

Figure 8.16. Cell proliferation % for Caco-2 cell treated with Zeolite 2.....	219
Figure 8.17. Cell proliferation % for Caco-2 cell treated with digested Zeolite 2 .....	219
Figure 8.18. Cell proliferation % for MCF-7 cell treated with Zeolite .....	220
Figure 8.19. Cell proliferation % for MCF-7 cell treated with digested Zeolite 1 .....	220
Figure 8.20. Cell proliferation % for MCF-7 cell treated with Zeolite 2 .....	221
Figure 8.21. Cell proliferation % for MCF-7 cell treated with digested Zeolite 2 .....	221
Figure 8.22. A Representative plot of cell cycle analyses results for MCF-7 cells treated with Z1. ....	223
Figure 8.23. A Representative plot of cell cycle analyses results for MCF-7 cells treated with Z2. ....	224
Figure 8.24. A representative plot for cell cycle analyses results for MCF-7 cells untreated(control).....	225
Figure 8.25. Representative dot plots for the apoptosis analyzes for Caco-2 and MCF-7 cells using Z1 and Z2.....	226
Figure 8.26. Representative population histograms for the apoptosis analyzes for Caco-2 and MCF-7 cells using Z1 and Z2.....	227

## LIST OF TABLES

<b><u>Table</u></b>	<b><u>Page</u></b>
Table 2.1. Properties of <i>E. coli</i> GUS, EC 3.2.1.31. ....	12
Table 2.2. $\beta$ -glucuronidase activities in the small intestinal and colonic contents of pigs.....	22
Table 2.3. <i>E. coli</i> GUS (EC 3.2.1.31) inhibitors and percentage inhibition .....	22
Table 2.4. <i>E. coli</i> GUS (EC 3.2.1.31) inhibitors and inhibition types.....	25
Table 3.1. Characteristics and methods .....	28
Table 3.2. Comparison of the characteristics of chemical and physical adsorption.....	34
Table 3.3. External mass transfer models and determination of kinetic parameters. ....	52
Table 3.4. Intraparticle diffusion models and determination of kinetic parameters. ....	53
Table 3.5. Reaction models and determination of kinetic parameters.....	53
Table 3.6. Diffusion models used for the modeling of adsorption kinetic data.....	57
Table 3.7. Reaction models used for the modeling of adsorption kinetic data.....	58
Table 5.1. Experimental conditions of various kinetic adsorption experiments for the GUS adsorption onto digested zeolite (Z1) at a constant working volume of 2 ml. ....	86
Table 5.2. Experimental conditions of various kinetic adsorption experiments for the casein adsorption onto digested zeolite (Z1) at a constant working volume of 10 ml. ....	87
Table 6.1. Elementary composition .....	95
Table 6.2. Analysis results of ASAP2010 .....	97
Table 6.3. Changes in major element content of the zeolites. ....	115
Table 7.1. Effect of casein on GUS activity. ....	128
Table 7.2. Comparison of inhibitory potentials for casein and zeolites on GUS activity. ....	129
Table 7.3. Apparent Kinetic Parameters.....	131
Table 7.4. Variations in zeta potential of GUS enzyme with pH .....	141
Table 7.5. Langmuir and Freundlich constants for GUS adsorption. ....	147
Table 7.6. Langmuir and Freundlich constants for casein adsorption at 25 and 37°C. ....	148
Table 7.7. Thermodynamic parameters for GUS adsorption on zeolite. ....	150
Table 7.8. Thermodynamic parameters for casein adsorption on zeolite. ....	151



Table 7.9. Effect of initial concentration on external diffusion model parameters .....	157
Table 7.10. Effect of initial concentrations on intraparticle diffusion model parameters .....	162
Table 7.11. Effect of initial concentration on reaction model parameters.....	165
Table 7.12. Effect of shaking rate on external diffusion model parameters.....	166
Table 7.13. Effect of shaking rate on intraparticle diffusion model parameters .....	166
Table 7.14. Effect shaking rate on reaction model parameters.....	167
Table 7.15. Effect of particle size on external mass transfer model parameters .....	168
Table 7.16. Effect of particle size on intraparticle diffusion model parameters (37oC, 150 rpm, S/L:5mg/ml, pH 6.8, Ci: 100 µgGUS/ml, Ci:0.125 mg casein/ml).....	168
Table 7.17. Effect of particle size on reaction model parameters (37oC, 150 rpm, S/L:5mg/ml, pH 6.8, Ci: 100 µgGUS/ml, Ci:0.125 mg casein/ml).....	169
Table 7.18. Effect of temperature on external diffusion model parameters .....	169
Table 7.19. Effect of temperature on intraparticle diffusion model parameters.....	170
Table 7.20. Effect of temperature on reaction model parameters.....	170
Table 7.21. Effect of zeolite incubation on casein amount and its antioxidant activity .....	176
Table 7.22. Zeta potential of casein hydrolysate in SIF solution during adsorption ....	178
Table 7.23. DSC Results of Samples.....	184
Table 7.24. Effect of different zeolite concentrations on growth of E.coli .....	194
Table 7.25. Specific growth rates and generation times of E.coli at various casein concentrations .....	196
Table 8.1. pH and conductivity values of zeolite treated media.....	207
Table 8.2. pH and conductivity values of zeolite treated media after storage at +4oC for 21 days.....	207
Table 8.3. Analysis of zeolite treatments by ICP-MS. ....	210
Table 8.4. Results of cytotoxicity tests for MCF-7 cells treated 18 h with metal salts (µM).....	210
Table 8.5. Results of cytotoxicity tests for MCF-7 cells treated 24 h with metal salts (µM).....	210
Table 8.6. Percentage viability of two types of cancer cell lines after zeolite treatment (Z), .....	213
Table 8.7. Comparison of GUS activities for two cancer cell lines.....	214

Table 8.8. GUS activity of cancer cells in terms of relative fluorescence unit (RFU) per $\mu\text{g}$ total protein of cell lysates (Z:zeolite treated). .....	215
Table 8.9. pH and conductivity changes in cancer cell growth media treated (24h) with digested (Z1D) and non-digested (Z1)zeolite samples with different doses (control: no zeolite). .....	216
Table 8.10. pH and conductivity changes in cancer cell growth media treated (24h) with digested (Z2D)and non-digested zeolite (Z2) samples with different doses (control: no zeolite). .....	216
Table 8.11. Summary of cell cycle analyses results for zeolite treated MCF-7 cells...	223
Table 8.12. Summary of apoptosis results in percentages of populations.....	227

# CHAPTER 1

## INTRODUCTION

Zeolites are crystalline, hydrated aluminosilicates of alkali and alkaline earth cations, consisting of three dimensional frameworks of  $\text{SiO}_4^{4-}$  and  $\text{AlO}_5^{4-}$  tetrahedra linked through the shared oxygen atoms. Both natural and synthetic zeolites are porous materials, mainly characterized by adsorption property, or acting as molecular sieves and their ion-exchange property. These properties make use of zeolites possible in a wide range of industrial and agricultural applications and particularly in animal nutrition (Mumpton, 1999).

Natural zeolite clinoptilolite has been reported to be inert and non-toxic matter for poultry and zeolite supplemented diets reported to support biomass production and improve the health status of the animals (Papaioannou et al., 2004; Papaioannou et al., 2005) and non-toxic to animals (Ortatlı and Oğuz, 2001). Many researches in literature provide evidence of a growth promoting effect when zeolites are used as additives in animal nutrition. Improved weight gain rates have been obtained in fattening pigs and lambs, better feed efficiency and egg productivity has been achieved in laying hens by the dietary use of zeolites (Papaioannou et al., 2004; Martin-Kleiner et al., 2001; Prvulovic et al., 2007). Zeolite with structural stability and with its ability to host useful pharmaceutical species, can be used as a controlled release matrix in the human body. Besides, clinoptilolite has demonstrated good stability in its transit through the gastrointestinal tract, and found to be harmless to the human body (Papaioannou et al., 2002; Ortatlı and Oğuz, 2001; Rivera et al., 2000) and it is used as drug carrier (Rivera et al., 2003; Farias et al., 2003). Based on such properties, natural zeolites have been used for different pharmaceutical forms for the treatment of several pathologies in animals and humans. For the gastrointestinal track, it is used as antimicrobial agent, used to treat stomach ulcers incision, and used as antidiarrheic drug (Rodriguez-Fuentes et al., 1997; Rivera et al., 1998; Rodriguez-Fuentes et al., 2006) and mechanism behind this therapeutic action suggested to encapsulation and/or adsorption of different ions and molecules in its open framework. But detailed mechanisms behind their therapeutic effect are still unknown and should be investigated.

More recent studies indicate that zeolites play a role in modulating immune system and results showed that clinoptilolite is used as potential adjuvant in anticancer therapy in animals. Pavelic et al. (2001) reported a novel use of micronized clinoptilolite as a potential adjuvant in anticancer therapy. It was used in anticancer treatment of mice and dogs and it resulted prolonged of life span, improvement of health status, decrease in some tumor sizes (Pavelic et al., 2001; Zarkovic et al., 2003). As well as their antimetastatic activity and their immunostimulatory modulatory effect was also reported where it was reported that zeolite treatment resulted reduction in melanoma metastases in mice (Pavelic et al., 2002). Therefore, to identify the mechanism behind the therapeutic effect of zeolite, investigation of the interactions of natural zeolites with digestion system and related cancer diseases have crucial importance.

Human intestinal system is a complex microbiota and exhibits variety of enzymatic activities with potential impact on human health through biotransformation of secondary products and xenobiotic compounds. Bacterial microflora of the intestinal system is capable of changing the activity of exogenous carcinogens through stimulating intestinal conditions and modulating metabolic activation and/or detoxification. It was reported that this biotransformation by bacterial metabolism, can lead to the generation of genotoxic and carcinogenic products (Hughes and Rowland, 2000). Therefore understanding the roles of bacterial flora is of great importance for the overall health status of the living metabolisms. From this point of view, intestinal system as a part of digestive system, and it is the first step to evaluate the beneficial effect of zeolite to interact with its surrounding.

In this study, positive health role of natural zeolite was proposed to act as a potent inhibitor of bacterial  $\beta$ -glucuronidase (GUS) enzyme. This enzyme is secreted by some microorganisms in intestine and related to drug metabolite detoxification and responsible for producing reactive metabolites related to some diseases and cancer development (Goldin and Gorbach, 1977; Beaud et al., 2005; De Moreno and Perdigon, 2001). In humans, fecal  $\beta$ -glucuronidase activity was shown to be higher in colorectal cancer patients as compared to healthy controls suggesting a role of this enzyme in carcinogenesis (Rafter et al., 2004). Besides, results of different studies implied that GUS activity can be considered as a cancer risk biomarker where its activity is related to cancer development and results showed that number of carcinogens being produced by this bacterial enzyme in the intestine (Fujisawa et al., 2001; Cardona, et al., 2006).

Aim of this study is to investigate inhibitory and adsorptive potential of natural zeolites against *E.coli* GUS and to determine interactions of zeolites with colon cancer (Caco-2) cells. Besides, inhibitory potential of casein which is an antioxidant nutritive compound, was investigated as an alternative inhibitor towards GUS. Since the intake of zeolite will actually be important for the digestive system, simulated digestion studies for the zeolite samples were performed. In Chapter 6, characterization of the digested and non-digested zeolite samples were given. Thus, the effect of in-vitro simulated digestion conditions on zeolite and possible interactions of zeolite with its surrounding media were revealed. In Chapter 7, inhibition studies of GUS by zeolite and casein were expressed. Additionally, adsorption studies for GUS onto zeolite were performed in order to investigate the dominant mechanism controlling the adsorption kinetics. Casein was investigated as another alternative inhibitor to zeolite, detailed interaction studies between two inhibitors were performed and mechanism behind the casein adsorption onto zeolite was investigated and discussed. In Chapter 8, interactions studies of zeolites with different cancer cell lines: Caco-2 (human colon adenocarcinoma) and MCF-7 (human breast cancer) were presented and possible affects of zeolites toward cancer cell lines at DNA level were analyzed.

Based on those investigations in this study, possible mechanisms of natural zeolites behind their therapeutic effects could be revealed. Besides, in the near future, bases of this present study could be helpful to identify most of the interaction mechanisms between these compounds and might help the utilization of our natural source “zeolite” as a high value added material for medical applications in our country.

## CHAPTER 2

# INTESTINAL SYSTEM AND $\beta$ -GLUCURONIDASE ENZYME

Human intestinal system is an important part of digestive system where digestion and absorption of the most nutrients occur. In general intestinal health is closely related to the integrity and mechanical barrier function of intestinal wall and also microbial growth in the intestine (Ya-Ling et al., 2007). Microbial flora with its composition and activities in the systematic physiology, can be considered as an organ of that intestinal system. Members of the microbiota in the human intestine exhibit a variety of enzymatic activities with potential impact on human health through biotransformation of secondary products and xenobiotic compounds. Therefore bacteria were also risk factors for colon cancer.

A number of carcinogens being produced by hydrolysis of glucuronide in the intestine with bacterial enzymes.  $\beta$ -glucuronidase which is an enzyme produced by a number of intestinal bacterial species has been suggested to be related to cancer development (Marta et al., 2008). Therefore it is important to understand the basic mechanisms in intestinal system and its microflora to evaluate beneficial effects of different therapeutic compounds to change the activity of exogenous carcinogens through stimulating intestinal conditions and modulating metabolic activation and/or detoxification.

### 2.1. Human Intestinal System

Human intestinal system is an important portion of gastrointestinal (or alimentary) system which is between the stomach and anus. It consists of two segments; the small intestine and the large intestine. The small intestine is about 6 m long, where the most extensive part of digestion occurs and most food products are absorbed. The large intestine has a larger diameter and is about 1.5 m where water is absorbed and from which solid waste material is excreted.

### **2.1.1. Small Intestine**

The structure of small intestine is consisted of four concentric layers which are mucosa, submucosa, muscularis externa, and serosa. In intestine, finger like structure arise from the luminal side of mucosal membrane is known as villi. Villi consists of a single layer of tall, columnar epithelial absorptive cells (enterocytes) that contain microvilli. Those structures increase the absorptive surface and give it a brush-like appearance and their surface membrane contains digestive enzymes and transport systems (Barltrop and Brueton, 1990).

Small intestine begins with the pylorus at the upper portion, the opening at the lower part of the stomach, through which the contents of the stomach pass into the duodenum. It ends at the ileocecal valve. It is also divided into different portions: duodenum, the mobile jejunum, and ileum (Adrouny, 2002). The duodenum surrounds the pancreas and the pancreatic duct and ducts from the liver and gall bladder that open into it. Middle part of the small intestine is called jejunum. Jejunum extends from the duodenum to the ileum. The terminal portion is called ileum and ileum is connected to the first part of the large intestine the cecum.

### **2.1.2. Digestion in Small Intestine and Importance of Liver and Bile**

Small intestine is an important part of whole intestine where the most of the digestion and absorption of food constituents occurs. Also it is a major site for absorption of water and electrolytes. Transport of the products of digestion and of vitamins, minerals, and water across the intestinal epithelium to the lymphatic or blood circulatory systems is performed in small intestine (Adrouny, 2002).

Mucosa of the small intestine has a unique structure which is suitable for the digestion and absorption. Digestion in the small intestine requires the biliary and pancreatic secretions that are emptied into the duodenum (Adrouny, 2002). Duodenum has a role in the digestion of food in the small intestine where enzymes are used. Also hormones such as secretin and cholecystokinin were released by the cells in the duodenal epithelium and rate of emptying of the stomach via hormonal pathways are regulated.

Material absorbed from the small intestine is taken to the liver. Liver is

responsible for synthesis, storage, secretion, excretion, and specific modification of endogenously and exogenously derived substances. It is mainly supplied by venous blood arriving from the gastrointestinal tract. Also it releases bile with gallbladder and the pancreas to release bicarbonate and digestive enzymes such as trypsin, lipase and amylase into the duodenum as they are needed.

The liver is anatomically divided into lobules which consist of functional aggregates of hepatocytes. Those cells are polygonally shaped liver parenchymal cells and bile is produced and secreted continuously into the bile canaliculi by them. In bile there are bile acids, bile pigments, cholesterol, phosphatidylcholine (lecithin), and electrolytes and glucuronide conjugates of bile pigments as bilirubin and biliverdin derived from the degradation of heme, a prosthetic group of many proteins (Adrouny, 2002). Also other endogenous (e.g., steroids) and exogenous (e.g., drugs, dyes) compounds are secreted via bile.

An aqueous alkaline buffering component (e.g.,  $\text{HCO}_3^-$ ) is added to the bile by the hepatic bile duct cells that carry the secretion toward the common bile duct. Then, hepatic bile flows into the gallbladder and in gallbladder it is concentrated. Also it is stored and then emptied into duodenum from gallbladder when partially digested foods from stomach enter the duodenum (Adrouny, 2002).

Infection problems in human and bile stagnation results increase in the production of bile pigments and such as bilirubin.  $\beta$ -glucuronidase enzyme is responsible for conversion of glucuronide conjugates to their free forms. Bilirubin diglucuronide is converted to insoluble free bilirubin and forms calcium-bilirubinate which is called pigment stones (Adrouny, 2002). Also cholesterol can be precipitated to form stones (known as gallstones) which are common health problems in the world.

### **2.1.3. Large Intestine**

Last part of the digestive system is large intestine. At this part of digestion system, foods are no longer broken down. In large intestine, water is absorbed from the indigestible foods during transit. Also it simply absorbs vitamins which are produced by the colon microflora. The human large intestine is about 1.5 metres long and consists of the caecum, ascending colon, transverse colon, descending colon, sigmoid colon and rectum (Claire et al., 2006). Bacteria in the colon convert undigested food material into



its final fecal form.

The large intestine has a smooth mucosal lining (only the rectum has folds) that secretes mucus to lubricate the waste materials. By peristaltic movements of the rhythmic contractions of intestinal muscles, undigested food material is moved through the large intestine and reaches at the exit of the rectum called anus.

## **2.2. Role of Microbial Flora in Human Intestinal System**

Microbial flora with its composition and activities, affect both intestinal and systematic physiology of human therefore it can be described as a metabolically adaptable and rapidly renewable “organ”. It is very complex ecosystem because more than 75% of the wet weight of our fecal output is composed of bacterial cells. Besides it was reported that one gram of this output is thought to contain approximately  $10^{11}$  microbes, of an estimated 50 genera belonging to over 400 separate species (Dunne, 2001).

The principal role of the gastrointestinal flora is to salvage energy from non digested dietary substrates and endogenous mucus. The nature and extent of this metabolism depends upon the characteristics of the bacterial flora, colonic transit time and the availability of nutrients especially carbohydrates and proteins. Hughes and Rowland (2000) reported that metabolic activities of the gut microflora have also been associated with cancer development following the formation of toxic products by bacterial enzyme activities

The human intestine is part of a truly amazing ecosystem that is essential for the successful and efficient absorption of nutrients. The gut’s high absorptive capability is because of its immense surface. The lumen of the gut accommodates 100 trillion microorganisms, ten times the number of human cells in the adult body. Most of the intestinal microbes are bacteria, although archaea and eukaryotes are also present. It was reported that the gut’s immune system scans and inhibits growth of harmful pathogens while promoting growth of beneficial commensals (Saier and Mansour, 2005).

Today bacterial species, most of which are still poorly characterized, inhabit the human intestine. The majority of adult intestinal bacteria fall into two of the 55 known bacterial kingdoms. They are Gram-positive Firmicutes, and the Gram-negative Bacteroidetes and each of these two groups of microbes constitutes about 30% of the

intestinal microbial flora. However, the composition of the microbial ecosystem in our intestines constantly changes during development and in response to nutrient types ingested. Also in several studies it was shown that they were effected with the age and the health status of the host (Gilmore and Ferretti, 2003; Saier and Mansour, 2005). Related to this, intestinal track colonisation is markedly influenced by luminal pH, and by the progressively slower transit of food materials towards the colon. This slower transit times allows the establishment of a complex and relatively stable bacterial community in the large intestine. Thus near neutral pH and the relatively low absorptive state of the colon, it was reported to further encourage the extensive microbial colonisation and growth (Vernazza et al., 2006).

The cells of the gut flora can also be separated into two categories: beneficial species (i.e., *Bifidobacterium* and *Lactobacillus*) and detrimental species (i.e., *Enterobacteriaceae* and *Clostridium spp.*) (De Moreno and Perdigon, 2001). The beneficial species are mainly called as probiotic bacteria and are responsible for:

- (1) providing nutrients and cofactors
  - (2) successfully competing with pathogens
  - (3) stimulating host immune responses by producing specific polysaccharides
- (Saier and Mansour, 2005).

Besides, Chiara et al. (2005) reported that binding of carcinogens to those bacterial cell walls has been suggested to protect against colorectal cancer. Therefore probiotic bacteria are found in the intestines of humans and other mammals and they provide health benefits to the host. Detrimental ones cause disease or illness to its host by themselves and their harmful byproducts (Catanzaro and Gren, 1997). The large intestine can harbour pathogens that can be a part of the resident flora or exist as transient members. Attachment and overgrowth of the pathogens generally results in acute diarrhoeal infections but in some cases more chronic forms of intestinal disease also occur such as inflammatory bowel diseases (ulcerative colitis and Crohn's disease), colon cancer and pseudomembranous colitis(Claire et al., 2006).

### **2.2.1. Influence of Diet on Intestinal Microflora and Health**

For the microflora composition and activities diet is very important as it provides the major source for microbial growth. Composition of the microbial

ecosystem in our intestines constantly changes in response to nutrient types ingested. The concept of probiotics was developed from this idea and it based on impression of the gut microbiota in a beneficial manner.

Probiotics defined as live microbial food supplements that beneficially affect the host by improving the intestinal microflora balance (Dunne, 2001). Therefore consumption of soured (fermented) products had an important effect on improvement of gastrointestinal health and the prolongation of life for the balance of intestinal microflora.

Dietary compounds had an important affect on the metabolic activity of intestinal bacteria, which may play a role in the conversion of bile acids and neutral sterols to reactive metabolites that may possibly act as cocarcinogens and/or carcinogens. Especially effect of dietary fat on the composition of fecal bacterial flora was in research for this reason. It was reported that effect of high protein (beef or soybean) diet associated with high fat (beef fat, lard) diets resulted elevated levels of bacterial  $\beta$ -glucuronidase activity in the large intestine in rats (Indira et al., 1980) which is responsible for producing reactive metabolites related to cancer development.

Bioactive food compounds and dietary manipulation can affect DNA damage and cell growth, and these factors mediate the development and/or growth of cancer cells. Therefore considerable clinical interest has been expressed in the qualitative and quantitative aspects of different dietary compounds such as foods rich in dietary fiber, probiotics and antioxidants in human diet in relation to reduce different health problems such as colon cancer.

### **2.2.2. Bacterial Enzymes Associated with Cancer**

Chemical transformations of some compounds occur directly due to metabolic activities of the microbiota. Numerous pathogens exist in intestine produce various enzymes with different functions. Some of these enzymes form products which are known to be mutagenic and carcinogenic.

Several studies have shown that when the populations were compared for their risk for colon cancer it was found that populations at high risk for colon cancer have an intestinal microflora with an increased ability to metabolize steroids and to hydrolyze glucuronides (Goldin and Gorbach, 1977). Therefore enzymatic activities of the gut

microflora, towards ingested foreign compounds such as nitro-aromatics, azo compounds, and nitrate can have wide-ranging implications for health.

A wide range of enzymes are associated with gut microflora. Those enzymes are capable of generating potentially carcinogenic metabolites in the colon. They are usually assayed in fecal suspensions and appear to be present in many bacterial types (Rafter et al., 2004). It was reported that the bacterial metabolism of such compounds can lead to the generation of genotoxic and carcinogenic products (Hughes and Rowland, 2000). Bacteria may have mutagenic activity which may further increase procarcinogenic activity. Procarcinogenic substances such as food preservatives, dyes, additives, or pollutants can be transformed into carcinogenic substances by bacterial enzymes beta-glucuronidase, beta-galactosidase, beta-glucosidase, nitroreductase, azoreductase, 7-alpha dehydroxylase, and cholesterol dehydrogenase (Catanzaro and Gren, 1997). The main ones are  $\beta$ -glucuronidase, azoreductase, and nitroreductase.

It was important to note that activities of these enzymes produced by pathogens have been well correlated to the number of lactic acid bacteria in the intestine. It was reported that rats which have been experimentally fed beef and *Lactobacillus* have reduced fecal amounts. Therefore *Lactobacilli* was suggested to influence the metabolic activity of colonic flora and inhibit cancer potential by altering the enzymatic activity produced by pathogens (Catanzaro and Gren, 1997). Also Goldin and Gorbach (1976) had showed the relationship between diet and rat fecal bacterial enzymes implicated in colon cancer.

$\beta$ -glucuronidase hydrolyzes a wide spectrum of glucuronides related to tumor formation (Goldin and Gorbach, 1977). Bacterial beta-glucuronidase contributes to the toxicity of compounds which have been previously detoxified by liver glucuronidation. As  $\beta$ -glucuronidase is an enzyme responsible for the hydrolysis of glucuronides in the lumen of the gut, reaction generates toxic and carcinogenic substances which are detoxified by glucuronide formation in the liver and then enter the bowel via bile. In this way, toxic aglycones can be regenerated in situ in the bowel by bacterial  $\beta$ -glucuronidase. In humans, fecal  $\beta$ -glucuronidase activity was shown to be higher in colorectal cancer patients as compared to healthy controls suggesting a role of this enzyme in carcinogenesis.

Another enzyme which is important in colon cancer prevention is nitroreductase (De Moreno and Perdigon, 2001). Bacterial nitroreductase reduces nitrogenous compounds to aromatic amines via nitrosamines and n-hydroxy compounds, which are

suspected mutagens (Catanzaro and Gren, 1997). The end products and the highly reactive intermediates derived from these reactions such as reactive nitroso- and N-hydroxyintermediates and aromatic amines are mutagenic and carcinogenic.

The last one, azoreductase promotes the reduction of azo food dyes to substituted phenyl and naphthyl amines, which are potent carcinogens (Catanzaro and Gren, 1997). These enzymes are known to be potential mediators of colon carcinogenesis (De Moreno and Perdigon, 2001). Of these enzymes,  $\beta$ -glucuronidase was reported to be the most extensively investigated as a biomarker of colon-rectum cancer risk (Rafter et al., 2004).

## **2.3. $\beta$ -Glucuronidase**

$\beta$ -glucuronidase is one of the most important hydrolytic enzymes in living systems (Ünak et al., 2005). Enzyme has an essential role in the detoxification pathway of toxic materials incorporated into the metabolism. It was first isolated and named by Fishman in 1948. This enzyme is widely distributed in mammalian tissues. It is reported in the literature that small changes in this enzyme level can cause the development of certain important diseases, especially specific types of cancers. In addition, some tumor tissues and bacteria have high  $\beta$ -glucuronidase activities. (Ünak et al., 2005)

### **2.3.1. Structure and Function**

$\beta$ -glucuronidase activity has been detected both in intestinal tissues and in intestinal bacteria. It was demonstrated that the greatest part of the activity in the caecum and in the large intestine of rats has, however, been attributed to bacterial enzymes (Beaud et al., 2005).  $\beta$ -glucuronidase activity has been detected among bacterial genera belonging to the dominant human intestinal microbiota, such as *Bacteroides*, *Bifidobacterium*, *Eubacterium* and *Ruminococcus*. Among bacteria, genes encoding  $\beta$ -glucuronidase have been described for *Escherichia coli*, *Lactobacillus gasseri* and *Staphylococcus sp.*, and identified in *Clostridium perfringens*, *Staphylococcus aureus* and *Thermotoga maritima*, for which whole genome sequences are available (Beaud et al., 2005).

As mentioned above, two main origins of the enzyme in human body are

bacteriologic or host cells. Between these two,  $\beta$ -glucuronidase of intestinal bacteria (GUS, EC 3.2.1.31) has received a great deal of attention as a promising indicator for evaluating dietary mediated effects of inherent colon cancer risk. This activity is in fact responsible for hydrolysis of xenobiotic glucuronide conjugates in the gut, and can thus produce toxic aglycones and carcinogenic substances. Caldini et al., (1999) reported that GUS production is constitutive in a large number of *Escherichia coli* strains and is a suitable marker for this species. The intestinal organisms *Escherichia coli*, *Enterococcus faecalis*, *Lactobacilli* and *Clostridia* have been associated with the production of  $\beta$ -glucuronidases (Cardona, et al. 2006). In Table 2.1, some properties of *E. coli* GUS were given.

Table 2.1. Properties of *E. coli* GUS, EC 3.2.1.31.

<b>Molecular Weight</b>	~290 kDa (tetramer) 68,259 Da (monomer)
<b>Optimal pH:</b>	6-7
<b>Isoelectric point (pI)</b>	4.8

This enzyme's expression is influenced by the physiological conditions of the bacteria and environment (Caldini, et al. 1999).  $\beta$ -glucuronidase (EC 3.2.1.31) catalyzes the reaction given below:

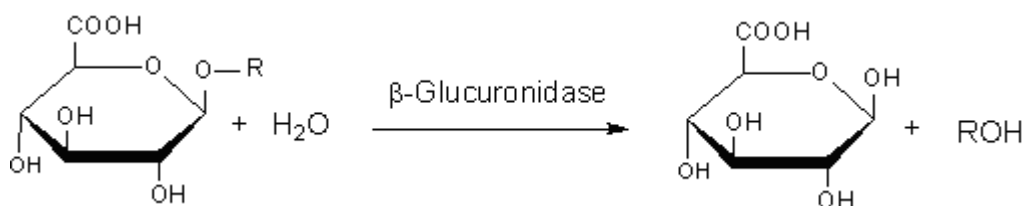


Figure 2.1. Catalyzed reaction for GUS ( $\beta$ -D-glucuronoside (glucuronide) +  $H_2O$   $\leftrightarrow$  D-glucuronate + an alcohol)

Human  $\beta$ -glucuronidase is mainly found in the lysosomes and microsomes of normal tissues, with plasma levels of enzyme quite low.  $\beta$ -glucuronidase is normally excreted in urine with cells of the urinary tract the primary source of enzyme. Increased urinary levels of enzyme are observed in conditions that affect the urinary tract, such as acute renal necrosis, active pyelonephritis, and cancer of the kidney and bladder. The enzyme has a characteristic acidic pH optimum. In contrast, it was reported by Zenser,

et al. (1999) that *Escherichia coli*  $\beta$ -glucuronidase has a much higher pH optimum. *E.coli*  $\beta$ -glucuronidase may also be present in urine due to urinary tract infection

### 2.3.2. Clinical Importance of GUS

$\beta$ -glucuronidase is an enzyme capable of splitting compounds that are conjugated with glucuronic acid as mentioned above. It liberates toxins and mutagens that have been glucuronated in the liver and excreted into the gut with the bile (Dabek et al. 2008). Many exogenous (e.g. drugs, pesticides) as well as endogenous compounds (e.g. bilirubin, steroids, bile acids) are conjugated with glucuronic acid in the liver and excreted by the bile. This formation of glucuronides has been considered a 'detoxification mechanism' named as glucuronidation (Cardona et al., 2006)

These exogenous compounds are poorly reabsorbed into the bloodstream and are efficiently eliminated from the body unless they are hydrolyzed (Beaud et al., 2005). But some of the glucuronides are secreted through the biliary route into the intestine and these compounds may be hydrolyzed by the action of bacterial  $\beta$ -glucuronidases present in the intestine (Cardona et al., 2006) and their hydrolysis may liberate free toxins and mutagens which can lead to high local concentrations of carcinogenic compounds where colon mucosa exposed. If glucuronide hydrolysis is a rate limiting step in this process, then the activity of microbial  $\beta$ -glucuronidase in the colon may influence the risk of colon carcinogenesis. Furthermore, it was reported in several studies that reuptake of the deconjugated compound from the gut and reglucuronidation in the liver leads to an enterohepatic circulation of xenobiotic compounds, which increases their retention time in the body (Nalini et al., 1998; Dabek et al., 2008). For example,  $\beta$ -glucuronidase exhibits its harmful effects by hydrolysing glucuronic acid-heterocyclic amine (HCA) conjugates into reactive metabolites to damage both the colon and the liver through the enterohepatic circulation (Chiara et al., 2005).

Besides the relation of colon cancer with microbial  $\beta$ -glucuronidase activity, it was found that its activity is increased in the cerebrospinal fluid (CSF) of patients with bacterial meningitis. Beratis et al. (2003) measured indicative parameters of illnesses such as, cell number, protein concentration, CSF/blood glucose ratio and  $\beta$ -glucuronidase activity and results showed that the  $\beta$ -glucuronidase activity was the best prognostic index. To better understand the importance of  $\beta$ -glucuronidase and its

relation with certain diseases it is important to know the glucuronidation mechanism in the body.

### **2.3.2.1. Glucuronidation**

Glucuronidation is the process of chemically binding a substance to glucuronic acid via a glycosidic bond. The resulting glucuronide is typically much more water soluble than the original substance. The human body uses glucuronidation to excrete a large variety of molecules, including drugs, pollutants, bilirubin, androgens, estrogens, mineralocorticoids, glucocorticoids, fatty acid derivatives, retinoids and bile acids. Most of this is done by the liver.

Conjugation with glucuronic acid is probably the most important detoxification reaction as it occurs extensively in mammals and other animals. The widespread occurrence of glucuronidation is due to the fact that glucuronic acid is readily available. Glucuronic acid is derived from glucose and its stored form, glycogen. In addition, there are several functional groups such as hydroxyl, amino, carboxyl and sulfhydryl to which glucuronic acid can be transferred enzymatically. Glucuronidations are catalyzed by UDP-glucuronosyltransferases, located in the endoplasmic reticulum. They catalyze the transfer of glucuronic acid from an uridinediphosphoglucuronic acid (UDPGA) cofactor to the above mentioned functional groups.

The effect of glucuronidation is to produce an acidic compound that is more water-soluble than the parent precursor at physiological pH. Therefore, these compounds will be entirely ionized at pH values between 3 and 4. Kaushik et al. (2006) showed that the properties of high acidity and high water-solubility in physiological conditions support the concept that glucuronide formation is a detoxification process. Therefore, this is a major drug-metabolizing reaction in humans. In the metabolic transformation of the drugs in the body, two general types of enzymatic reactions that foreign compounds undergo are denoted as Phase I and Phase II metabolism. Phase I metabolism is the enzymatic transformation (e.g., oxidation, hydroxylation, dealkylation, and reduction) of functional groups on compounds. Phase II metabolism involves changing the structure of a drug or Phase I metabolite via conjugation with an endogenous substance (e.g., glucuronide, glutathione, and sulfate) where glucuronidation occurs (Kaushik et al., 2006).



Shipkova and Wieland (2005) reported that glucuronidation accounts for approximately 40–70% of xenobiotic elimination. All classes of drugs are substrates for this pathway. Biotransformed xenobiotics gain increased polarity and hence they can be easily excreted. This mechanism serves as an essential clearance of compounds, including drugs from all therapeutic classes, dietary chemicals, environmental pollutants, and endogenous compounds (e.g., bilirubin, bile acids, hydroxysteroids) (Shipkova and Wieland, 2005).

### **2.3.2.2. $\beta$ -Glucuronidase in Drug Release and Prodrug Applications in Cancer Therapy**

Enzyme-controlled drug release relies on the existence of enzyme producing microorganisms in the colon. The colonic microflora produce a variety of enzymes, including azoreductase, various glycosidases and, at a lower concentration, esterases and amidases, that can be exploited for colon-specific drug delivery (Leopold, 1999).

Improvements in cancer chemotherapy will depend on discovery of efficiently site-specific targeting new anticancer drugs. In this respect, different researches were based on non-toxic prodrugs which may be activated at the tumor site by enzyme-catalyzed hydrolysis (Huang and Oliff, 2001).

The term "prodrug" or "proagent" signify pharmacologically inactive chemical derivatives that could be used to alter the physicochemical properties of drugs, in a temporary manner, to increase their usefulness and/or to decrease associated toxicity. Therefore, in literature they were reported to be used in order to release the active drug from an inactive precursor (Papot et al., 2000; Hyo-Kyung and Amidon, 2000). In this particular case, selectivity can be managed by an enzymatic cleavage. A more convenient strategy is the use of an already present enzyme. By taking advantage of these enzymes, prodrugs, hydrogels, matrices and biodegradable coating materials have been developed for enzyme-controlled drug release.

The colonic microflora produce a variety of enzymes that are not present in the stomach or the small intestine and could therefore be used to deliver drugs to the colon after enzymatic cleavage of degradable formulation components or drug carrier bonds (Leopold, 1999). Besides, enzymatic conversion of chemotherapeutic prodrugs to active drugs in or in the vicinity of tumors provides a means for delivering active drugs more

selectively to tumor cells versus normal cells of a host (Wei et al., 2005).

In prodrug therapy, GUS plays an important role. The main reason of this important role is their source. The source of  $\beta$ -glucuronidase, which is a lysosomal enzyme, is the inflammatory cells that are commonly found in the necrotic areas of tumors (Shipkova and Wieland, 2005). As a lysosomal enzyme,  $\beta$ -glucuronidase accumulates in necrotic areas surrounding the tumor. Due to elevated glucuronidase activity in tumors as compared to normal tissue an increased specificity and reduced systemic toxicity might be expected. For this purpose glucuronide prodrugs of anti-cancer medicaments such as doxorubicine, epirubicine, 5-fluoruracil, and paclitaxel have been synthesized (Shipkova and Wieland, 2005; Huang and Oliff, 2001).  $\beta$ -glucuronidases are capable of selectively activating low-toxicity glucuronide prodrugs into highly cytotoxic agents at the tumour site, leading to a better anti-tumour effect and a reduction of systemic toxicity. In addition, these enzymes may play a beneficial role by releasing aglycone residues with protective effects, such as lignans, flavonoids, ceramide and glycyrrhetic acid. These molecules are active against tumours, platelet aggregation, viral infection, and allergic or inflammatory responses. Some of them have antioxidant effects (Beaud et al., 2005).

#### **2.4. Inhibition of $\beta$ -Glucuronidase**

Inhibition of GUS and its possible interactions with the selected inhibitors requires the knowledge of enzymes and their roles as catalyses. GUS enzyme is a protein which posses catalytic properties. As a catalyst, it lowers the energy of activation of a reaction ( $E_a$ ), thereby increasing the rate of that reaction without affecting the position of equilibrium. To understand the mechanism behind the inhibition, detailed information about the enzyme catalyzed reactions were given below.

In the presence of enzymes, forward and reverse reactions are affected to the same extent (Figure 2.2). Since the rate of a chemical reaction is proportional to the concentration of the transition-state complex ( $S^\ddagger$ ), lowering the activation energy effectively leads to an increase in the reaction rate. The equilibrium constant for that reaction is unaltered (Marangoni, 2003; Segel, 1993). The rate of reaction is increased by an enzyme mostly by specifically binding to, and thus stabilizing, the transition-state structure.

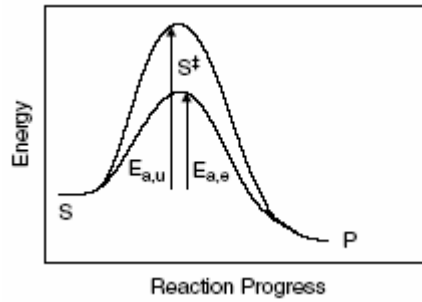


Figure 2.2. Changes in the internal energy of a system undergoing a chemical reaction from substrate S to product P.  $E_a$ : energy of activation for the forward reaction of enzyme-catalyzed (e) and uncatalyzed (u) reactions.  $S^{\ddagger}$ : the putative transition-state structure

General rate equation for the reactions involving enzymes was firstly derived in 1903 by Henri. Henri's equation accounted for the observation that the initial rate of the reaction was directly proportional to the concentration of enzyme but increased in a nonlinear manner with increasing substrate concentration up to a limiting maximum rate (Segel, 1993)

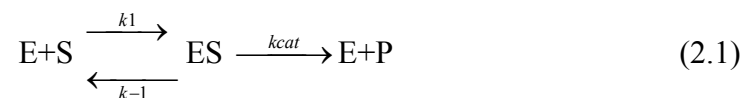
In enzyme catalyzed reactions, reaction velocity (i.e., the slope of the curve) decreases in time. The reasons of decreases are;

1. The enzyme becomes unstable during the course of the reaction.
2. As the substrate is consumed, the degree of saturation of the enzyme by substrate decreases.
3. The reverse reaction becomes more predominant as product accumulates.
4. In some cases the products of the reaction can act as inhibitors of the enzyme.

Also the combinations of those factors given above may act as factors of drop in velocity. Therefore according to the given factors above, progress curves for enzyme-catalyzed reactions do not fit standard models for homogeneous chemical reactions. A different approach is therefore required and enzymologists use initial velocities as a measure of reaction rates. For the initial stages of an enzyme catalyzed reaction, conversion of substrate to product is small and can thus be considered to remain constant and equal to initial substrate concentration ( $[S_t] \approx [S_0]$ ). Also very little product has accumulated ( $[P_t] \approx 0$ ) which means reverse reaction can be considered to be negligible. Therefore and any possible inhibitory action of the product on enzyme activity is also insignificant. And besides all, at initial stage of the reaction, the enzyme

can be considered to remain stable (Marangoni, 2003). So, to determine the initial velocities a tangent to the progress curve is drawn as close as possible to its origin of the progress curve and slope of this line. Using linear regression, the slope of this tangent line will give the initial velocity.

An enzyme catalyzed process can be shown as a two step process. In the first step single molecule of enzyme (E) combines reversibly with a single molecule of substrate (S) to form an enzyme-substrate complex (ES), which is transformed irreversibly to free enzyme and the product (P) of reaction kinetically. This is a monomolecular chemical reaction in which the enzyme plays a role of a recycling catalyst:



Two models; “Equilibrium Model” and “Steady State Model” were given below to give information of the kinetic behavior of enzyme as catalysts.

#### 2.4.1. Equilibrium Approach

The enzyme has a kinetic behavior consistent with a role of a recycling catalyst, which led Michaelis and Menten to propose the following kinetic mechanism of action after 10 years later based on the Henri’s work (Segel, 1993). Michaelis and Menten imposed two restrictions on the enzymatic reaction by dividing it into a fast reversible and a slow irreversible part. In the equilibrium model of Michaelis and Menten, the substrate-binding step is assumed to be fast with respect to the rate of breakdown of the ES complex.

$$k_{cat} \ll k_1 \quad (2.2)$$

In this kinetic model simple kinetics can be assumed such as there is no intermediate or product inhibition. Also it is assumed that there is no allostericity which means there is no binding a site other than the protein's active site. Also it was assumed that there is no cooperativity. Cooperativity is a special case of allostery which means

changing affinity for its ligand with respect to the amount of ligand already bound. Cooperative binding requires that the macromolecule have more than one binding site, since cooperativity results from the interactions between binding sites. Besides in kinetics, substrate is not “sticky” on enzyme and substrate dissociates from the collision complex faster than it reacts to give products. Therefore it is assumed that the enzyme–substrate complex is in a thermodynamic equilibrium with the free enzyme and the free substrate;

$$K_s = \frac{k_{-1}}{k_1} = \frac{[E] \cdot [S]}{[ES]} \quad (2.3)$$

where E, S, and ES are the concentrations of free enzyme, free substrate and enzyme–substrate complex, respectively (Leskovac, 2003). To write the velocity, first of all the total enzyme ( $E_T$ ) and the total substrate ( $S_T$ ) are written in terms of its free and complex bound forms:

$$[E_T] = [E + ES] \quad (\text{total mass balance}) \quad (2.4)$$

$$[S_T] = [S + E] \quad (\text{total mass balance}) \quad (2.5)$$

From Eq.5,

$$[ES] = \frac{([E_T] - [ES]) \cdot [S_T]}{K_s} \quad \text{or} \quad [ES] = \frac{[E_T][S_T]}{K_s + [S_T]} \quad (2.6)$$

The irreversible part of reaction is a slow monomolecular process with a rate constant  $k_{cat}$  thus the initial rate of ( $V_o$ ) the overall reaction is equal:

$$V_o = \frac{k_{cat}[E_T][S_T]}{K_s + [S_T]} \quad (2.7)$$

After substituting the constant value

$k_{cat}[E_T] = V_{max}$  Eq. 2.7; the kinetic law for reaction can be obtained:

$$V_o = \frac{V_{\max} [S]_T}{K_s + [S]_T} \quad (2.8)$$

Equation 2.8 is the fundamental equation of enzyme kinetics, generally known as the *Michaelis–Menten Equation*, the constant value  $K_s$  as the Michaelis constant and the constant value  $V_{\max}$  as the maximal velocity of reaction (Lescovac, 2003). Thus the Michaelis constant  $K_m$  corresponds to substrate concentration at  $1/2 V_{\max}$ .

### 2.4.2. Steady State Approach

In 1925, Briggs and Haldane derived a kinetic law examined for the general mechanism for reaction (Eq.4) allowing all rate constants to vary within wide limits. They assumed that the steady state is achieved shortly after the beginning of reaction and that the concentration of enzyme–substrate complex remained nearly constant over a prolonged period of time which means that the concentration of enzyme–substrate complex remains constant in time (i.e.,  $d[ES]/dt = 0$ ) (Segel 1993, Marangoni 2003).

When the differential equation is written in terms changes in ES concentration, with respect to time it should be equal to zero:

$$\frac{d[ES]}{dt} = k_1[E][S] - k_{-1}[ES] - k_2[ES] = 0 \quad (2.9)$$

steady state

When we rearrange and simplify this equation, it gives an expression for the Michaelis constant,  $K_m$ :

$$K_m = \frac{[E].[S]}{[ES]} = \frac{k_{-1} + k_2}{k_1} \quad (2.10)$$

It is important to note that this  $K_m$  value will be same as the dissociation constant; of the ES complex ( $K_s$ ) (mentioned in Equilibrium model) only for the case where  $k_{-1} \gg k_2$  where  $K_m = k_{-1}/k_1$ . As the enzyme catalyzed reactions are two step reactions and the rate-limiting step is the breakdown of the ES complex, velocity term

can be written as:

$$v = k_{cat}[ES] \quad (2.11)$$

where  $k_{cat}$  is the effective first-order rate constant for the breakdown of ES complex to free product and free enzyme. When we substitute the [ES] term with  $[E][S]/K_m$  according to the Eq.2.7 and normalize of the rate equation by total enzyme concentration,  $[E_T] = [E + ES]$  yields:

$$\frac{v}{[E_T]} = \frac{k_{cat}([E][S]/K_m)}{([E] + [E][S]/K_m)} \quad (2.12)$$

When the numerator and denominator were multiplied by  $K_m$ , both were divided by [E], and  $V_{max}$  was substituted for  $k_{cat}[E_T]$ ;

$$v = \frac{V_{max}[S]}{K_m + [S]} \quad (2.13)$$

This equation yields the familiar expression for the velocity of an enzyme catalyzed reaction where for the steady-state case,  $K_s$  has been replaced by  $K_m$ . In most cases, though, substrate binding occurs faster than the breakdown of the ES complex, and thus  $K_s \approx K_m$ . This makes the steady state model and equilibrium models equivalent (Marangoni, 2003).

### 2.4.3. Types of Inhibition

In some cases, existing of a substance reduces the velocity of an enzyme catalysed reaction. Any substance that reduces the velocity of an enzyme-catalysed reaction is called “an inhibitor”. In the presence of inhibitors those inhibition studies give us information about the specificity of an enzyme, physical and chemical nature of their active sites responsible for the catalyses and the kinetic mechanism of the reaction.

Development of specific inhibitors for GUS is of pharmacological importance because inhibitors may take a role in cancer prevention. Recent studies showed that also

some plants have potential to alter the GUS activity.

Xia et al.(2005) performed studies related to gastrointestinal using montmorillonite (MMT). They checked the  $\beta$ -glucuronidase activity which was potentially important in the generation of toxic and carcinogenic substances as many compounds. Results were shown in Table 2.2. This study was important because they related the release of potential harmful metabolites by glucuronidase activity to hindered growth performance or reduced feed utilization where inhibition of this enzyme is of great importance.

Table 2.2.  $\beta$ -glucuronidase activities in the small intestinal and colonic contents of pigs (Source: Xia et al., 2005)..

	Control	MMT <sup>C</sup>
<i>Small intestine</i>		
$\beta$ -Glucuronidase activity	128	102
<i>Proximal colon</i>		
$\beta$ -Glucuronidase activity	186	149

Table 2.3. *E.coli* GUS (EC 3.2.1.31) inhibitors and percentage inhibition (Source: Brenda Enzyme Database, 2008).

Inhibitor	Inhibition
CaCl <sub>2</sub>	2 mM, 14.8% inhibition
D-Glucuronate	IC50: 7.5 mM
glycyrrhizin	IC50: 0.08 mM
MgCl <sub>2</sub>	2 mM, 24.8% inhibition
NiCl <sub>2</sub>	2 mM, 52% inhibition
p-nitrophenol	IC50: 0.3 mM
saccharic acid 1,4-lactone	IC50: 0.09 mM
silybin	IC50: 1 mM
TLCK	IC50: 0.3 mM

Different inhibition studies were also took a part in enzyme databases performed by different scientist. A summary of reported inhibition studies were given in Table 2.3



in Brenda database. In this database  $\text{Cu}^{2+}$  and  $\text{Ag}^+$  were also reported as other  $\beta$ -glucuronidase inhibitors.

Gacche et al. (2005) used Coumarin Schiff-bases as  $\beta$ -glucuronidase inhibitors where coumarin is a flavonoid and is a natural constituent of many plants and essential oils. Experimental evidences suggest that compounds in some dietary spices (Rafter et al., 2004), *Pistacia terebinthus* leave extract with its main flavonoids as luteolin, luteolin-7-glucoside and apigenin-7-glucoside (Kavak et al., 2010), D-glucaro 1,4-lactone in vegetables (Lampe et al., 2002) had a inhibitory effect on  $\beta$ -glucuronidase activity.

Lee et al. (2003) used tectorigenin as  $\beta$ -glucuronidase inhibitor. Tectorigenin was isolated from the flowers of *pueria thunbergiana*. They reported that liver damage caused an increase of  $\beta$ -glucuronidase in blood, and liver cancer could be related to glucuronidase enzyme and could be inhibited by tectorigenin.

Fujisawa et al. (2001) found that possibility of cancer development due to the intake of a high fat diet may be inhibited by the presence of organic acids produced by intestinal bacteria such as lactic acid or butyric acid. In another study it was found that supplementation of fenugreek seeds in the diet inhibits colon carcinogenesis, by modulating the activities of  $\beta$ -glucuronidase (Devasena et al., 2003).

Besides, it was reported that activity of GUS enzyme extracted from the plant tissues was also influenced by interfering secondary plant compounds. Those secondary compounds were phenolic compounds, endogenous flavonols and proanthocyanidins and were reported as likely the inhibitor groups (Serres et al., 1997).

Loss of activity in the presence of an inhibitor might be either reversible or irreversible. Therefore inhibitors were divided into two groups as:

- I) irreversible inhibitors
- II) reversible inhibitors

For the reversible inhibitors, activity loss may be restored by the removal of the inhibitor. But if the inhibitor is irreversible, the loss of activity is time dependent and cannot be recovered during the timescale of interest. More important class for most enzyme-catalysed processes is the study of enzyme kinetics of reversible inhibitors. Reversible inhibitors usually form non-covalent complexes with enzymes and bind to enzyme by electrostatic bonds, hydrogen bonds and van der Waal's forces and tend to

form an equilibrium system with the enzyme. Non-covalent bonding results lower the amount of enzyme available for participation in the normal reaction sequence. All reversible inhibitors form complexes with the enzyme in a dynamic equilibrium system where complexes have different catalytic properties from those of the free enzyme. According to their effects on the kinetic behavior and on kinetic parameters of the enzymatic reaction, reversible inhibitors are divided into three major groups:

- (1) competitive
- (2) noncompetitive
- (3) uncompetitive.

Detailed information and equations for the inhibition models were given in Appendix D.

In literature, different kinetic experiments were performed in order to define the type of inhibitions for  $\beta$ -glucuronidase enzyme using different compounds. Thus inhibitor types such as competitive, noncompetitive, uncompetitive were determined.

Hashimoto et al. (2006) studied inhibition of GUS enzyme. Since the discharge of toxic compounds were enhanced by the inhibition of the activity of  $\beta$ -glucuronidase, they reported that a kind of aldaric acid, D-glucaric acid, and derivatives behaved as inhibitors on the hydrolysis of the  $\beta$ -Dglucuronide conjugates by  $\beta$ -glucuronidase in the small intestine. They specially synthesized two polymers. Glycopolymer (P(VB-1-GlcaH-co-AAm) inhibited the hydrolysis of model compound p-nitrophenyl  $\beta$ -D-glucuronide, uncompetitively where in contrast, second synthesized glycopolymer (P(VB-6-Glco-co-AAm) showed competitive inhibition

Kavak et al. (2010) studied inhibition of *E.coli* glucuronidase (GUS) by a plant extract of *Pistacia terebinthus*. 92.4% GUS enzyme inhibition was achieved with  $8.3 \mu\text{g ml}^{-1}$  crude extract concentration. Kinetic studies by nonlinear regression revealed that inhibition type caused by plant extract was mixed type (noncompetitive and competitive together).

Other reported inhibitors presented in enzyme database were given in Table 2.4 below:

Table 2.4. *E.coli* GUS (EC 3.2.1.31) inhibitors and inhibition types (Source: Brenda Enzyme Database, 2008).

<b>Inhibitor</b>	<b>Inhibition type</b>
D-Glucuronate	competitive
glycyrrhizin	competitive
p-nitrophenol	competitive
saccharic acid 1,4-lactone	competitive
silybin	non-competitive

## CHAPTER 3

### ZEOLITES

Natural zeolite; clinoptilolite demonstrated good stability in its transit through the gastrointestinal tract, and was harmless to the human body. Based on such properties, it was used as raw material for different pharmaceutical forms for the treatment of several pathologies in animals and humans and recently there were different researches for its use in cancer therapies. But reasons behind its positive health effects observed in cancer treatments are still unknown. It is possible that this mode of action is due to its property of pH regulating or encapsulation and/or adsorption of different ions and molecules in its open framework, and the subsequent delayed release. Based on those properties as well as being a natural compound it can act as an inhibitor in some undesired reactions which may be related to generation of carcinogenic/mutagenic or toxic compounds such as activity of microbial  $\beta$ -glucuronidase responsible for deglucuronidation of liver glucuronides.

Positive role of zeolite behind cancer studies was supposed to be a potent inhibitor of bacterial  $\beta$ -glucuronidase. Therefore in this Chapter, to better investigate these mechanisms, zeolite structure and its main properties were given in details.

#### 3.1. Structure

Zeolite is the crystalline, hydrated aluminosilicate of alkaline or alkaline earth metals, especially, sodium, potassium, calcium, magnesium, strontium and barium. Structurally, zeolite has aluminosilicate framework composed of infinitely extended three-dimensional network of  $\text{AlO}_4$  and  $\text{SiO}_4$  tetrahedra that form channels and interconnected voids, which are occupied by cations and water molecules. It may be expressed in two different formulas; oxide formula and idealized formula represented as follows. Oxide formula is  $\text{M}_{2/n}\text{O} \cdot \text{Al}_2\text{O}_3 \cdot x\text{SiO}_2 \cdot y\text{H}_2\text{O}$  and idealized formula is  $\text{M}_{x/n}[(\text{AlO}_2)_x(\text{SiO}_2)_y] \cdot w\text{H}_2\text{O}$ .

In the oxide formula, M represents the cation of valence n as in the idealized formula and x is generally equal to or greater than 2 since  $\text{AlO}_4$  tetrahedra can join only

to  $\text{SiO}_4$  tetrahedra. The structural formula of a zeolite may be best expressed by the idealized formula for the crystallographic unit cell where  $w$  is the number of water molecules and the ratio  $y/x$  varies between 1 and 5 depending on the structure. The sum  $(x + y)$  represents the total number of tetrahedra, while the portion with [ ] defines the framework composition (Breck, 1974).

As stated earlier all zeolites have framework three-dimensional structures constructed by joining  $\text{SiO}_4^{4-}$  or  $\text{AlO}_4^{5-}$  coordination polyhedra. By definition these tetrahedra are assembled together such that the oxygen at each tetrahedra corner is shared with that an identical tetrahedra (Si or Al). Since the positive charge of an silicon atom is higher than an aluminium atom the net charge on the each site of an aluminium tetrahedron is negative and it is balanced by one the exchangeable cations present in the framework.

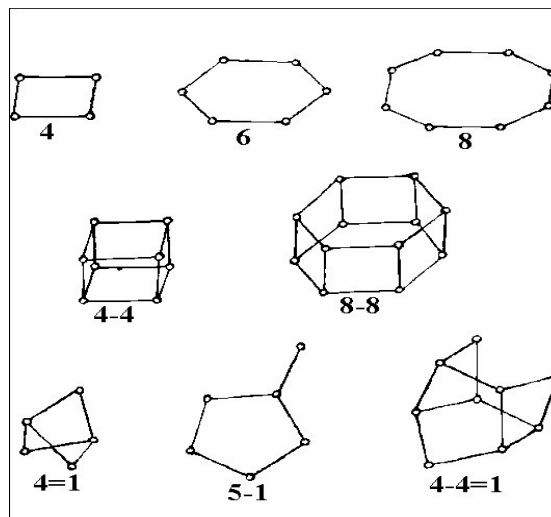


Figure 3.1. The secondary building units recognized in zeolite framework a) single four ring b) single six ring c) single eight ring d) double four ring e) double six ring f) complex 5-1 complex 4-4-1 (Source: Breck, 1974).

Therefore zeolite structure can be summarized as an aluminosilicate framework, with exchangeable cations and zeolitic water. Aluminosilicate framework is the most stable component and defines the structure. Exchangeable cations surrounded with water molecules and oxygen atoms fill the channels and cavities in the zeolite framework and balance framework charge, while water molecules distribute the framework charge hence, act as a stabilizer (Tsitsishvili et al., 1992).

At least 40 different types of naturally occurring zeolites have been found, beginning with the discovery of stilbite (STI) in 1756. The principal natural zeolites are

chabazite, gmelinite, mordenite, heulandite, clinoptilolite, levynite, faujasite (Yang, 2003). The main uses of natural zeolite are as drying agents, deodorants, adsorbents for air separation, ion exchangers for water purification especially for removing ammonium ion and heavy metal ions and for water softening, soil upgrading etc (Suzuki, 1990).

Some zeolitic crystal structures can be synthesized by hydrothermal reaction. The synthetics can, of course, be manufactured in a uniform, phase-pure state. Since the principal raw materials used to manufacture zeolite are silica and alumina, which are among the most abundant mineral components on earth, the potential to supply zeolites is virtually unlimited. More than 150 types of zeolite have been synthesized and are designated by a letter or group of letters (Type A, Type X, Type Y, Type ZSM, etc.) (Yang, 2003).

Zeolites have different applications. Due to their specific application, it is necessary to characterize the zeolite to see whether it confirms that desired properties or not. To determine the characteristics of zeolite there are different techniques. In Table 3.1 below, main characteristics to be identified and suitable methods are given.

Table 3.1. Characteristics and methods

Characteristic	Method
Structure, Adsorbed species	IR Spectroscopy
Textural properties	Physical Adsorption Measurement
Thermal stability, Dehydration behavior	Thermal Analysis (TGA, DTA, DSC)
Chemical composition	ICP-AES

### 3.2. Fundamental Properties

Physical and chemical properties of zeolites vary among zeolite types. The differences are primarily due to differences in crystal structure, and chemical composition. Properties such as particle density, theoretical CEC (Cation exchange capacity), cation selectivity, void volume, molecular pore size, and crystal shape vary depending on the zeolite type under consideration.

As mentioned before zeolites are crystalline porous solids with pores and channel systems in the molecular size range of 0.3 to 3 nm. They are tectosilicates

consisting of corner-sharing  $\text{AlO}_4$  and  $\text{SiO}_4$  tetrahedra. The  $\text{Si}/\text{Al}_2$  ratio of zeolites can be varied during synthesis or postsynthetically. The  $\text{Si}/\text{Al}_2$  ratio is also used to denote the hydrophobicity of zeolites, with higher ratios indicating a higher degree of hydrophobicity and lower ion-exchange capacity. The morphology of the structure can also be varied. These physicochemical characteristics are thought to be the basis for their immense importance in catalysis reactions, adsorption, separation, and ion exchange (Chiku et al., 2003).

### ***Catalysis***

Zeolites have the ability to act as catalysts for chemical reactions which take place within the internal cavities. The cations located at different sites would be expected to affect catalytic properties in different ways. In some catalytic applications, it is desirable to incorporate metal cations into the sieve, to modify the number and nature of the acid sites, and to affect the diffusion of reactants and products. Changing the framework aluminum concentration provides an additional way of controlling the number, strength, and distribution of the acid sites, and catalytic activity (Kaduk and Faber, 1995).

### ***Ion Exchange***

Ion exchange is an important mechanism for surface interaction in zeolite-aqueous solution system. Rigid three dimensional crystal structure of zeolite accommodate micropores interconnected within the lattice, capable of hosting extra-framework, i.e., exchangeable cations ( $\text{Na}^+$ ,  $\text{K}^+$ ,  $\text{Ca}^{2+}$ ,  $\text{Mg}^{2+}$ ) in association with mobile  $\text{H}_2\text{O}$  molecules (Logar et al., 2006). This exchange of ions is a chemical reaction between two phases and necessarily stoichiometric and each ion removed from the solution is replaced by an equivalent amount of ion in the exchanger of the same sign by conserving electro neutrality (Tsitsishvili et al., 1992). Thus exchangeable cations are the cations that are balancing the framework charge (Inglezakis, 2005) and the part of the exchangeable cations is dependent on the experimental conditions such as temperature, the cationic species, degree of hydration etc. (Yang, 2003).

### ***Adsorption and Separation***

The most fundamental consideration regarding the adsorption of chemical species by zeolites is molecular sieving. Species with a kinetic diameter which makes

them too large to pass through a zeolite pore are effectively "sieved." This "sieve" effect can be utilized to produce sharp separations of molecules by size and shape. They also adsorb molecules with permanent dipole moment with selectivity not found in other adsorbents (Breck, 1974)

The ability preferentially to adsorb certain molecules, while excluding others, has opened up a wide range of molecular sieving applications. Size and shape of pores are important parameters for controlling access of species into the zeolite. Besides particular affinity of species for an internal zeolite cavity depends on electronic considerations. The strong electrostatic field within a zeolite cavity results in very strong interaction with polar molecules such as water. Non-polar molecules are also strongly adsorbed due to the polarizing power of these electric fields. Thus, excellent separations can be achieved by zeolites even when no steric hindrance occurs.

Adsorption based on molecular sieving, electrostatic fields, and polarizability are always reversible in theory and usually reversible in practice. This allows the zeolite to be reused many times, cycling between adsorption and desorption. This accounts for the considerable economic value of zeolite in adsorptive applications.

### **3.3. Zeolites for Protein Adsorption**

Proteins are complex structures and they are amphoteric molecules i.e. they contain both acidic and basic moieties. Besides they are amphiphilic molecules as they both contain hydrophilic and hydrophobic sites. This chemical character results proteins to be adsorbed on a wide range of different surfaces. Zeolites with their large specific surface area, ion exchange/adsorption property and with their structural stability can be used as adsorbants or carrier matrices for the proteins.

During adsorption, protein changes from their native conformations to forms that depend largely on hydrophobic interactions between the surface and the amino acid side chains in the protein. Hydrophobic side chains will be close to the hydrophobic surface, if there exist, and hydrophilic residues will favor the aqueous phase. But this interaction may be restricted by the distribution of the amino acid residues in the protein. Dalglish (1997) showed that the conformation that is adopted also depends on the surface area that the protein is required to cover and the interactions depend on the physical state of the adsorbent and protein surface and the intimate solution environment. Therefore



protein adsorption is affected by numerous factors including protein size, charge, shape, hydrophobicity, pH, surface charge, surface topology, coadsorption of low-molecular-weight ions, intermolecular forces between adsorbed molecules, strength of functional groups bonds, composition of the protein solution, chemistry of the solid surface and surface energetics (Rovira-Bru et al. 2001).

Hydrophobicity of the protein play a key role for the protein structure and similarly play a key role for protein adsorption according to the surfaces hydrophobic interactions. Exposure of the hydrophobic site of protein to the water is energetically unfavorable and enthalpy of such interactions is generally small and negative. The free energy will increase due to the negative entropic contribution (Roach et al., 2005). If a hydrophobic protein residue adsorbs onto the hydrophobic surface a free energy of the system will decrease. During adsorption dehydration occurs and the dehydration of a hydrophobic domain of protein and a hydrophobic surface releases bound water. Therefore during this adsorption process binding is energetically favorable and entropy change is large and positive.

Solutions containing ions cause protein surfaces to gain charges. In such cases the electrostatic interaction may be more dominant in protein adsorption kinetics. Because of the nature of the electrostatic interactions, protein may change conformation and its orientation when it approaches an oppositely charged adsorbent. Although a charged protein is expected to prefer adsorption onto an oppositely charged surface, the osmotic pressure of counter ions, charged group desolvation and burying of the charges into a low dielectric medium may, in fact, counteract protein adsorption. Therefore electrostatic interactions are not only the main reasons of adsorption of proteins to the charged surfaces. If the protein and surfaces are like charges, an energy barrier to adsorption may occur. In some cases overall charge of protein may be zero where protein is at its isoelectric point. In this case it is also possible to talk about the electrostatic interaction between protein and surface. Electrostatic interaction may still exist due to the non uniformity of the charge distribution on the protein surface. Therefore adsorption of proteins is very complicated phenomenon and it is hard to analyze the possible interactions between surface and adsorbed molecule.

In recent years, there has been much interest in the applications of zeolite in immobilization of proteins or enzymes (Serralha et al., 1998) since the inorganic zeolite has good biocompatibility, high mechanical, thermal, and chemical stability, large surface areas, and unique hydrophilic and electrostatic property (Xie et al., 2007). Klint

and Eriksson (1997) showed that zeolites are able to adsorb proteins on surfaces although their pore size is smaller to allow proteins to pass or enter. In addition, the external surface may also be exploited since it is known that the presence of surfactants on solid surfaces can induce or enhance the co-adsorption of different organic molecules. This may lead to the use of zeolites as drug delivery systems (Rivera et al., 2005). Also zeolites for adsorption of proteins are used in biotechnology to achieve highly efficient and economical separation processes. Ismail et al. (2005) performed the adsorption of two proteins, cytochrome c and  $\alpha$ -chymotrypsin onto H-Beta zeolite.

Protein surface is heterogenous in its nature therefore interactions between protein and zeolite surface are very complex in nature. During protein adsorption conformational changes or change in lateral interactions may run concurrently and it may take longer times to reach the equilibrium. Therefore type of possible interactions (and their strength) between zeolites and proteins are very complicated. There can be acid–base reactions between the amino groups of the protein and the surface hydroxyl groups of the zeolites (silanol groups) or van der Waals and/or electrostatic interactions. Zeolite properties can influence the protein adsorption. Those properties are the zeolite structure, the chemical composition of the crystalline framework, the crystal morphology and size, the Brønsted acidity, the number and the distribution of defect and hydroxyl groups. These groups can be seen as a silanol groups whose acidity can be enhanced by the interaction with a strong Lewis center ( $Al^{3+}$ ) (Tavolaro et al., 2007).

Understanding complex adsorption mechanism requires detailed theoretical studies about adsorption isotherms, adsorption kinetics, conformation of adsorbed bioactive component. This experimental and theoretical information can answer questions about the mechanism of protein adsorption onto surfaces. Therefore following section is about the principles of the adsorption.

### **3.3.1. Adsorption Phenomena**

Adsorption is a physical and/or chemical process in which compounds are accumulated at the interface of solid – liquid or solid-gas mixtures. Solid material on which the solutes of interest adhere is called “adsorbent”. The material adsorbed on to the solid is called as “adsorbate. This accumulation provides separation of the components from the fluid phase to solid phase. In contrast, desorption is the reverse

process of adsorption in which the amount adsorbed decreases and removed from the solid phase.

Adsorbent must possess certain engineering properties depending upon the applications such as large surface area, porous structure, rigidity, mechanical stability etc. Most common adsorbents are activated carbon, silica, zeolites and polymers. Also there are composite adsorbents carrying advantages of its components in combination.

Affinity of the solute towards solid plays a critical role in the adsorption of a solute from a solution onto a solid phase. Main driving forces for the change in the affinity may be due to the electrostatic, chemical or van der Waals attractions. According to these interaction mechanisms adsorption process can be classified into the two types. The first type is known as physical adsorption (physisorption) and the second one is called as chemical adsorption (chemisorption).

*i) Physical Adsorption:* Adsorption in which the forces involved are intermolecular forces adsorption is generally regarded as physical adsorption. In physical adsorption adsorbed molecule is not affixed to a specific site and free to undergo translational movement within the interface. Therefore in physical adsorption bonds are weaker and process is reversible. The forces involved in physical adsorption are van der Waals forces and electrostatic interactions and dipole-dipole interactions between adsorbate molecule and the atoms which compose the adsorbent surface.

The electrostatic forces are due to the ionic atoms and polar groups on the surface. Therefore physical interactions during adsorption, based on electrostatic forces, include dipole-dipole interactions, dispersion interactions and hydrogen bonding. Adsorption due to the electrostatic forces (Coulombic forces), result from the charged sites on the surface. If there exist a separation of positive and negative charges within molecule, dipole moment occurs and attraction between those two dipole molecules is dipole-dipole interaction. In hydrogen bonding, hydrogen atom in a molecule has a partial positive charge and attracts another negatively charged molecule therefore H-bonding is a special case of dipole-dipole interaction. When two molecules with no permanent dipoles approach each other, a weak polarization is induced because of quantum mechanical interactions between their distributions of charge. This weak attraction is known as the dispersion interaction or the London-van der Waals force (Montgomery, 1985; Yang, 1999).

*ii) Chemical Adsorption:* Chemical adsorption is the result of a chemical bond, involving substantial rearrangement of electron density, is formed between the

adsorbate and adsorbent. Attraction between them is more powerful and this strength of the chemical bond may vary considerably. In chemical adsorption covalent or electrostatic chemical bonds with shorter bond length and higher bond energy occur between atoms. These bonds are specific to particular sites or functional groups on the surface of the adsorbent. In Table 3.2, distinguishing characteristics of chemical and physical adsorption are given.

Table 3.2. Comparison of the characteristics of chemical and physical adsorption.

<b>Properties</b>	<b>Chemical adsorption</b>	<b>Physical adsorption</b>
Binding force	Due to chemical forces or bonding	Due to physical force of attraction
Nature of adsorption	Often dissociative, may be irreversible, highly specific	Non-dissociative, reversible, non specific
Temperature range	Adsorption can take place even at higher temperatures	Adsorption is appreciable at lower temperatures
Molecular uptake	Usually monolayer	Monolayer or multilayer
Kinetics of adsorption	Variable, often an activated process	Rapid since it is a non-activated process

### 3.3.2. Adsorption Kinetics

Adsorption kinetics gives information about the performance of an adsorption process and its mechanisms. Scale of the adsorption system can also be established using kinetic information.

There are several mathematical models established to describe the kinetic process of adsorption. Those models can be classified as adsorption reaction models and adsorption diffusion models. Adsorption reaction models originating from chemical reaction kinetics are based on the whole process of adsorption. However, adsorption diffusion models are established on the basis of four consecutive steps (Qiu et al., 2009):

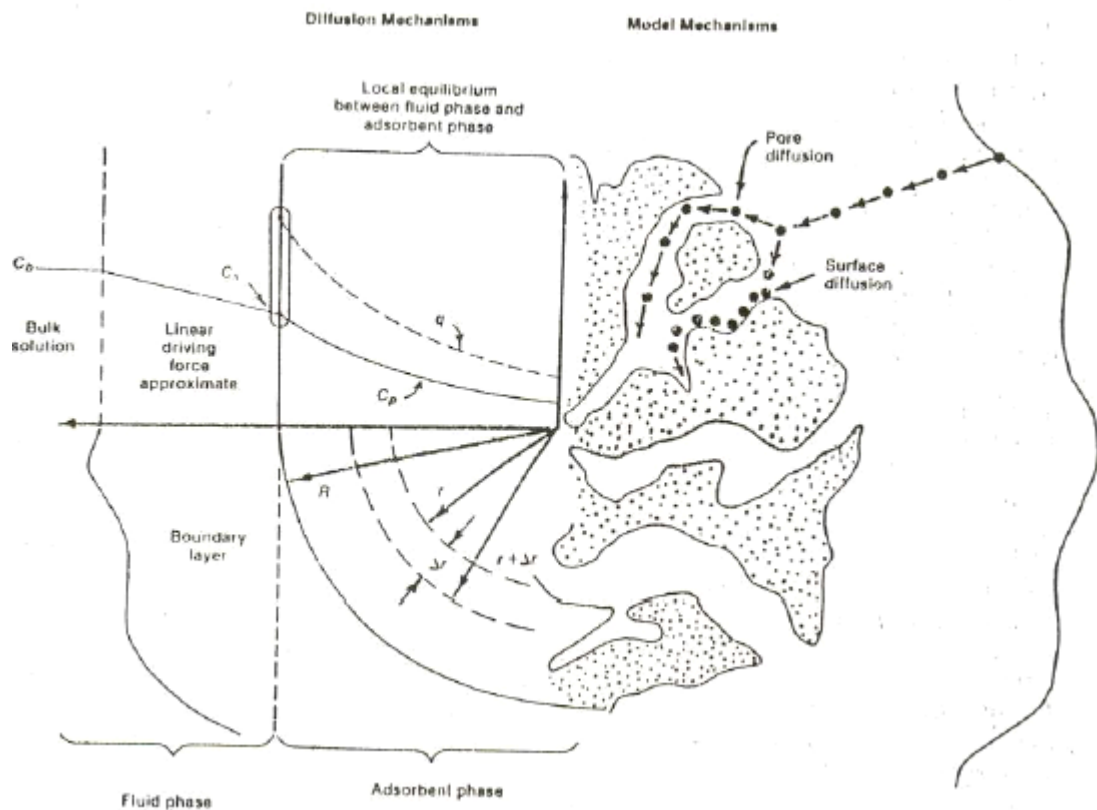


Figure 3.2. Concentration gradients in adsorption process. (Source: Abdelrasoul, 2006).

1. transport in the bulk of the solution;
2. diffusion across the liquid film surrounding the sorbent particles;
3. particle diffusion in the liquid contained in the pores and in the sorbate along the pore walls;
4. sorption and desorption within the particle and on the external surface.

The rates of those steps are depended on physical properties of the adsorbent, adsorbate and as well as the nature of the fluid surrounding the particle. If one of these steps is much slower than the others, it is the rate controlling step for that overall sorption process. Therefore, changing the process conditions can also change the rate-controlling steps. Such as; when agitation rate is increased, the influence of film mass transfer control in the system will also reduce. Additionally, initial rate controlling process may change throughout the sorption process (Ho et al., 2000) and more than one step might control the adsorption. This situation was explained well by an example reported by Gerente et al. (2007). It was reported that during the initial stage of metal

ion adsorption, film diffusion may be rate-controlling because large external site bearing surface areas are available. By the increase in the contact time, the external surface layers become saturated and the rate-controlling step moves to either reaction at a site (reaction kinetic control) or to internal diffusion, either by pore, surface, or pore with surface. Therefore, to identify the rate controlling mechanism, it is necessary to carry out different kinetic experiments involving important parameters in adsorption kinetics such as initial concentration, sorbent particle size, solution temperature, solution pH and agitation.

The physicochemical nature of the adsorbent can have profound effects on both rate and capacity for adsorption. Surface polarity corresponds to affinity with polar substances such as water. Therefore polar adsorbents are thus called "hydrophilic" and aluminosilicates such as zeolites, porous alumina, silica gel or silica-alumina are examples of hydrophilic adsorbents. On the other hand, nonpolar adsorbents are generally "hydrophobic" and carbonaceous adsorbents, polymer adsorbents and silicalite nonpolar adsorbents of this type (Suzuki, 1990). In addition to adsorbent, nature of the adsorbate is important in adsorption. Proteins are consisted of different amino acids and they gain polar, nonpolar, hydrophilic or hydrophobic property due to their amino acid content. Their behaviour at solid/liquid interface in adsorption is highly influenced with their structural property because it influences the orientation of protein and interaction of protein with the adsorbent at solid/liquid interfaces during adsorption.

Decreasing the particle size leads to increase in the surface area. Thus provide more active sites available for the adsorption. Kinetic experiments with varying particle size give also information to analyze the rate controlling mechanism in adsorption. If adsorption rate is controlled by macropore diffusion, there exists a concentration gradient within the particle. The adsorption rate is dependent to the particle size. But in case of micropore diffusion controlling system, the assumption of constant concentration gradient through the particle is applicable. Thus the rate of adsorption is not dependent to the particle size of adsorbent (Ülkü and Mobedi, 1991).

The pH of the solution is an important variable governing the adsorption process. It affects the charges of the both adsorbate and adsorbent. The pH of the solution determines the charge of the proteins that are comprised of both charged amino and carboxyl groups and the interacting surfaces consequently is responsible for the attractive and repulsive effects (Tavolaro et al., 2007). In case of adsorption at ionic surfaces, opposite charges are the main factors for the protein molecule and adsorbate.

Depending on the nature of the electrostatic interaction or ionic interaction rate of reaction is changed such as for stronger interactions (ie.ionic bonding) rate of reaction is increased.

Temperature changes can affect the diffusion rates of the adsorbate molecules and also equilibrium capacity of the adsorbent. For the chemically controlled adsorption, rate of reaction is more dependent on temperature. Increase in the temperature will increase the rate of diffusion of the adsorbate across the external boundary layer and also rate of diffusion in the internal pores of the adsorbent particle will increase (Guo et al., 2009). In physical adsorption bond forces are weaker and energy requirements are small. Therefore it is more independent of the temperature compared to chemical adsorption. Since there were stronger bond forces in chemically controlled adsorption, activation energy and enthalpy changes were also high which helps the decision of the adsorption either physical or chemical in nature.

Adsorbent amount in solution also affects the adsorption. When the adsorbent concentration is increased, number of particles will be increased. Therefore, there will be more surface area and active sites available for the adsorption.

Changes in the shaking rate affect distribution of the adsorbate in the solution and also it affects the thickness of the external film. External mass transfer resistance is proportional to the film thickness of the liquid layer. Therefore higher shaking rate decrease the film thickness and results a decrease in external mass transfer resistance. Additionally as the agitation speed is changed, the rate controlling process may also change from film to reaction or diffusion (Ho et al., 2000).

All these parameters are important in the determination of the dominant step controlling the adsorption mechanism. Additionally, data can be analysed by different diffusion and reaction models. Correlation coefficients between experimental and theoretical data will provide the best fit model. Some of these diffusion and reaction models were given below.

### **3.3.2.1. External Mass Transfer**

When an adsorbent material is in contact with a solution containing adsorbate, adsorbate molecules first migrate from the bulk solution to the surface of the liquid film.

This surface exerts a diffusion barrier. The involvement of a significant quantum of diffusion barrier indicates the dominant role taken up in the adsorption process (Karthikeyan et al., 2010). Therefore, diffusion takes place through the laminar film surrounding the external surface of the particle and reaction takes place on the external surface.

A mathematical approach for external mass transfer is based on the linear adsorption isotherm was developed by Furusawa and Smith (Choy et al., 2004; Ho et al., 2000) where they studied adsorption of benzene on activated carbon in a well agitated tank. In well agitated media, the sorbate concentration with respect to time ( $C_t$ ) is related to the fluid-particle mass-transfer coefficient:

$$\frac{\partial C_t}{\partial t} = -k_f S_s (C_t - C_s) \quad (3.1)$$

where  $k_f$  is the external mass transfer coefficient,  $S_s$  is the surface area of the particles. Assuming smooth spherical particles, the surface area for mass transfer to the particles is:

$$S_s = \frac{6m_s}{d_p \rho_s (1 - \varepsilon_p)} \quad (3.2)$$

where  $d_p$  is mean particle diameter,  $\varepsilon_p$  is particle voidage,  $\rho_s$  is particle density and  $m_s$  is the concentration where  $W$  is the mass and  $V$  is the volume of the adsorbent in the liquid phase:

$$m_s = \frac{W}{V} \quad (3.3)$$

Based on the Fick's second law and assuming constant effective intraparticle diffusivity ( $D_{eff}$ ), the differential mass balance within the particles can be written as follows:

$$D_{eff} \left\{ \frac{\partial^2 C_r}{\partial r^2} + \frac{2}{r} \frac{\partial C_r}{\partial r} \right\} - \rho_p \frac{\partial q_r}{\partial t} = \varepsilon_p \frac{\partial C_r}{\partial t} \quad (3.4)$$

For a single resistance model, intraparticle diffusion is neglected,  $C_r$  (concentration at



any distance of  $r$ ) is equal to  $C_s$  (concentration at surface) for any  $r$ , and  $q$  is uniform throughout the particle and equilibrium is assumed for adsorption at an interior site. For a linear adsorption isotherm, where  $1 \geq a_L C_r$  and for constant equilibrium value ( $K_L$ ), boundary conditions are:

$$\frac{\partial C}{\partial r} = 0 \text{ at } r=0, \quad (3.5)$$

$$C_r=0 \text{ at } t=0 \text{ for } 0 \leq r \leq R \quad (3.6)$$

$$\frac{\partial q}{\partial t} = K_L \frac{\partial C_s}{\partial t} \text{ at } qt=0 \quad (3.7)$$

when  $t=0$ ;  $C_t=C_0$  and  $t=t_0$ , following equation is obtained:

$$\frac{C_t}{C_o} = \frac{1}{1 + m_s K_L} + \frac{m_s K_L}{1 + m_s K_L} \exp \left[ - \left( \frac{1 + m_s K_L}{m_s K_L} \right) k_f S_s t \right] \quad (3.8)$$

by rearrangement of eqn 3.8, following linearized form is obtained:

$$\ln \left( \frac{C_t}{C_o} - \frac{1}{1 + m_s K_L} \right) = \ln \left( \frac{m_s K_L}{1 + m_s K_L} \right) + \left[ - \left( \frac{1 + m_s K_L}{m_s K_L} \right) k_f S_s t \right] \quad (3.9)$$

As  $t \rightarrow 0$ , surface mass transfer will be dominant and assumptions of negligible intraparticle diffusion and a linear isotherm ( $q_e = K_L C_e$ ) are valid. A plot of  $\ln(C_t/C_0 - 1/(1 + m_s K_L))$  versus  $t$  will give a straight line as  $t \rightarrow 0$  of intercept  $m_s K_L / (1 + m_s K_L)$  and slope  $-((1 + m_s K_L) / m_s K_L) k_f S_s$  at  $t = 0$ . By this plot, surface mass-transfer coefficient  $k_f$  can be obtained.

Following mathematical expression is based on linear, isothermal systems. Different than the previous equation where equilibrium is assumed for adsorption at an interior site, this equation assumes that adsorbed phase concentrations through the particle is at equilibrium with the fluid phase concentration at the surface. There is no gradient of concentration through the particle and equilibrium relationship ( $q^* = K C^*$ ) is a linear. The standard linear rate expression is used to express the transport rate through the external laminar film can be expressed as follows:

$$\frac{d\bar{q}}{dt} = k_f S_s (C - C^*) \quad (3.10)$$

In this equation,  $k_f$  is the film mass transfer coefficient,  $S_s$  is the specific surface area for the spherical adsorbent particle.  $S_s = 3/R_p$  where  $R_p$  is the particle radius.

The value of  $q$  averaged over a particle is presented as  $\bar{q}$  obtained by the following equation:

$$\bar{q} = \frac{3}{R^3} \int_0^R q r^2 dr \quad (3.11)$$

For the boundary conditions:

$$t < 0, C = q = 0 \quad (3.12)$$

$$t > 0, C = C_\infty = q_\infty / K \quad (3.13)$$

Equation 3.11 can be integrated to yield:

$$\frac{\bar{q}}{q_\infty} = 1 - \exp\left[-\frac{3k_f t}{KR_p}\right] \quad (3.14)$$

Rearranging the equation gives;

$$\ln\left(1 - \frac{\bar{q}}{q_\infty}\right) = -R' t \quad (3.15)$$

where

$$R' = \frac{3k_f}{R_p K} \quad (3.16)$$

When the film diffusion is the rate limiting step, the plot of  $\ln(1 - q_t/q_e)$  versus  $t$  should be a straight line and the slope is  $-R'$  thus  $k_f$  can be determined.

Another expression for external mass transfer is proposed by Spahn and Schlunder in 1975 (Quek and Balasubramanian, 2010) where  $t$  is the time of reaction, and  $C_t$  and  $C_0$  are the initial concentration and concentration at time  $t$  respectively, and

$k_f$  is the external diffusion coefficient assuming isothermal linear system, nonporous spherical adsorbent where no concentration gradient exist through the particle.

$$\ln\left(\frac{C_t}{C_o}\right) = -k_f t \quad (3.17)$$

Initial portion of the kinetic data is widely used for external mass transfer models. When  $C_t \rightarrow C_0$ , using the differential mass balance of the solute within the particle, equation 3.1 can be respresented as follows. In this expression, it is assumed that external mass transfer occured in the “proposed” initial time interval with a linear relationship between slope of tangent or slope of the polymominal fitted curve with  $k_f$ . This simple mathematical approach can be used to determine the external mass transfer coefficient:

$$\left[ \frac{d(C_t / C_0)}{d_t} \right]_{t=0} = -k_f S_s \quad (3.18)$$

Hence, at  $t=0$ , a plot of  $C_t/C_0$  will yield a slope of  $-k_f.S_s$  form which  $k_f$  can be determined (Walker et al., 2003).

### 3.3.2.2. Macropore Diffusion

If the porous adsorbent has macropores, those sites will be accessable for the adsorptive which will first diffuse through the macropores of the adsorbent after it is transferred trough the external surface of the particle. In macropore diffusion; molecular diffusion, Knudsen flow, surface diffusion and Poiseuille flow are important mechanisms for the solute transport and their importance are depended on the system conditions (Ülkü, 1991). However, molecular diffusion is the most dominant mechanism in liquid sorption processes especially in the large pores at higher pressures which results from the collision between diffusing molecules. Effective pore diffusivity for the molecular diffusion can be expressed as follows:

$$\varepsilon_p D_p = \frac{\varepsilon_p D_m}{\tau} \quad (3.19)$$

where  $\varepsilon_p$  is porosity of the particle,  $D_m$  is the molecular diffusivity, and  $\tau$  is the tortuosity factor.

However in small pores and at low pressure, collision of diffusing molecules with the pore walls will be more dominant compared to the collision within each other which is expressed as Knudsen diffusion. Knudsen diffusivity for a straight cylindrical pore is:

$$D_K = 9700 \bar{r} \left( \frac{T}{M} \right)^{0.5} \quad (3.20)$$

where  $D_K$  is the Knudsen diffusivity (cm<sup>2</sup>/s),  $\bar{r}$  is the average pore diameter, T is the Temperature and M is the molecular weight.

If molecular diffusion and Knudsen diffusion are both effective a system, overall diffusivity can be estimated by the following formula:

$$\frac{1}{\varepsilon_p D_p} = \frac{1}{\varepsilon_p} \left( \frac{1}{D_K} + \frac{1}{D_m} \right) \quad (3.21)$$

For the pore diffusivity of independent of concentration, macropore diffusion for a spherical geometry can be expressed by the following equation:

$$(1 - \varepsilon_p) \frac{\partial q}{\partial t} + \varepsilon_p \frac{\partial C}{\partial t} = \varepsilon_p D_p \left( \frac{\partial^2 C}{\partial R^2} + \frac{2}{R} \frac{\partial C}{\partial R} \right) \quad (3.22)$$

With the validity of the linear equilibrium ( $q^* = KC^*$ ), equation can be written as;

$$\frac{\partial C}{\partial t} = \frac{\varepsilon_p D_p}{\varepsilon_p + (1 - \varepsilon_p)K} \left( \frac{\partial^2 C}{\partial R^2} + \frac{2}{R} \frac{\partial C}{\partial R} \right) \quad (3.23)$$

In equation 3.23, the term  $\frac{\varepsilon_p D_p}{\varepsilon_p + (1 - \varepsilon_p)K}$  is the effective macropore diffusivity.

For the following boundary conditions;

Along the radial direction, at  $t=0$ ,

$$C(R,0) = C_o \quad (3.24)$$

$$q(R,0) = q_o = KC_o \quad (3.25)$$

At the surface of the particle for  $R = R_p$  and  $t=t$ ;

$$C(R_p, t) = C_o \quad (3.26)$$

$$q(R_p, t) = q_o \quad (3.27)$$

$$\left. \frac{\partial C}{\partial R} \right|_{R=0} = \left. \frac{\partial q}{\partial R} \right|_{R=0} = 0 \quad (3.28)$$

Using boundary conditions, equation 3.22 can be expressed in the following form:

$$\frac{m_t}{m_\infty} = 1 - \frac{6}{\Pi^2} \sum_{n=1}^{n=\infty} \frac{1}{n^2} \exp\left(-\frac{n^2 \Pi^2 \varepsilon_p D_p t}{R_p^2 (\varepsilon_p + (1 - \varepsilon_p)K)}\right) \quad (3.29)$$

where

$\frac{\varepsilon_p D_p}{R_p^2 [\varepsilon_p + (1 - \varepsilon_p)K]}$  is the diffusional time constant for macropore diffusion.

### 3.3.2.3. Micropore Diffusion

During adsorption, solutes may diffuse through interior sites of the microparticle after they pass through the macropores. When the system is isothermal and diffusion within the microparticle is the rate controlling step, the diffusion equation for a spherical particle can be written as follows

$$\frac{\partial q}{\partial t} = \frac{1}{r^2} \frac{\partial}{\partial r} \left( r^2 D_c \frac{\partial q}{\partial r} \right) \quad (3.30)$$

If there is small change in adsorbed phase concentration during the uptake, diffusivity may be assumed as constant:

$$\frac{\partial q}{\partial t} = D_c \left( \frac{\partial^2 q}{\partial r^2} + \frac{2}{r} \frac{\partial q}{\partial r} \right) \quad (3.31)$$

For the following boundary conditions:

$$t < 0 \quad C = C_0 \quad q = q_0 \quad (3.32)$$

$$t \geq 0 \quad C = C_\infty \quad q(r_c, t) = q_\infty \quad (3.33)$$

$$t \rightarrow \infty \quad C = C_\infty \quad q(r, t) = q_\infty \quad (3.34)$$

$$\left. \frac{\partial q}{\partial t} \right|_{r=0} = 0 \quad \text{for all } t. \quad (3.35)$$

If the spherical particle is initially free of solute, and the concentration of solute at the surface remains constant, external film resistance can be neglected according to the constant surface concentration. With constant diffusivity and using the following boundary conditions (concentration change is small), Crank proposed the following equation:

$$\frac{q_t}{q_\infty} = 1 - \frac{6}{\pi^2} \sum_{n=1}^{\infty} \frac{1}{n_i^2} \exp\left( \frac{-n_i^2 \pi^2 D_c t}{r_c^2} \right) \quad (3.36)$$

which can also be expressed as:

$$\frac{q_t}{q_\infty} = 6 \left( \frac{D_c t}{r_c^2} \right)^{1/2} \left[ \frac{1}{\sqrt{\pi}} + 2 \sum_{n=1}^{\infty} i \operatorname{erfc} \left( \frac{nr_c}{\sqrt{D_c t}} \right) \right] - 3 \frac{D_c t}{r_c^2} \quad (3.37)$$

In the earlier stages of the adsorption process  $\left[ \frac{q_t}{q_\infty} < 0.3 \right]$ , when  $t$  is relatively small, this equation can be simplified as:

$$q_t = \frac{6q_\infty D_c^{0.5}}{\pi^{0.5} r} t^{0.5} \quad (3.38)$$

This equation can be represented by the following expression used as Weber Morris equation representing the plot of uptake versus the square root of time should be linear:

$$q_t = k_d t^{0.5} \quad (3.39)$$

where  $k_d$  is the intraparticle rate constant;

$$k_d = \frac{6D_c^{1/2} q_\infty}{\sqrt{\pi} r_p} \quad (3.40)$$

and for long time,

$$\left[ \frac{q_t}{q_\infty} > 0.7 \right] \quad (3.41)$$

thus, final equation is,

$$1 - \frac{q_t}{q_\infty} \cong \frac{6}{\pi^2} \exp\left(-\frac{\pi^2 D_c t}{r_p^2}\right) \quad (3.42)$$

Equation 3.39 which is expressed as Weber Morris equation is widely used equation for the intraparticle diffusion models. This equation is very practical and also helpful to give idea about the rate controlling mechanisms in adsorption process. When the  $t^{0.5}$  vs  $q_t$  graph is plotted, it gives a straight line passing through the origin if the intraparticle diffusion is the rate controlling step. However, if it does not pass through the origin, intraparticle diffusion is not the sole controlling mechanism.

Another mathematical model to check whether sorption proceeds via film diffusion or intraparticle diffusion mechanism was developed by Boyd et al. (1947). Model assumes that system is linear and isothermal, with a spherical adsorbent initially

free of solute. The concentration of solute at the surface remains constant thus external film resistance can be neglected according to the constant surface concentration. For sufficiently small  $t$ ; equation is expressed as follows:

$$F = 1 - \frac{6}{\pi^2} \exp(-B_b t) \quad (3.43)$$

where  $B_b$  is a constant and  $F$  is the fractional attainment of equilibrium at time  $t$  given by:

$$F = \frac{q_t}{q_e} \quad (3.44)$$

Using equations 3.43 and 44, the kinetic expression becomes:

$$B_b t = -0.4977 - \ln\left(1 - \frac{q_t}{q_e}\right) \quad (3.45)$$

The value of  $B_b t$  was calculated for each  $F$  value and then plotted against time. Those plots are called Boyd plots. Linearity of this plot is used to distinguish between external transport-(film diffusion) and intraparticle transport- controlled rates of sorption (Mohan and Singh, 2002). A straight line passing through the origin indicates that sorption processes governed by particle-diffusion mechanisms; otherwise they are governed by film diffusion (Das et al., 2010)

Dumwald-Wagner proposed an intraparticle diffusion model similarly based on the Crank equations which is expressed as follows:

$$F = \frac{q_t}{q_e} = 1 - \frac{6}{\pi^2} \sum_{n=1}^{\infty} \frac{1}{n^2} \exp(-n^2 K t) \quad (3.46)$$

where  $K$  ( $\text{min}^{-1}$ ) is the rate constant of adsorption. This equation can be simplified as

$$\log(1 - F^2) = -\frac{K}{2.303} t \quad (3.47)$$



A plot of  $\log(1-F^2)$  vs  $t$  should be linear and the rate constant  $K$  can be obtained from the slope. Dumwald-Wagner model proved to be reasonable to model different kinds of adsorption systems, e.g., p-toluidine adsorption from aqueous solutions onto hypercrosslinked polymeric adsorbents (Qui et al., 2009).

Following intraparticle diffusion model was proposed by Urano and Tachikawa (1991) (U&T) where the sorption rate is considered to be independent of the stirring speed and external diffusion to be negligible relative to the low overall sorption rate. The (U&T) model is given by the following equation:

$$f\left(\frac{q_t}{q_e}\right) = -\left[\log\left(1 - \left(\frac{q_t}{q_e}\right)^2\right)\right] = \frac{4\pi^2 D_i t}{2.3 d_p^2} \quad (3.48)$$

where  $q$  and  $q_m$  are the solute concentrations in the solid at  $t$  and  $t \rightarrow \infty$ ,  $d_p$  the particle diameter and  $D_i$  the diffusion coefficient in the solid (Sağ and Aktay, 2000).

Vermeulen approximation is also based on the Crank equations similar to Eq 3.44:

$$F(t) = 1 - \frac{6}{\pi^2} \sum_{n=1}^{\infty} \frac{1}{n^2} \exp\left(\frac{-n^2 \pi^2 D_c t}{r_c^2}\right) \quad (3.49)$$

where  $F_t$  is the fraction uptake at any time  $t$ :

$$F(t) = \frac{q_t}{q_e} \quad (3.50)$$

Vermeulen approximation fits the whole range  $0 < F(t) < 1$ , for adsorption on spherical particles assuming diffusion is the rate controlling step (Srihari and Das, 2008).

$$F(t) = \left[1 - \exp\left(\frac{-\pi^2 D_c t}{r_c^2}\right)\right]^{1/2} \quad (3.51)$$

This equation can be simplified to:

$$\ln \left[ 1 - \frac{1}{1 - F^2(t)} \right] = \frac{\pi^2 D_c}{r_c^2} \quad (3.52)$$

thus slope of the plot of  $\ln[1/(1-F^2(t))]$  vs  $t$  would give  $D_c$ (effective diffusion coefficient)..

As well as the rate equations, dimensionless numbers are other important tools for the decision of the rate controlling mechanism. Following equation for the Biot number is widely used to compare if external or internal resistance controls the mass transfer mechanism.

$$Bi = \frac{k_f r}{3\epsilon D_p} = \frac{Sh D_m}{6 \epsilon D_p} \quad (3.53)$$

where  $k_f$  is the external mass transfer coefficient,  $r$  is the radius of particle (m),  $\epsilon$  is the porosity of particle,  $D_p$  is the pore diffusivity ( $m^2/sec$ ) and  $Sh$  is the Sherwood number. There are several approaches for the limitation of Biot number for the discrimination between external mass transfer and internal mass transfer mechanisms. For Biot number  $\ll 1$ , the adsorption rate is external mass transfer resistance controlled. For  $Bi \gg 100$ , pore diffusion is the predominant mass transfer controlling mechanism (Maiti et al., 2009).

### 3.3.2.4. Adsorption Reaction Models

#### *1<sup>st</sup> Order Kinetic Model*

1<sup>st</sup> order reaction model is known as Lagergren equation which is the earliest model describing the adsorption rate with respect to the adsorption capacity. This model includes all steps in the adsorption process such as external diffusion, pore diffusion and binding to active sites (Chang et al., 2006). Model is represented as follows:

$$\frac{dq}{dt} = k_1 (q_e - q_t) \quad (3.54)$$

where  $k_1$  is the first order reaction rate constant,  $q_e$  and  $q_t$  are the adsorption capacities

at equilibrium and at any time t.

This model is very similar to the external mass transport model based on the linear driving force for the liquid film controlled systems.  $k_1$  of the Lagergren equation is depended on concentration of the sorbate however,  $k_f$  varies inversely with the particle size and film thickness (Ho et al., 2000).

For the boundary conditions

$$t=0 ; q_t =0 \quad (3.55)$$

$$t = t ; q_t = q_t \quad (3.56)$$

Integrated form of the equation is :

$$\log(q_e - q_t) = \log q_e - \frac{k_1}{2.303} t \quad (3.57)$$

$\log(q_e - q_t)$  vs t plot can be used to determine  $k_1$  where  $k_1$  can be calculated from the slope of the plot.

### ***2<sup>nd</sup> Order Kinetic Model***

Another simple kinetic analyzes for the adsorption is 2<sup>nd</sup> order rate equation. 2<sup>nd</sup> order adsorption kinetic rate equation is expressed as:

$$\frac{dq}{dt} = k_2 (q_e - q_t)^2 \quad (3.58)$$

where,  $k_{2ads}$  is the rate constant of pseudo second-order adsorption ( $\mu\text{g}/\text{mg min}$ ).

For the boundary conditions

$$t=0 ; q_t =0 \quad (3.59)$$

$$t = t ; q_t = q_t \quad (3.60)$$

the integrated form of equation becomes:

$$\frac{1}{(q_e - q_t)} = \left( \frac{1}{q_e} \right) + k_2 t \quad (3.61)$$

which is the integrated rate law for a pseudo second-order reaction. It can be rearranged to obtain:

$$\frac{t}{q_t} = \left( \frac{1}{k_2 q_e^2} \right) + \left( \frac{1}{q_e} \right) t \quad (3.62)$$

The plot of  $(t/q_t)$  against  $t$  of equation should give a linear relationship from which  $q_e$  and  $k_2$  can be determined from the slope and intercept of the plot, respectively.

### ***Elovich Equation***

The Elovich equation is a kinetic equation of chemisorption was established by Zeldowitsch in 1934 (Kumar et al., 2010; Qui et al., 2009). It is another rate equation based on the biosorption capacity where absorbing surface is heterogeneous (Theivarasu and Mylsamy, 2010). It is expresses as follows:

$$\frac{dq}{dt} = a e^{-\alpha q} \quad (3.63)$$

where  $q$  represents the amount of adsorbed at time  $t$ ,  $a$  the desorption constant, and  $\alpha$  the initial adsorption rate. Eq.(3.65) can be rearranged to a linear form:

$$q = \left( \frac{2.3}{\alpha} \right) \log(t + t_0) - \left( \frac{2.3}{\alpha} \right) \log t_0 \quad (3.64)$$

with

$$t_0 = \frac{1}{\alpha a} \quad (3.65)$$

The plot of  $q$  versus  $\log(t + t_0)$  should yield a straight line. Using equation 3.65, “ $a$ ” is determined which obviously represents the initial rate of adsorption for  $q = 0$ . (Qui et al., 2009; Kumar et al., 2010). But, due to the complexity of the original Elovich equation, Chien and Clayton simplified it by assuming that  $\alpha a t \gg 1$  and by applying the boundary conditions of  $q = 0$  at  $t = 0$  and  $q = q$  at  $t = t$ . Final simplified integrated form of Eq. (3.64) is given below:

$$q = \alpha \ln(a\alpha) + \alpha \ln(t) \quad (3.66)$$

Equations explained above can be used to model different adsorption systems. Adsorption mechanisms depend on the sorbate-sorbent interaction and the system conditions. Reaction and diffusion models applied for various sorbate-sorbent systems in the literature were given in Table 3.3-3.5 below. Table summarizes the model equations and graphical methods used in literature to determine kinetic rate parameters.

Table 3.3. External mass transfer models and determination of kinetic parameters.

Kinetic Model & Equation	Linear Form	Plot	References
<i>External Mass transfer Models</i>			
Mass Transfer Classical Model $\frac{\partial C_t}{\partial t} = -k_f S_s (C_t - C_s)$	$\left[ \frac{d(C_t/C_0)}{dt} \right]_{t=0} = -k_f S_s \text{ or } \ln\left(\frac{C_t}{C_0}\right) = -k_f t$	Ct/C <sub>0</sub> vs t, ln(Ct/C <sub>0</sub> ) vs t	<ul style="list-style-type: none"> <li>- methylene blue by almond peel (Benaissa H., 2009)</li> <li>- metal by cyanobacterial mat (Kumar and Gaur, 2011)</li> <li>- dye onto dolomite (Walker et al., 2003)</li> <li>- lysozyme by NaY (Chang et al., 2006).</li> </ul>
Furusawa Smith Model $\frac{C_t}{C_0} = \frac{1}{1+m_s K_L} + \frac{m_s K_L}{1+m_s K_L} \exp\left[-\left(\frac{1+m_s K_L}{m_s K_L}\right)k_f S_s t\right]$	$\ln\left(\frac{C_t}{C_0} - \frac{1}{1+m_s K_L}\right) = \ln\left(\frac{m_s K_L}{1+m_s K_L}\right) + \left[-\left(\frac{1+m_s K_L}{m_s K_L}\right)k_f S_s t\right]$	$\frac{\ln(C_t/C_0 - 1/(1+m_s K_L))}{t}$ vs t	<ul style="list-style-type: none"> <li>- Benzene by activated Carbon (Furusawa and Smith, 1973).</li> <li>- Cd, Zn by activated carbon from begasse (Mohan and Singh, 2002)</li> <li>- Lead by rice husk (Naiya et al., 2009)</li> </ul>
Boyd Model $\frac{\bar{q}}{q_\infty} = 1 - \exp\left[-\frac{3k_f t}{KR_p}\right]$	$\ln\left(1 - \frac{q}{q_\infty}\right) = -R' t$	ln(1-q/q <sub>e</sub> ) versus t	<ul style="list-style-type: none"> <li>- Dye by Zeolites Synthesized from Fly Ash (Wang et al., 2009)</li> <li>- Methylene blue by Palm kernel coat (Oladoja et al., 2008).</li> <li>- Mn(II) by clay (Eba et al., 2010.)</li> <li>- carminic acid dye by glass powder (Atun and Hisarli, 2003)</li> </ul>

Table 3.4. Intraparticle diffusion models and determination of kinetic parameters.

Intraparticle Diffusion Model	Linear Form	Plot	References
<p>Weber Morris Model</p> $q_t = k_d t^{0.5}$		$q_t$ vs $t^{0.5}$	<ul style="list-style-type: none"> <li>- methylene blue by almond peel (Benaissa H., 2009)</li> <li>- dye onto dolomite (Walker et al., 2003)</li> <li>- tartaric acid by modified amberlite resin (Sminiceanu et al., 2010)</li> <li>- Lead by rice husk (Naiya et al., 2009)</li> </ul>
<p>Boyd Model</p> $F = 1 - \frac{6}{\pi^2} \exp(-B_b t)$	$B_b t = -0.4977 - \ln(1 - F)$	$B_{bt}$ vs $t$	<ul style="list-style-type: none"> <li>- Cd, Zn by activated carbon from begasse (Mohan and Singh, 2002)</li> <li>- Ag(I) by <i>Pleurotus platypus</i> (Das et al., 2010)</li> <li>- Na Exchange by resin (Reichenberg, 1952)</li> </ul>
<p>Vermeulen Model</p> $F(t) = \left[ 1 - \exp\left(\frac{-\pi^2 D_c t}{r_c^2}\right) \right]^{1/2}$	$\ln\left[1 - \frac{1}{1 - F^2(t)}\right] = \frac{\pi^2 D_c}{r_c^2} t$	$\ln[1/(1-F^2(t))]$ vs $t$	<ul style="list-style-type: none"> <li>- phenol by agro-based carbon (Srihari and Das, 2008)</li> <li>- Cu, Cd, Pd by modified zeolite (Apiratikul and Oavasant, 2008).</li> <li>- phenol by bagasse fly ash and activated carbon (Srivastava et al., 2006.)</li> </ul>
<p>Dumwald-Wagner Model</p> $F = \frac{q_t}{q_e} = 1 - \frac{6}{\pi^2} \sum_{n=1}^{\infty} \frac{1}{n^2} \exp(-n^2 K t)$	$\log(1 - F^2) = -\frac{K}{2.303} t$	$\log(1-F^2)$ vs $t$	<ul style="list-style-type: none"> <li>- tartaric acid by modified amberlite resin (Sminiceanu et al., 2010)</li> <li>- naphthalene and 2-naphthol by polymeric adsorbent of LM-6 (Yuan et al., 2006).</li> </ul>
<p>Urano and Tachikawa Model</p> $\left(1 - \left(\frac{q_t}{q_e}\right)^2\right) = e^{-\frac{4\pi^2 D_i t}{d_p^2}}$	$-\left[\log\left(1 - \left(\frac{q_t}{q_e}\right)^2\right)\right] = \frac{4\pi^2 D_i t}{2.3 d_p^2}$	$\text{Log}[1-(q_t/q_e)^2]$ vs $t$	<ul style="list-style-type: none"> <li>- Phosphorus by Modified alophene/activated alumina (Urano and Tachikawa, 1991)</li> <li>- hexacyanoferrate(III) anion by biomass (Chergui et al., 2009)</li> </ul>

Table 3.5. Reaction models and determination of kinetic parameters.

Reaction Models	Linear Form	Plot	References
1st Order Kinetic Model $\frac{dq}{dt} = k_1(q_e - q_t)$	$\log(q_e - q_t) = \log q_e - \frac{k_1}{2.303}t$	$\log(q_e - q_t)$ vs t plot	<ul style="list-style-type: none"> <li>- metal by cyanobacterial mat (Kumar and Gaur, 2011)</li> <li>- methylene blue onto pres mud (Kumar et al., 2010)</li> <li>- Dye by Zeolites Synthesized from Fly Ash (Wang et al., 2009)</li> <li>- tartaric acid by modified amberlite resin (Sminiceanu et al., 2010)</li> <li>- lysozyme by NaY (Chang et al., 2006).</li> </ul>
2nd Order Kinetic Models $\frac{dq}{dt} = k_2(q_e - q_t)^2$	$\frac{t}{q_t} = \left(\frac{1}{k_2 q_e^2}\right) + \left(\frac{1}{q_e}\right)t$	(t/qt) against t	<ul style="list-style-type: none"> <li>- metal by cyanobacterial mat (Kumar and Gaur, 2011)</li> <li>- methylene blue onto pres mud (Kumar et al., 2010)</li> <li>- lysozyme by NaY (Chang et al., 2006)</li> <li>- lead by palm kernel fiber(Ho and Ofojama, 2006)</li> <li>- Cr(IV) onto impregnated microspheres (Illanes et al., 2008)</li> <li>- tartaric acid by modified amberlite resin (Sminiceanu et al., 2010)</li> </ul>
Elovich Equation $\frac{dq}{dt} = a e^{-\alpha q}$	$q = \left(\frac{2.3}{\alpha}\right)\log(t + t_0) - \left(\frac{2.3}{\alpha}\right)\log t_0$	q versus $\log(t + t_0)$	<ul style="list-style-type: none"> <li>- methylene blue onto pres mud (Kumar et al., 2010)</li> <li>- Cr(IV) onto impregnated microspheres (Illanes et al., 2008)</li> <li>- Lead by pumpkin seed shell activated carbon (Okoye et al., 2010)</li> <li>- Rhodamine-B by cocoa shell (Theivarasu and Mymlsamy, 2010)</li> </ul>



### ***Equations Used for the Modeling of Casein and GUS Adsorption onto Zeolite***

Kinetic studies should be performed in order to analyze the GUS and casein adsorption onto zeolite. These adsorption systems were typical liquid/solid adsorption involves bulk and film diffusion, intraparticle diffusion, and reaction. Then, these kinetic processes of adsorption for GUS and casein can be analyzed by those mathematical models where in case one or more than one step can be a rate determining step.

Reaction and diffusion models expressed above are useful for the investigation of rate controlling mechanism. Last step in adsorption is usually rapid process thus kinetic process of adsorption is usually controlled by liquid film diffusion or intraparticle diffusion (Qui et al., 2009) and one of the processes can be the rate limiting step. However, each model has its own limitation especially in application using the experimental data.

The external mass transfer coefficient for GUS and casein adsorption can be calculated from any of the solution methods depending on the particular experimental and system conditions. For the external mass transfer, model developed by Furusawa and Smith given as equation 3.9 was complicated to perform since it included long expressions and equilibrium parameters. More simplified form for external mass transfer derived from the linear adsorption isotherm was given in equation 3.18. However, during linearization of the plot, there were different applications such as plotting the experimental data in logarithmic scale or performing curve fitting to a proper polynomial. Slope of the curve can be determined by taking derivative of the fitted equations at  $t=0$  which leads variations in the results. Additionally, in most cases, it was not possible to take experimental data for the initial stages of the sorption especially where the measurements were performed at the time of sorption experiments such as in GUS and casein adsorption. Thus lack of initial data limits the applicability of equation 3.18. External mass transfer coefficients can be calculated using equation 3.14 assuming zeolites as spherical particles. Model involves whole range of the experimental data and proper assumptions such as no gradient of concentration through the particle, adsorbed phase concentrations through the particle is at equilibrium with the fluid phase concentration at the surface, and there is a linear equilibrium relationship ( $q^*=KC$ ).

Widely used intraparticle diffusion equations given in Section 3.3.2 (Weber and Morris, Boyd, Dumwald-Wagner, Urano and Tachikawa) were all derived from the Crank's solutions. Intraparticle diffusion coefficients of GUS and casein adsorption can

be calculated by Weber Morris equation which was most widely applied intraparticle diffusion equation for sorption systems (Gerente et al., 2007). This model is the most simplified form. Besides, this model can be used to analyze the sorption systems such as different linear portions in the plot of  $qt$  vs square root of time in Weber Morris plot could characterize the steps in diffusion mechanism in the overall adsorption process. Additionally, the intercept of Weber Morris plot reflects the boundary layer effect where the larger the intercept, the greater the contribution of the surface sorption in the rate limiting step (Kumar and Porkodi, 2007).

In order to investigate the mechanism of sorption of GUS and casein, pseudo first and second order kinetic reaction models can be used to test experimental data. Elovich equation can be another alternative however it is commonly used to determine the kinetics of chemisorption of gases onto heterogeneous solids. Additionally, it was reported to be quite restricted, as it only described a limiting property ultimately reached by the kinetic curve and there could be some problems in fitting the data for the early stages (Aharoni and Ungarish, 1975). Besides, this model required a correctly chosen  $t_0$  thus the plot of  $q$  as a function of  $\log(t + t_0)$  should yield a straight line with a slope of  $2.3/\alpha$ . The analyze of curve involved one single disposable parameter,  $t_0$ , which is found by trial. Therefore if  $t_0$  was too small, the curve would be convex, and if  $t_0$  was too large, it would concave to the axis of  $\log(t + t_0)$  which would affect the calculation of rate parameter (Ho, 2006; Taylor and Thon, 1952)

The pseudo-first-order kinetic model has been reported to be used extensively to describe the sorption of metal ions onto sorbents however it does not fit well for the whole range of contact time. Deviations were attributed to the differences in the  $q_e$  values where there was a time lag possibly due to a boundary layer or external resistance controlling at the beginning of the sorption process. Gerente et al. (2007) reported that it was generally applicable for the contact time range of the initial 20 to 30 min of the sorption process Thus comparison with a second-order rate model seems more likely which has been the most widely tested model and it can be simply applicable model for the sorption of GUS and casein onto zeolite surface. The pseudo-second-order equation is based on the sorption capacity on the solid phase. Contrary to the other models, pseudo second order is well correlated to predict the behaviour over the whole range of sorption studies.

Diffusion and reaction models used in modeling of kinetic data for GUS and casein adsorption were given in Table 3.6 and 3.7 below.

Table 3.6. Diffusion models used for the modeling of adsorption kinetic data.

Diffusion Models	Assumptions	Boundary Conditions & Equations
<b>External Mass Transfer</b>	<ul style="list-style-type: none"> <li>- isothermal linear system</li> <li>- rapid diffusion within sorbent</li> <li>- nonporous spherical adsorbent</li> <li>- no concentration gradient through the particle</li> <li>- adsorbed phase concentrations through the particle is at equilibrium with the fluid phase concentration at the surface</li> <li>- linear equilibrium relation ship (<math>q^*=KC</math>),</li> </ul>	<p><b>B.C:</b></p> $t < 0, C = q = 0$ $t > 0, C = C_{\infty} = q_{\infty} / K$ <p><b>Equation:</b></p> $\frac{q}{q_{\infty}} = 1 - \exp\left[-\frac{3k_f t}{KR_p}\right]$
<b>Macropore Diffusion</b>	<ul style="list-style-type: none"> <li>- isothermal linear system</li> <li>- pore diffusivity of independent of concentration</li> <li>- spherical geometry</li> </ul>	<p><b>B.C:</b></p> <p>at <math>t=0</math>: <math>C(R,0) = C_o</math>, <math>q(R,0) = q_o = KC_o</math></p> <p>at <math>R = R_p</math> &amp; <math>t=t</math>: <math>C(R_p, t) = C_o</math>, <math>q(R_p, t) = q_o</math></p> $\left. \frac{\partial C}{\partial R} \right _{R=0} = \left. \frac{\partial q}{\partial R} \right _{R=0} = 0$ <p><b>Equation:</b></p> $\frac{m_t}{m_{\infty}} = 1 - \frac{6}{\Pi^2} \sum_{n=1}^{n=\infty} \frac{1}{n^2} \exp\left(-\frac{n^2 \Pi^2 \varepsilon_p D_p t}{R_p^2 (\varepsilon_p + (1 - \varepsilon_p) K)}\right)$
<b>Micropore Diffusion</b>	<ul style="list-style-type: none"> <li>- isothermal linear system</li> <li>- spherical geometry initially free of solute</li> <li>- constant diffusivity</li> <li>- constant concentration of solute at the surface</li> <li>- neglected external film resistance</li> </ul>	<p><b>B.C:</b></p> $t < 0 : C = C_o, q = q_o$ $t \geq 0 : C = C_{\infty}, q(r_c, t) = q_{\infty}$ $t \rightarrow \infty : C = C_{\infty}, q(r, t) = q_{\infty}$ $\left. \frac{\partial q}{\partial t} \right _{r=0} = 0 \text{ for all } t.$ <p><b>Equation:</b></p> $\frac{q_t}{q_{\infty}} = 1 - \frac{6}{\pi^2} \sum_{n=1}^{\infty} \frac{1}{n_i^2} \exp\left(\frac{-n_i^2 \pi^2 D_c t}{r_c^2}\right)$ <p>Weber Morris expression for sufficiently small t:</p> $q_t = k_d t^{0.5}$

Table 3.7. Reaction models used for the modeling of adsorption kinetic data

Reaction Models	Assumptions	Boundary Conditions & Equations
<b>1<sup>st</sup> Order Reaction</b>	- irreversible - rate of sorption is first order mechanism	<b>B.C:</b> t=0 ; qt =0 t = t ; qt = qt  <b>Equation:</b> $\frac{dq}{dt} = k_1(q_e - q_t)$
<b>2<sup>nd</sup> Order Reaction</b>	- rate of sorption is second order mechanism	<b>B.C:</b> t=0 ; qt =0 t = t ; qt = qt  <b>Equation:</b> $\frac{dq}{dt} = k_2(q_e - q_t)^2$

### 3.3.3. Adsorption Equilibrium and Adsorption Isotherms

Adsorption analyses are based on equilibrium properties of a system and mass transfer kinetics. For equilibrium properties statistical thermodynamics provides a useful tool for prediction of adsorption equilibria (Ruthven, 1989). Mass transfer kinetics took into account of internal, external and surface diffusion of adsorbate molecules related to solid-liquid contacting process (Dabbrowski, 2001). Therefore to analyze adsorption process and to estimate practical or dynamic adsorption capacity, adsorption equilibrium is the most fundamental property.

The fundamental concept in adsorption science is the adsorption isotherm. It is the equilibrium relation between the quantity of the adsorbed material and the pressure or concentration in the bulk fluid phase at constant temperature (Dabbrowski, 2001). At equilibrium there is a defined distribution of solute between the solid and liquid phases. The distribution ratio is a measure of position of equilibrium in the adsorption process and the relation between amount adsorbed,  $q$ , and concentration in the fluid phase  $C$  at temperature,  $T$  (Suzuki, 1990) where:

$$q = q(C) \text{ at } T \quad (3.67)$$

Therefore adsorption isotherms describe the equilibrium conditions for an adsorbate onto surface of an adsorbent. Usually the amount of material adsorbed is some complex function of the concentration of adsorbate and many theories and models have been developed to describe different types of isotherms. Some of them are Langmuir isotherm, Freundlich isotherm and BET isotherm.

*i) Langmuir Isotherm:* The Langmuir adsorption model assumes that adsorption is a reversible mass transfer process and valid for monolayer adsorption. Adsorption proceeds at a rate proportional to the product concentration of adsorbate in solution and the concentration of free adsorbent. Adsorption take place on an energetically uniform surface without any interaction between adsorbed molecules and energy of adsorption is constant. The reverse rate is proportional to the amount of adsorbate bound to the adsorbent. The rate equation can be given as:

$$\frac{dq}{dt} = K_a C(q_m - q) - K_d q \quad (3.68)$$

where C is the concentration of the adsorbate in solution and q is the concentration of the adsorbed amount,  $K_a$  and  $K_d$  are forward and reverse rate coefficients and  $q_m$  is the maximum capacity of the adsorbent. By kinetic and equilibrium and mass transfer experiments  $K_a$ ,  $K_d$  and  $q_m$  can be determined and to derive the final equation adsorption equilibrium is attained when  $dq/dt = 0$   $C \rightarrow C_e$  and written;

$$K_a C_e (q_m - q) = K_d q \quad (3.69)$$

$$K_a C_e \frac{(q_m - q)}{q_m} = K_d \frac{q}{q_m} \quad (3.70)$$

$$K_a \left(1 - \frac{q}{q_m}\right) C_e = K_d \frac{q}{q_m} \quad (3.71)$$

$$\frac{K_a}{K_d} = K = \text{dissociation constant} \quad (3.72)$$

$$\theta = \frac{q}{q_m} = \text{surface coverage or fraction of filling} \quad (3.73)$$

$$K = \frac{\theta}{(1-\theta)C_e} \quad (3.74)$$

$$\theta = \frac{KC_e}{1+KC_e} \quad (3.75)$$

$$q = \frac{q_m C_e}{K + C_e} \quad (3.76)$$

where it is derived due to the assumptions of Langmuir Isotherm. Mass adsorbed,  $q$  is assumed to approach a saturating value,  $q_0$ . A plot of  $1/q$  versus  $1/C_e$  approximates a line with slope of  $K/q_m$  and intercept of  $1/q_m$ .

*ii) Freundlich Isotherm:* The Freundlich isotherm is empirical and special case for heterogenous surface energies and approximates data for many physical adsorption systems. Expression is an exponential equation and therefore assumes theoretically an infinite amount of adsorption can occur. Freundlich equation is based on monolayer adsorption by the adsorbent with a heterogeneous energy distribution of active sites and equation is given as;

$$q = KC_e^n \quad (3.77)$$

In this equation  $K$  and  $n$  are the Freundlich constants characteristic on the system.  $K$  and  $n$  are indicators of adsorption capacity and heterogeneity factor, respectively. The Freundlich equations agree well with the Langmuir equation; it does not reduce to the linear isotherm at low surface and provides no information on the monolayer adsorption capacity. However unlike Langmuir equation, it does not reduce to a linear adsorption expression at very low concentrations, and does not agree well with the Langmuir equation at very high concentrations since  $n$  must reach a limit when the surface is fully covered. To determine the constants  $K$  and  $n$ , logarithmic plots may be used to linearize the equation and linear form of the equations may be used to calculate Freundlich constants. From slope and intercept of the graph, we can calculate  $n$  and  $K$  values respectively.

*iii) BET Isotherm:* Derivation of the Langmuir isotherm expression was based on the idea of coverage of the surface with single layers of adsorbent. In some cases,

isotherms curves for adsorption rather than flatten out after initial stage of adsorption suggest a secondary adsorption stage. S. Brunauer, P.H Emmett, and E.Teller have worked out to describe this process and derive an expression for the corresponding adsorption isotherm known as the BET isotherm.

Bet model assumes that a number of layers of the adsorbate molecules form at the surface and that the Langmuir equation applies to each layer. Given layer does not need to complete formation prior to initiation of subsequent layers. Layer beyond the first have equal energies of adsorption for adsorption from solution.

$$q = \frac{Kq_m C_e}{(C_s - C_e)[1 + (K - 1)\frac{C_e}{C_s}]} \quad (3.78)$$

where  $C_s$  is the saturation coefficient of the solute,  $C_e$  is the measured concentration in the solution at equilibrium and  $K$  is a constant expressive of the energy interaction of the surface and  $q_m$  is the amount of adsorbed adsorbed per unit weight adsorbent by monomolecular coverage on the surface.

### 3.4. Zeolites in Industrial Applications

Both natural and synthetic zeolites are porous materials, characterized by the ability to lose and gain water reversibly, to adsorb molecules of appropriate cross-sectional diameter (adsorption property, or acting as molecular sieves) and to exchange their constituent cations without major change of their structure (ion-exchange property) (Papaioannou et al., 2005). All commercially useful zeolites owe their value to one or more of these three properties. The exploitation of these properties underlies the use of zeolites in a wide range of industrial and agricultural applications and particularly in animal nutrition since mid-1960s (Papaioannou et al., 2005). They are widely used as drying agent in separation process, in laundry detergents, as catalyst and catalyst supports, in waste water treatment, nuclear effluent treatment etc. In recent years, many studies were performed to investigate the uses of zeolite for health issues. Some important applications are given in Figure 3.3 below.

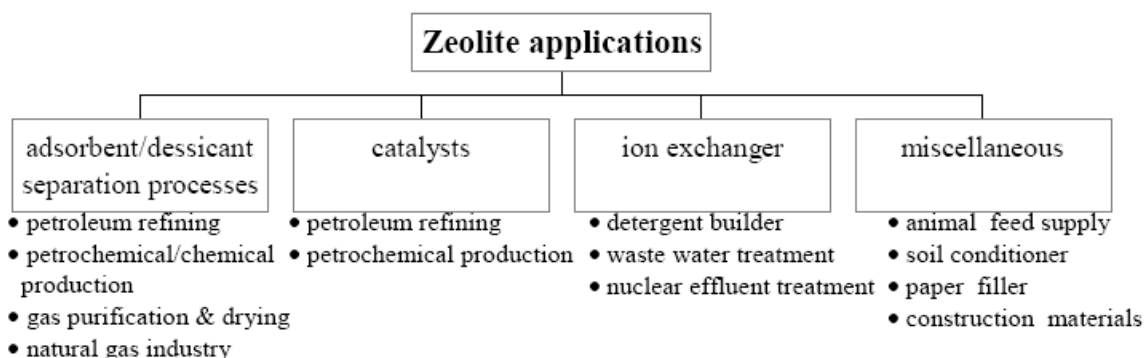


Figure 3.3. Zeolite applications.

### 3.5. Zeolites in Biomedical Applications

Minerals are traditionally employed in pharmaceutical products. Generally, they act as a carrier, binder, lubricating, diluent, disaggregating or radiopaque compound, but sometime they are also involved in therapeutical processes (Cerria et al., 2004; Dahm and Eriksson, 2004).

Most of the health effect studies were done using natural zeolite; clinoptilolite. Clinoptilolite has been reported as inert and non-toxic matter for poultry and approved by EU 2000 onwards (Ortatlı and Oğuz, 2001) which make clinoptilolite very advantageous. Trckova et al. (2004) indicated that zeolite supplemented diets are well tolerated by the animals; they support biomass production and improve the health status of the animals. Many researches in literature provide evidence of a growth promoting effect when zeolites are used as additives in animal nutrition. Improved weight gain rates have been obtained in fattening pigs and lambs, while a better feed efficiency and egg productivity has been achieved in laying hens by the dietary use of zeolites. Kyriakis et al. (2002) reported that the extent of these beneficial effects seems to be related to the species and the geographical source of the involved zeolite, its purity and physicochemical properties, as well as the supplemental level used in the diets. Besides, Papaioannou et al. (2005) reported that the particle size of the zeolitic material, crystallite size and the degree of aggregation, as well as the porosity of individual particles were reported to determine the access of ingesta fluids to the zeolitic surface during passage across gastrointestinal tract and strongly affect its ion exchange, adsorption and catalytic properties

When zeolite is used in dietary applications, it is important to check the systemic



effects of zeolites on hematopoiesis. Clinoptilolite added to food in high percentages would affect serum electrolytes, basic liver and kidney functions. Martin-Kleiner et al. (2001) investigated the effects of natural zeolites on hematopoiesis, serum electrolytes essential biochemical indicators of kidney and liver function in mice. They reported 20% increase in potassium level, detected in mice receiving zeolite rich diet without any other changes in serum chemistry. Erythrocyte, hemoglobin and platelet levels in peripheral blood were not materially affected.

The reasons of advantageous usage of zeolite as animal feed may be related to some of its types that show antimicrobial property. Antimicrobial properties of natural and synthetic zeolites conditioned in some cation forms, generally silver and zinc, are well constrained and tested in a variety of applications, as documented by several patents and papers. Some of these researches were developed by using natural zeolites, in particular clinoptilolite, which is one of the most diffused natural zeolite in the world. Top and Ülkü (2004) found that Ag-clinoptilolite seemed to be promising antibacterial material. They observed that antibacterial activity of Ag clinoptilolite against *Proteus* spp. and *Pseudomonas aeruginosa* is competitive to commercial antibiotics. As bactericidal the effect of zeolites in the control of urinary tract infections against *Pseudomonas aeruginosa*, *Staphylococcus aureus* and *Escherichia coli*, which has been demonstrated in vitro (Rivera and Farias, 2005). Therefore it is clear that some types of zeolites effect gastrointestinal flora.

Zeolite with structural stability, its ability to host useful pharmaceutical species, can be used as a controlled release matrix in the human body and to release them with a kinetics that suits the specific medical application. As most of the pharmaceutical studies were related to natural zeolites, Dahm and Eriksson used synthetic zeolite-Y particles as a carrier of bioactive molecule N-nitro-L arginin methyl ester (L-NAME) to inhibit the cellular NO production in peripheral monocytes and they found that zeolites were ten times efficient as a carrier of the inhibitor as opposed to addition of the inhibitor to the culture alone. Rivera et al. (2000) was reported that purified natural clinoptilolite has demonstrated good stability in its transit through the gastrointestinal tract, and to be harmless to the human body. Based on such properties, it has been used as raw material for different pharmaceutical forms for the treatment of several pathologies in animals and humans In Cuba, inexpensive, indigenous natural zeolites are being studied as buffers to reduce stomach acidity and to treat stomach ulcers incisions (Mumpton, 1999). A new antidiarrhetic drug for humans has been developed

by Rodriguez-Fuentes et al. (1997). It was based on the physical and chemical properties of the purified natural clinoptilolite (NZ). Possible mechanisms that zeolite act as antidiarrheic drug is, NZ adsorbs bile acids, one of the endogenic causes of the diarrhea. Also glucose may be adsorbed whose high content in intestinal fluid act as an irritant factor and whose transport through the intestinal cell is reversed during diarrhea. Hydrothermal modified NZ act as a selective adsorber of glucose. In September 1995, The Cuban Drug Quality Control Agency approved Enterex as a new drug.

One of the many exciting potential pharmacological applications of zeolites is the possible encapsulation and/or adsorption of different ions and molecules in their open framework, and the subsequent delayed release. Klint and Eriksson (1997) showed that zeolites are able to adsorb proteins on surfaces although their pore size is smaller to allow proteins to pass or enter. Also many enzyme-immobilization studies are carried out using zeolites as adsorbents and also related to this aim, zeolites used as biosensor based studies. Rivera et al. (2003) studied on preliminary characterization of drug support systems based on natural clinoptilolite. Their results showed that, the presence of surfactant and drugs on the zeolite does not produce structural changes, and results in a strong decrease of the specific surface area. The overall results indeed suggest that the zeolitic materials are able to support drugs of very different nature.

Other important studies related to gastrointestinal system were done using montmorillonite (MMT). Montmorillonite is in the group of clays but as zeolites it has high adsorptive property. Result showed that it had high adsorptive property against different bacteria. It was shown that MMT could adsorb *Escherichia coli* and *S. aureus* in vitro, but showed no bacteriostatic or bactericidal effect in pigs gastrointestinal track. Previous unpublished results showed that Cu-MMT adsorbed *E. coli* and reduced bacterial numbers by more than 97% and MMT only produced reductions of 20%. The addition of MMT to the diet also produced a positive effect on the intestinal mucosa. It is reported that MMT, a mucus stabilizer, effectively acts by attaching to the mucus to reinforce intestinal mucosal barrier and helps in the regeneration of the epithelium (Xia, et al., 2005).

### **3.6. Natural Zeolites as Adjuvants in Cancer Therapy**

New in vitro and in vivo research results indicate that some dietetic supplements indeed show anticancer activity. The strongest anticancer action has been demonstrated by natural compounds with multifunctional activity (Colic and Pavelic, 2000).

Natural silicate materials, including zeolite clinoptilolite, have been shown to exhibit diverse biological activities. Pavelic et al. (2001) reported that a novel use of finely ground clinoptilolite was possible as a potential adjuvant in anticancer therapy. According to their results effects of zeolite on tumor growth in vivo was found as diverse. Its effect was ranged from negative antitumor response, to normalization of biochemical parameters, prolongation of life span, and decrease in tumor size. In experiments where mice and dogs suffering from a variety of tumor types were used, clinoptilolite treatment provide improvement in their overall health status, prolongation of life-span, and decrease in tumors size. Very important results in animal models were observed in the treatment of skin cancer in dogs and this data suggested that adsorption of some active components was responsible for micronized zeolite activity. Also to check negative side effects, toxicology studies on mice and rats were performed and they demonstrated that the treatment does not have negative effects (Pavelic and Hadzija, 2003).

Complementary in vitro studies were performed in tissue culture. Results indicated that micronized zeolite treatment affects proliferation and survival of several cancer cell lines. Inhibited cell proliferation when zeolite was added depended on concentration (Figures 3.4 and 3.5).

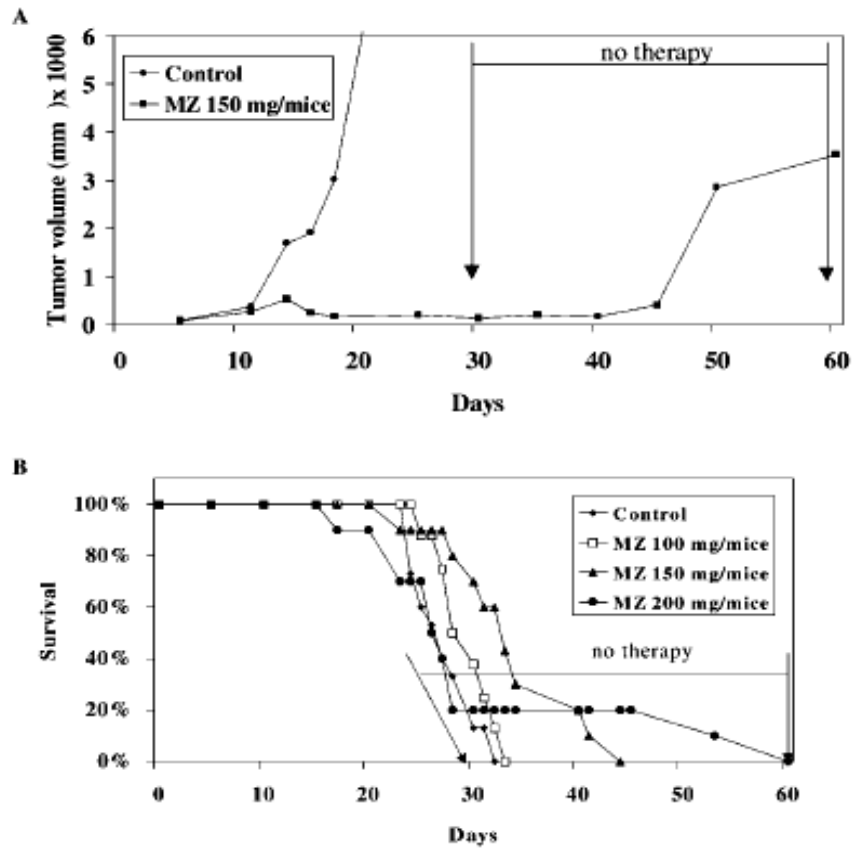


Figure 3.4. Growth rate of melanoma B16 treated with 150 mg micronized zeolite (MZ) / mouse per day(A), Survival of melanoma-bearing mice treated with three different doses of MZ (B) (Source: Pavelic et al., 2001).

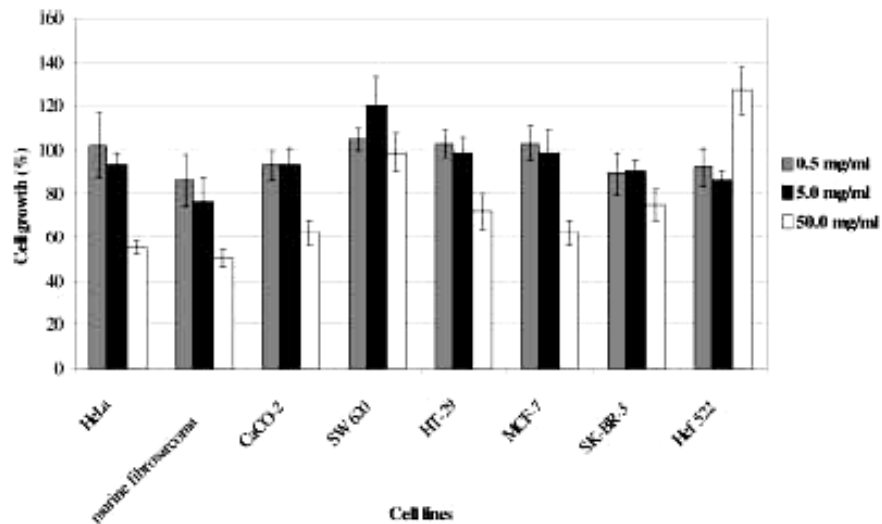


Figure 3.5. Effect of the medium pretreated with 0.5, 5.0, and 50.0 mg/ml MZ on growth of various cell lines (Source: Pavelic et al., 2001).

Mück-Seler and Pivac (2003) investigated the effect of tribomechanically micronized zeolite (MZ) on the binding of 3H-8-OH-DPAT to 5-HT1A and 3H-5-HT to

5-HT<sub>1B</sub> receptors in the brain of nontumorous (control) and mammary carcinoma bearing female mice where those have an important role in the chemotherapy-induced emesis. Results showed that there was a reduced binding of 3H-8-OH-DPAT to 5-HT<sub>1A</sub> receptors in mammary carcinoma bearing mice.

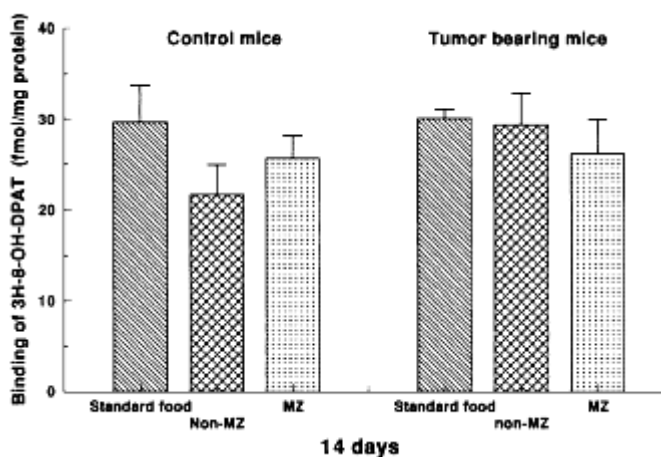


Figure 3.6. Binding of 3H-8-OH-DPAT to 5-HT<sub>1A</sub> receptors in the mouse brain (Source: Mück-Seler and Pivac 2003).

Control and tumor bearing mice were fed for 14 days with standard food, and with the mixture of standard food with 25% of non-MZ, or 25% of MZ. Results suggested a time dependent alteration of 5-HT<sub>1A</sub> receptors in mammary carcinoma (Figure 3.6).

In vitro culture studies showed that finely ground clinoptilolite inhibited protein kinase B (c-Akt), induced expression of p21WAF1/CIP1 and p27KIP1 tumor suppressor proteins, and blocked cell growth in several cancer cell lines. These data indicate that clinoptilolite treatment might affect cancer growth by attenuating survival signals and inducing tumor suppressor genes in treated cells. Alternatively, particles engulfed by phagocytosis have been reported to stimulate production of reactive oxygen species but redox regulation of gene expression is a general phenomenon in most cells (Pavelic et al., 2001)

## CHAPTER 4

### CASEIN

Caseins are phosphoproteins containing approximately 80% of the total protein content of milk proteins (Phadungath, 2005) and due to their high percentage in milk, caseins play a fundamental role of in human nutrition and in the dairy and food industry (Bramanti et al., 2001).

Besides being a natural nutritive compound, caseins were reported to be dynamic in nature and contain number of bioactive peptides possess many activities, such as immunoregulatory, antioxidant, or antihypertensive (Xue-Ying et al., 2007, Charles and Slatte, 1976). Also in different studies it was shown that its micropeptides bind cholera and *Escherichia coli* enterotoxins, inhibit bacterial and viral adhesion, modulate immune system responses (Worringer et al., 2006), stimulated phagocytosis by macrophages (Kazlauskaite et al., 2005), its peptides showed radical-scavenging activities in aqueous solution (Almajano et al., 2007) and inhibited activities of some enzymes. Therefore in this study, casein as well as being a protein and a nutritive compound, is thought to be an alternative inhibitor towards  $\beta$ -glucuronidase. Thus in this chapter, detailed information will be given about structure and function of casein with respect to health area.

#### 4.1. Structure

Cow milk constitutes a major part of the diet of developed nations and it contains an average 32 g of protein per liter, mostly casein (82%) and whey (18%). Caseins are phosphoproteins and made up of many components. The main types are  $\alpha$ 1- casein,  $\alpha$ 2-casein,  $\beta$ -casein, and  $\kappa$ -casein as defined and validated by analysis of DNA sequences. Kauf and Kensinger (2002) reported that caseins four subclasses,  $\alpha$ 1,  $\alpha$ 2,  $\beta$  and  $\kappa$ , major function is to transport calcium phosphate. There is another class for casein named as  $\gamma$ - casein. It is in trace amounts and occurred naturally on account of limited proteolysis of  $\beta$ -casein by plasmin. The main casein components contain

variable numbers of phosphoserine residues.  $\alpha$ -Caseins is the major casein proteins containing 8-10 seryl phosphate groups.  $\beta$ -Casein is the second most abundant casein behind  $\alpha_1$  and is essential for curd formation and important in determining the surface properties of micelles (Kauf and Kensinger, 2002).  $\beta$ -casein contains about 5 phosphoserine residues, it is more hydrophobic than  $\alpha$ s-caseins and  $\kappa$ -casein. In those 4 subclasses, especially  $\alpha_2$ -casein exhibited a large variability in phosphorylation. Because  $\alpha$ s-caseins and  $\beta$ -caseins are highly phosphorylated, they are very sensitive to the concentration of calcium salts, that is, they will precipitate with excess  $\text{Ca}^{2+}$  ions. Different than others,  $\kappa$ -casein contains only one phosphoserine residue and it is glycosylated. Unlike other caseins,  $\kappa$ -caseins are glycoproteins, and they have only one phosphoserine group. Hence, they are stable in the presence of calcium ions, and they play an important role in protecting other caseins from precipitation and make casein micelles stable.

It is important to note that basic structural property of caseins is due to the large amount of proline residues, especially in  $\beta$ -casein. This proline group greatly affects the structure of caseins, because the proline residues disrupt the formation of  $\alpha$ -helical and  $\beta$ -sheet. In addition, all casein proteins have different hydrophobic and hydrophilic regions along the protein chain (Phadungath, 2005).

Casein isn't heat sensitive; only temperatures up to or above 120°C causes the casein to gradually become insoluble, whereas it is sensitive to pH and will precipitate at its isoelectric pH. On the one hand caseins have extremely flexible structure and they are highly surface active. This is the concept of caseins as rheomorphic proteins which suggests that the caseins are dynamic in nature and that their conformation adapts to their environment (Horne, 2002). Casein was described as having an essentially random conformation, although several authors have estimated the amount of secondary structure in  $\alpha$ - and  $\beta$ -caseins by Raman spectroscopy. The lack of tertiary structure accounts for the stability of caseins against heat denaturation and for a considerable exposure of hydrophobic residues. The common compositional factor is that caseins present phosphate group(s) esterified to serine residues. These phosphate groups are important to the structure of the casein micelle. This results in strong association reactions of the caseins, which render them insoluble in water (Bramanti et al., 2001).

## 4.2. Casein Micelle

In milk nearly 80-95% of the casein is in the form of colloiddally dispersed particles, known as micelles. These micelles have ability to scatter light thus the white color in milk is mainly because of light scattering by casein micelles. Electron microscopy studies showed that the shape of casein micelles as spherical colloids, ranging in size from 50-500 nm in diameter (average about 120 nm) and a molecular mass from 106-109 Da (Phadungath, 2005).

Casein micelles take role in transport of large proportion of the minerals (calcium and phosphate) which the newborn requires for bone growth (Horne, 2002). Casein micelles were effected by changing the chemical properties of the environment, e.g. pH and ion strength. Such changes can influence the size and the structure of the casein micelles (Karlsson et al., 2000). In the micelle the caseins are held together by hydrophobic interactions and by bridging of calcium–phosphate nano-clusters bound to serine–phosphate residues of the caseins. Sturcture of micelle is important for their biological activity in the mammary gland. Structural stability of micelles in milk provides stability during processing of milk into various products. Also it is important for good digestibility of the nutrients comprising the micelles. The micelles are very stable to processing, and retain their basic structural identity through most of these processes (Semo et al., 2006).

There are different models for casein micelle structure. The most commonly accepted model in the sub-micelle model category was proposed by Walstra in 1984. In this model, it is suggested that casein micelles are built of roughly spherical subunits or sub-micelles. The composition of sub-micelles is variable and the size is in range 12-15 nm in diameter, and each sub-micelle has 20-25 casein molecules. The sub-micelles are kept together by hydrophobic interactions between proteins, and by calcium phosphate linkages. There are two main types of sub-micelles; one mainly consisting of  $\alpha$ s- and  $\beta$ -caseins, hydrophobic regions buried in the center of the sub-micelle, another type consisting of  $\alpha$ s- and  $\kappa$ -caseins, which is more hydrophilic because of the sugar residues on  $\kappa$ -caseins. The  $\kappa$ -caseins are located near the outside of the micelle with the hydrophilic part of the C-terminal end protruding from the micelle surface to form a 'hairy' layer that will avoid further aggregation of sub-micelles by steric and electrostatic repulsion. Consequently, micelles are stable, and they do not usually



flocculate (Phadungath, 2005). Figure 4.1 shows the structure of casein micelles from the submicelles model.

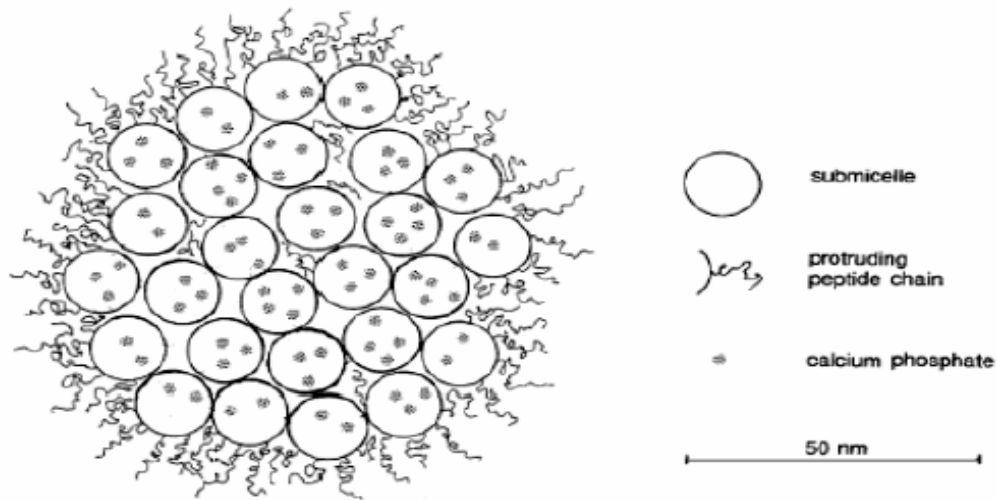


Figure 4.1. The structure of casein micelle in the sub-micelles model showing the protruding C-terminal parts of  $\kappa$ -casein as proposed by Walstra (Source: Phadungath, 2005).

### 4.3. Casein and Health

Casein is one of two major protein fractions in milk. It is about 40% of the protein in human milk and between approximately 78% and 86% of the protein in cow, sheep, goat milks. It is a nutritional source for young mammals and also it is source of a number of bioactive peptides with immunostimulating, antimicrobial, antioxidant activities (Field et al., 2008; Almajano et al., 2007).

#### 4.3.1. Casein as a Nutritive and Immunomodulatory Compound

As the casein is one of the major proteins in milk, with its high percentage; it plays a fundamental role in human nutrition. Until recently, the main physiological role of casein in the milk system was widely accepted to be a source of amino acids required by growth of the neonate. However, the dominant physiological feature of the casein micelle system has more recently been proven to be the prevention of pathological calcification of the mammary gland (milk in an aggregated form known as casein micelles). In several studies these casein micelles were also reported to transport a large

proportion of the minerals (calcium and phosphate) which the newborn required for bone growth (Phadungath 2005; Chatrles and Slatte, 1976).

While no specific physiological property has been proposed for the whole casein system, different peptides, active or inactive are hidden in the amino-acid sequence. They have been the subject of increasingly intense studies according to their biological activities in health area (Silva and Malcata, 2005). Caseinophosphopeptides (CPP) derived from the tryptic hydrolysis of casein, represent phosphoseryl rich peptides with divalent metal sequestering activity. Kitts (2005) indicated that their possible role is to enhance mineral bioavailability and they have been associated with binding of bivalent ions and enhanced solubility of many important minerals, such as calcium and iron

Caseinomacropptide (CMP) is a hydrophilic glycopeptide derived from the action of chymosin on casein during the milk-clotting process (Janer et al., 2004). It comprises the 64 amino acids in the hydrophilic C-terminal portion of  $\kappa$ - casein. CMP may exert important biological activities and this explains the growing interest in CMP as an ingredient in dietetic food and pharmaceutical products.

In Figure 4.2, different roles of the bioactive peptides derived from caseins on different biological systems are given. Different researches have highlighted the ability of CMP to bind cholera and *Escherichia coli* enterotoxins, inhibit bacterial and viral adhesion, modulate immune system responses, promote bifido-bacterial growth, suppress gastric secretions and regulate blood circulation, which are promising applications of the peptide (Worringer et al., 2006).

Presence of several other immunostimulating peptides has been detected in casein and casein peptides were found to exhibit immunostimulatory properties, such as stimulation of phagocytosis by macrophages and enhancement of resistance of animals to a bacterial infection. Also antimicrobial peptides of casein-born were also determined and behavior of those peptides showed similarity with the behavior of some immune system components (Kazlauskaite et al., 2005).

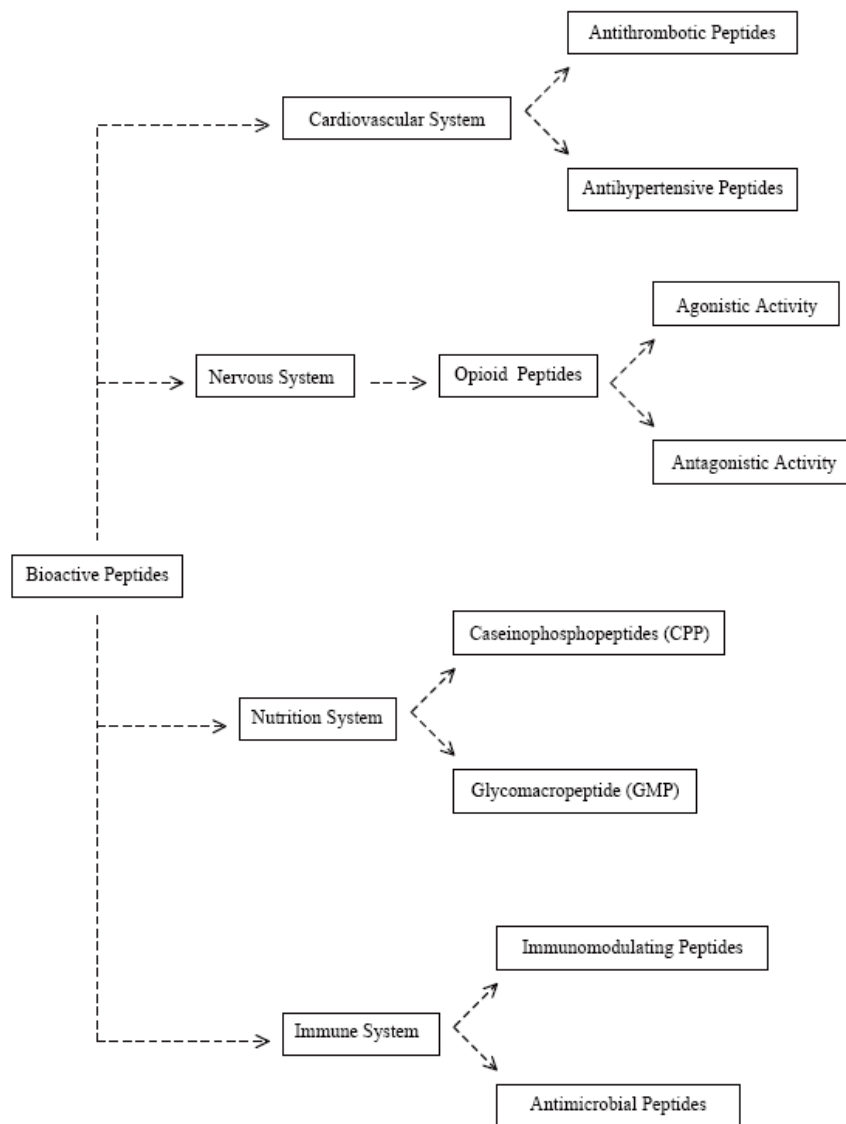


Figure 4.2. Functions of bioactive peptides from caseins (Source: Silva and Malcata, 2005).

### 4.3.2. Antioxidative Property of Casein

Antioxidants are molecules that slow or prevent the oxidation of other chemicals. Oxidation reactions can involve the production of free radicals, which can form dangerous chain reactions. Antioxidants can terminate these chain reactions by removing radical intermediates and can inhibit other oxidation reactions by being oxidized themselves.

$\beta$ -Casein and  $\alpha$ -casein showed radical-scavenging activities in aqueous solution (Almajano et al., 2007). Bzducha and Wolosiak (2006) suggested that antioxidant

activity of casein may be due to capability of free radicals capturing (histidine residues) or reducing them on the way of making the hydrogen atom available e.g. tyrosine, phenylalanine. As it was reported in previous sections that the major casein fractions ( $\alpha$ ,  $\beta$  and  $\kappa$ ) differ from each other in their phosphate content. This phosphate could confer antioxidant activity on casein molecules (Cervato et al., 1999).

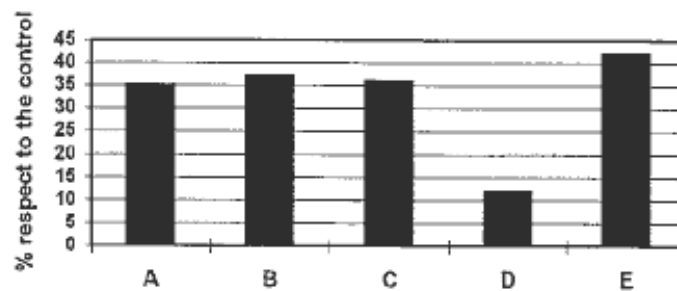


Figure 4.3. Superoxide radical formation for different forms of casein. A:  $\alpha$ -casein, B: dephosphorylated  $\alpha$ -casein, C:  $\beta$ -casein, D: dephosphorylated  $\beta$ -casein, E:  $\kappa$ -casein (Source: Cervato et al., 1999).

Less is known of the affinity of these bioactive peptides to prevent oxidation reactions through possible primary or secondary antioxidant mechanisms. The presence of phosphate groups originating from phosphorylated serine residues in close proximity to the peptide chain creates a polar, acidic domain that is favorable for sequestering divalent metals such as calcium, zinc, copper, manganese and iron. In the case of milk protein casein, the phosphate-bound phosphoserine residues which sequester iron through intermolecular iron bridging have been shown to also act to potentially scavenge superoxide, hydroxyl radicals and stable 1,1-diphenyl-2-picrylhydrazyl (DPPH) and 2,2'-azino-bis(3-ethylbenzothiazoline-6-sulfonic acid) (ABTS) radicals, as well as lower oxidation in iron-induced peroxidation of liposomes containing arachidonic acid (Kitts, 2005). Figure 4.3 shows the capacity of the different caseins to inhibit hydroxyl radical formation:  $\alpha$ -casein,  $\beta$ -casein and dephosphorylated  $\alpha$ -casein, demonstrated the greatest scavenging activity, less activity was shown for  $\kappa$ -casein, and dephosphorylated  $\beta$ -casein proved to have particularly poor scavenging properties (Cervato, et al. 1999).

### 4.3.3. Casein as Enzyme Inhibitor

Casein is source of number of bioactive peptides possess many activities, such as immunoregulatory, opioid, antioxidant, or antihypertensive (Xue-Ying et al., 2007). Therefore based on those properties and as well as being a natural nutritive compound, casein was used in enzyme inhibition studies.

Angiotensin-I-converting enzyme (ACE) is an important enzyme for high blood pressure, heart failure, diabetic nephropathy and type 2 diabetes mellitus. Casein was used as natural ACE inhibitor alternatively to synthetic drugs and it was found that casein hydrolysates of yak milk might be possible health-enhancing ingredient in the production of functional foods (Xue-Ying et al., 2007).

In different studies, it was reported that casein had inhibitory action on glucuronidase enzyme due to its aspartic acid content. The aspartic acid content of casein is of the order of 6 percent. Calculating from the known nitrogen content of aspartic acid and of casein, it was found that about 5 per cent of the total nitrogen of casein is aspartic acid nitrogen (Frost and Hainsen, 1945). Aspartic acid is an  $\alpha$ -amino acid with the chemical formula  $\text{HO}_2\text{CCH}(\text{NH}_2)\text{CH}_2\text{CO}_2\text{H}$ . The L-isomer is one of the 20 proteinogenic amino acids and it is classified as an acidic amino acid, together with glutamic acid (Aspartate, 2007).

In a study, Nutramigen, (United States Patent 6416783), enzymatically hydrolyzed casein, was used to investigate effect of casein on GUS activity. It was reported by Kramer et al (2001) that infants who consume casein hydrolysate formula have been shown to have lower neonatal jaundice levels than infants who consume routine formula or breast milk. Bilirubin is a compound which results from mainly from the breakdown of heme. It is removed from the body via conjugation with glucuronic acid in the liver and excretion as bilirubin glucuronides into the intestine. However, intestinal  $\beta$ -glucuronidases can cleave the glucuronide linkage, releasing free bilirubin that is absorbed from the intestine back into the blood stream. When the bilirubin levels increased in the blood that are associated with neonatal jaundice, it is the most common reason for hospital readmission of newborns. It was found that stool from Nutramigen-fed infants consistently demonstrated significant inhibition of this enzyme activity. It was found that activity was ranging from 45% to 85% of that in controls. Reason behind this was thought to contain a beta-glucuronidase inhibitor in casein structure. This

inhibitor caused blockage of the enterohepatic circulation of bilirubin (Gourley et al.,1997).

Unmodified casein and different milk proteins such as bovine lactoferrin, human lactoferrin, lactoperoxidase  $\beta$ -lactoglobulin,  $\alpha$ -lactalbumin, lactogenin, glycolactin etc. were tested by Wang et al. (2000) according to their  $\beta$ -glucuronidase inhibitory activity and it was found that unmodified casein with 19.27% inhibition showed highest inhibition towards GUS enzyme. In the same study casein showed no inhibitory activity towards HIV-1 reverse transcriptase enzyme which is crucial for HIV-1 replication.

## CHAPTER 5

### MATERIALS AND METHODS

#### 5.1. Materials

In the experimental part of this thesis two natural zeolites were used. Zeolites Z1 (in the rock form) and Z2 (in the powder form) was kindly supplied from Enli Madencilik (Gördes Manisa). In bacterial culture studies, stock *E.coli* (ATTC 8739) cultures obtained from National Center for Agricultural Utilization Research (Peoria, Illinois), nutrient agar, Mueller-Hinton broth and agar were purchased from Sigma-Aldrich Chemical Company (Germany). In cell culture studies Caco-2 (Human, colon adenocarcinoma cell line), MCF-7 (human breast adenocarcinoma cell line) cells were purchased from Şap Institute (Ankara). Dulbecco's Modified Eagles Medium (DMEM), RPMI-1640, fetal bovine serum (FBS), PBS buffer, L-glutamine and penicillin/streptomycin antibiotics were purchased from Biological Industries (Israel). MTT solution and DMSO were purchased from Sigma. Cell Proliferation Kit (XTT) was purchased from Roche (Switzerland). Annexin V-FITC Apoptosis Detection Kit 1 was purchased from BD Pharmingen (US). Culture well plates (12-24-96) and 25-75cm<sup>2</sup> culture flasks were purchased from Corning Incorporated (US). For enzymatic analyses  $\beta$ -glucuronidase (from *E.coli*) and its substrate 4-Methylumbelliferyl- $\beta$ -D-glucuronide and standard 4-Methylumbelliferone sodium salt were purchased from Sigma-Aldrich Chemical Company (Germany). For fluorescent measurements 96-well plates were purchased from Thermo Fisher Scientific (US). For the analytic studies ABTS (2,2-Azino-bis-(3-Ethylbenz-Thiazoline-6-Sulfonic acid), bovine serum albumin (BSA), porcine bile extract, pepsin and pancreatin were purchased from Sigma Chemical Company. Casein was purchased from Merck (Germany). All other reagents used were analytical grade.

## 5.2. Methods

Experimental studies were outlined in six sections. First section was composed of sample preparation and characterization methods. In the enzymatic studies, interactions of the inhibitors and experiments for  $\beta$ -glucuronidase (GUS) inhibition were given. Following section was about the interactions of the inhibitors with *E.coli*, which was a GUS producing bacteria. Then, adsorption studies for casein and GUS onto zeolite and their interactions were explained. Experiments to determine the behaviour of inhibitors in simulated intestinal conditions were also presented. The last section was about experiments for the determination of interactions of zeolite with different cancer cell lines.

### 5.2.1. Sample Preparation and Characterization

#### *Preparation of Zeolites*

Clinoptilolite-rich minerals were crushed, sampling was performed and homogenized zeolite powders were obtained. Crushed samples were settled in distilled water for one day to remove the floating debris. To fractionate the samples, wet-sieving was performed and thus zeolite samples with different particle sizes were obtained. Each fraction was boiled in distilled water before use and were dried overnight at 100 °C in oven and then stored in controlled atmosphere (in fully hydrated dessicator using saturated  $\text{NH}_4\text{Cl}$ ) for further analysis. The 45-75  $\mu\text{m}$  size range was used in further analyzes. Additionally, zeolites at < 25 $\mu\text{m}$  size were purified to obtain clinoptilolite rich minerals. For purification, 15 g of zeolite sample was firstly shaken with 15 ml of boiling deionized water for 5 minutes in a beaker. Boiled sample was settled for 10 minutes and settled phase was separated from the suspended clinoptilolite phase (liquid phase including fine zeolite particles). Then centrifugation was applied to suspended phase at 1000 rpm and settled fine zeolite pellets were collected. This procedure was applied stepwise in triplicate for every suspended phase using fresh distilled-boiling water. Collected phase (coded as CR) was dried and stored in controlled atmosphere (fully hydrated dessicator using saturated  $\text{NH}_4\text{Cl}$ ) for further analyzes.



### ***Preparation of Digested Zeolites***

Simulated digestion studies were important to investigate the effect of in-vitro simulated digestion conditions on zeolites (Z1, Z2, CR) and possible interactions of zeolite with surrounding media. This section included methods for analyzes of both liquid and solid phases obtained from in-vitro simulated digestion and their characterization studies.

To perform these studies, first of all gastric fluid was prepared with 0.1 M HCl including by pH adjustment to 2 using 0.1 N NaOH including pepsin with a final concentration of 3.2 mg/ml. Experiments were performed with or without zeolite (control) samples where zeolite concentrations were 3 g/100ml. Zeolites with different purities used in simulated digestion studies. They were coded as Z1 and Z2 and their purities were 67 % and 87 %, respectively which were determined by RIR method. Digestion fluids were incubated at 37 °C in a water bath shaking at 95 rpm for 1 h. Samples obtained after this step were named as gastric digested samples. Then, the pH of the gastric digested fluid was raised to 5.5 by adding 1 M NaHCO<sub>3</sub> followed by the addition of a mixture of bile extract and pancreatin prepared in 0.1 N NaHCO<sub>3</sub> including amylase, lipase and protease which met the USP specifications. Final concentrations for the bile extract and pancreatin were 2.4 and 0.4 mg/mL, respectively. The pH of each sample was increased to 7.5 by the addition of 1 N sodium hydroxide. Samples were incubated at 95 rpm at 37 °C for 2 h to complete the intestinal phase of the in vitro digestion process. Samples obtained after this complete simulated digestion were named as intestinal digested samples. Then characterization studies were performed for each solid and liquid phases. For ATR-FTIR and ICP analyses, liquid phase of the digested media were immediately placed at -18°C in cryovials for 2h and then they were preserved in liquid N<sub>2</sub> until the day of analysis. For the XRD, SEM and FTIR analyses, samples were frozen at -18 °C for 2 hours and they were freeze dried for 24 h by lyophilizator for the analyses. Same digestion procedure was also applied for the purified clinoptilolite rich sample (CR) which was going to be used in Confocal microscopy analyzes. Flow diagram about the following steps and analyzes for the digested samples were given in Figure 5.1 below.

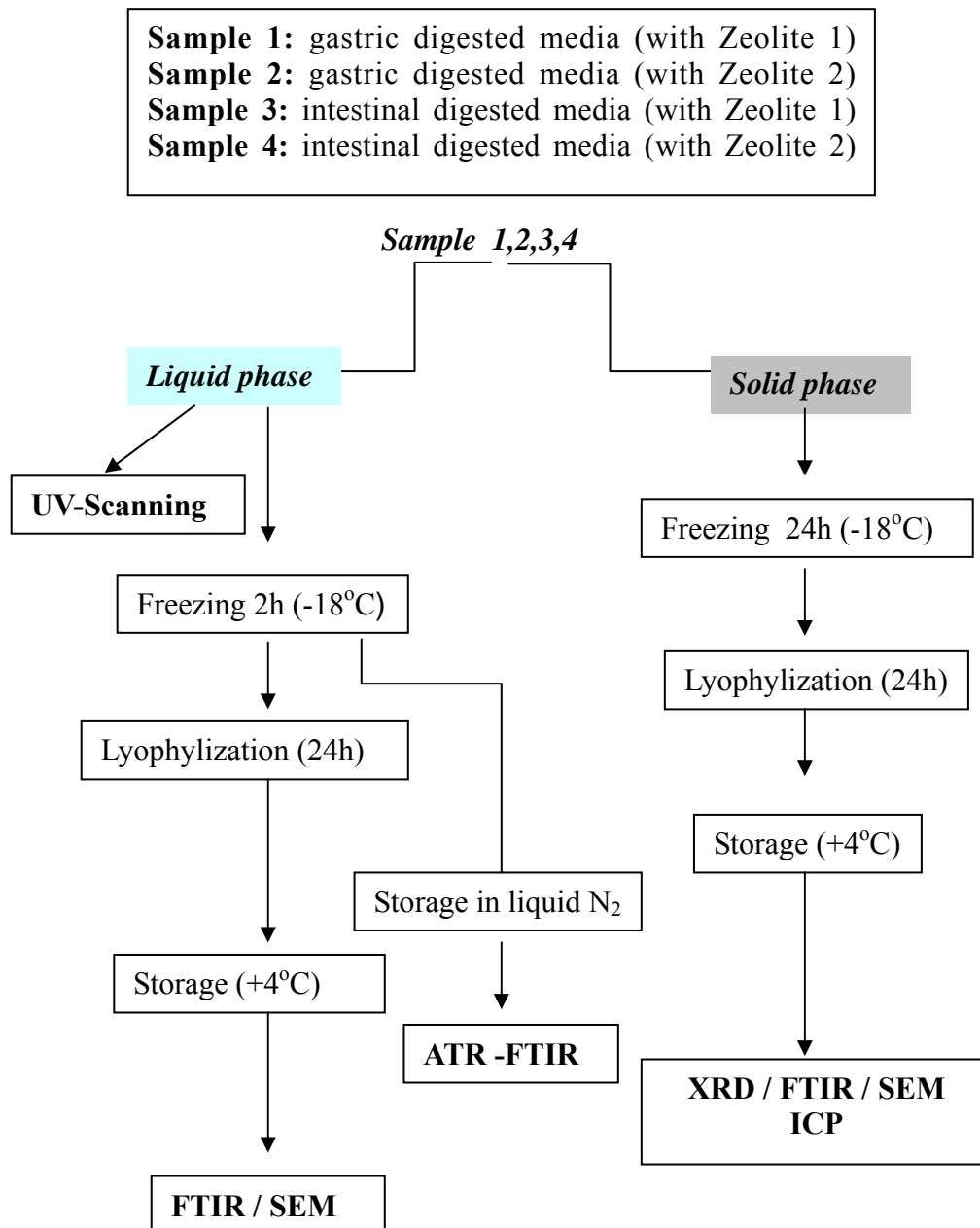


Figure 5.1. Preparation of the digested samples and following characterization steps.

### ***Characterization of the Samples***

To view the surface morphology of zeolite and protein samples, scanning electron microscopy (SEM) was used. Photographs were taken at an accelerating voltage of 15 kV, depending upon the sample at different magnifications in a Phillips XL30S FEG electron microscope. Additionally, using EDX detector qualitative and quantitative analyzes were performed for elemental analysis in 5 replicate and the results were given as the average of those measurements.

IR characterizations for zeolite and protein samples were carried out between

400 and 4000  $\text{cm}^{-1}$  with Shimadzu FTIR-8201 model Fourier Transformed Infra-red Spectrometer using KBr pellet and ATR technique. KBr pellets were prepared by pressing 2 mg sample and 200 mg KBr.

Thermogravimetric analyses for the zeolite samples were performed using Shimadzu TGA-51/51H. The thermal analysis was carried under a nitrogen stream at a heating rate of  $10^{\circ}\text{C}/\text{min}$  from 25 to  $800^{\circ}\text{C}$ .

3000 HAS model Zeta Sizer was used in order to determine the zeta potentials and surface charges of the zeolite and protein samples in the solution (pH 5.5-6.8-8 potassium phosphate buffer).

To determine the chemical compositions of the zeolites, solid samples were prepared by fusion dissolution method and liquid samples were diluted using 5 v/v %  $\text{HNO}_3$ . Fused samples and working solutions (SIF) samples were analyzed using Varian ICP /AES (Inductively Coupled Plasma Atomic Emission Spectrometer) or ICP/MS. For solid samples; 0.1 g of sample was mixed with 2 g of lithium tetraborate. Mixture was fused in furnace at  $1000^{\circ}\text{C}$  for 1h minutes. Formed glass bead was dissolved in 1.6 M  $\text{HNO}_3$  solution on a magnetic stirrer. Solution was completed to 250 ml by ensuring 5 v/v % of 65 %  $\text{HNO}_3$  and diluted if necessary. Standard solutions were prepared at different concentrations and samples' elementary concentrations were determined after analyses according to those calibration curves.

Mineralogy of the original zeolite and the crystallinities of the treated zeolite were determined by powder X-ray Diffraction techniques (Philips X-Pert Pro) using  $\text{CuK}\alpha$  radiation in the range of  $2\theta$ :  $2^{\circ}$ - $40^{\circ}$  with  $0.2^{\circ}$  step size. The quantitative mineralogical analysis was carried out using the Reference Intensity Ratio (RIR) technique (Narin, 2009, Nakamura et al., 1992) Reference mineral used for quantitative analysis is clinoptilolite with >90 % clinoptilolite content (27031, Castle Creek, Idaho; Mineral Research, New York) supplied kindly by F. Mumpton in powder form. Clinoptilolite contents of control samples were found 67 % for Z1 and 87 % for Z2 and 91% for CR, respectively.

The BET surface area of zeolites and adsorption capacity were determined by  $\text{N}_2$  physisorption studies performed at 77.45 K using Micromeritics ASAP 2010 model static volumetric adsorption instrument. The samples were dried in oven at  $200^{\circ}\text{C}$  for 3 hours prior to degassing and degas conditions were adjusted as  $350^{\circ}\text{C}$  and 24 hours under vacuum ( $10^{-5}$  mbar). Adsorption data were collected in the relative pressure range (P/Po) of 0.05 to 0.2.

Density of the zeolite was measured Helium Picnometer. Particle size measured was done by Sedigraph S100 Particle size analyzer. For analysis, 1 g zeolite sample was suspended in 50ml of 50% (w/w) glycerol-water solution. Samples were ultrasonicated for 10 minutes before analysis.

### **5.2.2. Enzymatic Studies**

Enzymatic studies were performed in order to investigate the inhibitory potential of two possible inhibitor “zeolite” and “casein” for microbial GUS enzyme activity, their interactions and effect of those inhibitors on *E.coli* bacteria which was the main microorganism responsible for the production of GUS. All experiments were performed in solution that simulates intestinal fluid (SIF) which was phosphate buffer at pH 6.8. This solution met optimum working conditions for GUS activity (recommended by the purchaser instructions) and also met the requirements of United States Pharmacopeia (2003).

#### ***Determination of Interactions for Zeolite, Casein and GUS***

To determine the possible interactions solutions containing enzyme, zeolite and casein were prepared and effect of time was investigated. Total volume of the solutions were 1.2 ml where 0.2 ml enzyme (from enzyme stock solution of 0.575 mg/ml) and 0.2 ml casein were added in well-plates. Final concentrations of casein and zeolite in mixture were 0.125 mg/ml and 25 mg/ml, respectively and in 24-well plates where incubations were performed at 150 rpm and 37°C. Changes in the enzyme activity (alone) and stability of components (combinations of solutions containing zeolite, GUS and casein) was measured at 375 and 200 -380 nm in UV region using microplate reader (Varioskan, Thermo) within the time intervals of 0, 2.5, 5, 10 and 0, 10, 30, 60, 120, respectively.

#### ***Enzyme Inhibition Experiments***

Inhibition studies were performed to investigate the inhibitory potential of two possible inhibitor “zeolite” and “casein” for GUS enzyme activity. Michaelis Menten approached was applied to determine the model constants;  $K_m$  and  $V_{max}$  in order to identify the types of the inhibition. Standard curve for the GUS enzyme activity was

performed using 4-MU (4 methylumbelliferone sodium salt) as a standard at a concentration range of 0-2000 nM. To measure GUS enzyme activity, substrate 4-MUG was added into treated and untreated cell lysates. Activity determination method and standard curve were given in App. A.1. To obtain model parameters effect of different initial substrate concentrations on velocity of enzymatic reaction was investigated. To perform these studies temperature and pH were kept constant at 37 °C and 6.8 (phosphate buffer), respectively which were the optimum working conditions for the enzymatic activity. Initial concentrations of substrate 4-Methylumbelliferyl- $\beta$ -D-glucuronide trihydrate (4-MUG) used in this experiments were 0.71, 1.42, 2.13, 2.84, 4.26, 4.97, 7.1, 9.93  $\mu$ mole/L. Total reaction volume of these solutions containing enzyme and inhibitors were 1.2 ml where 0.2 ml enzyme (from enzyme stock solution of 0.575 mg/ml) and 0.2 ml casein were added in well-plates. Final inhibitor concentrations in reaction mixture were 0.125 mg/ml and 25mg/ml for casein and zeolite, respectively. Solutions were incubated for 30 minutes in 24-well plates at 150 rpm at 37°C. After incubation, enzyme activities in sample solutions were analyzed for GUS activity in triplicate and results were given in terms of velocities where velocity of the reaction was defined as  $\mu$ M 4-MU formed per minute per  $\mu$ g solid. Double reciprocal plots were plotted and kinetic parameters for the inhibition studies were calculated (see information about double reciprocal plots in Appendix A.2).

To investigate the effect of different inhibitors at different concentrations on enzyme activity, 0.125 and 0.175 mg/ml for casein and 25 mg/ml for zeolite were used. Only enzyme samples were used as control samples and percentage (%) remaining activities were calculated for the samples containing inhibitors. Sample calculation for the remaining activity was given in (App.A.3.)

### **5.2.3. Zeolite, *E.coli* and Casein Interaction Experiments**

*E.coli* was one of major GUS producing bacteria in intestinal system therefore findings of any overgrowth inhibitory effect using casein or zeolite for this organism would be helpful for regulating intestinal flora. The first experiments were based on the confirmation that *E.coli* was GUS positive. For this aim, stock *E.coli* cultures were inoculated on Nutrient agar (Merk) and incubated at 37°C for overnight (o/n). One colony was picked up and dissolved in tube including 2 ml of distilled water at a cell

suspension density adjusted by McFarland 0.5 Standard. From this tube bacterial suspension was pipetted to test tubes including Mueller-Hinton broth and incubated o/n at 37°C. Enzyme of  $\beta$ -glucuronidase (GUS,) was extracted by cell lysis method. Phosphate buffer (pH.6.8) including 0.1% Triton X-100 (Sigma) was prepared and enzyme substrate 4-methylthium belliferone glucuronide trihydrate (4-MUG) was added at a final concentration of 2 or 4  $\mu$ g/ml. 0.5ml of cell suspension was added into that lysis solution and mixture was vortexed for 1 min (2000rev/min), then mixture was incubated for 5 or 10 minutes at dark, at 37°C and fluorescent luminance was checked under UV which indicates *E.coli* was GUS positive.

#### ***Antimicrobial Tests for E.coli using Zeolite***

To investigate the effect of zeolite on *E.coli* growth, antimicrobial tests were performed. Stock *E.coli* cultures (stored at -80°C) were inoculated on Nutrient agar and incubated at 37°C for overnight (o/n). One colony was picked up and dissolved in tube including distilled water (dw) at a cell suspension density adjusted by McFarland 0.5 Standard. From this tube bacterial suspension was pipetted to test tubes including Mueller-Hinton broth (Merk). To investigate the effect of zeolite concentration, zeolite samples added to the test tubes at concentrations of 10, 03 and 50 mg/ml and incubated o/n at 37°C. Following day, suspensions were diluted up to  $10^{-4}$  and suspensions inoculated on petri dishes in triplicate including Mueller Hinton agar (Merk) by spread plate technique, incubated o/n and colony count was performed. Results were given as cfu/ml and cell growth %. Bacterial suspension that cultured without adding zeolite were used as positive control and zeolite incubated in broth used as negative control. Results were given in cfu/ml.

#### ***MIC (Minimum Inhibitory Concentration) Tests for E.coli Using Casein***

To investigate the effect of casein on *E.coli* growth, 100 $\mu$ L of casein solution at different initial concentrations (0, 0.9, 1.5, 3, 7.5, 15  $\mu$ g/ml) and 95  $\mu$ L nutrient broth were added in 96 well microplate. Each well was inoculated with 5  $\mu$ L suspension of 6h incubated *E.coli* suspensions after being standardized by adjusting their optical densities at 420 nm by UV spectrophotometer (Perkin Elmer). The assay plates were incubated at 37 °C for 24 h. and the growth kinetic assays of *E.coli* strain were performed by growth curves and observed as turbidity which was determined by a microplate reader (Varioskan Flash, Thermo) at 620 nm. Collected data used for the determination of the

specific growth rates and generation times (App.A.4).

#### **5.2.4. Adsorption Experiments**

To understand the mechanism of casein and GUS adsorption and to propose appropriate models for the kinetics and equilibrium of adsorption, batch kinetic experiments were conducted against time using shaker water bath for 2.5 and 7 hours for casein and zeolite, respectively. 100  $\mu$ l of samples taken from the sorption media at different time intervals and were used in protein analyzes. Solutions of casein samples were analyzed by Bradford Method, (given in App.A.5) and GUS samples were analyzed for their UV absorbances at 255 nm which is the wavelength of the maximum absorbance. Zeolite free samples were used as control. Kinetic and equilibrium models were applied to determine the rate constants, thermodynamic and equilibrium parameters in order to identify the mechanism of the adsorption. Experimental conditions in kinetic experiments for the GUS and casein adsorption were given in Tables 5.1 and Table 5.2.

Table 5.1. Experimental conditions of various kinetic adsorption experiments for the GUS adsorption onto digested zeolite (Z1) at a constant working volume of 2 ml.

Parameter	Particle size*	Initial enzyme concentration ( $\mu\text{g/ml}$ )	Agitation speed (rpm)	Temperature ( $^{\circ}\text{C}$ )	pH	S/L
Particle size	Coarse, mid, fine	100	150	37	6.8	5
Initial casein concentration (mg/ml)	mid	20,50,100,150,200,300,500	150	37	6.8	5
Agitation speed (rpm)	mid	100	50, 100, 150	37	6.8	5
solid liquid ratio(s/L: mg/ml)	mid	100	150	37	6.8	3,5,10
pH	mid	100	150	37	5.5,6.8,8	5
Temperature ( $^{\circ}\text{C}$ )	mid	100	150	15, 25, 37	6.8	5

\*Coarse: 75-106, mid: 45-75; fine: 25-45 $\mu\text{m}$



Table 5.2. Experimental conditions of various kinetic adsorption experiments for the casein adsorption onto digested zeolite (Z1) at a constant working volume of 10 ml.

Parameter	Particle size*	Initial casein concentration (mg/ml)	Agitation speed (rpm)	Temperature (°C)	pH (constant)	S/L (mg/ml)
Particle size	coarse, mid, fine	0.125	150	37	6.8	5
Initial casein concentration (mg/ml)	mid	0.06, 0.125, 0.41, 0.7, 0.99, 1.2, 1.25	150	37	6.8	5
Agitation speed (rpm)	mid	0.125	50, 100, 150	37	6.8	5
solid liquid ratio(s/L: Ug/ml)	mid	0.125	150	37	6.8	2,5,7
Temperature (°C)	mid	0.125	150	15, 25, 37	6.8	5

\*Coarse: 75-106, mid: 45-75; fine: 25-45 $\mu$ m

### 5.3. Control of the Behaviour of Inhibitors in SIF Conditions

As the proteins may lose their stability for longer incubation times, effect of time on the stability of casein in SIF solution was investigated. Changes in absorbance of casein solutions of 1.25 mg/ml were recorded after incubations of 0, 10, 30, 120, 300, 420, 1440, 1800 minutes.

Effect of zeolite on the pH of the working solution was investigated for the same time range where zeolite concentration was 5mg/ml. Additionally ICP analyzes (Varian ICP -AES) were performed for the same conditions at different time intervals of incubations for batch solutions in order to analyze the change in the elementary composition of the working solution.

Antioxidant activities of zeolite, raw casein and casein in SIF conditions were investigated which was important for the compounds since that mechanism has a role in neutralization of harmful free radicals. Antioxidant activity determination procedure was given in App. A.6 where the working concentrations of the zeolite and casein were 0.5, 1 and 3 g/100ml; 0.9, 1.5, 3 mg/ml for zeolite and casein, respectively.

Effects of electrostatic charges in adsorption were also investigated. The zeta potential and average diameter of casein micelles during adsorption in pH 6.8 phosphate buffer were determined using a Zetasizer 3000 HS (Malvern instrument, Malvern, UK) and Zeta Potential Instrument, respectively. Samplings for the measurements were done at time of 0-4h-6h of incubation of the batch solutions. Before measurement, solutions including casein samples were 100 times diluted with SIF and measured in triplicate at 25°C. Results were expressed in absolute values and the experimental error was given as  $\pm$  mV.

As the spectrums of proteins were sensitive to micro-environment, fluorescence and UV spectrum data of the same samples were collected to investigate the possible interactions between zeolite and the casein. 100  $\mu$ l of casein solutions used in adsorption studies (casein concentration was 1.25 mg/ml) incubated in SIF at pH 6.8 for 0-4-6h and used for UV absorbance spectra in the range 200–380 nm using by microplate reader (Varioskan, Thermo). For the fluorescence measurements, 100  $\mu$ l of same samples from the same sets of solutions were used. Measurements were performed using 2 cm excitation light path and emission spectra in the range 300–500 nm and were recorded

with a fixed excitation wavelength of 295 nm using fluorometer (Varioskan Flash, Thermo). All spectra were averages of three scans, corrected by subtraction of the appropriate blank (caseins free samples) spectrum.

For the characterization of the interaction solutions including 5mg/ml zeolite and 1.25 mg/ml casein, solutions were incubated for 4h and 6h. Then, liquid and solid phase were frozen 2h at -18°C separately. After freezing, they were lyophilized for 24h. Lyophilized samples were gently collected and sealed in eppendorfs and kept at +4 °C until analyses of FTIR, SEM to investigate the effect of zeolite. Zeolite free samples (only casein) were used as control samples. To investigate the stability of casein in SIF during adsorption and to determine the thermodynamics of protein unfolding, thermal behaviour measurements were performed by Shimadzu Differential Scanning Calorimeter (DSC-50) using aluminum seal cells. Approximately 2.5 mg of sample was weighed into the aluminum pans. The pans were hermetically sealed and the measurements were performed under nitrogen atmosphere at a rate of 40 ml/ml where the temperature range was 25 to 220 °C and the heating rate was 10 °C/min. The onset temperature ( $T_{\text{onset}}$ ), the peak temperature ( $T_{\text{peak}}$ ) and the enthalpy of denaturation ( $H_D$ ) were calculated.

### **5.3.1. Zeolite-Cancer Cell Interaction Experiments**

Natural zeolite clinoptilolite, have been shown to exhibit diverse biological activities and reported as possible adjuvant in anticancer therapy. In this section, methods to investigate possible interactions of natural zeolite with different cancer cell lines: Caco-2 (human colon adenocarcinoma) and MCF-7 (human breast cancer) cell lines were given.

Caco-2 cells were cultured in Dulbecco's Modified Eagle Medium (DMEM) supplemented with 10% FBS, 1% L-glutamine, 1% nonessential amino acids, and 50 µg/mL penicillin-streptomycin. MCF-7 cells were cultured in RPMI-1640 supplemented with 10% FBS, 1% L-glutamine, 1% nonessential amino acids, and 50 µg/mL penicillin-streptomycin. The cell cultures were maintained at 37 °C in a 95% humidified atmosphere with 5% CO<sub>2</sub> where they were seeded onto collagen-coated 25 cm<sup>2</sup> area culture flasks. Caco-2 cells were feeded twice weekly and were subcultured (passaged) with 0.25% trypsin and 0.2% EDTA (5–10 min) at 37°C and seeded in new flasks for

every 10-14 days. MCF-7 cells were passaged every week.

For the zeolite treatments cells were harvested by trypsinisation after 80% confluency was reached during culturing. They were seeded at a density of  $10^5$  cells/cm<sup>2</sup> in 96-well plates (Becton Dickinson, Meylan, France). Culture medium was changed (feeding) two times a week systematically before zeolite treatments. Zeolite samples were sterilized and added in culture media so that the final zeolite concentrations were 25, 50 and 75 mg/ml. then culture media was incubated for 24, 48 and 72 h with the presence of zeolite. After incubation treated media was distributed into wells in triplicate where Caco-2 cells were seeded. Positive and negative controls were prepared and incubated in the same manner as the experimental specimens and after 24, 48 and 72 hours; cell proliferation assays of MTT and XTT (see App.A.7 and A.8 for MTT and XTT, respectively) were performed to measure the cell proliferation after zeolite exposure where possible metabolic events after exposure might lead to apoptosis or necrosis, the reduction in cell viability.

### ***Confocal Microscopy Experiments***

To determine the possible internalization of the zeolite particles by Caco-2 cells, Z1 and CR samples were hand-milled by agate mortar to decrease their particle size. For the preparation of the cells, glass slides were incubated in methanol overnight, dried among the drying paper and autoclaved. Those slides were carefully placed on the 6-well plates. 2ml of culture media including cells were added and seeded overnight. 6 well plates Caco-2 cell were seeded on 6-well plate at a density of  $5 \times 10^5$  cell/well. Cells were incubated in culturing conditions overnight. Sterilized zeolites (digested Z1 and digested CR) were added in the culture media at concentrations of 0.5, 5 and 25 mg/ml and incubated for 1 and 2 hours. Slides were picked up from the culture surface and investigated under confocal microscope (Andor, Revolution, Disc Spinning Microscope, Camera:DV897-BV2751). Illumination time for the observation was 100-400ms where samples were excited at 488nm

### ***Determination of Zeolite -Culture Media Interactions***

During zeolite treatments, zeolite may interact with the cell culture media and may alter pH. Besides, there could be exchange of ions between media and zeolite. Those changes in pH and ion content in media were important parameters and should be determined for the cell growth. Media samples treated 18h and 24h with 25; 50 and

75mg/ml zeolite were used for the pH and conductivity measurements (WTW pH330i). Non-treated samples were used as control samples. Color changes in treated media and in control samples were displayed by digital photograph (Nikon L20). Then effect of zeolite treatment and on elementary composition of the media was investigated in triplicate by Inductively Coupled Plasma Mass Spectrometry (Agilent 7500 Series Octapole Reaction system).

### ***Determination Effect of Zeolite on Cancer Cell GUS Activities***

As the cancer cells produce GUS enzyme, effect of zeolite treatment for the cancer cell glucuronidase activity were determined. Lower concentrations of zeolite (25mg/ml) were chosen and time of zeolite treatment was 60 min. in order to preserve cell viability for checking glucuronidase activity. Sterile zeolite samples were added to media (RPMI-1640 and DMEM) and media was incubated at 37°C 120 rpm for 60 min and centrifugated for 3000 rpm 5 min to separate zeolite. Supernatants were added to cells in 25 cm<sup>2</sup> flask.

For the extraction of GUS enzyme from the cancer cells, Caco-2 cells and MCF-7 cells were cultured as culturing procedures given previously. After 80% confluency (for Caco-2) and confluency (for MCF-7) was reached, cells were washed with 5-10 mL PBS. Treated and control media were added on to flasks and cells were incubated for 60 min at 37 °C in a humidified atmosphere with 5% CO<sub>2</sub> for cell lysate preparation..

To prepare cell lysates, culture medium was decanted, and cells were washed with 5-10 mL of PBS. The cells were harvested by trypsinization. Cell suspensions were centrifuged at 800g for 5 min and washed twice with 5 mL of PBS. Supernatants were discarded and cell pellets resuspended in 2 mL of PBS at 0 °C and then placed on ice. Cold cells were lysed using a mini-bead beater (Biospec Products, Bartlesville, OK) for ~10 s at 4200 rpm. The lysates were centrifuged (Beckman GS-15R centrifuge) at 14000g for 10 min at 4 °C and supernatants that kept on ice were immediately used for GUS enzyme activity assays.

During assays, cell viability should be preserved in order to obtain GUS enzyme. Therefore cell viability was assessed using the trypan blue dye exclusion method. A suspension of ~10<sup>6</sup> cells/ml was prepared using brief trypsinization of treated and untreated cells. One hundred microliters of the cell suspension was mixed with 100 µl of trypan blue and left for 5 min at room temperature. Approximately 18 µL of this mixture was transferred using a micropipet to the counting chamber of a hemocytometer

and the stained (dead) cells and viable cells per were counted under an optic microscope (Olympus CX31).

To measure GUS enzyme activity, substrate 4-MUG was added into treated and untreated cell lysates. After 5 min incubation, reaction was terminated by carbonate stop buffer and enzyme activities in samples solutions were analyzed triplicate for GUS activities by microplate reader (Varioskan, Thermo) using 96-wells at 360  $\lambda_{ex}$ / 450  $\lambda_{em}$ .

### ***Cell Cycle and Apoptosis Analysis***

To define the cell cycle distribution and the apoptosis rate, treated MCF-7 cells were trypsinized, pelleted, fixed, and propidium iodide stained by using a detection kit from BD Biosciences (San Jose, CA) according to the manufacturer's instructions. Propidium iodide staining fluorescence of individual cells was analyzed by using a FACSCalibur flow cytometer apparatus (BD Biosciences, San Jose, CA) and the MODFIT DNA analysis software. For each sample, at least 20,000 events were stored.

Apoptosis was additionally evaluated to treated cells by using annexin V-FITC staining technique. Briefly, trypsinized MCF-7 cells were collected, including floating apoptotic cells and the cells spontaneously detached during washing procedure, and annexin V-FITC stained by using a detection kit from BD Biosciences (San Jose, CA) according to the manufacturer's instructions. Fluorescence analysis was performed by a flow cytometer apparatus (BD Biosciences) and the CELL QUEST analysis software. For each sample, at least 20,000 events were stored. Quadrant settings were based on the negative control.

## CHAPTER 6

### RESULTS OF CHARACTERIZATION STUDIES

Characterization of zeolites facilitates the closer examination of the critical properties of samples such as changes in their water and elementary content, their size, shape, and morphological properties at various stages in experimental applications. Those techniques improve understanding of the significance of the applications considering their reasons. Therefore in this chapter results of primary characterization studies were given for the main two zeolite samples with different purities used in experimental studies.

In sample preparation studies the obtained fractions after wet sieving were in the ranges of;  $<2\ \mu\text{M}$ ,  $2\text{-}25\ \mu\text{M}$ ,  $25\text{-}45\ \mu\text{M}$ ,  $45\text{-}75\ \mu\text{M}$ ,  $75\text{-}106\ \mu\text{M}$ , and  $>106\ \mu\text{M}$ . Size of zeolite was important because smaller sized particles result some difficulties in experimental applications especially in separation (settling, centrifugation) processes.

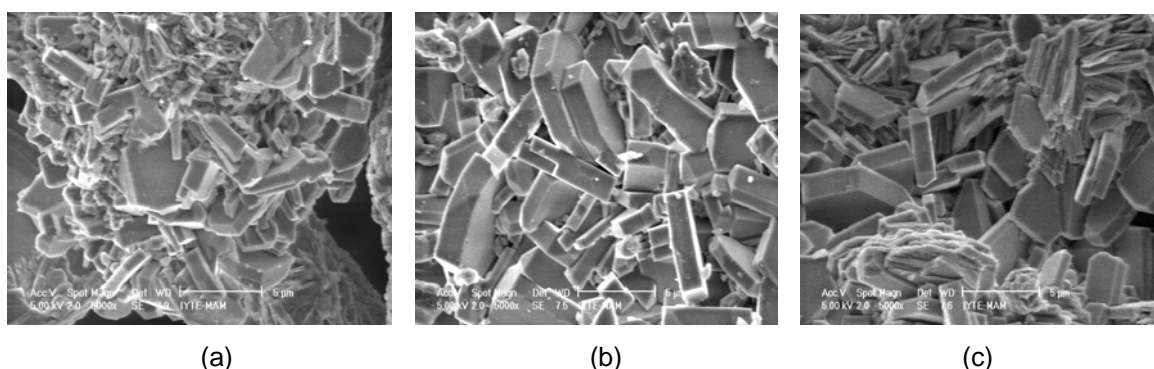


Figure 6.1. Scanning electron micrographs zeolite samples (a)  $25\text{-}45\ \mu\text{m}$  (b)  $45\text{-}75\ \mu\text{m}$  and (c)  $75\text{-}106\ \mu\text{m}$ .

By the SEM picture of the samples (Figure 6.1), in which classical clinoptilolite– heulandite family of zeolite crystals was observed. Crystals were easily seen in each fraction but better crystalline structures were in (b) and (c). It was important to note that zeolite samples with smaller particle size would have higher external surface area and also would have higher adsorption capacity. But in experiments especially where biological materials were also used, a non-soluble (zeolite) material would lead some important experimental problems. Such as, separation (centrifugation,

settling) of zeolite from the whole sample would be a time consuming step where rate of the experiment complementation is a limiting case especially in enzymatic studies. Thus, for the samples with smaller sizes, there would have some difficulties but with the larger sized samples, their high precipitation rate might help separation. Therefore fraction of 25-45 $\mu\text{m}$  was chosen for further analysis due to its high amounts, acceptable size for analyzes and high quality crystalline pictures obtained by SEM. Density of that fraction was calculated as 2.28 g/cm<sup>3</sup> with the aid of Helium piknometer.

Sample fraction of 25-45 $\mu\text{m}$  was coded as Z1 (from Enli Madencilik), and another clinoptilolite rich sample with high purity was coded as Z2 and they were used in further experimental studies. Additionally, this fraction was purified and characterization experiments were also performed for that sample. Purified sample was coded as CR. Purities of those samples were approximately calculated by Reference Intensity Ratio (RIR) technique and used for the determination of the clinoptilolite content of the zeolites (Narin, 2009; Nakamura et al., 1992). Purities of the samples were found as 67% and 87 %for Z1 and Z2, and 91 % for CR respectively.

Particle size analysis were performed for all samples and results were given in Figures 6.2-4.

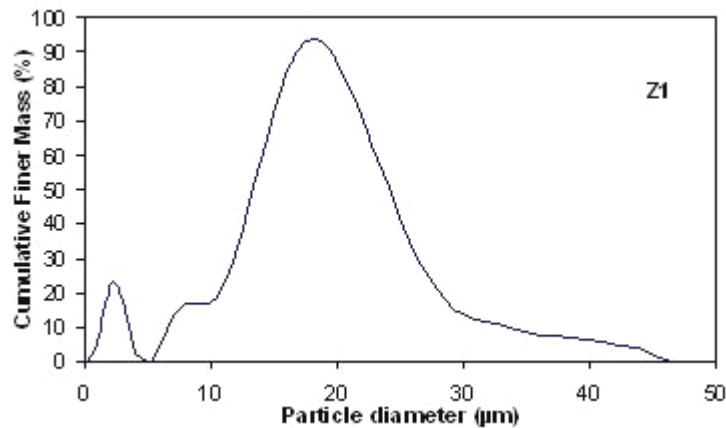


Figure 6.2. Particle size distribution for Z1.



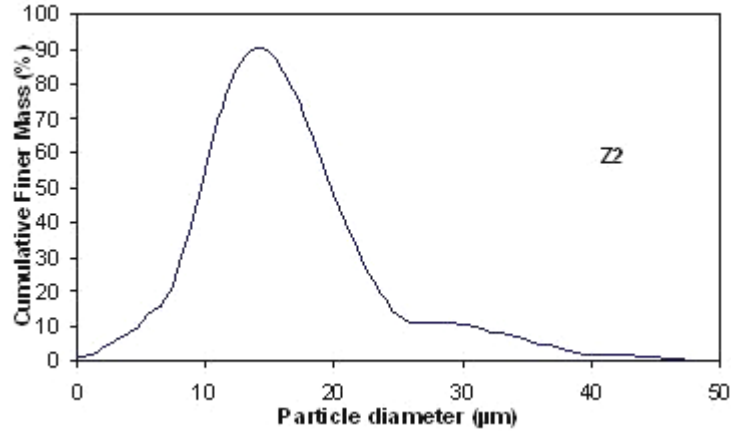


Figure 6.3. Particle size distribution for Z2.

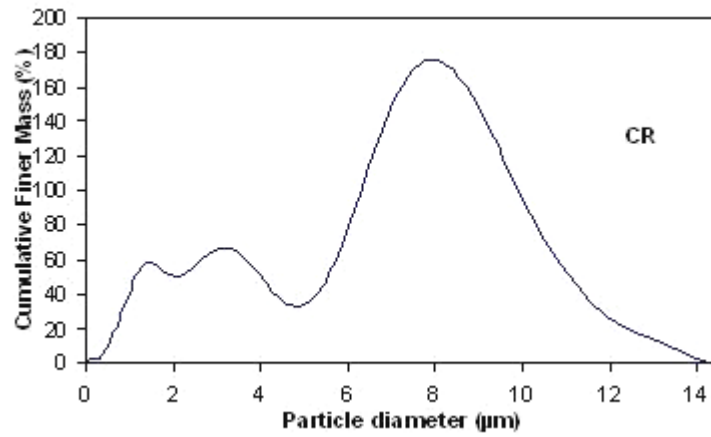


Figure 6.4. Particle size distribution for CR.

To determine elementary composition of zeolites elementary analysis using ICP/AES were performed. Elementary compositions of those two samples were given Table 6.1 below.

Table 6.1. Elementary composition (mg element/g zeolite sample).

Elements	Sample Z1	Sample Z2	Sample CR
Al	75.3	70.6	73.3
Ca	14.8	13.1	12.4
Fe	14.6	15.1	13.6
K	18.9	17.3	17.4
Mg	0.5	6.6	0.2
Na	11.9	3.5	2.6
Si	375.0	366.6	380.3
Si/Al	4.98	5.19	5.18

The Si/Al ratio was significant for the classification of the zeolitic material as Heulandite-Clinoptilolite rich. The material can be classified as high-silica heulandite, low-silica clinoptilolite and highsilica clinoptilolite for the Si/Al range of 3.5-4, 4.0-4.5 and 4.5-5.5 respectively (Tsitsishvili et al., 1992). ICP/AES results indicated that the Si/Al ratios were high for all three zeolite which indicated that samples were high silica clinoptilolite.

Intake of some trace elements with zeolite is also important because they could be toxic for the organism. It was known that some living microorganisms and humans need different concentrations of heavy metals for their metabolic activities such as iron, cobalt, copper, manganese and zinc. Besides tolerable intake values of heavy metals for human were determined by regulations for time periods. According to this, lead (Pb) and cadmium (Cd) were known as toxic. The oral intake of cadmium from food and water is estimated to be 10-35 mg per day (WHO 1993) and provisional tolerable weekly intake (PTWI) of Cd and Pb were 7 and 25 µg/kg body weight respectively. Akdeniz (2009) investigated the trace element composition of the zeolite sample and results were quite lower than PTWI values where <10 ppb and 48.72 ppb were determined for Cd and Pb, respectively. Other trace element composition for the zeolite sample were found as <30, <10, 150, <5 ppb for Co, Cr, Cu and Ni, respectively.

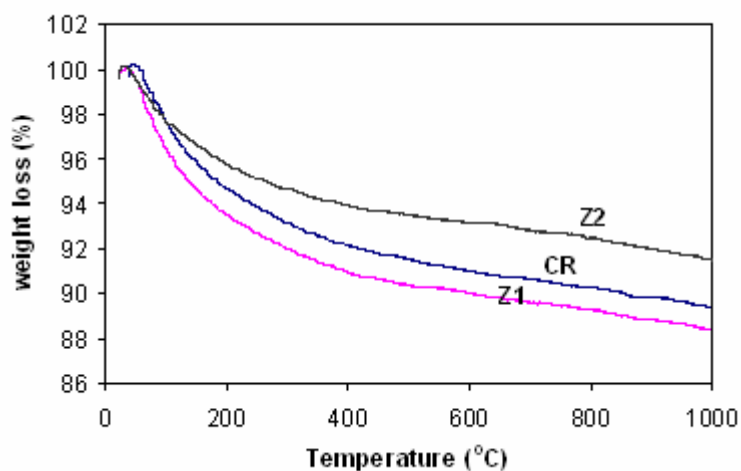


Figure 6.5. TGA curves for Z1, Z2 and CR

Results of the thermal gravimetric analyzes were given in Figure 6.5. The amount of water desorption, determined by TGA and no phase transformation occurred. The weight loss indicating water content was in the 11.02, 13.3 and 10.6 % for Z1, Z2 and CR, respectively. These values were close to clinoptilolite samples reported in the study performed by Akdeniz (1999).

Samples were also analyzed by ASAP2010 for sorption properties using N<sub>2</sub> gas at 77.6 K and results were given in Table 7.3 below. CR samples showed the highest surface area.

Table 6.2. Analysis results of ASAP2010

Sample	Langmuir	BET	Horvath-Kawazoe	
	Surface area (m <sup>2</sup> /g)	Surface area (m <sup>2</sup> /g)	Maximum pore volume (cm <sup>3</sup> /g)	Median pore diameter(A)
Z1	54.951	37.699	0.01842	8.6202
Z2	59.893	41.701	0.01861	9.273
CR	79.7968	55.7633	0.02472	8.1101

Pore size distributions of the samples were given in Figures 6.6-8 below. Results showed that zeolites have a mesoporous structure. Distributions of pore sizes were high approximately in the range of 25-120 Å.

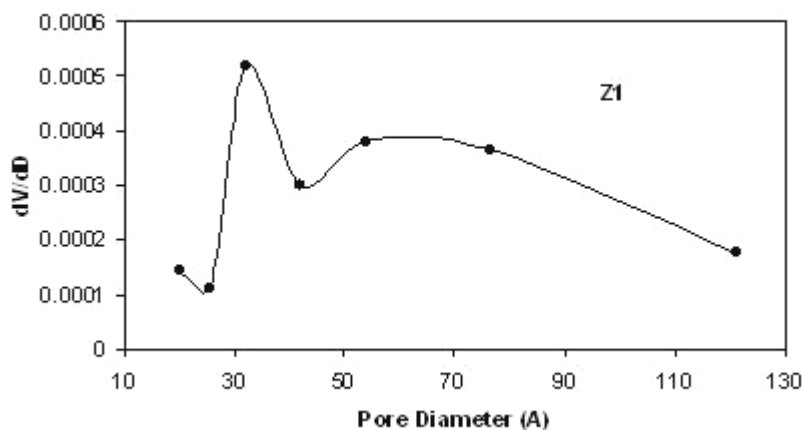


Figure 6.6. Pore size distribution for the Z1 sample.

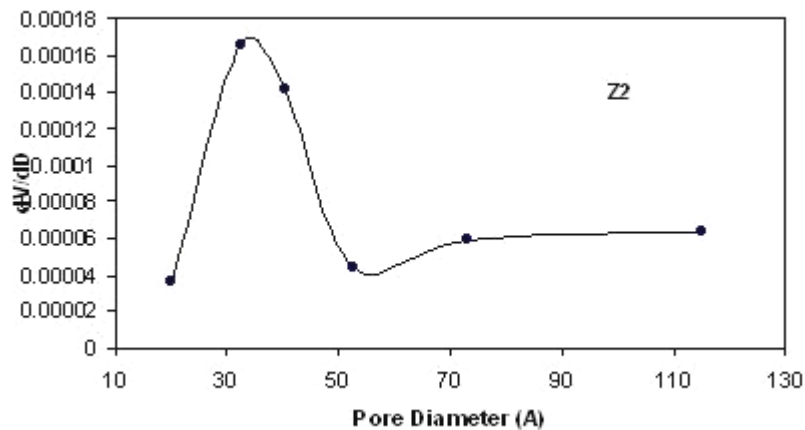


Figure 6.7. Pore size distribution for the Z2 sample.

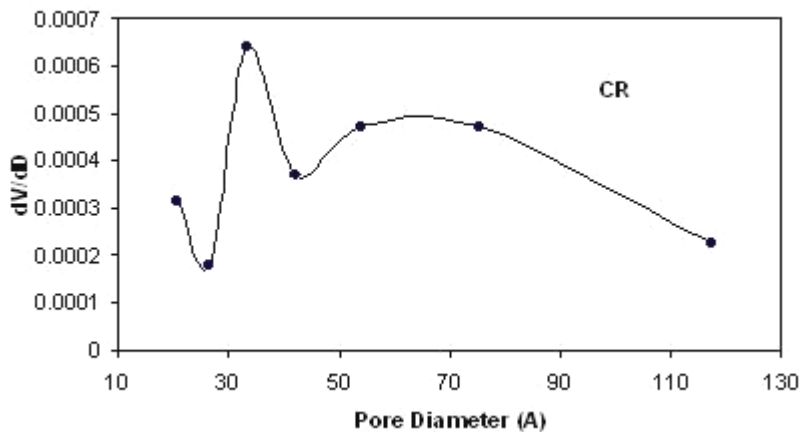


Figure 6.8. Pore size distribution for the CR sample.

XRD analyzes of the samples were performed in order to have information about crystallinity of the samples. Results were given in Figure 6.9-12 below. Three zeolites were identified as clinoptilolite and their characteristic peaks were recognized at  $2\theta=9.81^\circ$ ,  $22.3^\circ$ , and  $30^\circ$ . Additionally zeolite samples contained small amounts of quartz at  $2\theta=26.62$ , and anorhite at  $2\theta=24.465$ .

The quantitative mineralogical analysis for the control samples were performed by the method proposed by Nakamura et al. 1992. Reference mineral (Idaho) used for quantitative analysis is clinoptilolite with >90 % clinoptilolite content (27031, Castle Creek, Idaho; Mineral Research, New York) supplied kindly by F. Mumpton in powder form. Clinoptilolite contents of control samples were found 67; 87 and 91 % for Z1, Z2 and CR, respectively.

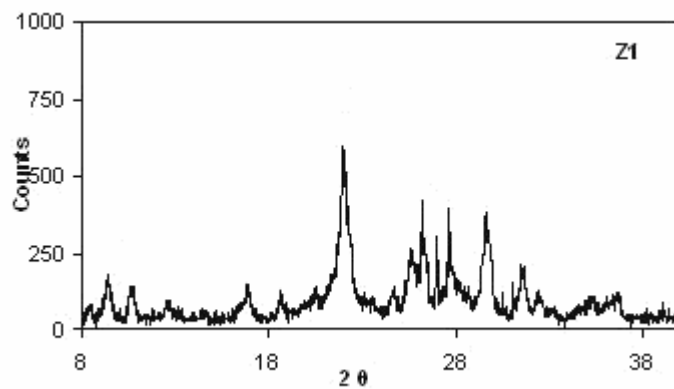


Figure 6.9. XRD patterns of natural zeolite Z1 (peaks coded as C: clinoptilolite A: anorhite, Q: quartz).

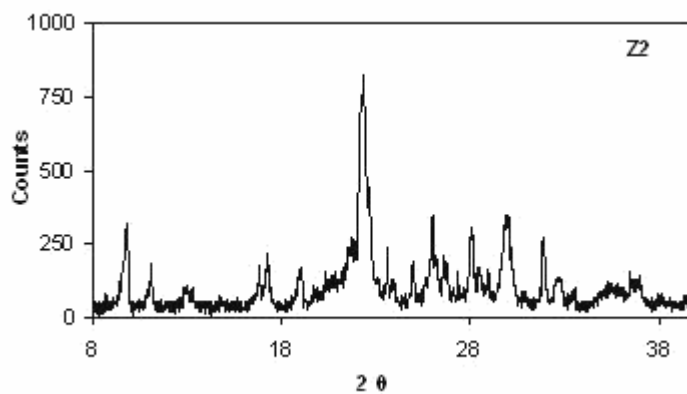


Figure 6.10. XRD patterns of natural zeolite Z2.

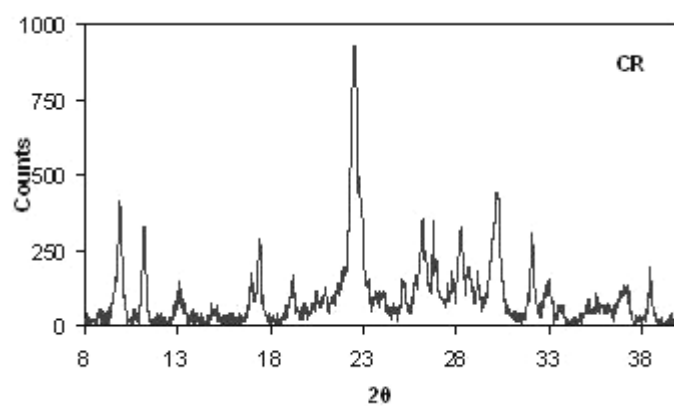


Figure 6.11. XRD patterns of natural zeolite CR.

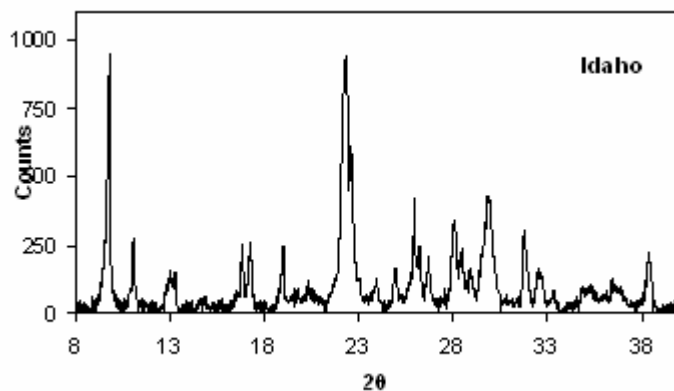


Figure 6.12. XRD patterns of reference natural zeolite Idaho.

FTIR spectrum data for the samples Z1, Z2 and CR were collected to have information about the characteristic molecular bonds of the samples. FTIR spectra showed characteristic peaks of zeolites for all samples (Figure 6.13). The  $472\text{ cm}^{-1}$  and  $615\text{ cm}^{-1}$  peaks were assigned to the internal and external Si (or Al)-O double ring respectively. The strong symmetric and asymmetric stretch vibrations were present at  $1058\text{ cm}^{-1}$ . Peaks related with isolated OH stretching was at  $3700\text{ cm}^{-1}$ , H-bonded O-H stretching was at  $3400\text{ cm}^{-1}$  (Breck, 1974). Results also indicated that characteristic peaks were sharper for the clinoptilolite rich sample (CR).

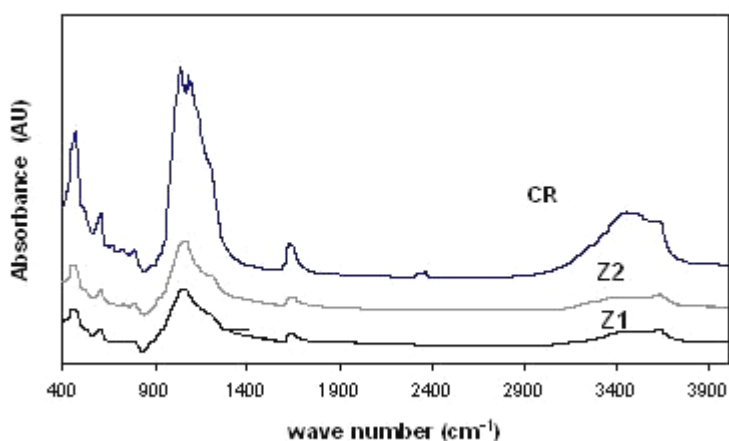


Figure 6.13. Infrared spectra of zeolite samples Z1, Z2 and CR.

To have an idea about surface morphology of the samples, electron micrographs of Z1, Z2 and CR were taken. Characteristic hexagonal clinoptilolite crystals were well defined in SEM results for both samples (Figure 6.16) and were identified in wide range of the surfaces on samples. However, crystals of the clinoptilolite rich samples were not

easily observed by the SEM images which might be attributed to the purification procedure.

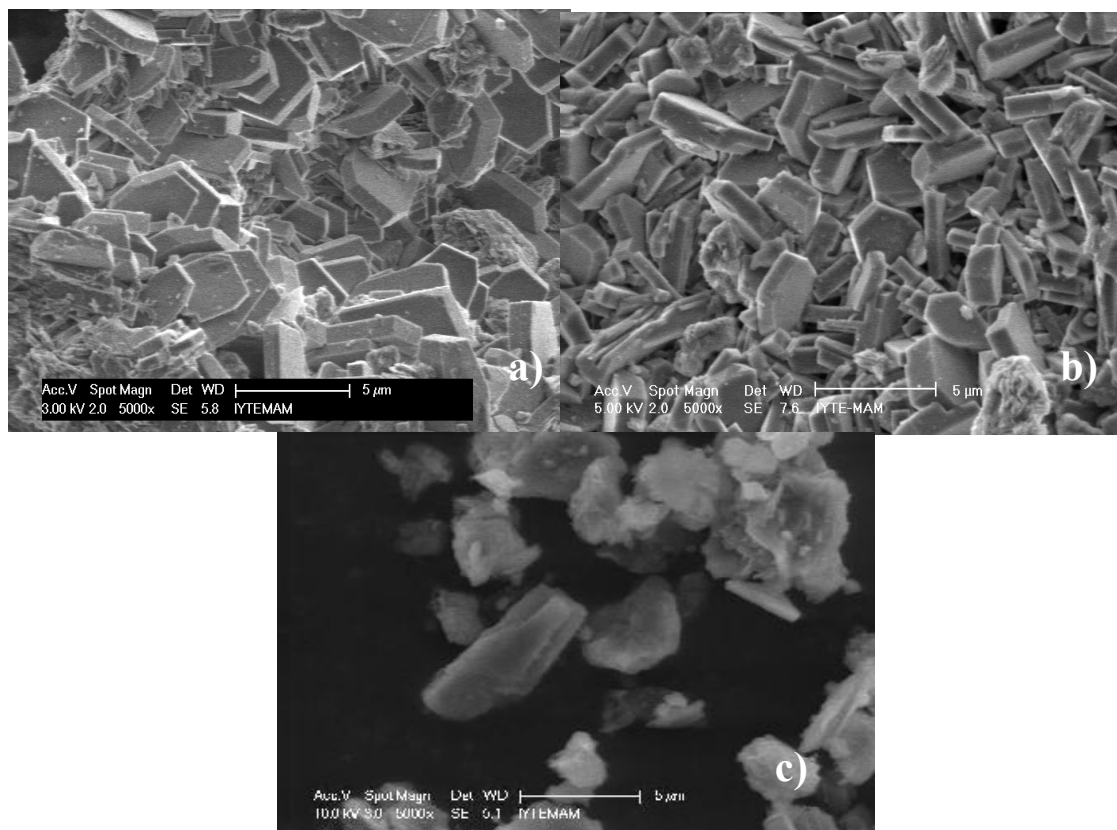


Figure 6.14. SEM images of zeolite samples a) Sample Z1, b) Sample Z2, c) Sample CR

## 6.1. Simulated Digestion Studies

Simulated digestion studies were performed to investigate the effect of in-vitro simulated digestion conditions on zeolite and possible interactions of zeolite with surrounding media which includes digestive enzymes such as pepsin, pancreatin (including amylase, lipase protease) and various bile salts. Zeolite with its complex structure will interact with its surrounding media according to its major adsorptive, catalytic and ion exchange properties. Therefore in this Section, results of the analyzes of either liquid phases or solid phases (zeolite) of digestive media were given to investigate possible interactions during simulated digestion Moreover, same experiments with their characterization studies were performed with low and high purity zeolites (Z1 and Z2, respectively).

### 6.1.1. Effect of Zeolite on UV Absorption Spectra of Digestion Media

To detect any possible decrease in pepsin levels in simulated gastric fluid as a consequence of possible interactions with zeolites, gastric fluids were analyzed for their UV absorption properties. In Figure 6.15, control samples excluding zeolite showed slightly different UV-spectrum with zeolite containing samples. Reason might possibly be the amount of protein structures in media. Media included pepsin and in the presence of zeolite, enzyme with its protein structures were possibly adsorbed on zeolite surfaces therefore samples showed different UV spectrum. Also it was reported (Chiku et al., 2006; Nara et al., 2009) that zeolites can be used as tools for protein folding. Therefore due to possible interactions with pepsin and zeolite, adsorption and/or conformational changes in protein might have happened and this might have resulted different UV-absorption patterns in the presence and absence of zeolite. On contrary, there were no considerable shifts in UV spectra for the simulated gastric solutions.

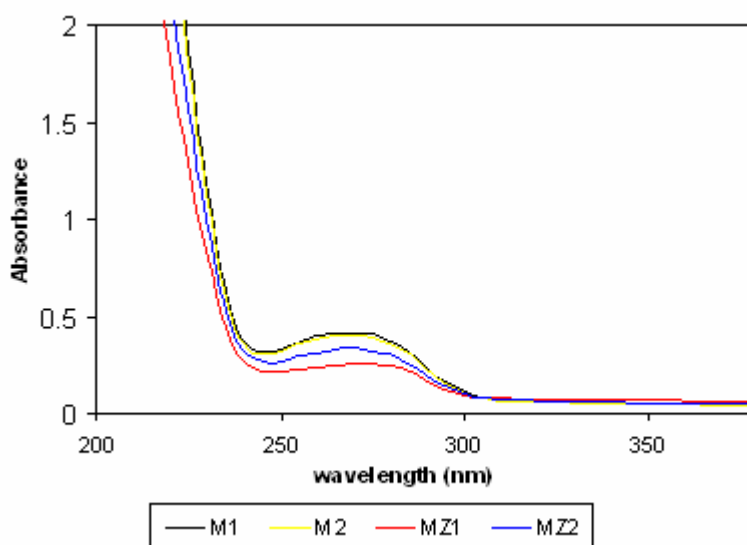


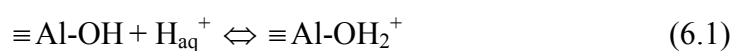
Figure 6.15. Comparison of UV spectra (240-300nm) of gastric fluids (M) for Z1 and Z2.

The UV absorption spectra of gastric and digested media treated with/without zeolite were given in Figure 6.16 and 6.17. UV absorbance at around 270 nm was corresponded to the digestive enzymes in protein structure. Since the intestinal digestive (code: D) media is rich in the concentration of the enzymes, higher absorbance values were achieved compared to the gastric media. Results for digested media (code: D)



suggest that there is not a considerable interaction between the zeolites (Z1 and Z2) and pancreatin mixture which consists of amylase lipase and protease. This is also important for the digestive role of enzymes and their stability. Slight fluctuations in absorbance might be due to the weak interactions between digested media, since in literature zeolites and mesoporous silicates were used as inorganic support for immobilization of enzymes such as amylase lipase and protease (Knezevic et al., 1998; Pandya et al., 2005; Phadtare et al., 2004). However higher interactions were detected in gastric media.

Rivera et al. (1998) studied the neutralizing property of zeolites/composites in synthetic gastric juice and found little or no interaction with the pepsin enzyme. On the contrary, it was found that sample with Z1 showed slightly different UV-spectrum compared to control sample for the gastric digested media indicative of interactions. Those interactions were complicated because pH and ionic strength continuously changes during the simulated digestion. The active groups on zeolite surface are  $\equiv\text{Si-OH}$  and  $\equiv\text{Al-OH}$  groups. In acidic to neutral pH range, protonation of negative and neutral surface hydroxyl groups:



were reported (Dolua et al., 2002). On the other hand, pepsin has only two basic groups and 20 carboxyl groups and at pH higher than 1 (pI), it has a negative electrical charge (Spelzini et al., 2008). Therefore, possibly electrostatic interactions between the  $\text{COO}^{-}$  groups and  $\equiv\text{Al-OH}_2^{+}$  groups might be active. Besides the electrostatic interactions, there could be hydrogen bonding between hydroxyl ( $-\text{OH}$ ) groups on the zeolite and H-bond acceptors on the enzyme depending on the chemical nature of the protein chains and zeolite. Thus further characterizations were performed. It is important to note that Z1 has lower clinoptilolite content compared to Z2, thus impurities such as quartz might be responsible for the interaction of pepsin enzyme where quartz was also reported to be used in protein adsorption (Kang et al., 1999).

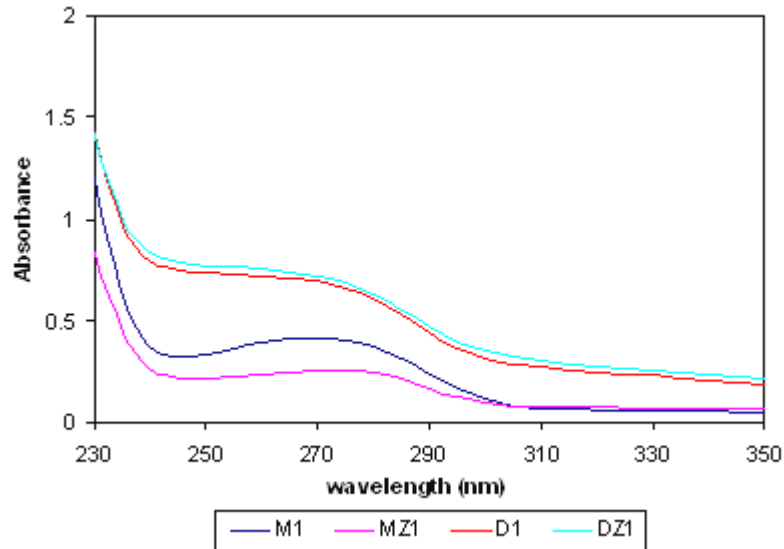


Figure 6.16. UV spectra of gastric (M) and intestinal digested (D) fluid with/without Z1

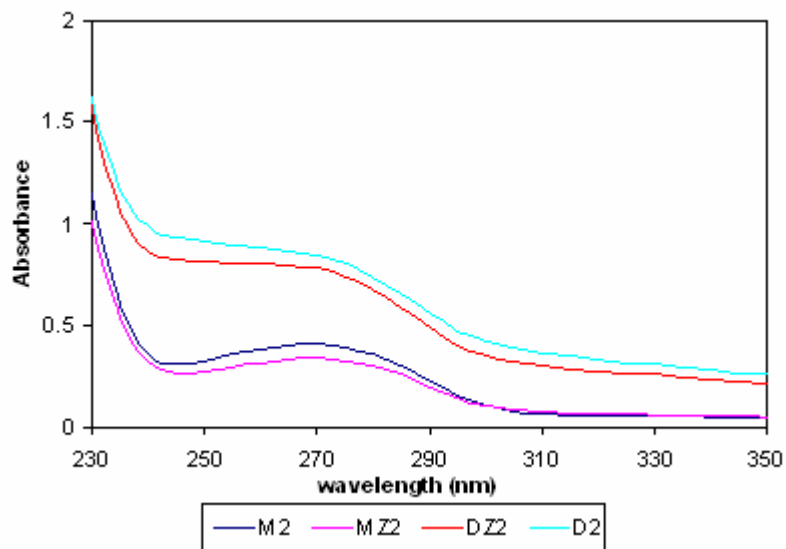


Figure 6.17. UV spectra of gastric and digestion fluid with /without Z2

Zeolite might have interacted with the pepsin existing in the gastric fluid. But this might be very weak and thus could not be observed in the same way for the intestinal digested samples where simulated conditions continued for additionally 2hs. This same result was also confirmed in the further studies of FTIR analysis where there was no additional peak observed in FTIR spectrum indicating no adsorbed protein on simulated digested zeolite samples. Same results were also confirmed by SEM analysis. These results were given in the following sections.

## 6.2. Characterization Results for Simulated Digestion

After simulated digestion was performed, samples were characterized in order to identify any differences in surface properties and structure. For characterization, XRD SEM, FTIR analyzes were performed.

### *XRD Analyzes*

XRD results given in Figure 10.5 indicated that zeolite could be identified as clinoptilolite and its characteristic peaks were recognized at  $2\theta = 9.81^\circ$ ,  $22.3^\circ$ , and  $30^\circ$ . The two zeolite samples also contained small amounts of quartz where  $2\theta = 26.62$ , and anorhite at  $2\theta = 24.465$ .

It was found that there were slight differences between the XRD patterns of simulated gastric treated (M coded) samples of Z1 and Z2 and untreated samples. Simulated gastric treatment media was acidic because contained 0.1 M HCl. Therefore in gastric digestion zeolite was treated with acidic solution. There were different studies in literature about acid treatments of zeolites to modify their structures. Arcoya et al. (1994) found that the treatment of natural zeolites with HCl increases both the acidity and the effective diameter of the channels and pores but it produces an important loss of zeolite phase. In Figure 6.18 (Z1M and Z2M) this structural loss was not observed. This may be related to the severity of the treatment. Arcoya et al. (1994) used higher concentrations of HCl and they observed decrease of the intensity of the lines and the appearance of a broad low baseline which were indicative of the transformation of zeolite into an amorphous phase. Also another important case for the loss of zeolite phase in their study might be the period of HCl treatment. Beside the higher concentrations, they treated zeolite with HCl for 5 h whereas in our study, treatment period was 2h.

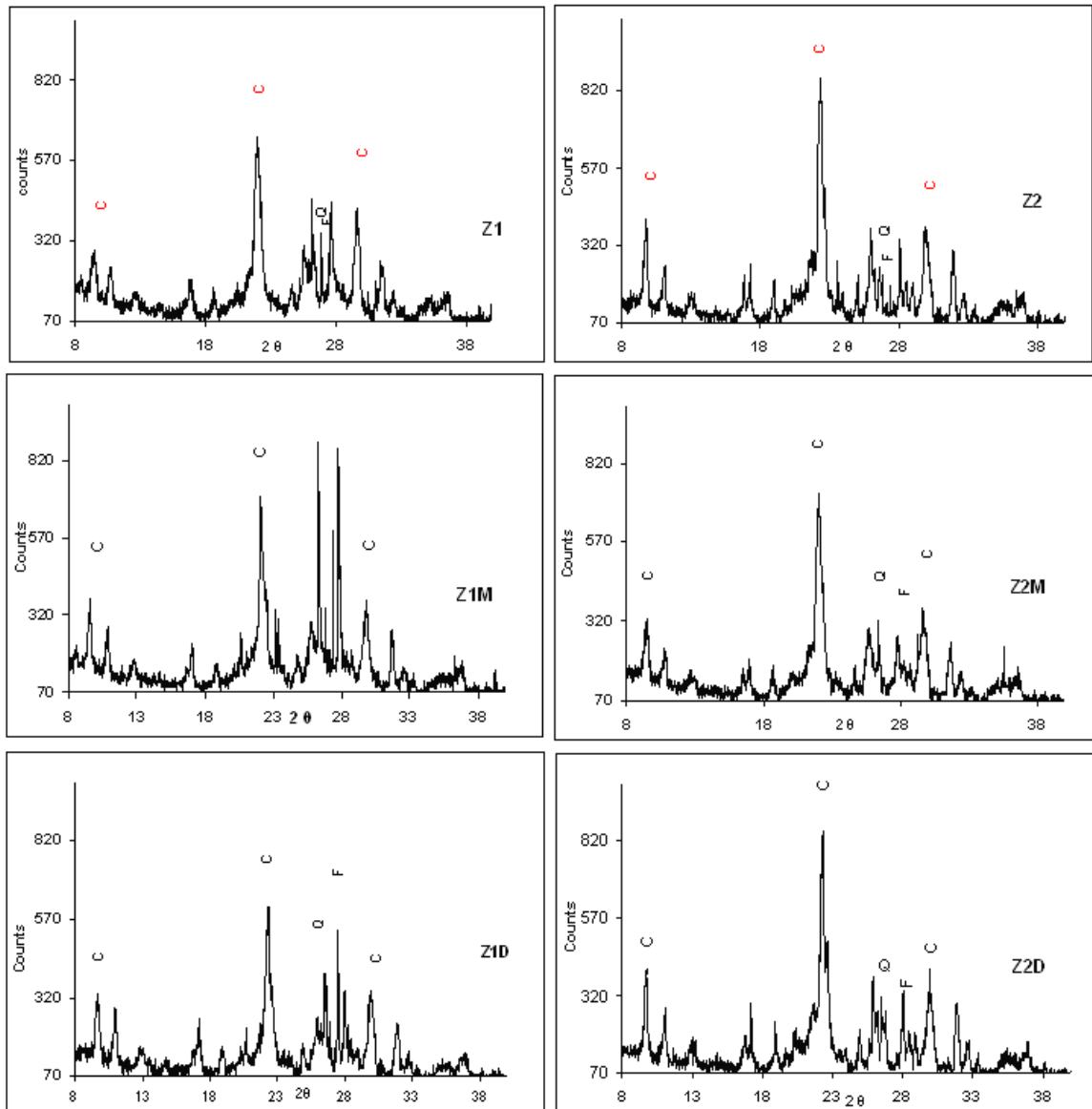


Figure 6.18. XRD patterns of natural zeolites. Z1: low purity control sample (untreated), Z2: high purity control sample (untreated), Z1M and Z2M: gastric treated low and high purity samples, Z1D and Z2D: digested low purity and high purity samples, respectively.

Results in Z1M and Z2M showed that characteristic peak intensities of clinoptilolite were very slightly reduced with the acid treatments. That could be regarded as insignificant because of the mild acidic conditions and lower temperature in gastric digestion. Polatoğlu (2005) studied the effects of HCl treatments on natural zeolites. They observed slight decreases in clinoptilolite characteristic peaks for 0.2 and 1 % HCl treatment. When the simulated digestion was completed, Figure 6.18 Z1D and Z2D showed that intensities of the clinoptilolite characteristic peaks slightly increased.

Simulated digestion media was very complex. Especially in the second step of the digestion procedure, to complete simulated digestion, pH of the media was increased and complex bile salts were added to the media. Therefore, in the presence of the complex media including especially bile salts, increase in the pH and addition of simulated digestion media might have caused changes in peak intensities.

It was important to note that, besides the slight changes in clinoptilolite characteristic peaks in simulated digestion treatments, the most significant changes was observed in the peaks that were characterized as “impurities” in XRD result. Major impurity observed in Z1 was quartz and its peak intensity was low in sample Z2. Therefore, considerable change in the intensity of the quartz peak was found in sample Z1 in simulated gastric treatment. The main reason for that change in gastric treatment might be because of the HCl. It was patented in U.S by Loritsch K. B. and James R.D (United States Patent, No:5037625) that HCl was a chemical used to purify the quartz mineral. Mineral impurities, especially alkali metal impurities within the quartz crystal lattice structure were removed with HCl treatment at high temperatures. In this process, HCl diffused the mineral impurities to the quartz crystal surface where they formed salts with chloride ion. By that way, salts were removed and purified quartz crystals were recovered. Therefore increase in peak intensity of the quartz might be suggested to be as a result of purification effect by HCl treatment. In complete digestion, with the increase in pH and with the complexation of the media, this purification was probably limited.

Those changes in structure of zeolite according to the quartz peak reported to have a little effect on the physicochemical behavior of clinoptilolite. Investigations showed that the present contaminants (mica and quartz) didn't participate in the ion exchange or in the surface complexation (Doula et al., 2002). Therefore, those changes observed after simulated digestion studies were not supposed to alter zeolite's possible bioactivity.

### ***FTIR Analyzes for Zeolite Phase***

The IR spectra of the gastric and intestinal digested samples were given in Figure 6.19 and Figure 6.20. When Z1 and Z2 were compared with respect to their IR spectrum, there were no significant differences. It was found that FTIR spectra showed characteristic peaks of zeolite for all treatments. The  $472\text{ cm}^{-1}$  and  $615\text{ cm}^{-1}$  peaks were assigned to the internal and external Si (or Al)-O double ring respectively. The strong symmetric and asymmetric stretch vibrations were present at  $1058\text{ cm}^{-1}$ . The water

vibrations of zeolite were also observed after  $3450\text{ cm}^{-1}$ . It was observed that there were no considerable differences in positions for the characteristic bands for both Z1 and Z2 sample given in Figures 6.19 and 20.

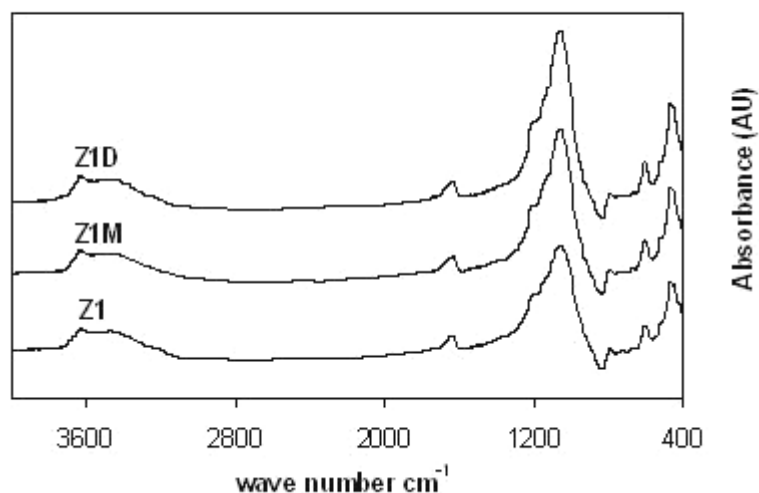


Figure 6.19. Infrared spectra of Z1 after different treatments. (Z1:untreated sample, Z1M:gastric digested sample, Z1D: digested sample).

With respect to treatment conditions such as concentration, contact time, and temperature, zeolite might have loose its structural stability and these results could be observed in FTIR spectra. Arcoya et al. (1994) reported that higher shifts at characteristic peaks at  $472$  and  $1056\text{ cm}^{-1}$  and reduction in their intensities result from dealumination and partial structural breakdown with HCl treatment. Besides, Özkan and Ülkü (2005) reported that in zeolite framework, the internal T-O vibrations were sensitive to the Si/Al ratio of the framework. In the study of Özkan and Ülkü, effect of HCl treatment on natural zeolite was observed as T-O asymmetric stretching vibrations of internal tetrahedral at position  $1056\text{ cm}^{-1}$ . Band shifted to  $1080\text{ cm}^{-1}$  as a result of increase in dealumination degree depending on the increase in HCl concentration used in treatments of natural zeolites. But when their HCl concentration was low, dealumination at lower degrees for  $25$  and  $40^\circ\text{C}$  with HCl lower than  $0.16\text{ M}$ , was insignificant. It was important to note that Rivera et al. (2003) reported that when natural zeolite submitted to an acid environment close to stomach conditions (pH 1.2) there were Al extraction from the framework.

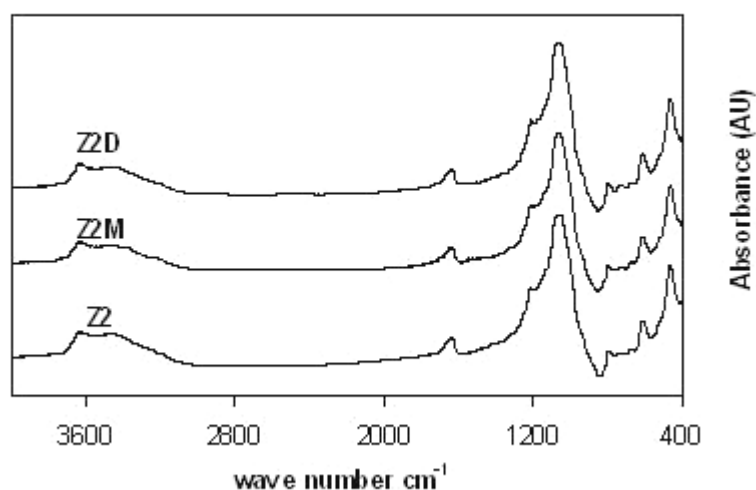


Figure 6.20. Infrared spectra of Z2 after different treatments. (Z2:untreated sample, Z2M:gastric digested sample, Z2D: digested sample).

In this study, concentration of HCl was 0.1M and pH was around 2; temperature was 37°C. Our results indicated that there was no reduction in peak intensities by acid treatment or no higher shifts at characteristic peaks at 472 and 1056 cm<sup>-1</sup> which indicated insignificant dealumination and no destruction of the structure

In previous section, XRD analyses showed minor structural changes especially in impurities for quartz. But in IR spectrums characteristics bands were observed and there was no shift at their position.

When a closer examination was performed for a narrow range of wave number, on contrary to Z2 (Figure 6.21) sample, sample Z1(Figure 10.8) showed slight increases like sharpening in peak intensities at 472 cm<sup>-1</sup> and in 1072 cm<sup>-1</sup> by increasing treatment severity as starting from the untreated to gastric digestion and at last; intestinal digestion.

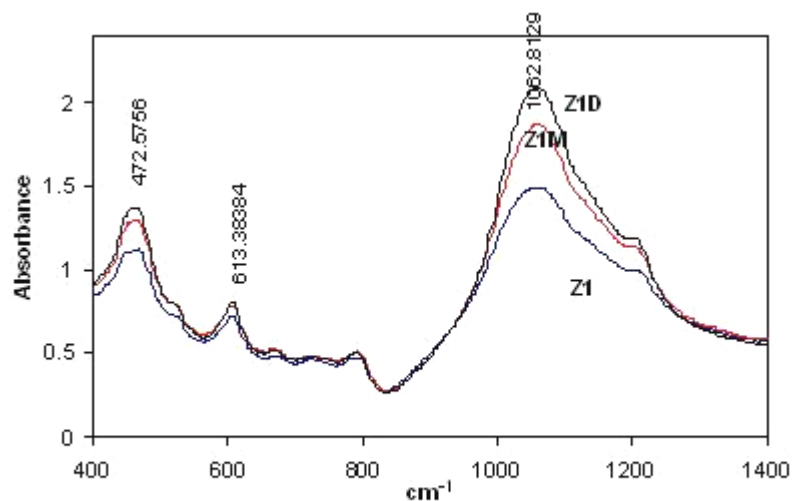


Figure 6.21. 400-1400  $\text{cm}^{-1}$  range showing the characteristic bands for Z1 (Z1:untreated sample, Z1M: gastric digested sample, Z1D: digested sample).

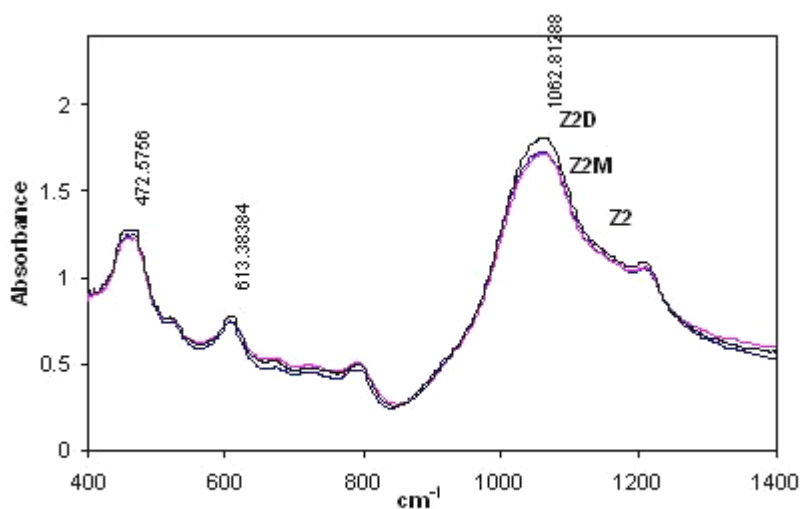


Figure 6.22. 400-1400  $\text{cm}^{-1}$  range showing the characteristic bands for Z2 (Z2:untreated sample, Z2M: gastric digested sample, Z2D: digested sample).

It was important to note that during simulated digestion experiments, media used was very complicated. It contained different ions, besides different enzymes in protein structure were used in media to simulate digestion. Results in Figure 6.21 and 6.22 indicated that there were no additional peaks observed indicating adsorption of some complex structures such as digestive enzymes. As it was given in previously, UV absorbances slightly changed especially for the gastric treatment in presence of zeolite which possibly indicated the changes of protein nature in liquid media. But this possible



interaction especially between enzymes and zeolite should be so weak and could not be observed in FTIR spectra after the zeolite sample preparation step.

### ***FTIR Analyzes for Digested Fluid Powder***

As zeolites were analyzed, it was important to analyze the fluid phase after simulated digestion experiments in order to investigate differences with respect to two zeolite treatments with different purities. Digestion media used was very complex including digestive enzymes and bile salts, also it contained zeolite. Therefore fluid separated fluid phase was lyophilized to obtain powder form and FTIR analyzes were performed.

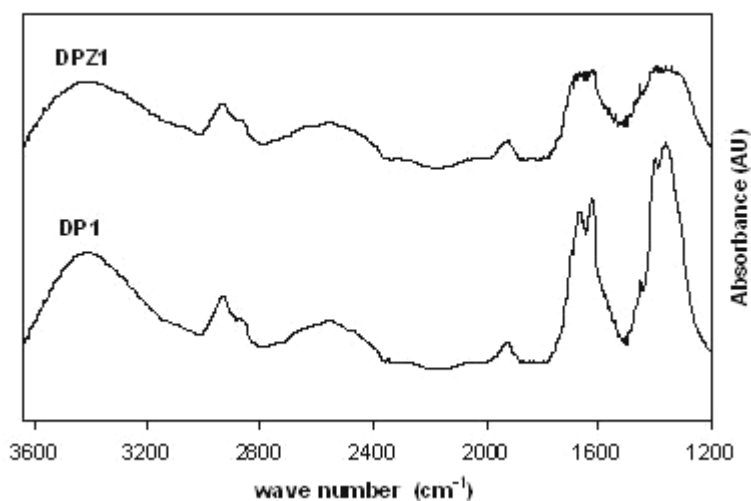


Figure 6.23. IR spectrum of simulated intestinal digestion fluid powders (DP1: digested powder without Z1, DPZ1: digested powder with Z1).

Results of IR spectrum of lyophilized digestion fluid powders were given in Figures 6.23-24. In both figures, the main bands for Amide 1 and Amide 3 were observed in the region around of 1650 and 1350, respectively. But Amide 2 bands (1500-1550  $\text{cm}^{-1}$ ) could not be observed. It was important to note that during digestion procedure, digestive enzymes were used (i.e. protein digestive enzymes). Since those enzymes were in protein structure they would interact with each other therefore IR spectrum should be observed different than the original protein structure data. Simulated digestion was experimentally set up as a continuous process with changing pH values. Those pH values were the main factors for altering protein structures. Also ionic strength due to the acids, bases, bile salts and due to zeolite made the media very

complex which reflected to the IR results as factors altering the media.

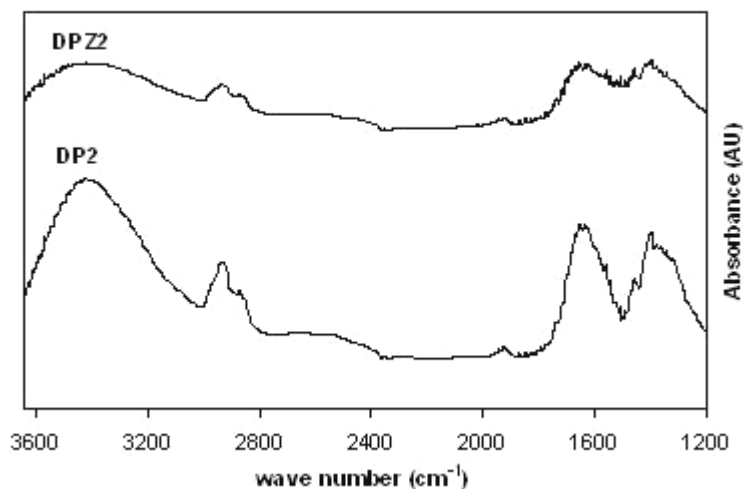


Figure 6.24. IR spectrum of simulated intestinal digestion fluid powders (DP2: digested powder without Z2, DPZ2: digested powder with Z2).

When the results were compared for zeolite treatments, it was observed that there were differences in IR spectra when the digestion treatments were done with Z1 and Z2. In both cases, intensities of the peaks reduced without losing their special band region. Those reductions in peak intensities might be due to the interactions of media components with zeolites. Further investigations for the liquid analysis using ATR-IR will be helpful to enlighten the situation.

#### ***ATR-FTIR Analyzes of Digested Fluid***

Simulated digestion fluids were analyzed by ATR-FTIR to investigate the possible changes with zeolite treatments in liquid phase. Results were given in Figure 6.25. Maximums at peaks indicated the regions specific for the protein structures which were very close. There were no significant shifts in the band regions. Characteristic band peaks at maximum and regions for both treatments were identified as follow: at 1358 and 1420  $\text{cm}^{-1}$  in Amide III, at 1539 and 1577  $\text{cm}^{-1}$  in Amide II and at 1620  $\text{cm}^{-1}$  at Amide I region.

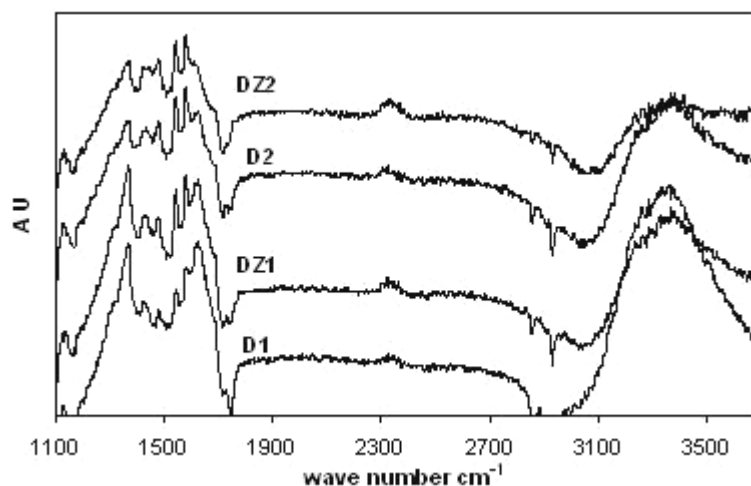


Figure 6.25. ATR-FTIR spectrum of simulated digestion fluid powders (D1: without zeolite 1, DZ1: with zeolite 1, D2: without zeolite 2, DZ2: with zeolite 2).

Considering the previous results for IR results of powder analysis of same samples and Figure 6.25, ATR-FTIR results also showed that Amide III bands were intense in both cases. The most intense peaks were observed in Amide III regions in liquid and powder analysis for sample Z1-D1 treatments. This might be due to the differences in the surface areas and Si/Al ratios of two zeolites which were important parameters for the interactions with the surrounding media.

### ***Elementary Composition Analyzes***

The chemical compositions of natural zeolites were investigated after gastric and digestion treatments. During simulated digestion pH was continuously adjusted with different chemicals therefore elementary composition of the media was dynamically changes. Changes in the pH values from acidic to alkaline ( pH 2 to 7.4) might affect the chemical composition of the zeolite with the possible interactions between the zeolite surface and digestive media. These interactions might be attributed to different physicochemical reactions as dissolution, ion exchange, sorption, and possibly surface precipitation (Trgo and Peric, 2006). Changes in the major elementary composition of two zeolites were analyzed and results given in Figures 6.26-27 and in Table 6.1 below:

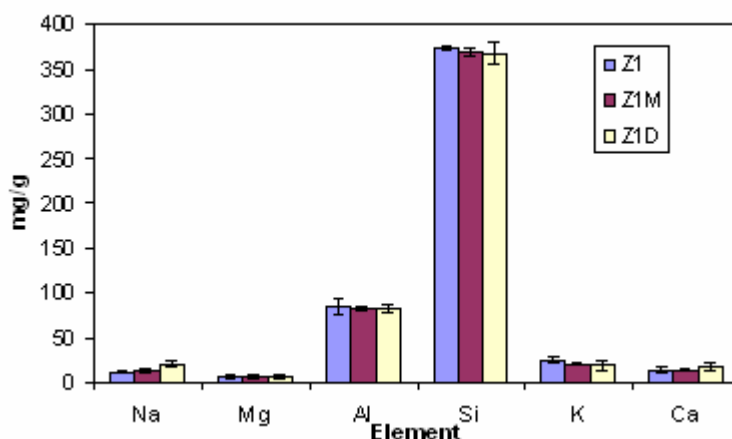


Figure 6.26. Elementary composition change in Z1 (Z1:control, Z1M:gastric treated, Z1D:digested).

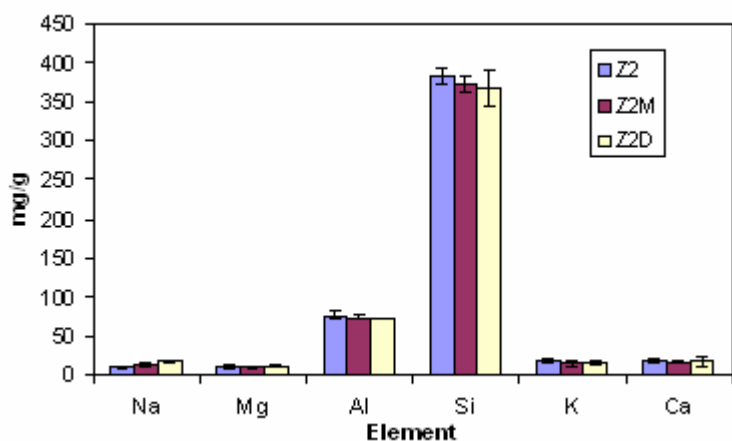


Figure 6.27. Elementary composition change in Z2 (Z2:control, Z2M:gastric treated, Z2D:digested ).

Interaction of zeolite with the digestive media might depend on Si/Al ratio and also the Brønsted and Lewis theory of acidic and basic sites in its structure. Such as, Si–O–Al species represents a negative charge of the lattice and represents the structural basic site. as a potential adsorption location. Therefore oxygen from the lattice acts as a proton acceptor. Since the pH adjustments were performed with  $\text{CaCO}_3$  and  $\text{NaOH}$ , they were in high amounts in the digestive media. Results showed that there were slight increments in the amounts of  $\text{Na}^+$  in both zeolites (79.1 and 66.3 % increase for Z1 and Z2 after intestinal digestion (D), respectively) and also in  $\text{Ca}^{2+}$  for Z1 (28.8% increase after intestinal digestion (D), which might be attributed to exchange of these ions from the digestive by this behaviour.

Table 6.3. Changes in major element content of the zeolites.

Elements (mg/g)	Zeolites					
	Z1	Z1M	Z1D	Z2	Z2M	Z2D
Na	11.0±2.3	12.9±3.0	19.7±2.7	9.8±2.1	13.0±1.5	16.3±1.8
Mg	6.5±2.0	6.1±1.4	6.4±1.7	11.2±2.8	10.6±1.1	11.7±0.5
Al	84.7±5.0	81.5±2.5	81.8±8.4	76.3±4.8	74.5±3.8	73.9±0.1
Si	373.8±12.6	368.8±4.2	366.9±1.5	382.5±11.4	372.0±10.2	367.9±24.5
K	24.2±5.2	19.5±0.7	18.4±3.5	17.8±3.5	14.6±2.7	14.7±2.1
Ca	13.2±3.7	13.5±2.2	17.0±4.0	19.2±3.3	16.0±1.8	17.7±5.8

It was important to note Al composition almost remain constant, however there were slight decrease in the Si composition with the increase in the pH of the digestive media. Such as for Z1, there was 1.3% and 1.8% decrease in Si content compared to untreated Z1 after gastric and intestinal treatments. This might be related to the dissolution process of aluminosilicates at the surface layer at the alkaline conditions. The dissolution process for the natural zeolites were affected by the H<sup>+</sup> or OH<sup>-</sup> in the solutions (Brønsted and Lewis theory) and they represent acidic or basic behaviour. Doula et al. (2002) reported that dissolution of Si was related to the decrease in ionic strength and increase in the pH of the solution. However, Al dissolution was reported to be increased with the increase in ionic strength but also it decreased with the decrease in solution pH. Therefore high ionic strength and pH might be important for the slight dissolution of Si. However, this dissolution might also be considered as statistically insignificant.

### ***SEM of Zeolite Phase***

To investigate possible surface morphological changes by digestion, SEM images were taken for the gastric treated and intestinal digested samples (Figure 6.28 and 6.29). In literature, effects of acid and alkali treatments were observed in SEM images in different studies (Ogura et al., 2001; Li et al., 2005; Rachwalik et al., 2006) and severe conditions resulted structural losses for both alkali and acid treatments.

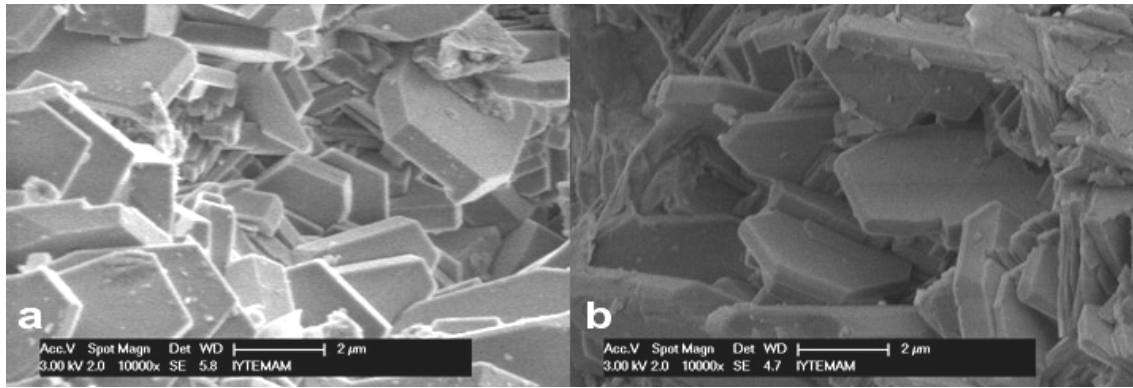


Figure 6.28. SEM images of Zeolite 1 a) gastric treated (Z1M) and b) intestinal digested (Z1D).

In XRD results, it was found that purity of Z2 sample was more than the Z1 sample (87 and 67 %, respectively). In SEM results it was observed that hexagonal clinoptilolite crystals were identified in wide range of the surfaces on Z2 compared to Z1. XRD results also indicated an increase in quartz peak intensities in Z1 after gastric treatment but there no indicators of dealumination confirmed in FTIR results. This was also confirmed with SEM results indicating no structural deformation on both surfaces in both zeolites (Figure 6.28 and 6.29). It was important to note that there were trace precipitates observed on both surfaces. But it was hard to define those precipitates if they were resulted from the digestion treatments or resulted from the nature of the impurities in zeolites themselves.

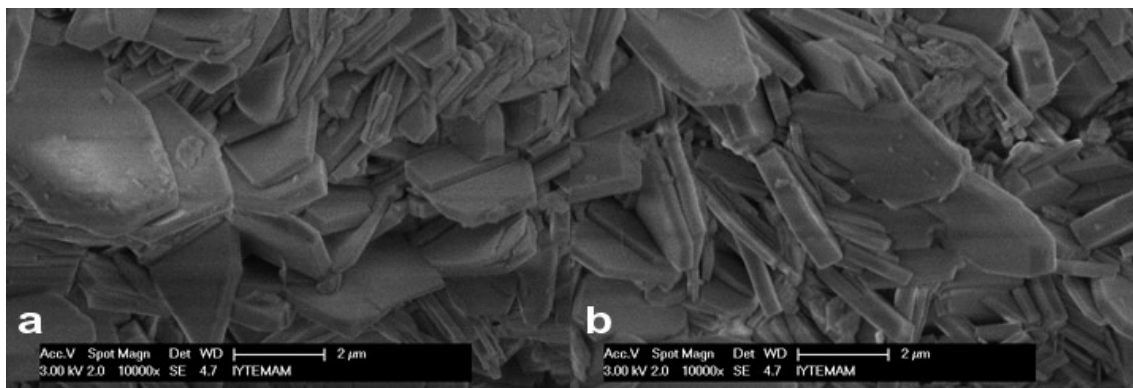


Figure 6.29. SEM images of Zeolite 2 a) gastric treated (Z2M) and b) digested (Z2D).

In structural deformation, surface morphology loses its original smooth crystal images. Some examples of structural deformation from literature with acid or alkali treated zeolites were given below in Figures 6.30 and 31 in order to represent the view of deformation for the comparison.

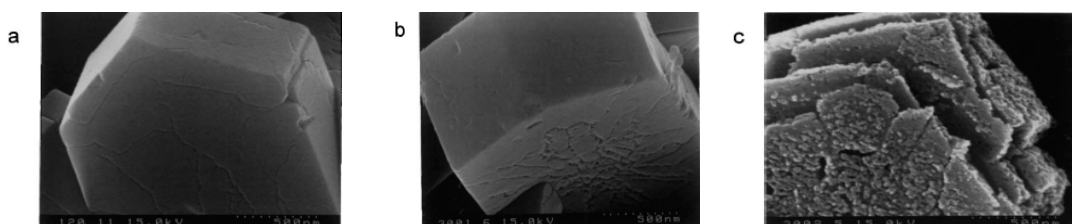


Figure 6.30. SEM images of alkali-treated ZSM-5. Treatment was carried out in a 0.1M NaOH solution at 338K for 120 min (a), 300 min (b), and in a 0.2M solution at 353K for 300 min (c). (Source:Ogura et al., 2001).

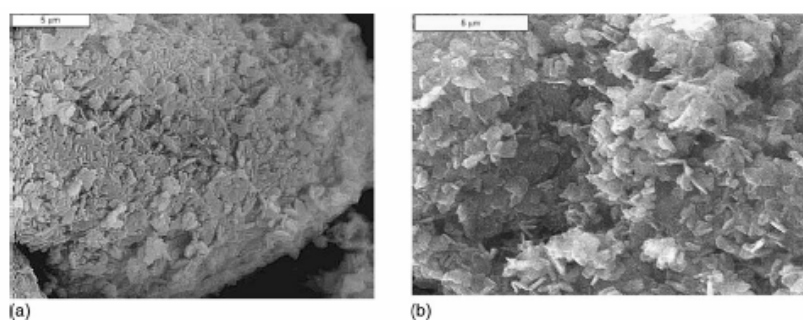


Figure 6.31. Scanning electron microscopy microphotographs Ferrierite (a) starting material NH<sub>4</sub>-Ferrierite, Si/Al = 9.2); and (b) dealuminated sample (Si/Al = 40.5) with 0.25M HCl treatment (Source: Rachwalik et al., 2006).

Main reasons behind structural stability should be the conditions of the digestion studies. First of all, treatment temperature was the body temperature of 37°C which was lower for acid or alkali treatments compared to literature studies where structural stability was lost (Arcoya et al., 1994; Ogura et al., 2001; Li et al., 2005, Özkan and Ülkü, 2005; Rachwalik et al., 2006). Another reason was the structural stability of zeolite itself. Besides gastric and intestinal digestion studies were different from those literature studies where pH was at around 2 and continuously raised to 7.5 in gastric and intestinal digestion treatment respectively. Also pH adjustments during experimental process were done using dilute acids or basis.

### ***SEM of Digested Media Powder***

To determine morphological differences in digested fluid powders with respect to zeolite treatments, SEM images were taken at 100x and 5000x scale. At higher magnifications, (Figure 6.32 and 6.33) surface porosity and irregularity was observed but there wasn't a significant differentiative factor or relevance with their treatment types. After zeolite treatments, it was observed in both figures that powders were in

more dense structures.

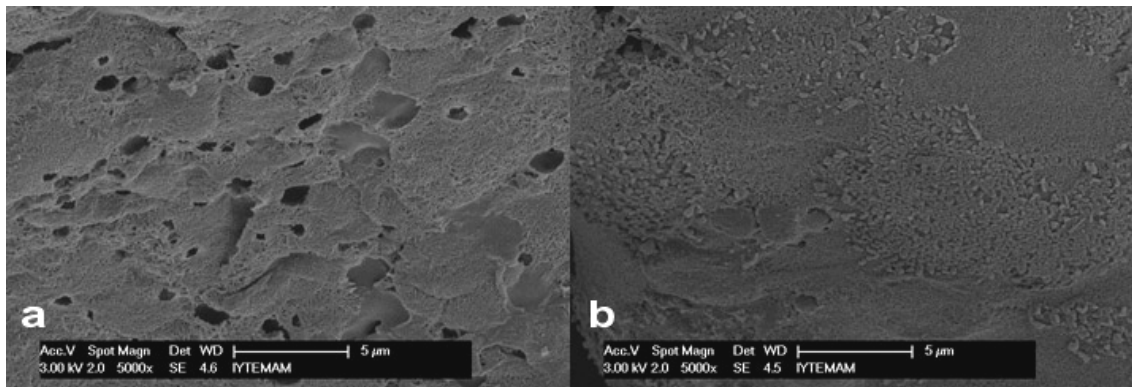


Figure 6.32. SEM images of digested powder with 5000x magnification a) without zeolite treatment b) treated with Z1.

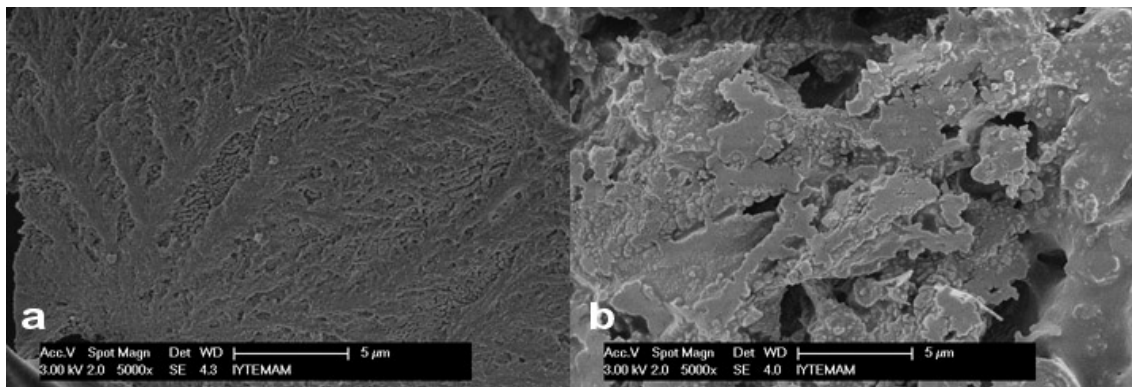


Figure 6.33. SEM images of digested powder 5000x magnification a) without zeolite treatment b) treated with Z2.

On the other hand it was interesting to observe with 100x magnification that all zeolite treatments resulted protein powders to form aggregates after treatments. In both Figure 6.34 and 6.35, digested samples (without zeolite) were smaller in size but zeolite resulted forming aggregates after treatments. This interesting case was much clear for sample Z2 in Figure 6.35

It was important to remind that, similar case was also observed in adsorption studies in the characterization experiments of casein after adsorption and discussed in details in Chapter 7. When casein was incubated with zeolite for 6h, SEM images of protein powders tend to form aggregates compared to control (without zeolite) treatments. Therefore one should consider the existence of possible and complex interactions between protein structures and zeolite in aqueous media such as hydrophobic/phylic interaction, ion exchange of B-acids (Bronsted) and water



substitution on L-acids (Lewis acids) etc. Besides novel usage of zeolites in protein folding (Chiku et al., 2006; Nara et al., 2009) should also be considered that all those factors might effect the final form of protein structures obtained after simulated digestion experiments.

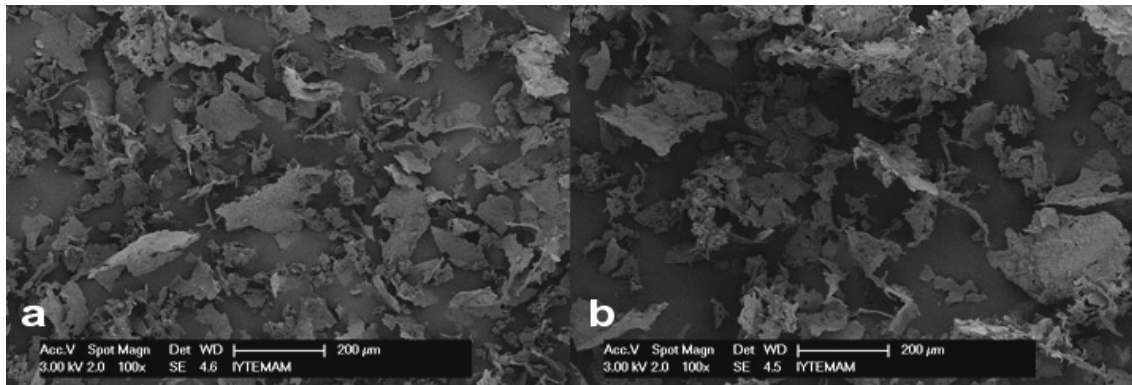


Figure 6.34. SEM images of digested powder 100x magnification a) without zeolite treatment b) treated with Z1.

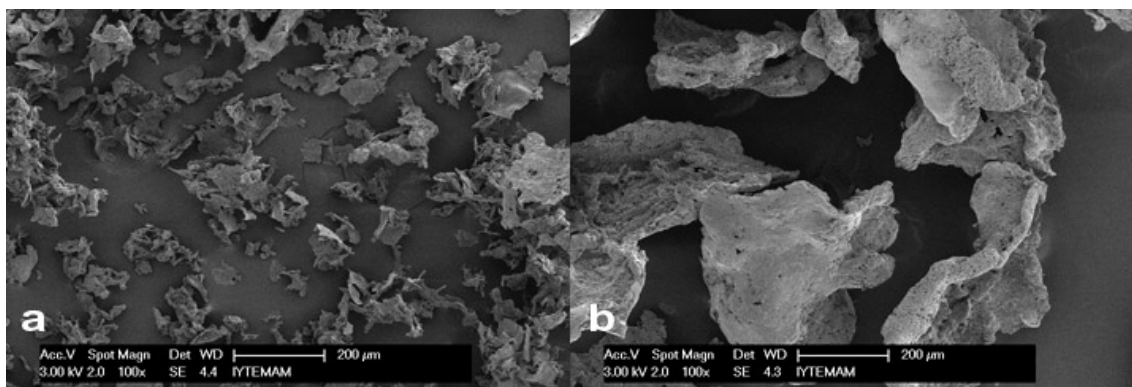


Figure 6.35. SEM images of digested powder 100x magnification a) without zeolite treatment b) treated with Z2.

Simulated digestion procedure was a continuous process with changing pH values and the digestion media contained complex additives such as enzymes in protein structure and bile extract including various salts. Therefore, to better understand these results of agglomeration, one should consider the conformational stability of the proteins in media.

It was reported that conformational stability of the protein native state plays an important role in aggregation. Thus, first of all; aggregation was accompanied by the loss of native protein structures and then those partially unfolded protein molecules were especially prone to aggregation as it was reported by Chi et al. (2003). In this

simulated digestion assay, digestion media contained all the factors to prone aggregation of protein structures such as altering pH values and ionic strengths. Temperature was same in both experiments with/without zeolite (37°C) thus it was not an effective factor. In this experiment, pH of the media changed continuously, and zeolites tended to neutralize the pH of the media. Therefore this competition should have more strong influence on aggregation rate which was obviously observed in Figure 6.35 (b). As it was reported, proteins were often stable against aggregation over narrow pH ranges and when pH was outside those ranges, they may aggregate rapidly in solutions (Chi et al., 2003).

Besides, to better understand the suggested role of zeolite on aggregation, one should also consider the charges of the two interacting site. Charges of the proteins form electrostatic interactions between themselves. When they were highly charged with identical signs there should be repulsive interactions between proteins that stabilize protein solution colloidal and in that case aggregation would be energetically unfavorable. In digestion experiments using zeolite, it was possible that zeolite resulted proteins to possess both positively and negatively charged groups at pH values close to the pI. Changes in pH (step by step; acidic to alkaline) and ionic strength of the media might have caused exchange of H<sup>+</sup> ions, binding of protons on the Lewis basic sites, removal of protons from the surface Bronsted acidic sites or removal of the protons that arrange the ion exchange (Na, K, Ca, Mg) on zeolites surfaces. Thus those complex mechanisms with zeolite treatments might have resulted proteins to possess anisotropic charge distribution. Thus anisotropic charge distribution on the protein surface with the zeolite treatments might have caused increase in dipoles where protein–protein interactions could be highly attractive, making assembly processes such as aggregation energetically favorable.

## CHAPTER 7

### RESULTS OF INTERACTION STUDIES FOR $\beta$ - GLUCURONIDASE, ZEOLITE and CASEIN

Some of the glucuronides that are secreted through the biliary route into the intestine may be hydrolyzed by the action of bacterial  $\beta$ -glucuronidase and that hydrolysis of those glucuronides (they were previously transformed to less toxic and excretable compounds by liver) may liberate free toxins (Dabek et al., 2008). Since it increases endogenous exposure of colon to carcinogens, this process is primary important. After hydrolysis by bacterial GUS, glucuronidation process is reversed and more toxic parent compound is absorbed from the intestine entering the enterohepatic circulation (Nalini et al., 1998; Dabek et al., 2008). If glucuronide hydrolysis is a rate limiting step in this process, then the activity of microbial  $\beta$ -glucuronidase in the colon may influence the risk of colon carcinogenesis.

In this section, two different materials; zeolite and casein were investigated for their possible inhibitory potential on GUS enzyme. Besides, adsorption and interaction studies between those materials were presented. Experiments were performed in solution that simulates intestinal fluid (SIF) which was phosphate buffer at pH 6.8. That solution met optimum working conditions for GUS activity which was recommended by the purchaser instructions and also met the requirements of United States Pharmacopeia (2003).

It was important to note that in literature there was an important study related to GUS activity inhibition using montmorillonite (MMT) performed by Xia et al. (2005). Montmorillonite is in the group of clays but as zeolites it has high adsorption capacity. It was shown that MMT could adsorb *Escherichia coli*. The addition of MMT to the diet also produced a positive effect on the intestinal mucosa. Also they checked the  $\beta$ -glucuronidase activity in pigs and found that in small intestine MTT reduced GUS activity from 128 to 102 units and in proximal colon activity reduced 186 to 149 (Xia et al., 2005). But in literature there was no study related to zeolites and GUS inhibition. Therefore studies especially about inhibition of GUS by zeolite will meet the inadequacy in literature.

## 7.1. Preliminary Results of the Interactions

Knowledge and understanding of the interactions and behavior of compounds with zeolite is important for the biomedical applications of zeolite, since their chemical and biological activity or stability can depend on those interactions. To understand the possible interactions of zeolite casein and GUS, different combinations of treatments were performed and UV and fluorescence spectra of samples were analyzed.

Effect of zeolite on GUS enzyme activity has the primary importance. To investigate the effect of zeolite on enzyme activity, firstly, time required for enzyme and substrate reaction was determined. GUS activity was measured at different time intervals and activity vs. reaction time graph was plotted to determine the linear region of the enzyme kinetics. Results were given in Figure 7.1 below. Considering addition of inhibitors will restrict the detection of residual enzyme activity, 5 minutes in the upper linear region was chosen for the reaction time in activity measurements. By this way, it would be possible to measure the enzyme activity although high inhibitions were achieved in the presence of the inhibitors.

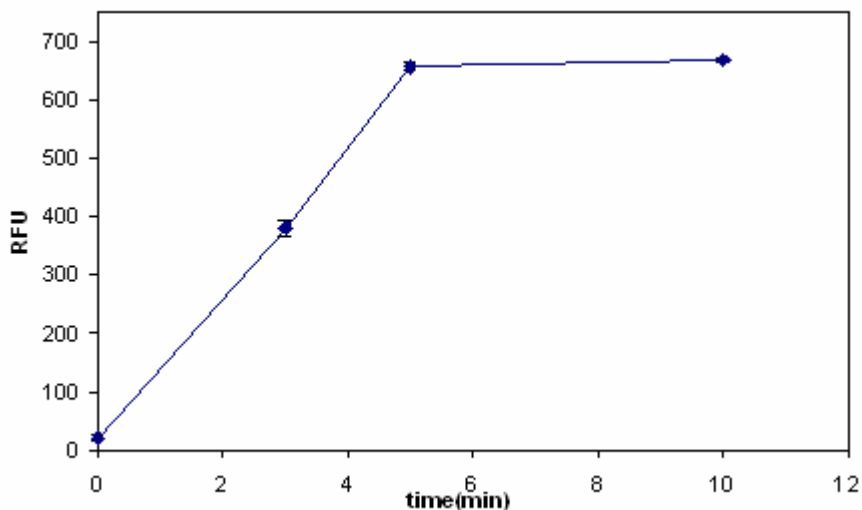


Figure 7.1. Change in relative fluorescent units (RFU) by time (95 $\mu$ g/ml GUS in SIF solution-pH 6.8 phosphate buffer).

Loss of enzyme activity is an important problem associated with enzymatic reactions where enzymes were very sensitive to microenvironments. Therefore effect of incubation times on enzyme stability was investigated in order to determine the time required for preservation of GUS stability. Results of incubations for different times

showed that although there were slight fluctuations, absorbance of the enzyme remained almost the same as its initial value during 30 minutes of incubation (Figure 7.2). This result was also in good agreement with optimum activity time recommended by the purchaser and incubation time for further studies was set as 30 minutes.

Effect of zeolite was also investigated for the same conditions. When the enzyme with zeolite sample was compared with zeolite free enzyme, it was important to note that there were only slight differences indicating weak adsorption of enzyme by zeolite. Moreover, as the time elapsed 30 minutes, differences between two treatments increased. For 60 and 120 minutes, difference was remained almost constant where the absorbance values were almost the same.

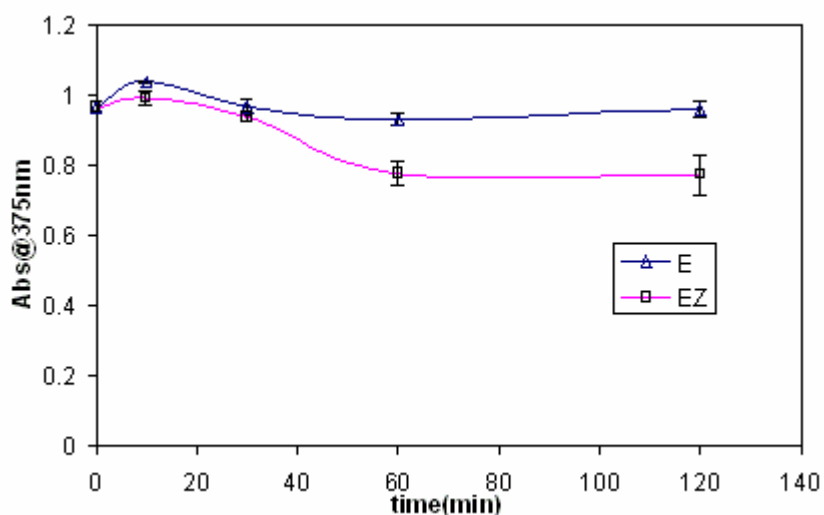


Figure 7.2. Kinetic absorbance change of GUS (E: control incubation without zeolite, EZ: GUS incubated with zeolite, 95 $\mu$ g/ml GUS and 25mg/ml zeolite in SIF solution-pH 6.8 phosphate buffer).

For the same sample, effect of zeolite treatment for kinetic UV absorption spectra was also investigated. UV absorption resulted from protein nature of casein and GUS enzyme with respect to aromatic side groups and double bonds (Phadungath, 2005) and it is directly proportional to sample's concentration in solution. Figure 7.3 shows the UV absorbance spectra of GUS solutions before ( $t=0$ , control sample) and after with the zeolite interaction for varying times. Results of UV absorption showed that differences between UV spectra of GUS solutions after contact with zeolite at different time intervals were very small, indicating negligible variations of GUS levels in solution after the interaction. Those results indicated the possibility of slight adsorption

of GUS enzyme by zeolite. Therefore results in these kinetic experiments implied that there were slight interactions between enzyme and zeolite and this interaction was more clearly observed at incubation times longer than especially 30 minutes. On the contrary, it is important to note that at incubation times longer than 30 min, enzymatic stability started to weaken. 30 minute was also the time recommended by the purchaser and incubation time for further studies was set as 30 minutes.

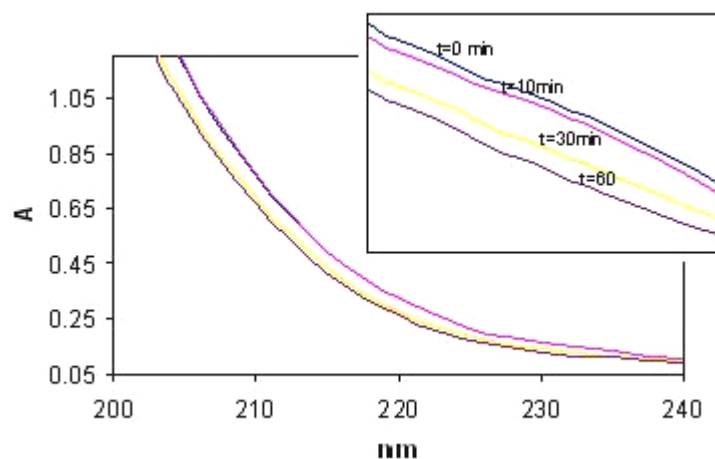


Figure 7.3. Kinetic change in UV absorption spectra of GUS (to: initial conditions before zeolite addition- control, 95 $\mu$ g/ml GUS and 25mg/ml zeolite in SIF solution-pH 6.8 phosphate buffer).

Detailed study for the effect of casein and zeolite inhibitors on UV spectrum of GUS were performed and results given in Figure 7.4. Concentrations of casein used in incubation studies were much higher than the enzyme concentrations. Therefore, highest UV absorbance was found for casein as expected. When casein was incubated with enzyme (E+C), it was found that their UV absorbances were lower than the casein itself. This might be due to the interaction of casein with enzyme and changes in their conformation and activity where this was observed in enzyme kinetic studies. This result suggested that protein free and in native form would have absorbed more UV light than protein in interaction.

When the zeolite added into the media of enzyme-zeolite-casein (E+Z+C), their absorbance reduced due to possible adsorptive effect of zeolite. If there was adsorption in the presence of zeolite, the amount of free protein in the solution would be reduced and at the same time reduction in UV absorbance would also be observed. This case was more easily observed in zeolite-casein (Z+C) studies compared to only casein (C) sample's UV absorbance spectra. In the presence of zeolite, high variations in UV

spectra were observed implying strong interactions of zeolite with casein compared to enzyme. These results suggested that casein was highly adsorbed with zeolite samples and those results were supported by the detailed adsorption studies and also by characterization studies which were presented in the following sections.

Additionally, results showed that in the following enzyme inhibition studies for GUS enzyme, studies about the effect of two inhibitors (together) would denote some limitations as they were highly interacted. One important result was related to UV absorbance spectrum of (E) and (E+Z) treatments. Slight differences in UV spectrum indicated the possibility of enzyme adsorption on zeolite.

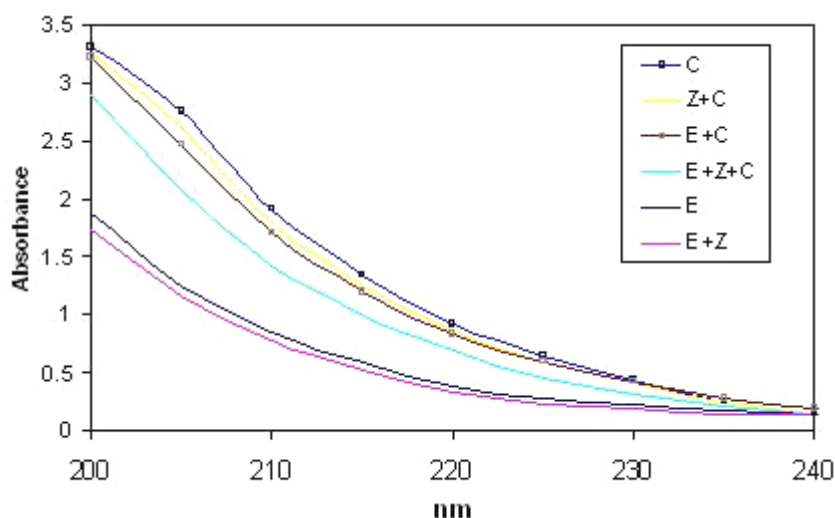


Figure 7.4. UV absorption spectra of enzyme incubations with different inhibitors (E:enzyme, C: casein, Z:zeolite, Results upper to lower: C, Z+C, E+C, E+Z+C, E, E+Z; 95 $\mu$ g/ml GUS, 25mg/ml zeolite and 0.125 mg/ml casein in SIF solution-pH 6.8 phosphate buffer).

To investigate the slight interaction of enzyme with zeolite, FTIR analyzes were performed for zeolite incubated with GUS. The adsorption of the protein (GUS) might probably be seen in Amide II band region. But in contrary, when enzyme and zeolite interaction was investigated, there were no differences in FTIR spectra. Results of the FTIR spectra were given in Figure 7.5 This result suggested that there was no strong chemical interaction with GUS and zeolite indicating GUS enzyme wasn't strongly adsorbed by zeolite. These results were also in agreement with UV spectrum analyzes. Therefore there might be physical interaction with the enzyme and zeolite such as van-der Waals interaction, electrostatic interaction or hydrogen bonding.

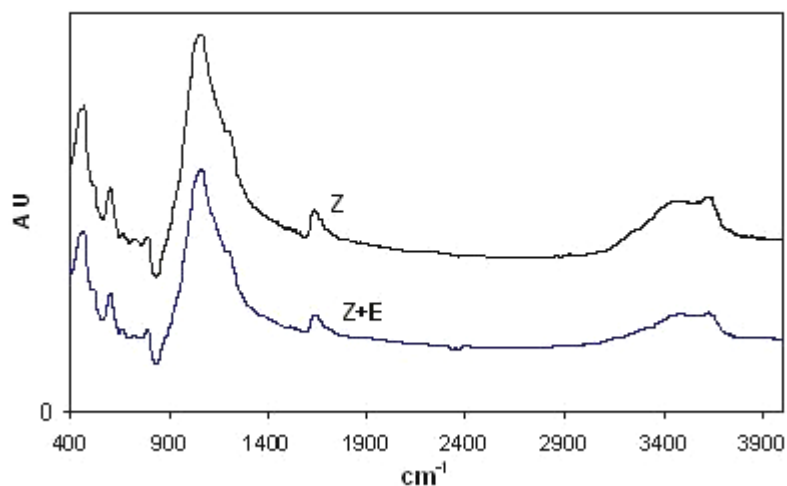


Figure 7.5. FTIR spectra of zeolite (Z: control, Z+E: zeolite 120 min. incubated with enzyme using 95 $\mu$ g/ml GUS and 25mg/ml zeolite in SIF solution-pH 6.8 phosphate buffer).

In UV absorbance studies, it was found that in solution UV absorbances corresponding to the enzyme concentration were slightly reduced with zeolite treatment zeolite. However, no chemical bonding was found in FTIR analyze. Therefore, a complementary analyze was performed using SEM. To complete characterization and obtain images of the surface morphology of the zeolite sample, SEM analyzes were performed.



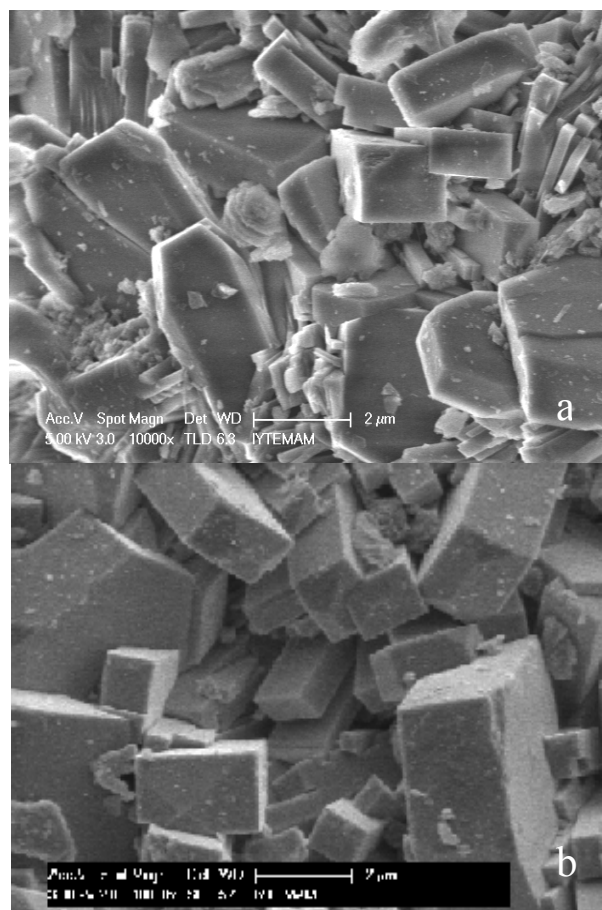


Figure 7.6. SEM image of zeolite; a) control sample (without enzyme), b) zeolite incubated with enzyme.

SEM images of zeolite- enzyme and control samples (zeolite without enzyme) were examined if there was possible protein structures coated on zeolite surface. SEM images confirmed that compared to control zeolite sample, there wasn't any protein like structure coating the surface. An image result was given in Figure 7.6. Those results were also in good agreement with UV and FTIR results.

Results of the preliminary interaction studies revealed that there was a strong interaction between the selected two inhibitor: casein and zeolite. Results indicated that casein was adsorbed by zeolite during the incubation studies using GUS, zeolite and casein. Therefore, this situation caused experimental difficulties to investigate the effect of two inhibitors on GUS in the same solution. Additionally, reductions in UV absorbance levels for GUS with zeolite treatment revealed possibility of adsorption of enzyme by zeolite. Therefore, as well as inhibitory potentials, mechanism behind the interactions between GUS and zeolite, casein and zeolite should be studied in details which are the following main topics in this chapter.

## 7.2. GUS Inhibition Studies and Application of the Michaelis Menten Approach for Zeolite and Casein Inhibitors

Inhibitory effect of potent inhibitors (zeolite and casein) and inhibition mechanism was studied to classify inhibition type of zeolite and casein for GUS enzyme activity. If the detailed mechanisms of inhibition are known then the classification can be made by identifying where on the enzyme the inhibitor binds or order of which the inhibitor binds relative to substrate. Therefore simple kinetic parameters were determined to classify the inhibitor.

Casein was used in different inhibition experiments (Swanson et al., 2002; Wang et al., 2000) due to its micellar structure. This structure provides interacting and binding of the surrounding constituents. Enzyme GUS could be activated or reversibly inhibited with different doses of inhibitors. Therefore different doses of casein were used to investigate GUS enzyme activity with respect to different concentrations of the casein. Results were given in Table 7.1 in percentage residual enzyme activities with respect to control experiment (enzyme without inhibitor). It was found that, the dose of 0.125 mg/ml inhibited the GUS enzyme 12.17%. When the dose was higher this inhibition increased to 17 %.

Table 7.1. Effect of casein on GUS activity.

(Control)	[I <sub>C</sub> ]=0.125mg/ml	[I <sub>C</sub> ]=0.175mg/ml	[I <sub>C</sub> ]=0.175mg/ml+[I <sub>Z</sub> ]=25mg/ml
100.00	87.83	82.92	87.08
±1.04	±1.68	±1.29	±2.62

This result was also confirmed by literature. Wang et al. (2000) investigated the inhibition potentials of different milk proteins. Unmodified casein and different milk proteins such as bovine lactoferrin, human lactoferrin, lactoperoxidase  $\beta$ -lactoglobulin,  $\alpha$ -lactalbumin, lactogenin, glycolactin etc. were tested for their  $\beta$ -glucuronidase inhibitory activity and it was found that unmodified casein with 19.27% inhibition showed highest inhibition towards GUS enzyme. In the same study casein showed no inhibitory activity towards HIV-1 reverse transcriptase enzyme which is crucial for HIV-1 replication

As the zeolite had an inhibitory effect on GUS, combination of casein and zeolite were studied and it was found that there was not a synergistic effect that

observed as an increase in inhibition percentages. On contrary, their combination effect was lower than the only casein sample. This was due to the adsorption of casein on zeolite surface (also previously observed in UV absorbance measurements in interaction studies) where this result was confirmed with further detailed adsorption studies. Hence, the casein was adsorbed, amount of free casein in solution reduced to interact with the enzyme.

Table 7.2. Comparison of inhibitory potentials for casein and zeolites on GUS activity.

(Control)	[I <sub>C</sub> ]=0.125mg/ml.	[I <sub>Z1</sub> ]=25mg/ml	[I <sub>Z2</sub> ]=25mg/ml
100.00	84.61	64.94	63.49
±1.01	±1.28	±2.13	±2.72

In inhibition of enzyme activity by zeolite; ion-exchange ability of zeolites might have a potent role where exchange H<sup>+</sup> for cations such as Na<sup>+</sup> and K<sup>+</sup> will tend to affect protonation state of the acidic groups in protein and, hence, enzymatic activity. Similar case was reported by Fontes et al. (2002). Slight adsorption was observed in UV-spectra which was reported previously.

In order to evaluate the inhibitory effect of two types of zeolite (Z1 and Z2, see Section 6.1), inhibition studies were performed using same doses of zeolite (Table 7.3). Those results were also compared with the inhibitor casein. When the inhibitory effect of casein and zeolites were compared, zeolite was found as more potent inhibitor for the GUS enzyme. Approximately, casein inhibited GUS enzyme 15% whereas zeolites inhibited GUS 35%. It was important to note that zeolite sample Z1 and Z2 had approximately same inhibitory potentials towards GUS enzyme.

To determine the kinetic parameters double reciprocal plots were performed (see information about double reciprocal plots in Appendix B.2). When the double reciprocal plots for the enzyme (control) and enzyme inhibitor systems were drawn (Figure 7.7 and 7.8), both of them showed complex inhibition mechanisms due to their intercept regions.

For the GUS-casein system, plots showed that intersecting lines converge to the left of the y-axis and below x-axis where  $\alpha < 1$ . It was known as the III quadrant in enzyme systems. For the GUS-zeolite system plots showed that intersecting lines converge to the left of the y-axis and above x-axis where  $\alpha > 1$ . That region was known as the IV quadrant in enzyme systems.

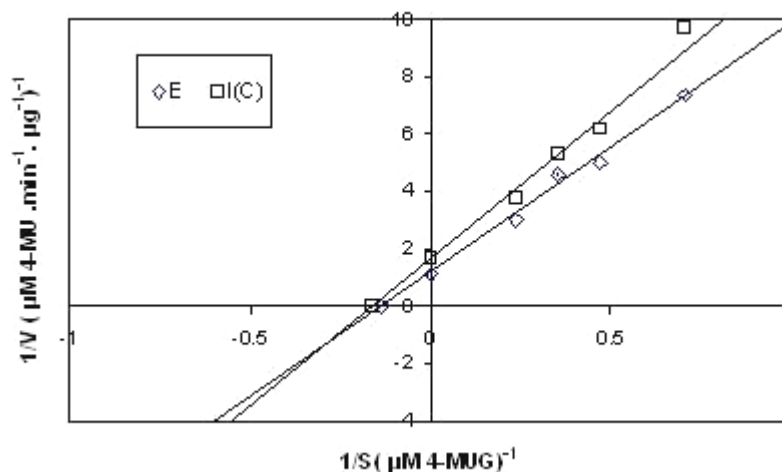


Figure 7.7. Double reciprocal plots for GUS enzyme:E and GUS enzyme incubated with casein inhibitor:I(C)

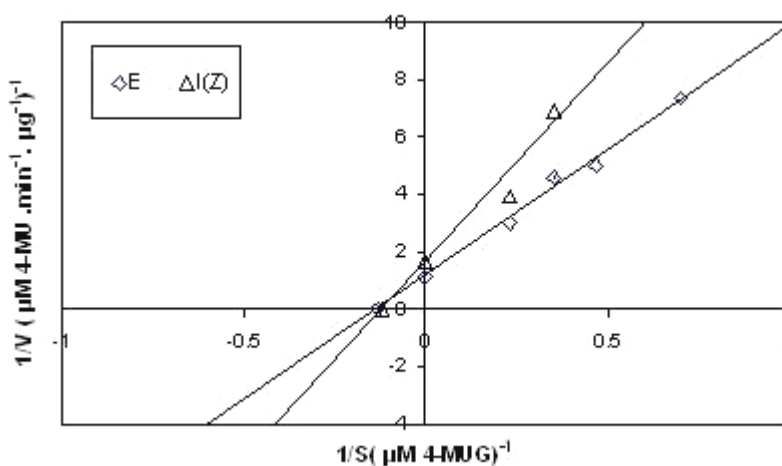


Figure 7.8. Double reciprocal plot for GUS enzyme:E and GUS enzyme incubated with zeolite inhibitor:I(Z).

Both figures showed that both casein and zeolite were found as mixed-type inhibitors related to changes in  $K_m$  and  $V_{max}$  values (Segel, 1993). In mixed inhibition, inhibitor compound can act either as competitive or uncompetitive inhibitor therefore it can interact with both the free enzyme and the enzyme–substrate complex at a site other than the active site. A mixed inhibitor binds to a site on the enzyme and interferes with both apparent substrate affinity and catalytic turnover, thus affecting both the observed  $K_m$  and  $k_{cat}$  (therefore  $V_{max}$ ) for the enzyme-catalyzed reaction (Segel, 1993).

Table 7.3. Apparent Kinetic Parameters.

Sample	$V_{max}^*$ ( $\mu\text{M 4-MU} \cdot \text{min}^{-1} \cdot \mu\text{g}^{-1}$ )	$K_s^*$ ( $\mu\text{M 4-MUG}$ )
E	0.87	7.60
I(C)	0.61	6.22
I(Z)	0.61	8.42

Simple kinetic parameters determined from the double reciprocal plots were given in Table 7.3. It was observed that apparent reaction velocity was reduced at the same degree with the two inhibitors. Both apparent  $K_m$  value, which indicated the affinity of enzyme to the substrate was reduced with the casein but increased with zeolite used as an inhibitor. As mixed inhibitors it was found that both zeolite and casein did not bind directly in the active site, and therefore did not block substrate binding (Segel, 1993; Marangoni, 20003). The interaction of inhibitors with GUS enzyme possibly distorted the active site of GUS enzyme to a non optimal conformation for catalysis which reduced the reaction velocity.

The reason of different apparent  $K_m$  values might be the nature of the inhibitors. Zeolite is a mineral and casein is a protein. Those both mixed inhibitors should have behaved differently in solution as protein was dissolved in solution. Mixed inhibitors could bind to free enzyme prior to substrate, distorting the active site to a non-optimal conformation for catalysis (Segel, 1993; Marangoni, 20003). The inhibitor-distorted active site has trouble converting the substrate to product before it dissociates, resulting in a lowered apparent substrate binding affinity. Casein might have behaved in that nature. As the casein was micelluar in nature, it has ability to coat its surrounding resulting inhibition of enzyme. But in some cases mixed inhibitors could bind after substrate to the enzyme-substrate complex. This case was proper for the zeolite where it was not dissolved in solution. Thus one could think that order of binding for the zeolite and casein different and that difference resulted at the way of increasing or decreasing the apparent  $K_m$  values.

### 7.3. Adsorption of $\beta$ -Glucuronidase and Casein onto Zeolite

Previous interaction studies indicated that there was slight interaction between zeolite and GUS enzyme. Those slight interactions might be physical interactions such as van-der Walls interaction, electrostatic interaction or hydrogen bonding which also

may alter the free GUS activity in solution. Additionally, casein was investigated for its inhibition potential against GUS enzyme previously and it was found that casein performed inhibitory activity on enzyme. But studies showed that, when casein was incubated with zeolite, casein was adsorbed by zeolite. Since casein was a natural nutritive compound and had many bioactive peptides that possess many activities, such as immunoregulatory, antioxidant, or antihypertensive (Xue-Ying et al., 2007; Charles, 1976), it was important to investigate zeolite and casein interactions and also mechanism behind adsorption. Besides, adsorption of casein might suggest higher transit time and better bioavailability in intestinal system, or zeolite-casein together might perform synergistic effect on other compounds during longer transit provided by zeolite.

To investigate adsorption mechanism of GUS and casein onto zeolite, detailed kinetic and equilibrium studies were performed. To identify the dominant mechanism involved in controlling the adsorption kinetics, adsorption experiments involving important parameters in adsorption kinetics such as initial concentration, sorbent particle size, solution temperature, solution pH, solid liquid ratio and agitation were performed. Additionally kinetic data were analyzed for diffusion and reaction models. Results of the detailed adsorption studies for GUS and casein were given below.

### **7.3.1. Adsorption Kinetics**

Kinetic experiments for GUS and casein adsorption were performed for the parameters; initial adsorbate concentration, pH, solid liquid ratio, shaking rate, particle size and temperature. Batch kinetic studies were performed for GUS and casein and their adsorption behaviours were investigated.

#### ***Effect of Initial Concentration***

To understand the differences in the behaviour of zeolite, first of all, digested and non digested forms of zeolite were used with different initial concentrations of casein. Results of the uptake curves were given below in Figure 7.9 for the non-digested (untreated/control Z1) and digested Z1 zeolites, respectively. Results showed that there was not a considerable difference with respect to uptake curves. Adsorbed amounts of casein were almost same for Z1 and Z1D and did not change with the increase in the

initial casein concentrations. Thus, further kinetic experiments were performed using digested zeolite for both GUS and casein to better simulate the intestinal conditions.

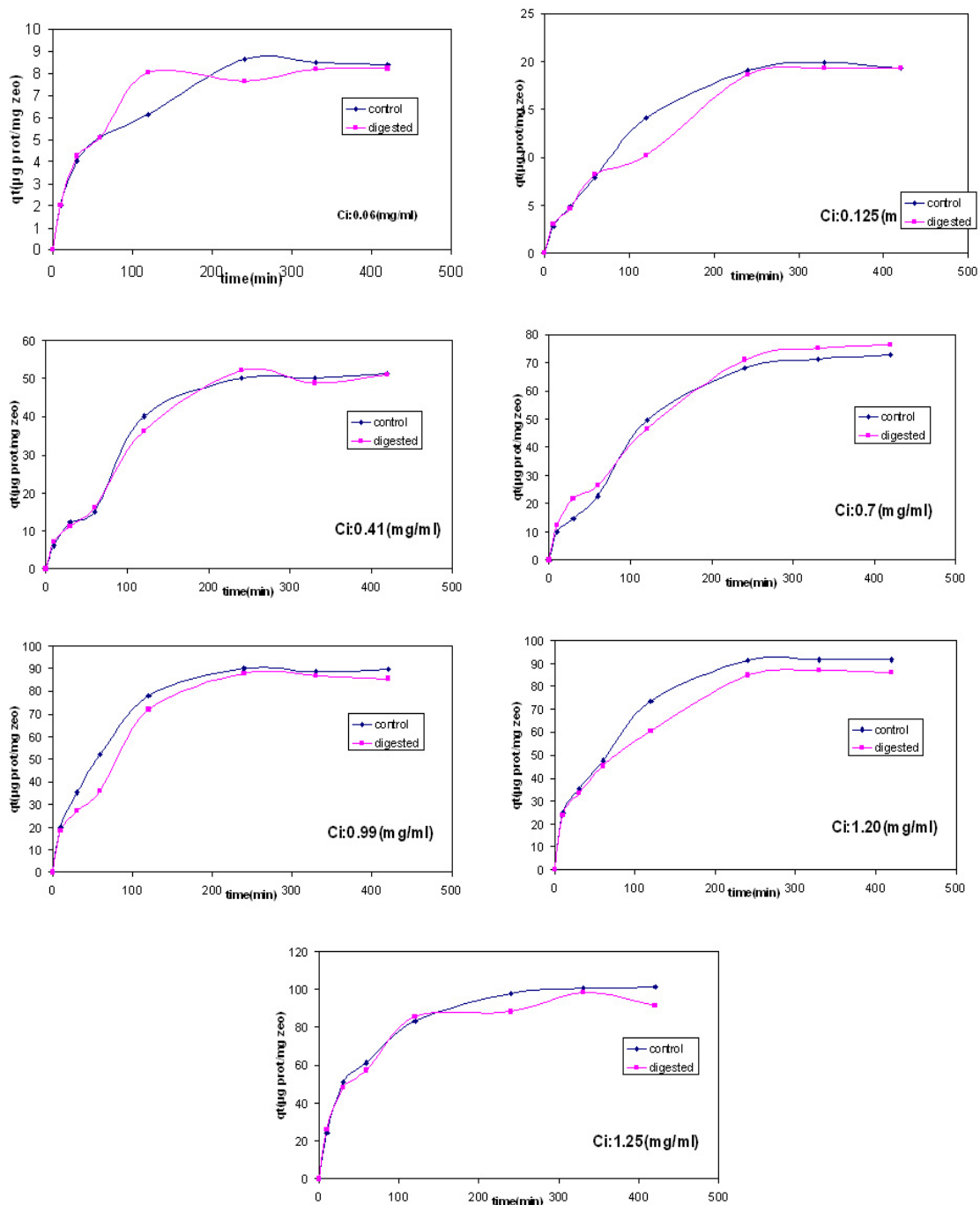


Figure 7.9. Comparison of the uptake curves for the digested and non digested (control) zeolite (37°C, 150 rpm, S/L:5mg/ml, pH 6.8, particle size: 45-75µm)

Results of the uptake values for GUS and casein adsorption at different initial concentrations were given in Figures 7.10-11. Results showed that adsorption equilibrium was reached after 60-120 and 330 and 420 minutes depending on the initial

adsorbate concentration. Initial concentrations lead an increase in adsorption rates in both uptake curves because when the initial concentration increased, concentration differences between the solid phase and the liquid phase was also increased which resulted higher driving force to overcome the mass transfer resistances.

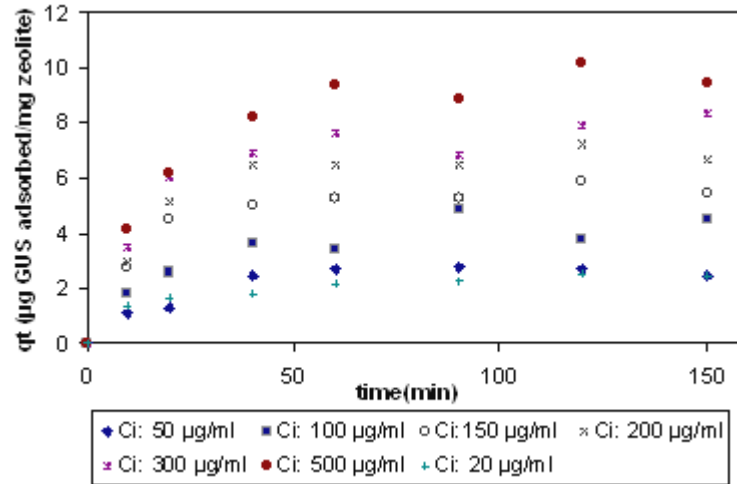


Figure 7.10. Uptake curves for GUS adsorption onto zeolite (37°C, 150 rpm, S/L:5mg/ml, pH 6.8, particle size: 45-75µm)

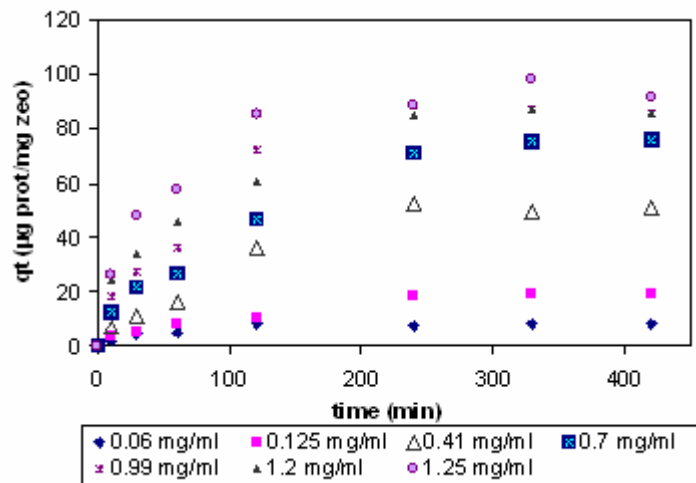


Figure 7.11. Uptake curves for casein adsorption onto zeolite (37°C, 150 rpm, S/L:5mg/ml, pH 6.8, particle size: 45-75µm)

To investigate the reduction ratios in the free amount of adsorbate, plot of  $C_t/C_0$  vs time was given in Figures 7.12-13. Results indicated that there were three distinct regions in both plots. Adsorption was faster at the initial period of the adsorption and especially within first 0-10 minutes for GUS and 0-30 minutes for casein. After the fastest step (I), a gradual decrease was observed in the amount of free adsorbates (II) and



at last, equilibrium was reached (III). Those distinct curves in adsorption were also observed in different studies (Nassar et al., 2008; Al-Ghouti et al., 2009). For 37 °C, reduction in the free GUS amounts were 9.4 and 54.4 % for the highest (500 µg/ml) and lowest (20 µg/ml) initial GUS concentrations, respectively. For free casein, reductions in percentages were varied in the range of 36.5 - 77.3 % for 1.25 -0.06 mg/ml casein. For both adsorbates, steep slope curve in the first (I) region might be due to the effect of surface acidic functional groups on zeolite which can be silanol groups (Tavolaro et al., 2007).

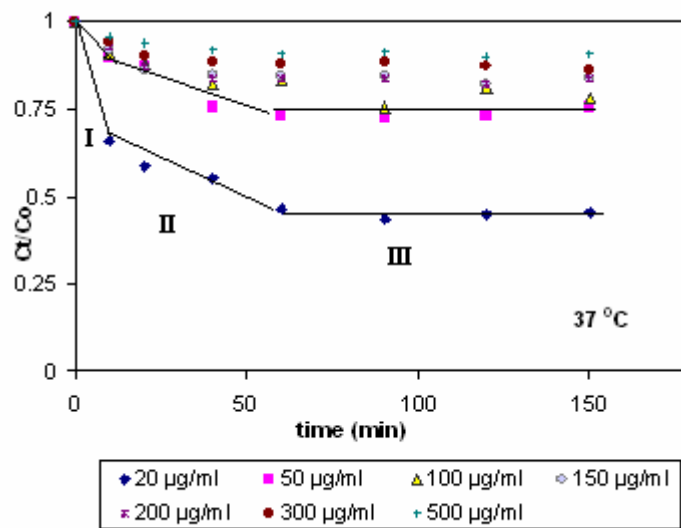


Figure 7.12. Uptake curves representing the reduction in the free GUS concentration (37°C, 150 rpm, S/L:5mg/ml, pH 6.8, particle size: 45-75µm).

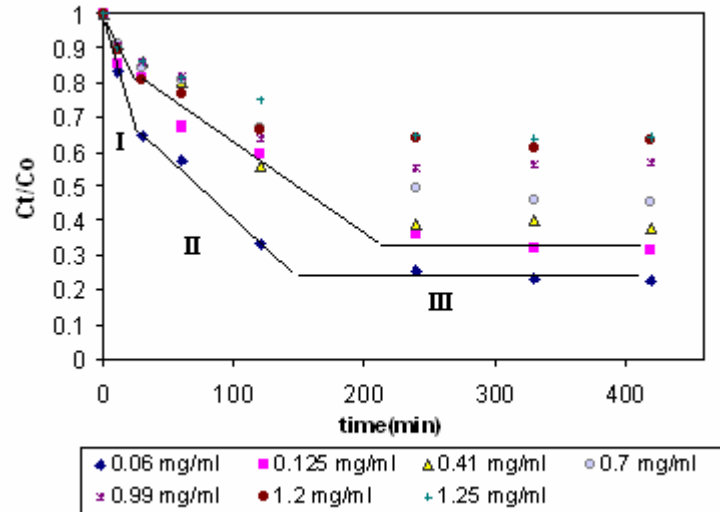


Figure 7.13. Uptake curves representing the reduction in the free casein concentration (37°C, 150 rpm, S/L:5mg/ml, pH 6.8, particle size: 45-75µm).

### Effect of Solid Liquid Ratio

Effect of solid liquid ratio on adsorption kinetics was investigated and results were given in Figure 7.14-16 below. Results showed that an increase in zeolite concentration increased the amount of GUS and casein adsorbed. Since higher amounts of adsorbent provided higher amounts of surface area, adsorbed amount might be increased.

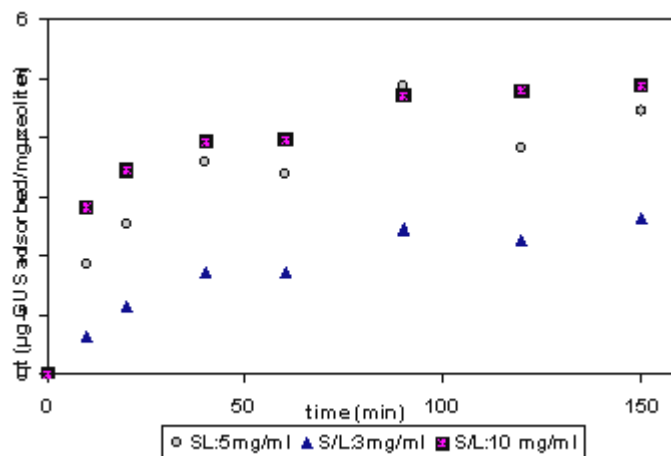


Figure 7.14. Effect of solid liquid ratio on adsorption kinetics of GUS by zeolite (37°C, 150 rpm, Ci:100µg/ml, pH 6.8, particle size: 45-75µm).

It was important to note that at the end of 150 minutes, adsorbed amount of GUS (67.3% increase) changed significantly for the adsorbent concentrations was increased from 3 to 5 mg/ml. However, increase in the adsorbed amount was lower and found as 9.6% when the adsorption capacities using 5 and 10 mg/ml zeolite were compared. This might be because of existence of complex interactions at higher zeolite concentrations. Similar case was reported by Sağ and Aktay (2000) where they studied Cr(IV) adsorption on chitin. They suggested increase in sorbent concentration triggered the interactions such as collision of adsorbent thus adsorbed amount was negatively affected.

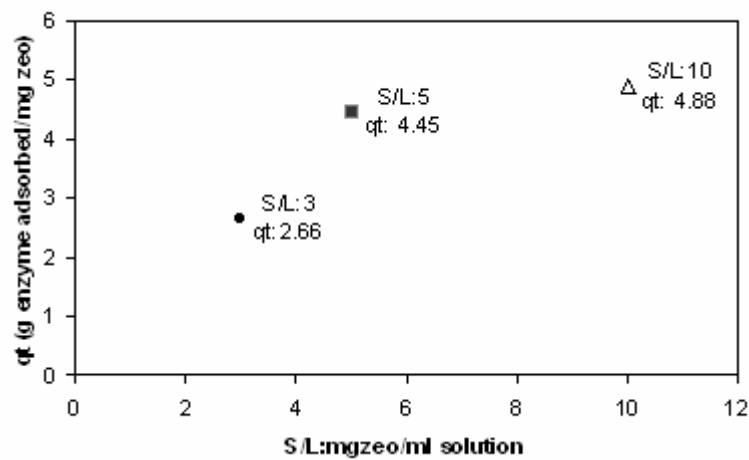


Figure 7.15. Effect of solid liquid ratio on adsorbed amounts of GUS at the end of 150 minutes.

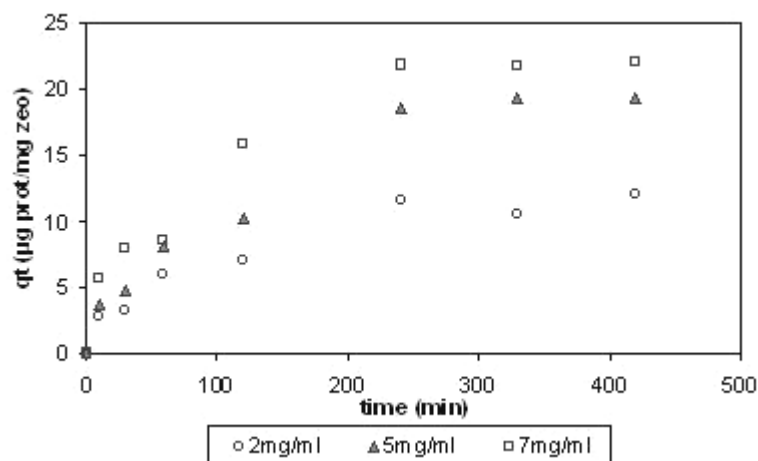


Figure 7.16. Effect of solid liquid ratio on adsorption kinetics of casein by zeolite (37°C, 150 rpm, Ci:0.125 mg/ml, pH 6.8, particle size: 45-75µm).

### Effect of Shaking Rate

Shaking rate is important for the distribution of the molecules in the bulk solution. Besides, it affects the film thickness of liquid layer surrounding the zeolite particle. A series of contact time experiments were conducted at various degrees of shaking rate for the adsorption of GUS and casein onto the zeolite and results were given in Figures 7.17-18 below.

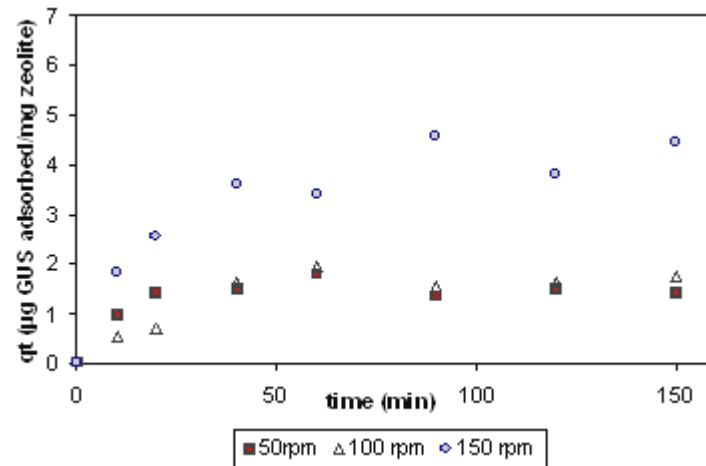


Figure 7.17. Effect of shaking rate on adsorption kinetics of GUS by zeolite (37°C, S/L:5mg/ml Ci:100µg/ml, pH 6.8, particle size: 45-75µm).

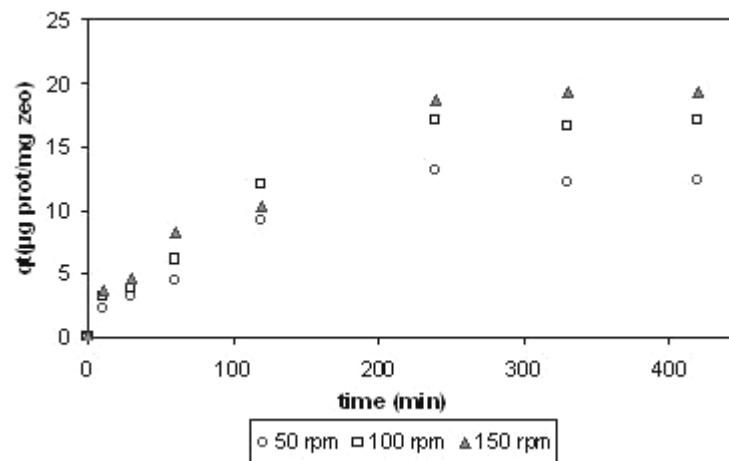


Figure 7.18. Effect of shaking rate on casein adsorption onto zeolite (37°C, Ci:0.125 mg/ml, S/L:5mg/ml, pH 6.8, particle size: 45-75µm).

Results showed that shaking rate was effective on adsorption kinetics. As the shaking rate was increased, adsorption rate was increased for both adsorbates. This can be explained by the differences in the external-mass transfer rates for the different

shaking rates. Since the external mass transfer resistance is proportional to the film thickness of the liquid layer, a higher shaking rate decreased the film thickness.

### ***Effect of pH***

Three different pH values were selected in order to see their effects on adsorption kinetics. Optimum pH for the GUS activity was 6.8. In this study, pH 5.5 and 8 were also investigated which might give idea about adsorption kinetics in the ranges of the intestinal pH with respect to pH ranges of fed and fasted conditions of the intestinal system. Results were given in Figure 7.19.

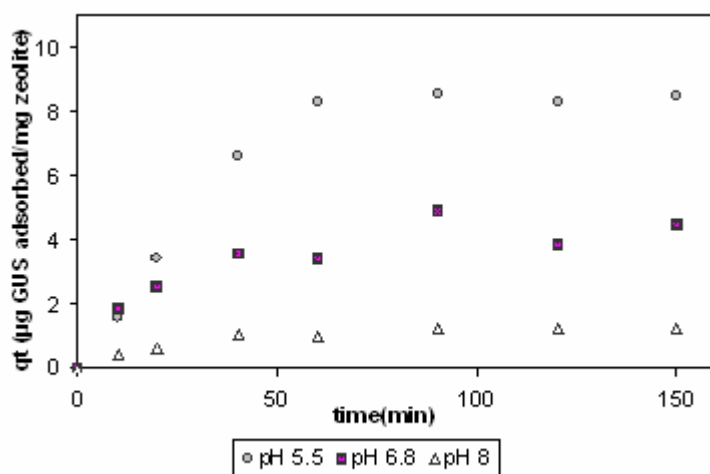


Figure 7.19. Effect of pH on adsorption kinetics of GUS by zeolite (37°C, S/L:5mg/ml Ci:100µg/ml, 150 rpm, particle size: 45-75µm).

Results showed that adsorption kinetics were affected with the pH of the solution. In pH 5.5, very low adsorbed amounts were achieved. Increase in pH resulted 7.1 times higher amount of GUS adsorbed and adsorbed amount increased from 1.19 to 8.46 µg/mg. It was important to note that change in adsorption capacities with different pH values is highly related to surface charges of both zeolite and GUS. Therefore effect of pH was discussed separately considering both GUS and zeolite phases.

At acidic conditions protonation of zeolite surface was reported whereas at alkaline conditions deprotonation of the zeolite occurred (Polatoğlu and Ozkan, 2010; Dolua et al., 2001). pH 5.5 can be considered as mild acidic condition. At pH 5.5 zeolite,  $\equiv \text{Si-OH}$  and  $\equiv \text{Al-OH}_2^+$  groups might be dominant yielding net positive charge. However, at pH 6.8 net surface charge will be lower thus neutral  $\equiv \text{Al-OH}$  and  $\equiv \text{Si-OH}$  groups might be dominant. Besides at pH 6.8 charged groups ( $\equiv \text{Al-OH}_2^+$ ;  $\equiv \text{Al-O}^-$ ;  $\equiv \text{Si-O}^-$ )

$O^-$  ;  $\equiv Si-OH_2^+$ ) will still exist on zeolite surface however they will be at very low concentrations (Doula et al., 2001). At pH 8; net charge of the zeolite surface will be negative where  $\equiv Si-O^-$  and  $\equiv Al-O^-$  groups will be dominant. Zeta potential measurements of zeolite in solutions with different pH values were performed and results showed that zeolite was net negatively charged (Figure 7.20).

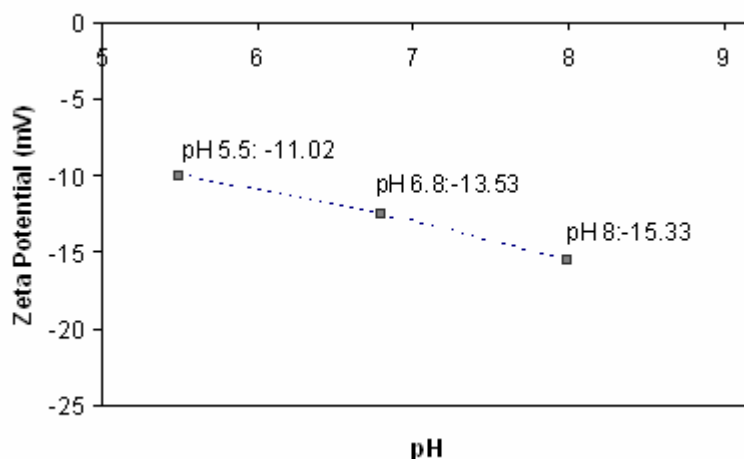


Figure 7.20. Variations in the zeta potential of zeolite (5mg/ml) in adsorption solutions (potassium phosphate buffer, pH 5.5-6.8-8 at 37°C).

Amount of released ions from clinoptilolite to the solution can change depending upon the presence of impurities, solution temperature and pH. Ersoy and Çelik (2002) investigated the changes in zeta potential of natural zeolites with respect to pH, ions and solid amount and they reported that amounts of released ions into the solution was very low (Al, Si, K, Ca, Na, Mg, and Fe), did not change with the change in the solid amount thus they did not affect the zeta potential of zeolite. This is because, ion exchange process in zeolites is a stoichiometric reaction therefore, equivalent amounts of cations generated to maintain the total electroneutrality.

Behaviour of zeolite with the presence of  $K^+$  in solution might be different and changes in the zeta potentials of zeolite might be attributed to presence of  $K^+$  ions in working solution. Adsorption working solution is potassium phosphate buffer at different pH values. Those ions could accumulate on the zeolite surface and might change the zeta potentials of zeolite. This case was reported by Ersoy and Çelik (2002) that monovalent counterions ( $NH_4^+$  and  $K^+$ ) accumulate at the negatively charged clinoptilolite because of the coulombic attraction. Thus, they change the magnitude of the zeta potential of clinoptilolite.

Table 7.4. Variations in zeta potential of GUS enzyme with pH (potassium phosphate buffer, pH 5.5-6.8-8 at 37°C).

<b>pH</b>	<b>ζ potential :domain-1 (mV)</b>	<b>ζ potential :domain-2 (mV)</b>
5.5	-42.0	-4.1
6.8	-52.1	-5.2
8	-46.4	9.6

For GUS enzyme, isoelectric point (pI) is 4.8 therefore it should have net negative charge at all three pH values. Zeta potential measurements of GUS were performed in same solutions (phosphate buffer at pH 5.5, 6.8 and 8). Results of the charge distributions at three pH values and change in the zeta potentials were given in Figure 7.21-7.23 and Table 7.4 respectively. Results showed that during zeta potential measurements GUS enzyme behaved as two domains and both domains had a negative charge for pH values 5.5 and 6.8. However, it was interesting to observe that at pH 8, a positive charged domain was observed. Although its average positive charge was small (+9.6 mV) it might be effective in adsorption process.

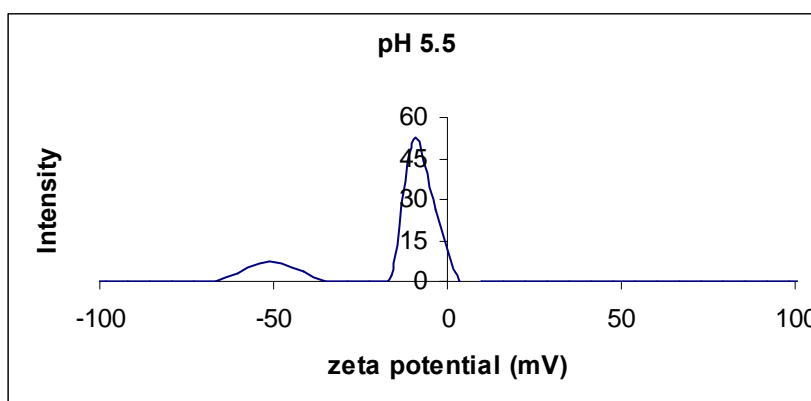


Figure 7.21. Charge distribution of GUS at pH 5.5.

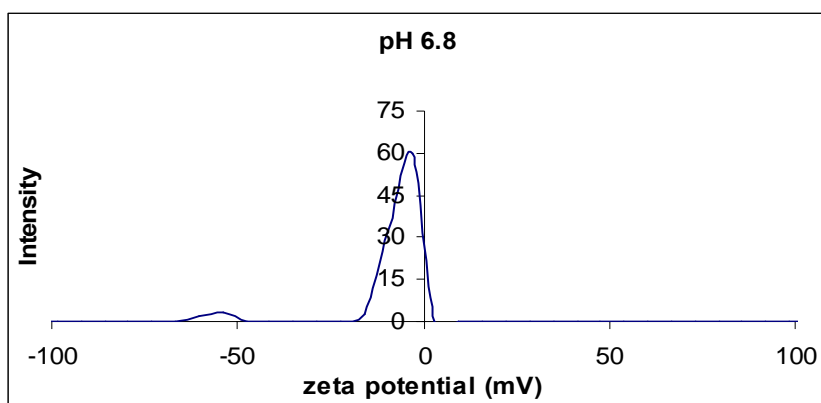


Figure 7.22. Charge distribution of GUS at pH 6.8.

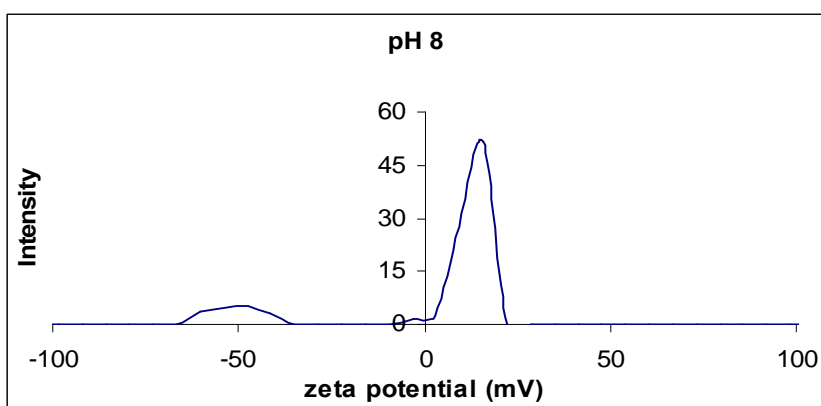


Figure 7.23. Charge distribution of GUS at pH 8.

Results of the size distribution of GUS (Figure 7.24) with respect to different pH values showed that size of the GUS molecule did not considerable changed with the pH. Mean size of the GUS was found as 97.5, 95.7 and 108.8 for the pH 5.5; 6.8; and 8 respectively. Results of the zeta potential measurements revealed that electrostatic repulsion between zeolite and GUS might be more dominant compared to electrostatic attraction except pH 8 in adsorption.



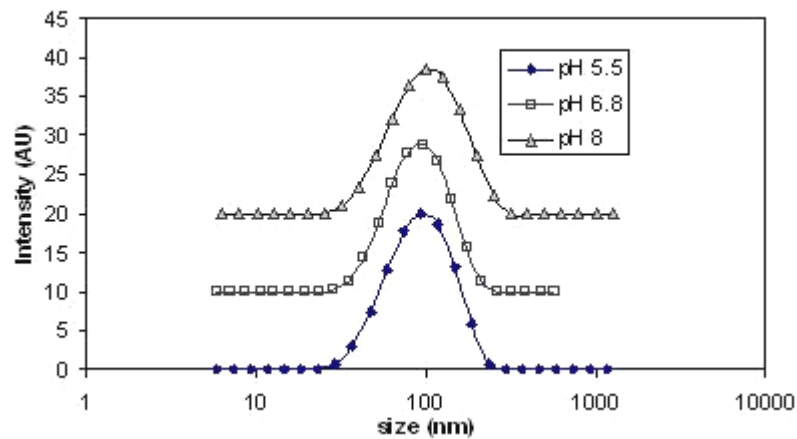


Figure 7.24. Size distribution of GUS at different pH values.

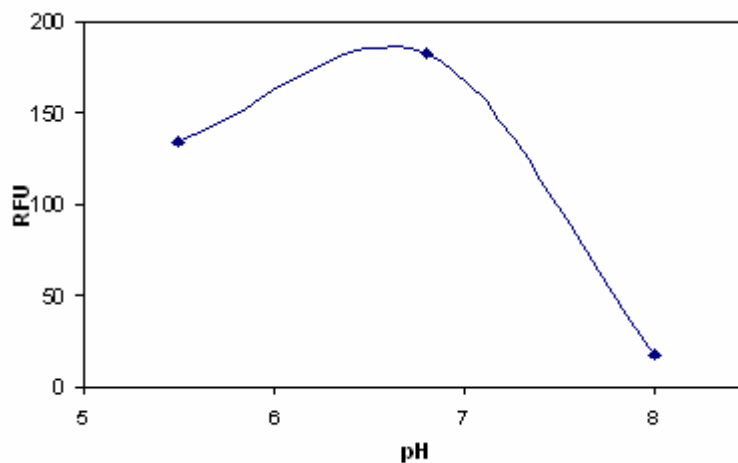


Figure 7.25. Variation in activity of GUS (relative fluorescence unit:RFU) with pH.

Higher adsorption capacities were achieved at pH 8 which might have due to the electrostatic attraction. Since both positive and negative groups exist at both surfaces electrostatic interactions between the  $\text{COO}^-$  and  $\equiv\text{Al-OH}_2^+$  groups might be active as well as  $\text{NH}_3^+$  and  $\equiv\text{Si-O}^-$  of enzyme and zeolite. However, effect of pH8 on the conformational stability of the enzyme was not clear which might be the reason behind the positively charged part of the GUS enzyme at pH 8. This unusual case can be explained by the possible denaturation of the GUS enzyme at that pH. Activity measurements were performed with respect to pH and results showed that activity of enzyme reduced 26.4% and 90.1 % when the pH of the working solution changed from 6.8 (optimum pH for GUS activity) to 5.5 and 8, respectively (Figure 7.25).

Similar case was reported by Jefferson et al. (1986) where enzyme was found to be stable at pH 5-7.5. Besides the difference in charge distribution at pH 8; possible denaturation or conformational change of enzyme in alkaline conditions might have altered the solubility and position of the ( $-\text{COOH}$ ) and ( $-\text{NH}_2$ ) functional groups on the GUS surface. Those changes might have lead stronger H bonding. Thus, cumulative effects of electrostatic interactions, solubility and position changes with respect to denaturation might have triggered multilayer adsorption thus higher adsorption capacities were achieved.

### ***Effect of Partice Size***

Effect of particle size on adsorption kinetics of GUS and casein were investigated using three different size ranges of zeolites. Results were given in Figures 7.26-27. Results showed that adsorption rates were increased with the decrease in particle size. Higher adsorption capacities were also obtained with the decrease in particle size. This might be because of the increase of the external surface area of the zeolite with the decrease in its size. Thus smaller particles provided greater surface area and more number of active sites became available for the same mass of adsorbent. Since the adsorption is a surface phenomenon higher equilibrium concentrations was reached with smaller particles.

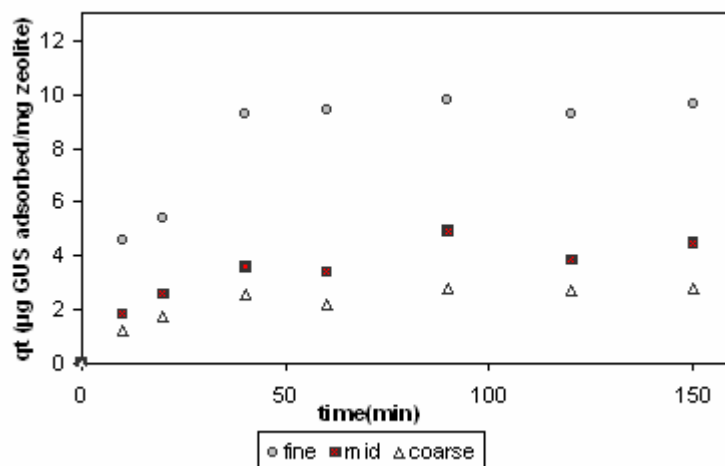


Figure 7.26. Effect of particle size on adsorption kinetics of GUS by zeolite. Fine: 25-45  $\mu\text{m}$ ; mid:45-75  $\mu\text{m}$ ; coarse 75-106  $\mu\text{m}$ . (37°C, S/L:5mg/ml Ci:100 $\mu\text{g/ml}$ , pH:6.8, 150 rpm).

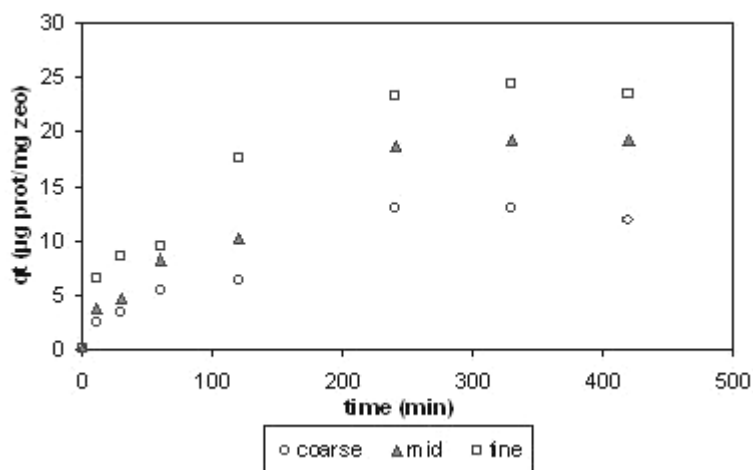


Figure 7.27. Effect of particle size on casein adsorption onto zeolite. Fine: 25-45  $\mu\text{m}$ ; mid:45-75  $\mu\text{m}$ ; coarse 75-106  $\mu\text{m}$  (37°C, S/L:5, 150 rpm, Ci:0.125 mg/ml, pH 6.8).

### ***Effect of Temperature***

Effect of temperature on adsorption kinetic was investigated at temperature values of 15°C; 25°C and 37 °C and results were given in Figures 7.28-29 below. Both results of GUS and casein adsorption indicated that, adsorption capacity of zeolite was increased with the decrease in temperature. This case was more obvious for GUS. At 15 °C and 25 °C, there was not a considerable difference in adsorption behaviour of zeolite. However at 37 °C adsorption capacity was considerably reduced. Such as, adsorbed

amount of GUS at 120 minutes were 9.33; 9.03 and 3.82 at 15, 25 and 37 °C, respectively.

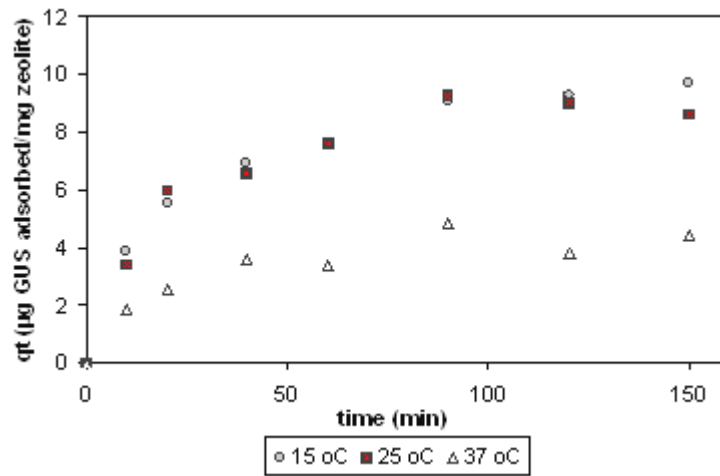


Figure 7.28. Effect of temperature on adsorption kinetics of GUS by zeolite (S/L:5 mg/ml, 150 rpm, Ci:100µg/ml, pH 6.8, particle size: 45-75µm).

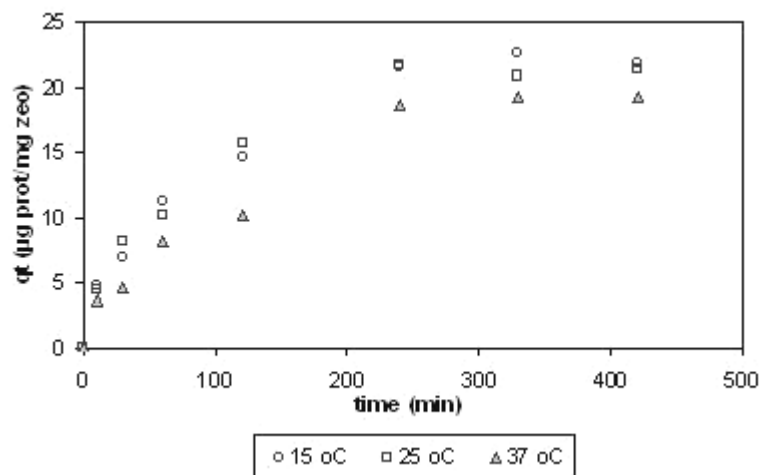


Figure 7.29. Effect of temperature on adsorption kinetics of casein by zeolite (37°C, 150 rpm, Ci:0.125 mg/ml, S/L:5, pH 6.8, particle size: 45-75µm).

Therefore, results in this study implied that adsorption was physical and exothermic for both adsorbates, and possible interactions between adsorbates and zeolite might be electrostatic, hydrogen bonding, and van der Waals interactions. The temperature increase would cause decrease of binding force between adsorbates and zeolite thus the adsorption capacity at higher temperature was lower compared to lower temperatures.

### 7.3.2. Adsorption Isotherms

The equilibrium data for GUS and casein adsorption onto zeolite were analyzed using Langmuir and Freundlich models. The Freundlich constants  $K_f$  and  $n$  were analyzed by drawing  $\log q_e$  versus  $\log C_e$  and Langmuir constants  $q_m$  and  $K_L$  were found by plotting  $1/q_e$  versus  $1/C_e$ . Characteristic constant for each isotherm were also determined. Results were given below.

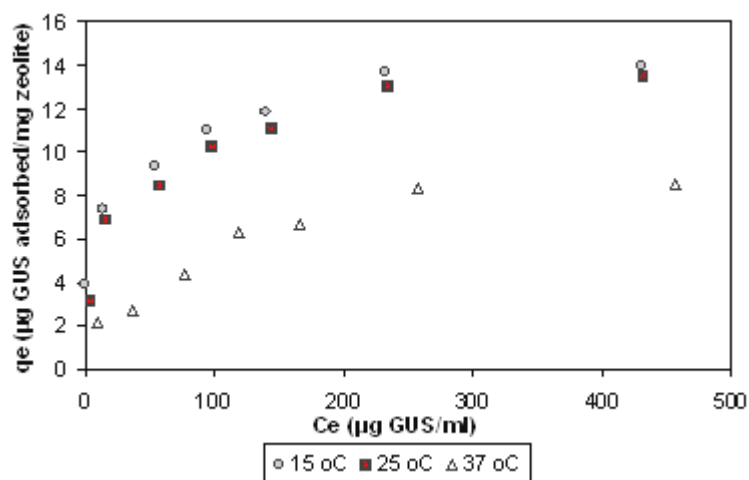


Figure 7.30. Adsorption isotherms for GUS (at 15, 25 and 37°C).

Table 7.5. Langmuir and Freundlich constants for GUS adsorption.

Temperature (°C)	Langmuir Isotherm			Freundlich Isotherm		
	$q_m(\mu\text{g}/\text{mg})$	$K_L(\text{ml}/\text{mg})$	$R^2$	$K_f(\mu\text{g}/\text{mg})$	$N$	$R^2$
15	14.41	54.60	0.9946	4.57	0.19	0.9937
25	14.20	36.79	0.9944	2.52	0.30	0.9401
37	10.00	13.73	0.9764	1.01	0.36	0.9023

Results for the Langmuir model which is based on the monolayer coverage demonstrated superiority to Freundlich model especially for higher temperatures. Results showed that maximum adsorption capacity were close to each other and at around 14µg/ml for the temperatures of 15 and 25 °C (Figure 7.30). However, it was reduced to 10µg/ml when the temperature was increased to 37 °C. At 15 °C, highest adsorption was achieved. It was interesting to note that  $R^2$  values (square of the

coefficient of linear correlation between  $q$  and  $C$  which is a measure of the fitting accuracy to models) for each model were close to each other (Table 7.5).

Similar case was also observed for casein adsorption. Adsorption isotherms at were shown in Figure 7.31 below. Results indicated that isotherm was concave to the concentration axis and has a long plateau, which indicated that this isotherm was type I isotherm. Type I isotherms were associated with the monolayer coverage of solutes.

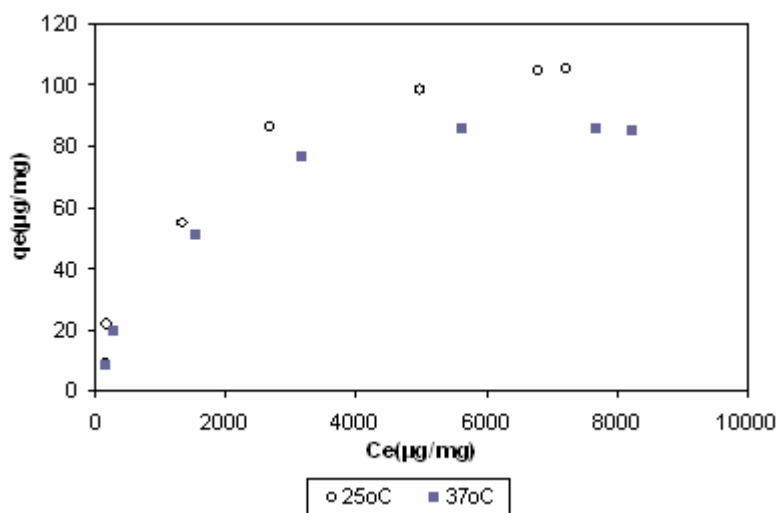


Figure 7.31. Adsorption Isotherms for casein (at 25 and 37°C).

Characteristic constant for each isotherm were calculated and results were given in Table 7.6 below.  $R^2$  was the square of the coefficient of the linear correlation between  $C$  and  $q$  whose proximity to 1 was a measure of the fitting accuracy of the models. Results of the Langmuir model demonstrated superiority to Freundlich model. Therefore results implied that adsorption of casein onto zeolite was occurred by monolayer coverage and maximum adsorbed amount of casein increased with the decrease in temperature.

Table 7.6. Langmuir and Freundlich constants for casein adsorption at 25 and 37°C.

Temperature (°C)	Langmuir Isotherm			Freundlich Isotherm		
	$q_m(\mu\text{g}/\text{mg})$	$K_L(\text{ml}/\text{mg})$	$R^2$	$K_f(\mu\text{g}/\text{mg})$	$n$	$R^2$
25	128.21	0.65	0.9855	0.80	0.57	0.9257
37	105.26	0.62	0.9870	0.59	0.57	0.9256

### 7.3.3. Thermodynamic Parameters

To understand how GUS adsorption onto zeolite proceeds, thermodynamic parameters were analyzed for three different temperatures; 15, 25 and 37 °C. Therefore free energy of change  $\Delta G^\circ$  (kJ/mol), change of enthalpy  $\Delta H^\circ$  (kJ/mol) and change of entropy  $\Delta S^\circ$  (j/mol K) for the adsorption were determined. These parameters were calculated using the equation given below where the Gibbs free energy change in adsorption is related to adsorption equilibrium constant by Van't Hoff equation.

$$\Delta G^\circ = -RT \ln K = \Delta H^\circ - T\Delta S^\circ \quad (7.1)$$

Since the Langmuir isotherm has superiority to represent the adsorption equilibrium for the three temperatures  $K_L$  was used to determine thermodynamic parameters (Lataye et al., 2006; Al-Degs et al., 2008). Therefore in the equation; K is the Langmuir constant, R is the universal gas constant, 8.314 (j/mol.K), T is the absolute temperature. Plot of the experimental data using the following Van't Hoff equation was given in Figure 7.21. Thus,  $\Delta H^\circ$  (kJ/mol)  $\Delta S^\circ$  (kJ/mol) were determined from the slope and the intercept of the Figure 7.32. Calculated parameters were given in Table 7.7 below.

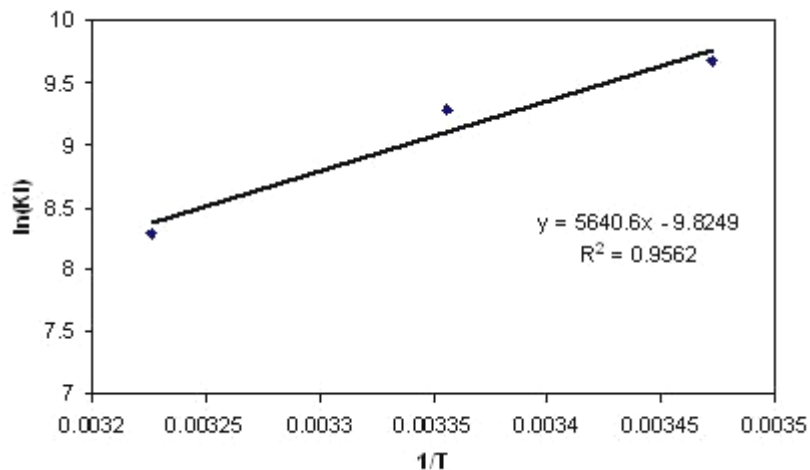


Figure 7.32. Van't Hoff's plot from Langmuir isotherm constants.

Table 7.7. Thermodynamic parameters for GUS adsorption on zeolite.

$\Delta H^\circ$ (kJ/mol)	$\Delta S^\circ$ (j/mol K)	$\Delta G^\circ$ (kJ/mol)		
		T=288 K	T=298 K	T=310 K
-46.89	-81.68	-23.15	-22.98	-21.36

For casein adsorption, to calculate the thermodynamic activation parameters of such as free energy change  $\Delta G^*$  (kJ/mol), change of enthalpy  $\Delta H^*$  (kJ/mol) and change of entropy  $\Delta S^*$  (j/mol K) for the adsorption, the Eyring equation was applied (Al-Ghouti et al., 2005). Eyring equation is a theoretical construct, based on transition state theory. The principles of transition state theory are: there is a thermodynamic equilibrium between the transition state and the state of reactants at the top of the energy barrier and the rate of chemical reaction is proportional to the concentration of the particles in the high-energy transition state. Assuming a rapid pseudo equilibrium between transition state molecules and reactant molecules, rate constant k is:

$$k = \frac{k_B T}{h_p} K^* \quad (7.2)$$

where  $k_B$  is the Boltzmann constant ( $1.3807 \times 10^{-23}$  J/K),  $h_p$  is the Planck constant ( $6.6261 \times 10^{-34}$  J s), k is the rate constant and  $K^*$  is equilibrium constant of thermodynamics.

using following Van't Hoff equation of thermodynamics :

$$\Delta G^* = -RT \ln K^* \quad (7.3)$$

Eyring Equation is:

$$\ln\left(\frac{k}{T}\right) = \left[ \ln\left(\frac{k_B}{h_p}\right) + \frac{\Delta S^*}{R} \right] - \frac{\Delta H^*}{R} \left(\frac{1}{T}\right) \quad (7.4)$$

Using Eyring equation activation (difference between transition state and ground state) enthalpy and entropy changes of adsorption were calculated from the slope and intercept of the  $\ln(k/T)$  vs  $1/T$  graph (Figure 7.33) and results were represented in Table 7.8



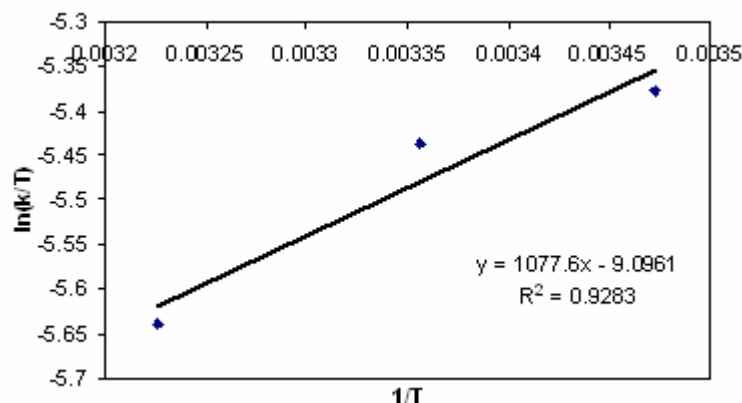


Figure 7.33. Eyring plot of  $\ln(k/T)$  vs  $1/T$  for the adsorption of casein onto zeolite.

Table 7.8. Thermodynamic parameters for casein adsorption on zeolite.

$\Delta H^*$ (kJ/mol)	$\Delta S^*$ (j/mol K)	$\Delta G^*$ (kJ/mol)		
		T=288 K	T=298 K	T=310 K
-8.96	-273.2	69.71	72.44	75.72

For both casein and GUS adsorption, free energy changes give idea about the feasibility of the adsorption process (Chang et al., 2006) thus the higher absolute values of free energy change implies higher adsorption property. The  $\Delta G^0$  values of GUS were negative which showed that free energy decreased with the adsorption. Besides, negative  $\Delta G^0$  indicates that adsorption of the GUS onto zeolite surface is spontaneous. The negative value of entropy change indicated that degree of freedom decreases at solid/liquid interface during the adsorption for both casein and GUS. Enthalpy changes showed that adsorption of GUS and casein onto zeolite was exothermic process, which was suggested by the negative values of the enthalpy changes.

In literature enthalpy changes were associated with adsorption behaviour and they indicated physical or chemical nature of the adsorption. Especially for the physical adsorption the enthalpy change was reported to be in the range of 10–30 kJ/mol (Wang et al., 2007) or <84 kJ/mol (Al-Degs et al., 2008). Additionally, free energy change was also associated with the adsorption behaviour and 0 to -20 kJ/mol was the reported range for the physical adsorption and -80 to -400 kJ/mol was referred to be the range for the chemical adsorption (Tu et al., 2009). Therefore, it was hard to decide the adsorption behaviours of both adsorbates either physical or chemical. The calculated value of enthalpy change for GUS adsorption was found as -46.89 kJ/mol. Although there was no study in literature about the adsorption of GUS on natural zeolite, synthetic

zeolite NaY was used for lipase and lysozyme and adsorption processes were found as physical adsorption (Knezevic et al., 1998; Chang et al., 2006). Considering both  $\Delta H^\circ$   $\Delta G^\circ$ ; results of thermodynamic data implied that adsorption was exothermic, and values of the enthalpy and entropy change might be accepted as in the range of physical adsorption. For casein, enthalpy change is smaller than GUS and it was found to be - 8.96 kJ/mol. Therefore, for both of the adsorbates, adsorption process was physical in nature and  $\pi$ - $\pi$  interaction, the Van derWaals force and hydrogen-bonding were possibly involved in the adsorption mechanism (Wang et al., 2007; Chang et al., 2006). It is important to note that In literature exothermic adsorption processed are commonly referred as enthalpy driven whereas endothermic processed are commonly referred as entropy driven processes (Tu et al., 2009). Additionally, enthalpy driven processes were reported to be affected by direct electrostatic interactions however entropy driven process were reported to be more affected by hydrophobic interactions (Kim and Lee, 2007; Tu et al., 2009). Therefore thermodynamic parameters implied that adsorption of GUS and casein onto zeolite might be enthalpy driven and electrostatic interactions might be effective at that point of view.

As well as the free energy, enthalpy and entropy changes, activation energies were also important to understand the physical and chemical nature of the adsorption. The rate constants for the 2<sup>nd</sup> order model or intraparticle diffusion model can be used to estimate the activation energies (Al-Ghouti et al., 2005). Assuming the correlation among the rate constant k, temperature T and activation energy Ea follows the Arrhenius equation activation energy value can be calculated by the following formula:

$$k = A_a - e^{EA/RT} \quad (7.5)$$

where R (=8.314 kJ/mol<sup>-1</sup>), Aa:is the frequency factor of adsorption, EA (kJ/mol<sup>-1</sup>) the activation energy of adsorption and T(K) is the solution temperature. When ln k is plotted versus 1/T, a straight line with slope EA/R was obtained.

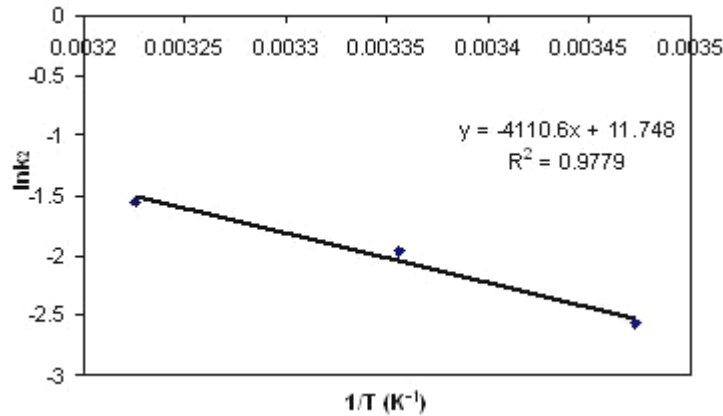


Figure 7.34. Arrhenius plot of  $\ln k_2$  vs  $1/T$  for the adsorption of GUS onto zeolite.

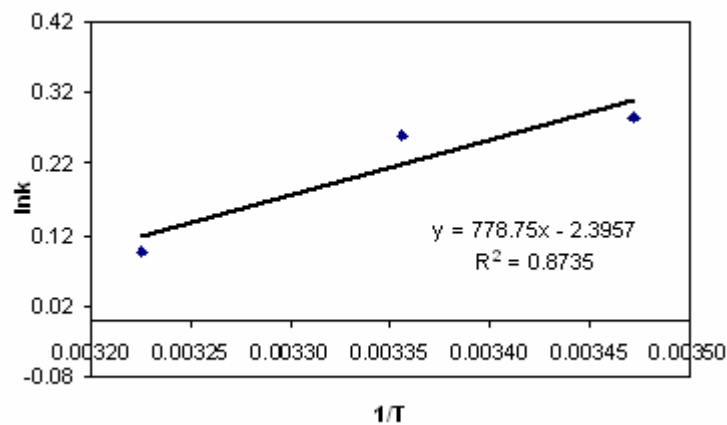


Figure 7.35. Arrhenius plot of  $\ln k_d$  vs  $1/T$  for the adsorption of casein onto zeolite.

From the Figures 7.34-7.35, activation energies for GUS and casein adsorption were found to be 34.14 and -6.5 kJ/mol. Since the rates of sorption reactions increase more rapidly than those of diffusion processes with temperature, activation energies should be high in chemical sorption compared to physical sorption. Therefore results of the activation energies implied that both GUS and casein adsorption onto zeolite were physical adsorption. Those results were also in good agreement with the results of enthalpy changes. Ho et al. (2000) reported that when  $k_d$  is plotted against reciprocal temperature using Arrhenius plot, the activation energy of adsorption is greater than 25–30 kJ/mol for chemically controlled processes. Additionally, studies in literature established that low activation energies <42 kJ/mol were attributed to diffusion controlled physical process and activation energies >42 kJ/mol were attributed to chemically controlled processes (Al-Ghouti et al., 2005). Based upon these values adsorption of the GUS and casein onto zeolite was exothermic and physical adsorption.

### 7.3.4. Adsorption Mechanism

Kinetic behaviour of the adsorbate and the adsorbant in solution during adsorption can be modeled by different equations. Those equations can be classified as reaction models and diffusion models and they were powerful tools to investigate controlling mechanism. Therefore different mathematical models were applied to examine the kinetic experimental data and adsorption rates and diffusion constants were calculated for GUS and casein adsorption onto zeolite.

It was important to note that GUS and casein adsorption was highly depended on pore size of zeolite and molecular weight and size of the proteins. This case is important to understand significance of the surface and pore diffusions in the adsorption rate control. Proteins are large molecules and they can not usually go through the pores of natural zeolites which are at A° level. Such as, BSA is an oval globular protein of 69kDa molecular weight and with a long radius of 7 nm (Sakaguchi, 2005; Chiku et al., 2003) and it is widely used in adsorption studies. Therefore, accessibilities of the casein and GUS molecule were controlled by dimensions of pore and channel systems of zeolite. Pore size distribution studies (Chapter 6) showed that pore size of zeolite (micropores and mesopores) varied in the range of 2.5 to 12 nm. However, size of the casein measured in SIF solution was 324 nm. It has miscelluar structure and it is highly hydrophobic thus mostly preserves its coil like shape in solution. On the other hand, GUS has a tetramer structure with high molecular weight of 290 kDa and its size distribution showed that its size was smaller than casein and varied in the range of 60-120 nm in SIF solution (phosphate buffer pH 6.8). Although its measured size was found to be too large, there was no literature study about the size of the GUS molecule.

Nakanishi et al. (2001) reported that molecular dimensions of proteins are represented by  $axbxc$  and are considered as having two conformations. One with a long axis is known as end-on-type and the other with a short axis called side-on type which is important for the orientation of proteins in the adsorption. They determined side-on and end-on orientations of globular proteins having considerably lower molecular weight (14-160 kDa). However, for fibrinogen (with higher molecular weight of 340 kDa), they could not categorize the orientation and determined that several orientations co-exist in fibrinogen (Nakanishi et al., 2001). Therefore, dynamic behaviour of GUS might change in solution and different orientations on the terminals of aminoacid side chains

can be formed for GUS. Casein also might behave in the same manner. Thus, terminals possibly having shorter amino acid chains could bend and might diffuse through the pores on zeolite surface.

The macropore sizes of the mineral pores among the zeolite crystals were measured by SEM analyzes. Results in Figure 7.36 showed that macropore sizes of the zeolites samples used in adsorption experiments ranged between 784-4400 nm and they were large enough for both casein and GUS to diffuse inside. SEM analyzes were successfully used to define the pore structures and macroporous morphologies of zeolite and silica (Sprynskyy et al., 2010; Kowalczyk et al., 2006; Basenger et al., 2006). The macroporous structure of the mineral might allow these proteins to enter the pores and diffuse inside. Therefore, in addition to external diffusion, pore diffusion is also possible for both proteins during the adsorption process.

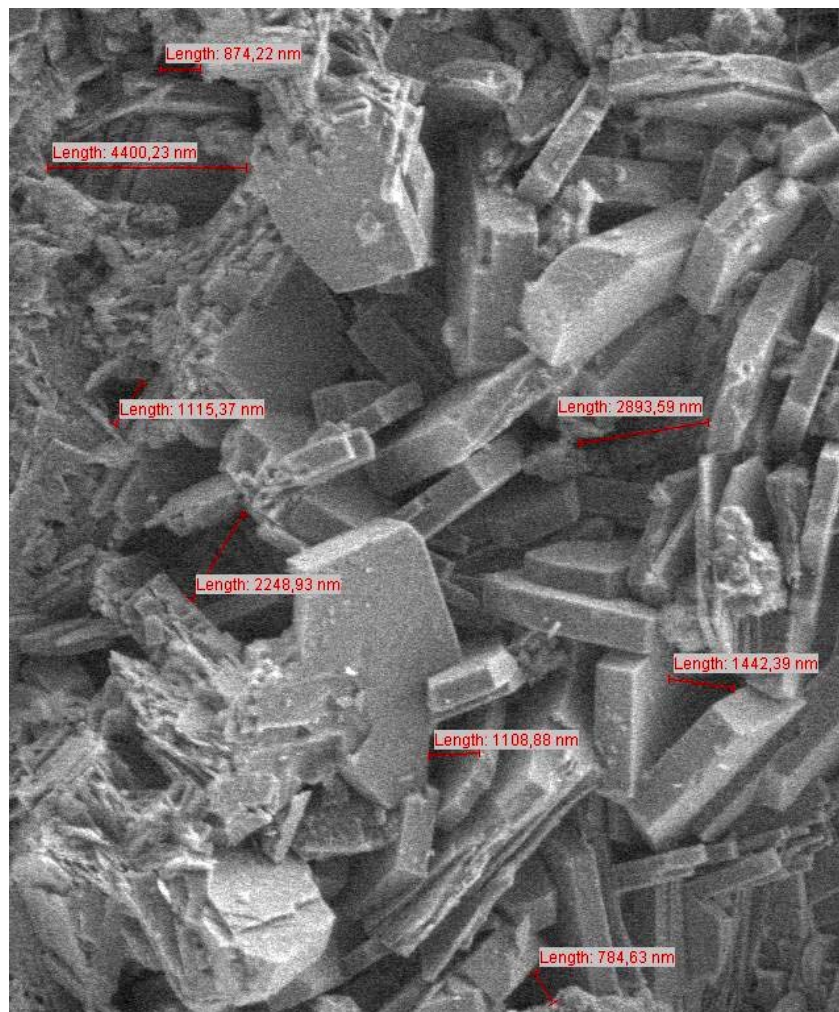


Figure 7.36. SEM image of zeolite sample and size of the macropore.

### ***Diffusion and Reaction Mechanisms***

Result in Section 7.2.1 showed that initial GUS and casein concentrations lead an increase in adsorption rates in the uptake curves where higher initial concentrations have higher driving force to overcome the mass transfer resistances. Adsorbed amounts were especially high in early stages of the adsorption especially for GUS where this indicates the instantaneous adsorption of the GUS on to zeolite. After the occupation of the surface active groups, GUS and casein molecules might diffuse through the pores between the crystals.

Considering the rate controlling mechanism is external mass transfer, effect of initial concentration on  $k_f$  values were investigated below. External mass transfer coefficient throughout the study was determined using the following equation (Eq. 3.15 given in Chapter 3):

$$\ln \left[ 1 - \frac{\bar{q}}{q_\infty} \right] = \left[ -\frac{3k_f t}{KR_p} \right] \quad (7.6)$$

the plot of  $-\ln \left[ 1 - \frac{\bar{q}}{q_\infty} \right]$  vs  $t$  gives the slope  $\frac{3k_f}{KR_p}$  where  $k_f$  can be determined.

A sample calculation was given below:

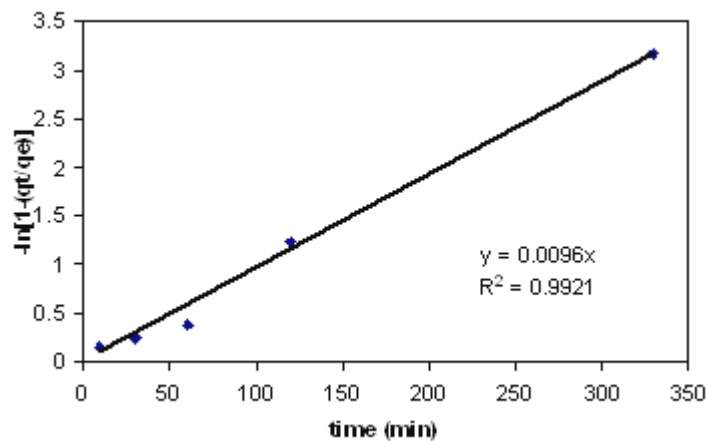


Figure 7.37. Representative plot used for the calculation of  $k_f$ .

For the initial concentration of 0.41 mg/ml casein slope is: 0.0096 which is obtained from the plot. For :

$$q_e = KC_e \quad (7.7)$$

$K = 0.0329$  ml/mg which is found from the initial linear region of the isotherm at  $37^\circ\text{C}$ .

Since the average radius of the zeolite is  $R_p = 2.12 \times 10^{-5}$  m;

$k_f = 2.23 \cdot 10^{-9}$  m/min.

Table 7.9. Effect of initial concentration on external diffusion model parameters ( $37^\circ\text{C}$ , 150 rpm, S/L:5mg/ml, pH 6.8, particle size: 45-75 $\mu\text{m}$ ).

Initial Concentration		External diffusion model		
GUS ( $\mu\text{g/ml}$ )	$k_f$ ( $\times 10^8$ (m/min))	SSE	$R^2$	
20	1.56	0.3994	0.977	
50	0.87	0.7044	0.893	
100	0.89	0.6484	0.910	
150	2.25	0.1082	0.962	
200	2.37	0.0399	0.975	
300	1.97	0.0934	0.942	
500	2.09	0.0412	0.977	
casein (mg/ml)	$k_f$ ( $\times 10^9$ (m/min))	SSE	$R^2$	
0.06	3.67	0.2596	0.982	
0.125	2.83	0.4801	0.957	
0.41	2.23	0.3076	0.983	
0.7	2.83	0.3810	0.972	
0.99	3.27	0.2812	0.978	
1.2	3.69	0.3001	0.967	
1.25	4.81	0.2191	0.962	

Results in Table 7.9 implied  $k_f$  values did not show a consistent trend and there were slight fluctuations in  $k_f$  values, especially for GUS with the increase in initial concentration. This behaviour might be attributed to the unhomogeneity in of the zeolite particles. Similar case was reported by Chang et al. (2006).

Both casein and GUS have protein structure and they have dynamic conformation. Thus terminals on their structure can orientate through the cavities and/or pores of the zeolite. Intraparticle diffusion model was also applied for the data

considering that intraparticle diffusion step is the controlling one. Linear portion in the plots can be attributed to intraparticle diffusion while the final plateau indicated the complete saturation of the zeolite with GUS and casein under equilibrium conditions (Nassar et al., 2009; Chen et al., 2010; Al-Ghouti et al., 2009). First region in the uptake plots given in Figures 7.39-42 were used for the analysis of the data. Weber Morris equation (Eq.3.39 in Chapter 3) was used in the determination of the intra particle diffusion constants ( $k_d$ ) :

$$q_t = k_d t^{0.5} \quad (7.8)$$

by plotting  $q_t$  values vs  $t^{0.5}$  (square root of time);  $k_d$  values can be determined from the early stages of the uptakes.

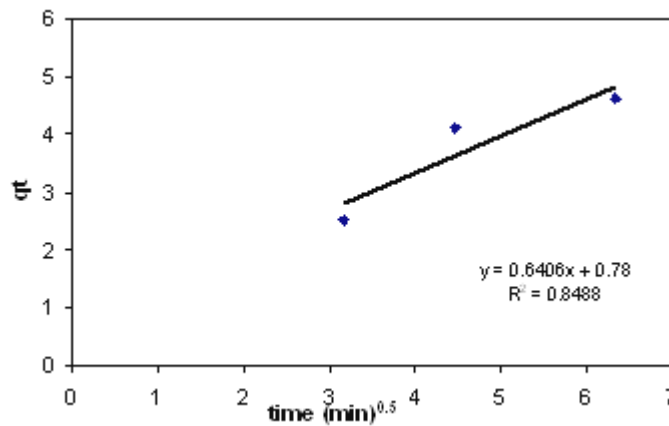


Figure 7.38. Representative plot used for the calculation of  $k_d$

For Ci.150  $\mu\text{g/ml}$  GUS, slope of the plot is: 0.6406

$$k_d = 0.6404 \text{ } (\mu\text{g/mg min}^{0.5})$$

Calculated  $k_d$  values were given in Figures 7.39-41 for different initial concentration ranges. Plots of  $q_t$  vs  $t^{0.5}$  for GUS did not pass through the origin which indicated that intraparticle diffusion was not the only rate-limiting step (Ho et al., 2000; Chen et al., 2010; Al-Ghouti et al., 2009). This was also confirmed with the lower correlation coefficients in Table 7.10. However, for casein they passed through the origin except Ci:1.2 and 1.25 mg/ml. Thus intraparticle diffusion seems to be



controlling one at lower concentrations.

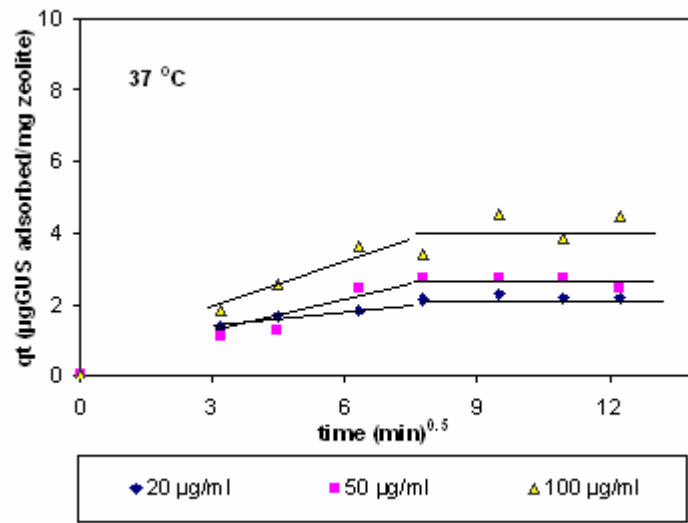


Figure 7.39. Intraparticle diffusion plot for the adsorption of GUS onto zeolite (Ci: 20-100 µg GUS/ml, 37°C, 150 rpm, S/L:5mg/ml, pH 6.8, particle size: 45-75µm).

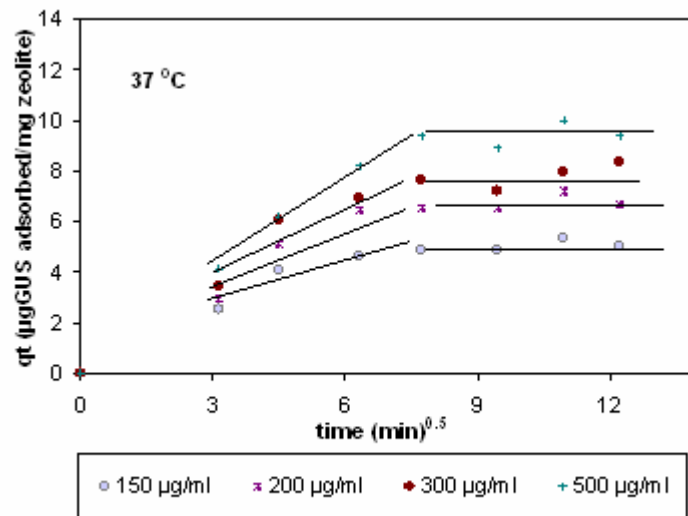


Figure 7.40. Intraparticle diffusion plot for the adsorption of GUS onto zeolite (Ci: 150-500 µg GUS/ml, 37°C, 150 rpm, S/L:5mg/ml, pH 6.8, particle size: 45-75µm).

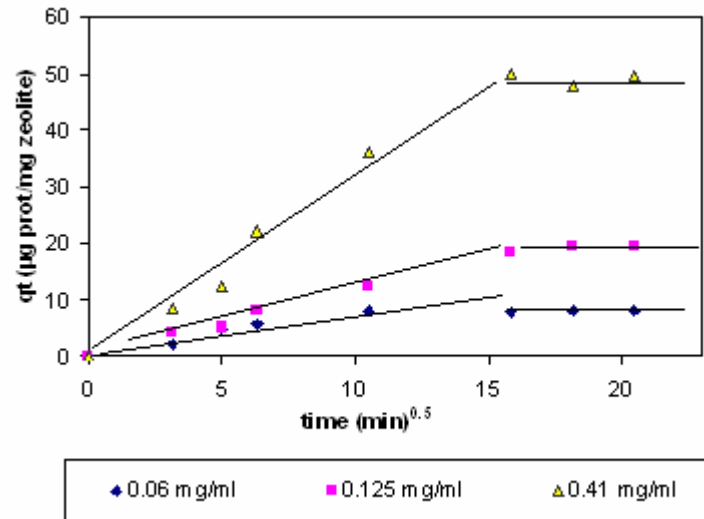


Figure 7.41. Intraparticle diffusion plot for the adsorption of casein onto zeolite (Ci: 0.06-0.41 mg /ml, 37°C, 150 rpm, S/L:5mg/ml, pH 6.8, particle size: 45-75µm).

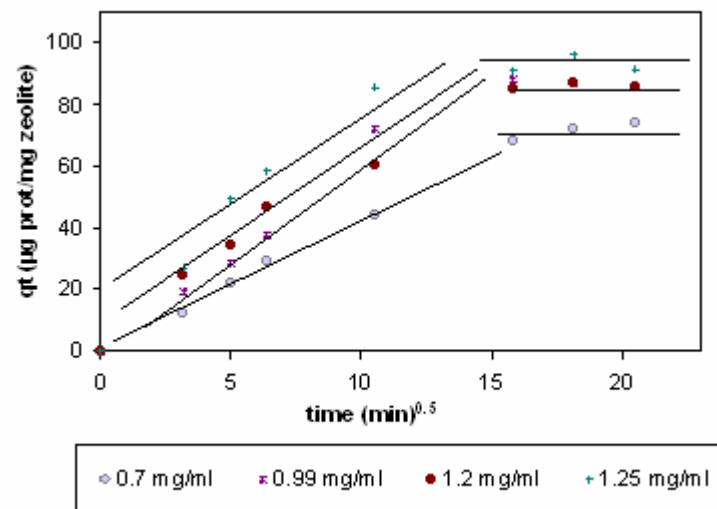


Figure 7.42. Intraparticle diffusion plot for the adsorption of casein onto zeolite (Ci: 0.7-1.25 mg /ml, 37°C, 150 rpm, S/L:5mg/ml, pH 6.8, particle size: 45-75µm).

Considering the rate controlling mechanism is macropore diffusion, macropore diffusivity of the samples were calculated from the equation ( Eq. 3.29 given in Chapter 3) given below:

$$\frac{m_t}{m_\infty} = 1 - \frac{6}{\pi^2} \sum_{n=1}^{n=\infty} \frac{1}{n^2} \exp\left(-\frac{n^2 \pi^2 \varepsilon_p D_p t}{R_p^2 (\varepsilon_p + (1 - \varepsilon_p)K)}\right) \quad (7.9)$$

for the uptake ratio  $>0.7$ , we obtain :

$$1 - \frac{m_t}{m_\infty} = \frac{6}{\pi^2} \exp\left(-\frac{\pi^2 \varepsilon_p D_p t}{R_p^2 [\varepsilon_p + (1 - \varepsilon_p)K]}\right) \quad (7.10)$$

this equation is linearized by taking ln of the both sides:

$$\ln\left(1 - \frac{m_t}{m_\infty}\right) = \ln\left(\frac{6}{\pi^2}\right) + \left(-\frac{\pi^2 \varepsilon_p D_p}{R_p^2 [\varepsilon_p + (1 - \varepsilon_p)K]}\right)t \quad (7.11)$$

by plotting  $\ln\left(1 - \frac{m_t}{m_\infty}\right)$  vs t:

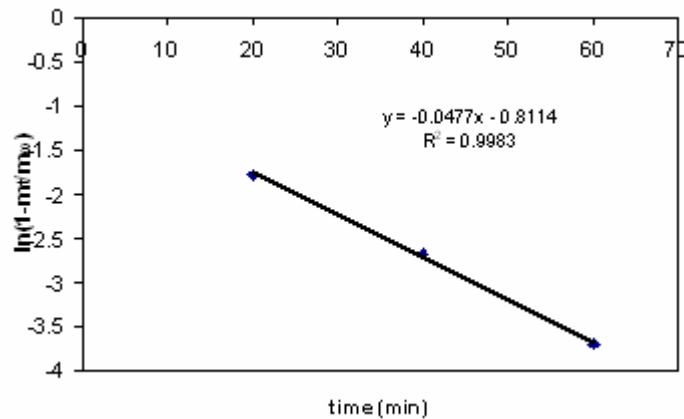


Figure 7.43. Representative plot used for the calculation of  $D_p$ .

slope of the plot is  $-0.0477$

Ci.150  $\mu\text{g/ml}$  GUS,  $\varepsilon_p:0.32$ ,  $R_p: 2.12 \times 10^{-5}$  m.

by the equation  $q_e = KC_e$  :

$K=0.0623$  ml/mg, which is found from the initial linear region of the isotherm at  $37^\circ\text{C}$ .

Using those data,  $D_p$  is calculated as:

$D_p$  is found as:  $1.47 \times 10^{-10}$  m/sec.

Intraparticle diffusion parameters were presented in Table 7.10. Results showed that  $k_d$  values were increased with the increase GUS concentration. For casein,  $k_d$  values were increased in 0.06-0.99 mg/ml concentration range. But decrease in the  $k_d$  values at 1.2 and 1.25 mg/ml casein was observed.  $t^{0.5}$  vs  $q_t$  plots gave intercept values of 12.63 and 22.1 for 1.2 and 1.25 mg/ml casein, respectively. Those intercepts were attributed to the external mass transfer resistance or existence of boundary layer. Although the calculated  $k_f$  values were increased by increase in the the last two initial concentration, reduction in  $k_d$  values designates blockage of the pores by the molecules.

Table 7.10. Effect of initial concentrations on intraparticle diffusion model parameters (37°C, 150 rpm, S/L:5mg/ml, pH 6.8, particle size: 45-75µm).

Initial Concentration		Intraparticle diffusion model		Macropore Diffusivity
GUS (µg/ml)	$k_d$ (µg mg <sup>-1</sup> min <sup>-0.5</sup> )	SSE	R <sup>2</sup>	Dp(x10 <sup>10</sup> m <sup>2</sup> /sec)
20	0.132	1.2750	0.906	0.708
50	0.162	0.3016	0.806	0.253
100	0.555	0.7671	0.868	1.165
150	0.641	0.9845	0.826	1.474
200	0.761	0.5737	0.818	1.758
300	1.055	1.0307	0.856	2.373
500	1.266	0.8128	0.881	3.402
casein (mg/ml)	$k_d$ (µg mg <sup>-1</sup> min <sup>-0.5</sup> )	SSE	R <sup>2</sup>	Dp(x10 <sup>10</sup> m <sup>2</sup> /sec)
0.06	0.815	2.2494	0.862	0.277
0.125	1.180	0.1092	0.982	0.225
0.41	3.200	0.2843	0.963	0.292
0.7	4.294	0.0728	0.986	0.321
0.99	5.955	0.2666	0.947	0.397
1.2	4.606	0.0928	0.975	0.387
1.25	4.896	0.3484	0.911	0.412

Pseudo first order and Pseudo Second order kinetic models were be applied to kinetic data of casein and GUS adsorption. Following equation (Eq. 3.57 in Chapter 3) is used to determine 1<sup>st</sup> order reaction rate constants:

$$\log(q_e - q_t) = \log q_e - \frac{k_1}{2.303} t \quad (7.12)$$

$\log(q_e - q_t)$  vs  $t$  plot was used to determine  $k_1$  where  $k_1$  can be calculated from the slope of the plot.

For Ci.150  $\mu\text{g/ml}$  of GUS plot is given below:

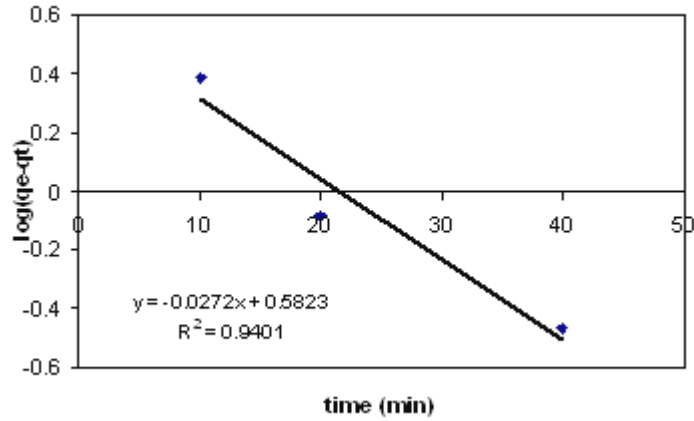


Figure 7.44. Representative plot used for the calculation of  $k_1$ .

slope is: -0.0272

$k_1 = 0.062642 \text{ min}^{-1}$

Following equation (Eq. 3.62 in Chapter 3) is used to determine 2nd order reaction rate constant where,  $k_{2\text{ads}}$  is the rate constant of pseudo second-order adsorption ( $\mu\text{g/mg min}$ ).

$$\frac{t}{q_t} = \left( \frac{1}{k_2 q_e^2} \right) + \left( \frac{1}{q_e} \right) t \quad (7.13)$$

The plot of  $(t/q_t)$  against  $t$  of equation should give a linear relationship from which  $q_e$  and  $k_{2\text{ads}}$  can be determined from the slope and intercept of the plot, respectively.

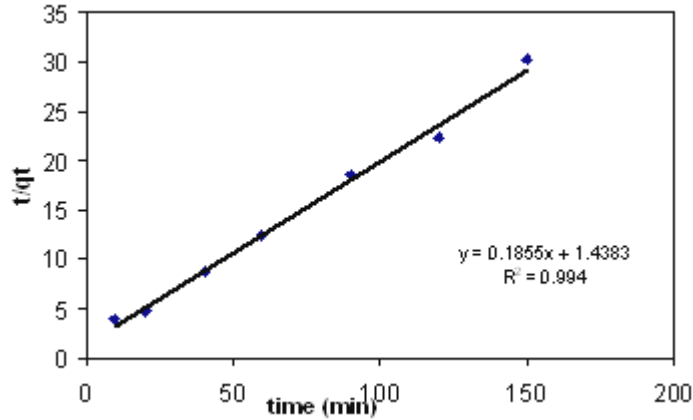


Figure 7.45. Representative plot used for the calculation of  $k_2$ .

For, Ci.150  $\mu\text{g/ml}$  GUS:

$$q_e = 1/0.1855 = 5.391 \mu\text{g/mg}$$

$k_2$  was calculated as follows

$$k_2 = 0.023924 (\text{mg} \times (\text{min}^{-1}))$$

Results of the 1<sup>st</sup> and 2<sup>nd</sup> order kinetic rate constant were given in Table 7.11. Results showed that correlation coefficients were close for each model. However, theoretical values,  $q_{e,\text{theo}}$  were not so close for the 1<sup>st</sup> order reaction model. On the other hand they agreed well for the 2<sup>nd</sup> order reaction model (ie, in GUS adsorption for Ci:20  $\mu\text{g/ml}$ ;  $q_{e,\text{theo}}$ :2.32 for 2<sup>nd</sup> order;  $q_{e,\text{theo}}$ :0.96 for 1<sup>st</sup> order where  $q_{e,\text{exp}}$ :2.2) possibly indicating that adsorption of casein and GUS onto zeolite followed 2<sup>nd</sup> order kinetic model. This was confirmed by the higher values of SSE in 1<sup>st</sup> order compared to 2<sup>nd</sup> order model. In the 2<sup>nd</sup> order model,  $k_2$  values showed a decreasing tendency with the increase in the initial concentration. This situation was explained well by Al-Ghouti et al. (2009). At low initial concentrations of both GUS and casein were bound to high energy sites on the zeolite surface at the early stages of the adsorption. Then, low energy sites will be occupied by adsorbates with the increase with its initial concentration thus higher value for rate parameter of pseudo-second order is to be expected.

Table 7.11. Effect of initial concentration on reaction model parameters (37°C, 150 rpm, S/L:5mg/ml, pH 6.8, particle size: 45-75µm).

<b>Initial</b>						
<b>Concentration</b>	<b>1st order reaction model</b>			<b>2nd order reaction model</b>		
GUS (µg/ml)	$k_1(x10^2min^{-1})$	SSE	R <sup>2</sup>	$k_2(x10^2(mg(µgmin)^{-1})$	SSE	R <sup>2</sup>
20	2.28	3.9402	0.958	5.88	0.0132	0.964
50	6.77	1.1830	0.930	2.75	0.2017	0.932
100	3.78	0.6960	0.917	1.27	0.0573	0.919
150	6.26	1.0580	0.945	2.39	0.0518	0.965
200	10.32	2.0525	0.963	1.47	0.0939	0.964
30	3.96	1.2752	0.927	0.91	0.0457	0.949
500	8.36	0.0986	0.972	0.74	0.0292	0.972
casein (mg/ml)	$k_1(x10^2min^{-1})$	SSE	R <sup>2</sup>	$k_2(x10^3(mg(µgmin)^{-1})$	SSE	R <sup>2</sup>
0.06	1.01	1.1926	0.954	3.43	0.0353	0.979
0.125	1.34	0.3080	0.963	0.36	0.2977	0.976
0.41	0.97	0.4048	0.977	0.11	0.2731	0.978
0.7	2.00	0.4684	0.958	0.09	0.2123	0.987
0.99	1.47	0.3360	0.974	0.13	0.2242	0.974
1.2	1.68	0.3362	0.980	0.18	0.1774	0.978
1.25	1.45	0.9672	0.982	0.24	0.0574	0.985

Results of the effect of shaking rate were given in Table 7.12 below. Results for the uptake values of casein and GUS adsorption studies given previously showed that the shaking rate affected the adsorption rate. As the shaking rate was increased, adsorption rate was also increased.  $k_f$  values in Table 7.12 were calculated by the same equations given previously in details.  $k_f$  values were increased with the increase in shaking rate. This can be explained by the differences in the external-mass transfer rates for the different shaking rates. Since the external mass transfer resistance is proportional to the film thickness of the liquid layer, a higher shaking rate decreased the film thickness. Therefore external mass transfer resistance was reduced.

Table 7.12. Effect of shaking rate on external diffusion model parameters (37°C, S/L:5mg/ml, pH 6.8, particle size: 45-75µm, Ci: 100 µgGUS/ml, Ci:0.125 mg casein/ml)

Shaking rate (rpm)		External diffusion model			
GUS adsorption	$k_f$ ( $\times 10^8$ (m/min))	SSE	$R^2$		
50	0.56	1.6119	0.456		
100	0.84	0.5439	0.852		
150	0.89	0.6484	0.910		
casein adsorption		$k_f$ ( $\times 10^9$ m/min)	SSE	$R^2$	
50	2.51	0.3552	0.977		
100	2.55	0.3814	0.981		
150	2.83	0.4801	0.957		

Effect of shaking rate on intraparticle diffusion model parameters were given in Table 7.13.  $C_d$  is the intercept of the  $qt$  vs square root of time plot, which is proportional to the boundary layer thickness.  $t^{0.5}$  vs  $t$  plots gave intercept values for 50 and 100 rpm which indicated contribution of external film/skin resistance at lower rpm values. Similar case was reported in literature (Ho and McKay, 2003; Al-Ghouti et al., 2010).

Table 7.13. Effect of shaking rate on intraparticle diffusion model parameters (37°C, S/L:5mg/ml, pH 6.8, particle size: 45-75µm, Ci: 100 µgGUS/ml, Ci:0.125 mg casein/ml)

Shaking rate (rpm)		Intraparticle diffusion model				
GUS adsorption	$k_d$ ( $\mu\text{g mg}^{-1} \text{min}^{-0.5}$ )	$C_d$	SSE	$R^2$		
50	0.1523	0.5932	1.0331	0.427		
100	0.1184	0.1683	0.4305	0.785		
150	0.5554	0.0789	0.7671	0.868		
Casein adsorption		$k_d$ ( $\mu\text{g mg}^{-1} \text{min}^{-0.5}$ )	$C_d$	SSE	$R^2$	
50	0.552	0.8	0.2405	0.956		
100	0.798	0.6	0.1929	0.969		
150	1.180	0	0.1092	0.982		

Effect of shaking rate on Pseudo 1<sup>st</sup> and 2<sup>nd</sup> order reaction models for GUS and casein adsorption were given in Table 7.14. Results showed that 2<sup>nd</sup> order reaction model had better correlation values especially for GUS adsorption for lower shaking rates. Since the external mass transfer resistance was high at lower rpm, less amount of



casein or GUS per active sites would be available and they would preferentially bind to higher energetic sites thus rapid sorption would take place.

Table 7.14. Effect shaking rate on reaction model parameters (37°C, S/L:5mg/ml, pH 6.8, particle size: 45-75µm, Ci: 100 µgGUS/ml, Ci:0.125 mg casein/ml)

Shaking rate (rpm)		1st order reaction model			2nd order reaction model		
GUS							
adsorption	$k_1(x10^2\text{min}^{-1})$	SSE	$R^2$	$k_2(x10^2(\text{mg}(\mu\text{gmin})^{-1}))$	SSE	$R^2$	
50	10.41	1.2367	0.674	57.61	0.1891	0.736	
100	7.32	0.5241	0.903	2.08	0.2485	0.890	
150	3.78	0.6960	0.917	1.27	0.0573	0.919	
1st order reaction model				2nd order reaction model			
Casein							
adsorption	$k_1(x10^2\text{min}^{-1})$	SSE	$R^2$	$k_2(x10^3 \text{mg}(\mu\text{g min})^{-1})$	SSE	$R^2$	
50	1.11	0.4823	0.970	0.61	0.3321	0.972	
100	1.13	0.4238	0.977	0.42	0.3315	0.980	
150	1.34	0.3080	0.963	0.36	0.2954	0.976	

Results of the effect of particle size on external diffusion model parameters for GUS and casein adsorption were given in Table 7.15 below. For GUS adsorption and for the particle size  $> 45 \mu\text{m}$ , external diffusion coefficient increased with the increase in particle size. That might be because of the reduction in the shear forces between the single particle and the surrounding liquid. When the size of the particle was increased it would show resistance to the shaking by its own moment of inertia. Therefore this resistance might cause stronger shear forces with the larger particles and its surrounding fluid (Al-Ghouti et al., 2009) which might have lead higher  $k_f$  values. This case was clearly observed for casein adsorption. However, in the finest particle range for GUS adsorption, similar case was not observed. This situation was hard to explain. One of the possible reasons might be because of unhomogeneity of zeolite particles. Another reason might be attributed to the blockage of the zeolite surface by the aggregation of GUS molecules. Large GUS molecules might have showed tendency to occupy surface without utilizing the whole area and they might show interaction with each other. Thus, this interactions between the GUS molecules itself on the surface might have give contribution to obtain higher  $k_f$  values in fine particles.

Table 7.15. Effect of particle size on external mass transfer model parameters (37°C, 150 rpm, S/L:5mg/ml, pH 6.8, Ci: 100 µgGUS/ml, Ci:0.125 mg casein/ml)

Particle size (µm)		external mass transfer model		
GUS adsorption	$k_f$ (x10 <sup>8</sup> (m/min))	SSE	R <sup>2</sup>	
25-45	1.63	0.1688	0.958	
45-75	0.89	0.6484	0.91	
75-106	1.29	0.2986	0.945	
casein adsorption	$k_f$ (x10 <sup>9</sup> (m/min))	SSE	R <sup>2</sup>	
25-45	2.6	0.4796	0.976	
45-75	2.83	0.4801	0.957	
75-106	5.09	1.9568	0.869	

Effect of particle size on intraparticle diffusion parameters were given in Table 7.16.  $k_d$  values decreased with the increase in particle size for both GUS and casein adsorption. When the particle size of the zeolite increased, time and pathway required to diffuse the interior parts of the zeolite for both molecules would also be increased. This case would lead higher intraparticle diffusion resistance thus  $k_d$  values would be lower. Similar case was also reported by Sağ and Aktay (2000).

Table 7.16. Effect of particle size on intraparticle diffusion model parameters (37°C, 150 rpm, S/L:5mg/ml, pH 6.8, Ci: 100 µgGUS/ml, Ci:0.125 mg casein/ml)

Particle size (µm)		Intraparticle diffusion model		
GUS adsorption	$k_d$ (µg mg <sup>-1</sup> min <sup>-0.5</sup> )	SSE	R <sup>2</sup>	
25-45	1.20	0.6632	0.833	
45-75	0.55	0.7671	0.868	
75-106	0.21	0.1040	0.884	
casein adsorption	$k_d$ (µg mg <sup>-1</sup> min <sup>-0.5</sup> )	SSE	R <sup>2</sup>	
25-45	1.511	0.2440	0.965	
45-75	1.180	0.1092	0.982	
75-106	0.734	0.1942	0.952	

Effect of shaking rate on 1<sup>st</sup> and 2<sup>nd</sup> order reaction model parameters were given in Table 7.17. The amount of external surface area available for rapid reaction would decrease with increasing particle size for constant sorbent mass. However, there was not an exact trend for both reaction model parameters with the increase in particle size.

Table 7.17. Effect of particle size on reaction model parameters (37°C, 150 rpm, S/L:5mg/ml, pH 6.8, Ci: 100 µgGUS/ml, Ci:0.125 mg casein/ml).

Particle size (µm)	1 <sup>st</sup> order reaction model			2 <sup>nd</sup> order reaction model			
	GUS adsorption	$k_1(x10^2min^{-1})$	SSE	R <sup>2</sup>	$k_2(x10^2(mg(\mu gmin)^{-1}))$	SSE	R <sup>2</sup>
25-45		8.94	2.9524	0.946	0.85	0.0931	0.946
45-75		3.78	0.6960	0.917	1.27	0.0573	0.919
75-106		6.49	0.1420	0.954	2.14	0.0369	0.954
		1st order reaction model			2nd order reaction model		
casein adsorption	$k_1(x10^2min^{-1})$	SSE	R <sup>2</sup>	$k_2(x10^3(mg(\mu gmin)^{-1}))$	SSE	R <sup>2</sup>	
25-45	2.00	0.3493	0.952	0.67	0.3555	0.966	
45-75	1.34	0.3080	0.963	0.36	0.2954	0.976	
75-106	0.92	0.5515	0.957	0.52	0.3282	0.954	

Effect of the temperature on the external mass transfer model parameters were given below. Results of the  $k_f$  values given in Table 7.18 showed that  $k_f$  values decreased with the increase in the temperature change for both casein and GUS adsorption.

Table 7.18. Effect of temperature on external diffusion model parameters (S/L:5mg/ml, pH 6.8, particle size: 45-75µm, Ci: 100 µgGUS/ml, Ci:0.125 mg casein/ml).

Temperature (°C)	external diffusion model		
GUS adsorption	$k_f(x10^8 (m/min))$	SSE	R <sup>2</sup>
15	10.63	3.5683	0.979
25	7.85	3.4718	0.968
37	0.89	0.6484	0.910
casein adsorption	$k_f(x10^9 m/min)$	SSE	R <sup>2</sup>
15	2.65	0.2681	0.988
25	2.62	0.3045	0.992
37	1.65	0.5315	0.985

Effect of temperature on intraparticle diffusion models were given in Table 7.19 below. Intraparticle diffusion parameters  $k_d$ , decreased with the increase in the temperature for both GUS and casein.

Table 7.19. Effect of temperature on intraparticle diffusion model parameters (S/L:5mg/ml, pH 6.8, particle size: 45-75 $\mu$ m, Ci: 100  $\mu$ gGUS/ml, Ci:0.125 mg casein/ml).

Temperature ( $^{\circ}$ C)	Intraparticle diffusion model		
GUS adsorption	$k_d$ ( $\mu$ g $mg^{-1}$ $min^{-0.5}$ )	SSE	$R^2$
15	0.954	0.1647	0.977
25	0.592	0.0523	0.948
37	0.554	0.7671	0.868
casein adsorption	$k_d$ ( $\mu$ g $mg^{-1}$ $min^{-0.5}$ )	SSE	$R^2$
15	1.377	0.1122	0.976
25	1.384	0.1584	0.971
37	1.180	0.1092	0.982

Table 7.20. Effect of temperature on reaction model parameters (S/L:5mg/ml, pH 6.8, particle size: 45-75 $\mu$ m, Ci: 100  $\mu$ gGUS/ml, Ci:0.125 mg casein/ml).

Temperature ( $^{\circ}$ C)	1 <sup>st</sup> order reaction model			2 <sup>nd</sup> order reaction model		
GUS adsorption	$k_1$ ( $\times 10^2 min^{-1}$ )	SSE	$R^2$	$k_2$ ( $\times 10^2$ ( $mg(\mu gmin)^{-1}$ ))	SSE	$R^2$
15	2.65	0.7530	0.996	0.46	3.3665	0.987
25	2.14	1.3507	0.978	0.85	3.3450	0.975
37	3.78	0.6960	0.917	1.27	0.0573	0.919
	1st order reaction model			2nd order reaction model		
casein adsorption	$k_1$ ( $\times 10^2 min^{-1}$ )	SSE	$R^2$	$k_2$ ( $\times 10^3$ ( $mg(\mu gmin)^{-1}$ ))	SSE	$R^2$
15	0.81	0.9323	0.992	0.53	0.1448	0.985
25	1.08	0.6516	0.989	0.65	0.0971	0.985
37	1.34	0.3080	0.963	0.36	0.2954	0.976

Effect of temperature on Pseudo 1<sup>st</sup> and 2<sup>nd</sup> order kinetic model parameters were given in Table 7.20. For GUS, adsorption rate parameter for the 1<sup>st</sup> order reaction model did not follow a regular trend with the increase in the temperature. Additionally, theoretical values,  $q_{e,theo}$  were much closer for the 2<sup>nd</sup> order reaction model compared to the 1<sup>st</sup> order reaction model (ie; for T:37  $^{\circ}$ C;  $q_{e,exp}$ :4.45,  $q_{e,the}$  is 4.81 for 2<sup>nd</sup> order, 3.9 for 1<sup>st</sup> order) possibly indicating that adsorption of GUS onto zeolite followed 2<sup>nd</sup> order kinetic model. For casein, adsorption rate parameter for the 2<sup>nd</sup> order reaction model did not follow a regular trend with the increase in the temperature. Lower values of SSE compared to 1<sup>st</sup> order reaction model indicated that 2<sup>nd</sup> order reaction model might be

appropriate for the adsorption of casein onto zeolite.

## **7.4. Behaviour of Inhibitors in SIF Conditions**

Casein is a bioactive compound and it has important roles related to antioxidative, nutritive and detoxification mechanism in intestine. In literature it was reported that synthetic or natural zeolites could adsorb some bioactive compounds and could be used as a carrier of those molecules (Klint and Eriksson, 1997; Sakaguchi et al. 2005). Sometimes adsorption of some molecules resulted higher transit time and better bioavailability in intestinal system, or resulted synergistic effect on other compounds during longer transit provided by zeolite. Therefore, stability of casein and zeolite, their anticancer effects due to their antioxidant activities in SIF were analyzed and characterization of samples was performed.

### **7.4.1. Stability of Casein in SIF**

Proteins are very sensitive to environmental conditions such as pH, ionic strength and temperature of the solutions. Due to these conditions, they could change their conformation, biological activity and also in some cases they could be denaturated. Therefore it was important to check stability of casein at incubation conditions which would be important to set time parameters to perform adsorption studies.

To determine casein stability in SIF, casein was incubated in phosphate buffer pH 6.8 (simulated intestinal fluid conditions-SIF) for 30h at 37°C. During incubation it was analyzed for its protein content and absorbance values were recorded by time. Results were given in Figure 8.1 and 8.2 as difference between absorbance values at initial time ( $t_0$ ) and at a particular time ( $t$ ). It was observed that casein lost its stability nearly after 360-420h where analysis results showed higher variations, which suggested possible conformational change or denaturation of the protein due to duration of protein solutions for longer times in 150 rpm and at 37°C. Casein was complex in structure and formed by subunits such as  $\alpha_1$ -2-3,  $\beta$  and  $\kappa$ . It was reported by Slattery C. W. in 1976 that submicelles were amphiphilic in nature.  $\alpha$ -s1 and 3 were hydrophobic while the  $\kappa$ -casein portion of the submicelle surface was hydrophilic. Since there were longer times in buffer, hydrophilic/hydrophobic interactions might have affected the stability of

casein.

Therefore adsorption period should be set as 6-7 hours. Same study was performed for shorter times to confirm the previous result. Absorbance values didn't considerable change as expected during 7 hours and results were given in Figure 7.46-47 below.

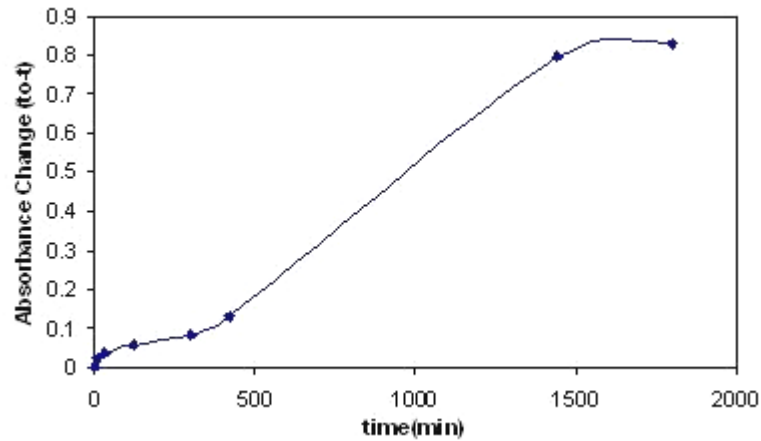


Figure 7.46. Stability change of casein for 30h incubation time ( $t_0$ : initial absorbance,  $t$ : absorbance at the time of measurement)

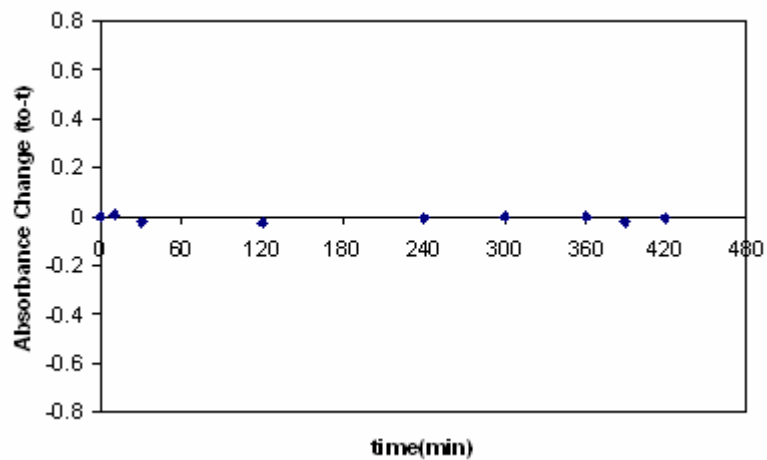


Figure 7.47. Stability change of casein for 7h incubation time

### 7.4.2. Effect of Zeolite on pH and Ion Concentration of SIF

Proton concentration in intestinal juice is an important parameter for acidity of media. Also enzymes are very sensitive to ion concentrations in their microenvironment. An abnormal change in the pH or in the other words hyperacidity, or changes in ion

concentrations can cause some gastric disturbances in human health where enzymatic activities might be effected. Based on this fact, effect of zeolite samples on simulated intestinal media were investigated in order to determine if there was any disturbances with respect to pH and elementary composition.. Their interactions were based on investigations about, pH, ion kinetics and stability.

### ***Effect on pH***

Zeolite samples incubated in SIF (pH 6.8) and media were analyzed according to changes in pH during 24 hours. Maximum fluctuation in pH was found as  $6.8 \pm 0.03$  (Figure 7.48) which was insignificant. This result was expected, because zeolites have capability to regulate gut and to have tendency to neutralize the media where the media pH of the study was 6.8 which was so close to neutral. These results were also in good agreement with the literature studies where Rivera et al. (1998 and 2000) reported and discussed the neutralizing properties of the natural clinoptilolite.

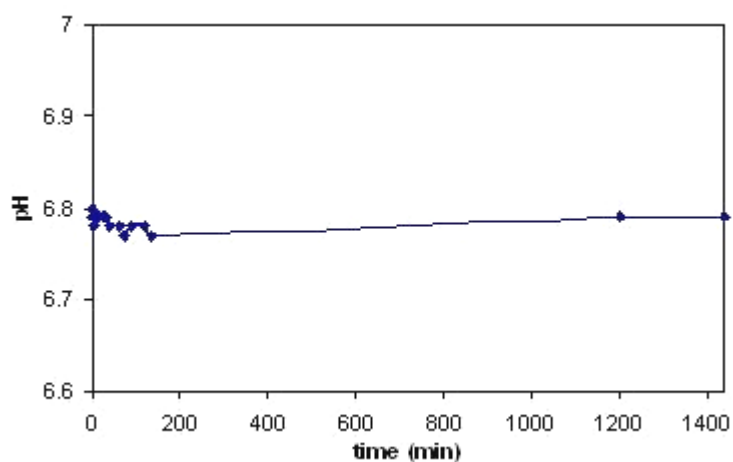


Figure 7.48. pH changes in SIF incubated with zeolite

### ***Effect on Ion Concentration***

Determination of changes in ionic concentrations was important because during intestinal transit, zeolite might encounter with different structures, especially proteins which were highly affected by the ionic strength). Proteins and also enzymes with protein like structures may alter their conformations due to changes in ionic strength of the media therefore their bioactivity may change.

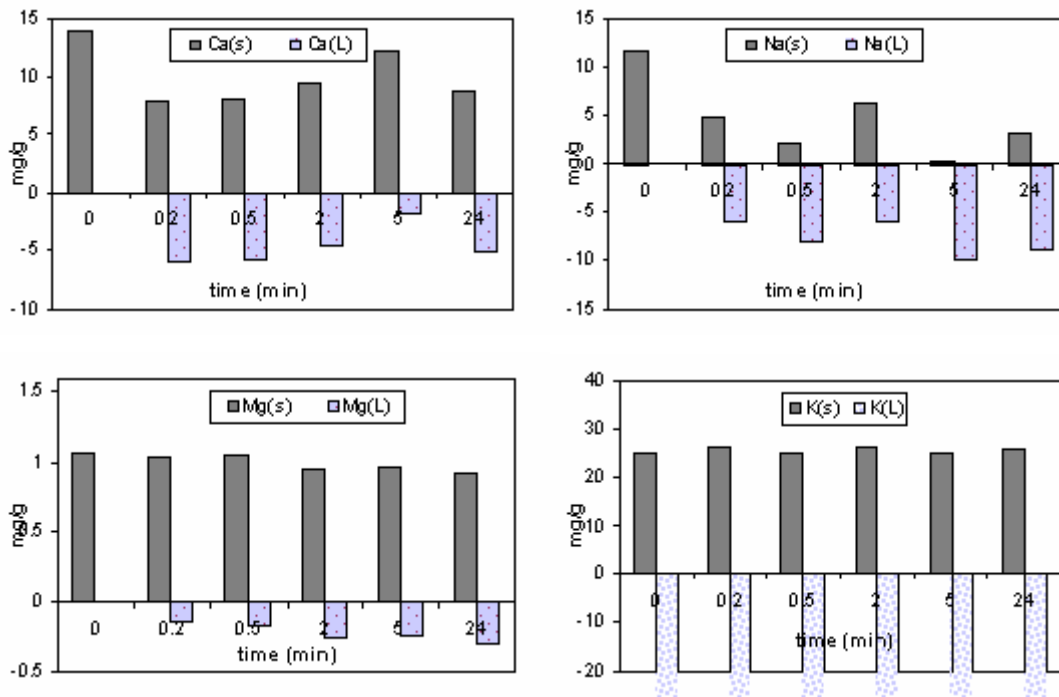


Figure 7.49. Change in  $[Ca^{2+}]$ ,  $[Na^+]$ ,  $[Mg^{2+}]$ ,  $[K^+]$  in SIF (s:element in solid-zeolite phase, L: element in liquid SIF phase)

Zeolites have ion-exchange capacity. Therefore in this study, interactions of zeolite with aqueous SIF solution were investigated with respect to elementary composition. It was important to note that SIF is potassium phosphate buffer. Since  $K(L)$  value is infinitely high compared to  $K(s)$ , it was not represented on the graph.

Kinetic results of the exchangeable cations during 24 h in SIF (L) and in solid phase (s) were given in Figure 7.49. All results indicated that there were fluctuations in ionic concentrations. Ion kinetics in solutions were reported to vary relative to quality and particle size of the zeolitic material, type of exchangeable cations, and hydrodynamics of the system during the process (Trgo et al., 2006).

It was found that approximately for 300min (5h), ionic concentrations were fluctuated highly for all ions. For  $Na^+$  and  $Ca^{2+}$  there were high fluctuations in solid and liquid phase. Also it was reported that this ion was the weakest bonded cation in clinoptilolite structure and therefore could be easily exchanged with cations from the working solution (Rozic et al., 2002). Also  $Ca^{2+}$  ion has a special importance on casein stability. It was reported in different studies that  $Ca^{2+}$  concentration may alter the casein stability and miscelle formation (Charles W. S., 1976; O'Connel, et al., 2003). It was found that there was a slight increase in  $Ca^{2+}$  concentration in SIF. After 300min,  $Na^+$  concentration in aqueous phase (L) and in solid phase (s) didn't significantly change



and it possibly indicated that it might have reached the equilibrium. After 350min, there were slight increases in aqueous concentrations of  $Mg^{2+}$ . Amount of  $K^+$  element was extremely high in SIF (L) because simulated fluid itself contained  $K^+$  ions. Due to strong bonding, removal of the  $K^+$  ion was reported to be hard compared with the other cations in the clinoptilolite structure (Jama and Yücel, 1990). Therefore its concentrations in zeolite was remained nearly same which suggested that it wasn't be exchanged significantly.

### 7.4.3. Antioxidant Activity of Casein

Previous studies showed that casein acted as potent GUS enzyme inhibitor. As a nutritive source, its antioxidant activity was checked because it might act as free radical inhibitor and prevent cell damage because oxidative stress plays a significant role in a number of diseases such as diabetes, cancer and atherosclerosis. Therefore, first of all radical inhibition capacity of raw casein powder using ABTS radical was determined at different concentrations and results were given in Figure 7.50 below.

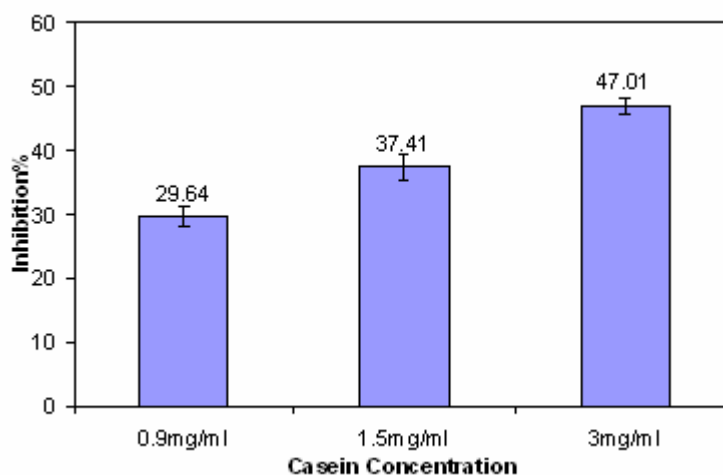


Figure 7.50. Radical inhibition capacity of casein at different concentrations

Results indicated that casein had high antioxidant capacity and this capacity was proportional to its concentration. Also this antioxidant activity was reported in literature by different studies (Bzducka and Wolosiak, 2006; Cervato et al., 1999). This high antioxidant capacity result might be important for the elimination of free radicals that could be generated by metabolism itself or for the elimination of free radicals that were taken with the diet.

Proteins were highly affected with their microenvironment. Hence, antioxidant activity of casein in SIF was also investigated which was an important parameter for determining their health effects. Previously it was found that antioxidant capacity was directly proportional to casein's concentration. 1.5mg/mL SIF casein was analyzed for its antioxidant capacity where adsorption was carried out with 0.5,1 and 3 mg/ml zeolites. Results were given in Table 7.37 below.

Table 7.21. Effect of zeolite incubation on casein amount and its antioxidant activity

Analysis	Treatment Type				
	Control t <sub>0</sub>	Control 6.5h	0.5(mg zeo/ml)	1(mg zeo/ml)	3(mg zeo/ml)
Free Protein(BSA meq/ml)	0.593	0.582	0.286	0.255	0.17
Antioxidant Capacity (trolox meq/ml)	0.016	0.020	0.014	0.013	0.012

Free protein results in Table 7.37 for the control studies showed that casein preserved its stability for 6.5 hours. Casein was adsorbed by zeolite and its adsorbed amount was directly proportional to the zeolite concentration. Free protein amount in the SIF indicated that zeolite with a concentration of 3mg/ml showed highest adsorption capacity as expected where 0.17 meq/ml free protein was remained after adsorption.

Although it was found that amount of free protein nearly remained unchanged, antioxidant capacities of the free casein in control studies were increased during incubation at 37°C from 36.66% to 46.55% (Figure 7.51). This change might be a results of conformational changes occurred during incubation. As it was incubated for longer times in 37°C ph 6.8 phophate buffer, electrostatic interactions within casein molecules and perhaps other pH-dependent forces might play a role in the stabilization of the three-dimensional structure of the molecule and therefore conformational stability might have affected.

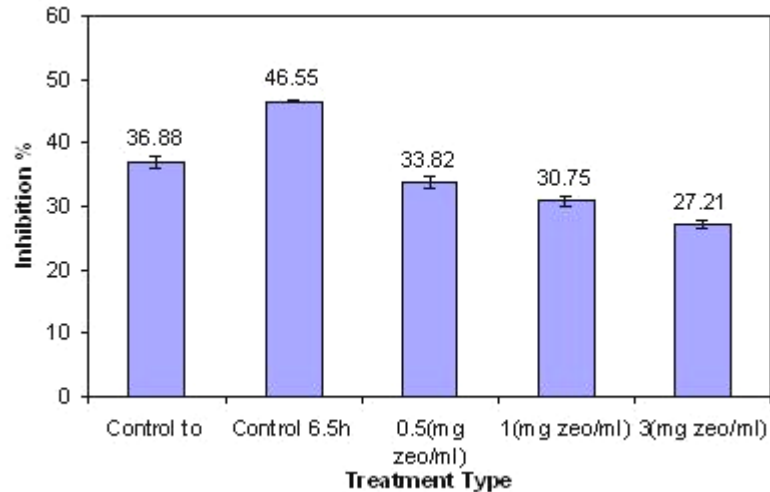


Figure 7.51. Antioxidant activity change in inhibition %

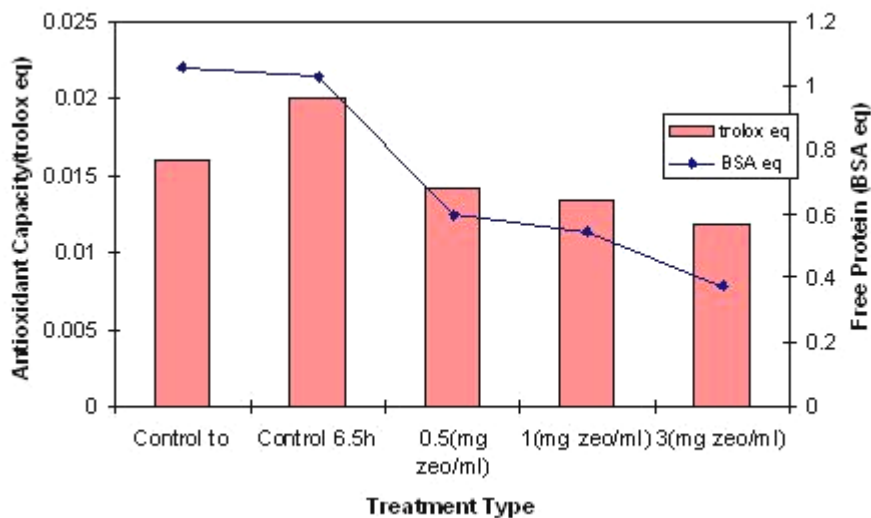


Figure 7.52. Protein content in SIF and their antioxidant capacity

As it was in many proteins, casein was a hydrophobic protein and its stability was also found to be related to hydrophobic interactions (McMahon and Brown, 1984). Since stability might have changed, antioxidant capacity (reaction of protein residues with  $ABTS^{+o}$  radical) might have altered and thus antioxidant capacity might have increased. It was reported by Gomez-Ruiz et al. (2008) that the  $\alpha$ -casein fraction in ovine casein was the most active with  $ABTS^{+o}$  radical decolorization assay on the contrary,  $\kappa$ -casein showed the lowest activity. Besides antioxidant activity of different amino acids assessed by  $ABTS^{+o}$  radical decolorization assay and reported that Cys was the most active amino acid followed by Trp, Tyr and His. The remaining amino acids

analyzed did not exhibit antioxidant activity by that method. Hence, it could be suggested that electrostatic or hydrophilic/phobic interaction might have changed the dynamic conformation of  $\alpha$ -subunit or Cys etc. subunits during incubation in SIF resulting a more appropriate condition for the radical reaction. Thus an increase in antioxidant activity was determined. Also results showed that zeolite addition to the SIF media decreased antioxidant activity of free casein (Figure 7.51) since free casein was adsorbed by zeolite in SIF (Figure 7.52).

#### 7.4.4. Effect of Zeolite Treatment on Charge and Size of Casein

As the surface charge of compounds play a key role in adsorption, zeta potentials of casein and zeolite were investigated. But it is important to note that  $\zeta$  - potential of casein could only be determined as a rough estimation and similar case was also reported by Pan et al. (2007) where the ionic strength for individual protein samples were not high.

Table 7.22. Zeta potential of casein hydrolysate in SIF solution during adsorption

Sample	Zeta potentials(mV)		
	to	4h	6h
Zeolite	-14.00	-9.60	-9.23
Casein	-18.57	-16.03	-14.87
Casein with Zeolite	-18.57	-18.20	-17.67

Zeta potentials of the casein and zeolite indicated that they were negatively charged in SIF during adsorption (Table 7.38). As the pI of the average casein molecule was reported as 4.8 by Guo and Liu (2008), charge of the casein should be negative when it was in media of pH 6.8. Results of zeta potential measurements confirmed this case. It was reported that in the pH range from 6.0 to 12.0, individual casein molecules become more negatively charged and were separated further from each other due to electrostatic repulsion. This leads to the looser structure of casein micelles and the size of the casein micelles increases (Guo and Liu, 2008). Results showed that negative value of casein charge was reduced during 6h in the absence of zeolite. In the presence of zeolite, it was interesting to note that negative charge of the casein was preserved and was more close to its initial value. This might be via presence of zeolite which was also negatively charged in SIF.

In zeolites each aluminum ion which exists in the zeolite framework yields a net negative charge and this charge is balanced by an extra framework cation, usually from the group IA or IIA (Dimirkou and Doula, 2008). It was found that zeta potential of zeolite was negative in all cases. Because in acidic to neutral solutions zeolite/media reacts leading the adsorption of protons in the solution by the neutral and negative surface hydroxyl groups of zeolite. Hence, proton binding occurred suggesting the negative surface charges. In the microporous structure of zeolites there are acidic and basic sites which are commonly defined by the Brønsted and Lewis theory. Oxygen atom in the Si–O–Al species have a negative charge of the lattice and behaves like a proton acceptor and represents the structural basic site as a potential adsorption location for the cations. Besides isomorphous Si/Al substitution account for a negative charge. All those reactions related to metal adsorption on zeolite were given and discussed in details by Doula et al. (2001).

As casein was negatively charged and Guo and Liu (2008) reported that it lead to the looser structure of casein micelles and the size of the casein micelles increased, size measurements were performed. Diameter of the casein in SIF at initial conditions was measured as 327.33 nm. The experimental error for diameter determination was  $\pm 12.6$  nm. During adsorption size of casein couldn't estimated correctly for 4h and 6h periods because of the higher experimental error values. This might be due to the complex structure of the protein nature and might be because of the effect of changes in media to its conformation. Casein has a micelluar structure and its conformation was highly effected with pH, temperature and ionic strength and also it was shown that heat stability of casein was very sensitive to the concentrations of cations present in solution (Philippe et al., 2005). During adsorption in SIF for 6h, ions concentrations present in SIF were varied due to the exchangeable cations especially in presence of zeolite (see Section 7.5.1). Thus they might affect its conformational stability. But pH should not be an effective factor for conformation because in previous studies, it was shown that pH of the solution didn't change in the presence of zeolite and was constant at around pH 6.8 for 24h.

#### 7.4.5. Effect of Zeolite on UV and Fluorescence Spectra of Casein

It was observed that casein showed fluorescence property in Figure 9.25 due to its tyrosine, tryptophan, and phenylalanine residues which were also confirmed by literature (Guo and Liu, 2008). The results were evaluated according to the Tryptophan which had much stronger fluorescence and higher quantum yield than the other two aromatic amino acids and whose fluorescence intensity, quantum yield, and wavelength of maximum fluorescence emissions were very solvent dependent. In the nature of casein,  $K_{s1}$ -casein contained two tryptophan residues at positions 164 and 199, and  $\beta$ -casein had a Trp residue at position 143, respectively. The three Trp residues were mainly located in a primarily hydrophobic portion of casein molecules, and could provide important information about the self-assembly of the casein molecules (Guo and Liu, 2008). As fluorescence spectrum of protein was sensitive to the microenvironment, fluorescence spectrum data were collected.

It was found that there was a slight difference in RFU intensities for casein at initial, 4h and 6h values. This might be due to slight conformational changes. It was reported that in the pH range of 5.5–12.0, the deprotonation of the carboxylic groups of aspartic acid (Asp) and glutamic acid (Glu) residues in casein gave rise to many changes in casein micelle formation, including electrostatic repulsions, the destruction of salt bridges and the formation of buried isolated charges (Guo and Liu, 2008). According to the results of only casein sample in Figure 7.53, considerable fluorescence spectrum shifts could not be observed during incubation in SIF.

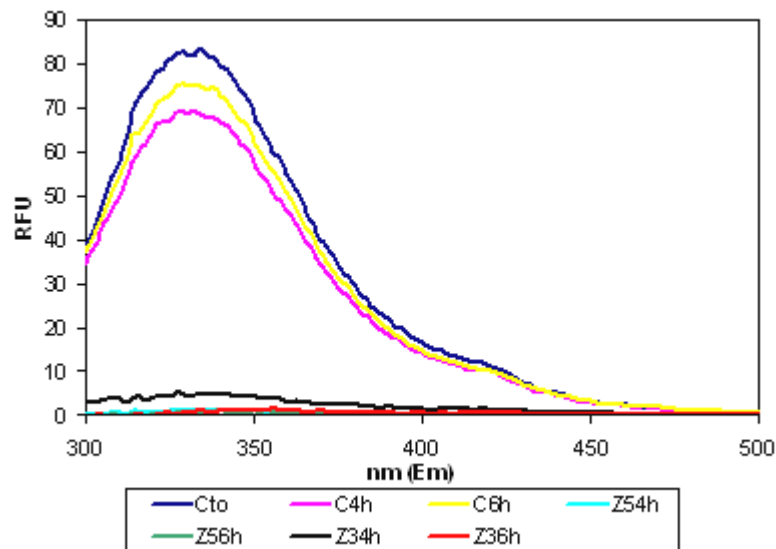


Figure 7.53. Fluorescence emission spectra of casein (1.5 mg/ml) in SIF at pH 6.8.(C:casein; to, 4h and 6h: incubation times ; Z3 and Z5: casein incubated with 3 and 5mg/ml zeolite)

For the casein samples taken at initially, maximum emission wavelength ( $\lambda_{max}$ ) measured was at 334 nm. The maximum emission wavelength ( $\lambda_{max}$ ) was very useful in estimating the hydrophobicity of the microenvironment around tryptophan residues.  $\lambda_{max}$  at 335–350 indicated that tryptophan residues were located in the less polar region, that was, they were buried in a hydrophobic domain in protein;  $\lambda_{max}$  at 350–353 nm suggested that tryptophan residues were much exposed to water (Guo and Liu, 2008).

Casein is one of the most hydrophobic proteins and it is important to note that hydrophobic interactions are very temperature sensitive. In Figure 7.54, after 4h in SIF maximum value was obtained at 336 and didn't change after 6h indicating no change in polarity of the solvent surrounding the tryptophane residue as expected. If there exist any shift, spectrum should have shifted to shorter wavelength and the intensity of the fluorescence should have increases as the polarity of the solvent surrounding the tryptophane residue decreased. For the casein samples incubated with two different doses of zeolite, very low RFU intensities were observed. This indicated that less amount of free casein in SIF was remained to be analyzed suggesting adsorption of casein by zeolite samples.

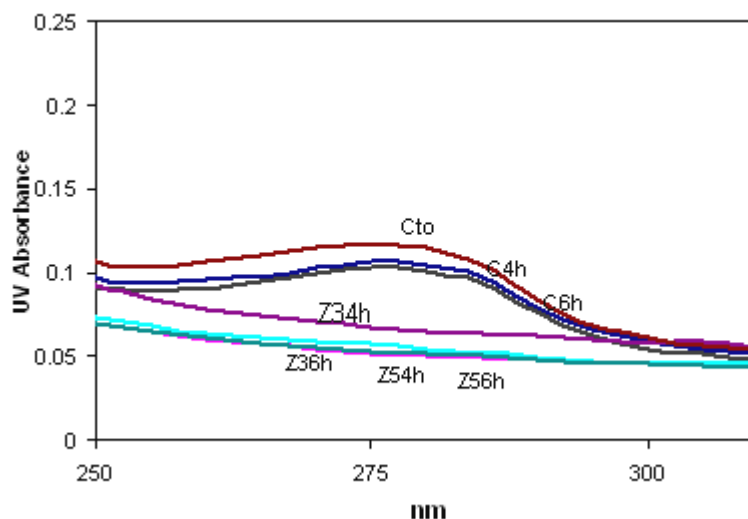


Figure 7.54. UV Absorption spectra of casein (1.5 mg/ml) in SIF at pH 6.8. (C:casein; to, 4h and 6h: incubation times ; Z3 and Z5: casein incubated with 3 and 5mg/ml zeolite)

Similar case for zeolite-casein treatments was also observed for UV absorption studies (Figure 7.54). UV absorption of casein resulted from its protein nature with aromatic side groups and double bonds (Phadungath, 2005). Results showed that, free protein (nonadsorbed) absorbed significantly more UV light than protein incubated with zeolite. This was due to the amount of free protein in the solution. In the presence of zeolite, casein was adsorbed therefore casein samples and casein with zeolite samples showed different UV spectrum which also supported the adsorption studies. Results of UV spectrum of casein incubated with two different doses of zeolite didn't show a considerable difference. Besides, insignificant change was observed for only casein samples incubated for 4h and 6h

#### 7.4.6. Effect of Zeolite on Thermal Behaviour of Casein

Protein functionality is closely related to its conformational state, which in turn is completely influenced by conditions. Temperature is one of the most important factors in a process performance, since high temperature causes protein unfolding and lost of functionality and denaturation of proteins has been extensively studied by differential scanning calorimetry (DSC), where denaturation is observed as an endothermic peak on the thermogram (Len et al., 2003).



Thermal analysis is a valuable tool for studying the effect of temperature which is associated with protein unfolding. As casein samples (incubated in SIF or control samples with/without zeolite) were heated, they would undergo thermal denaturation; which means that they became unfolded and became less ordered form of a random coil.

To investigate the stability of casein in SIF and to investigate thermodynamics of protein unfolding, differential scanning calorimetry was used. Figure 7.55 showed heating DSC curves for casein lyophilised from SIF solution initially, in the presence of zeolite and at the end of adsorption after 6h. Data was evaluated according to the enthalpy changes associated with the unfolding transition in addition to the temperature. Apart from the zeolite/casein samples, which showed a distinct single endothermic transition, all other samples showed two peaks. For only casein samples at time zero and for only casein samples after 6h incubations; transitions were observed around 48 and 60°C respectively. This difference might indicate the effect of interaction of solvent with casein for 6h where conformational changes could be occurred. It was suggested that the transitions at lower temperature around 30 degrees C occur primarily in the monomer and those middle ranged transitions, around 40 degrees C are more likely the reflection of hydrophobic changes in the core of beta-casein. As beta-casein undergoes self-association and increases in size, the transition at higher temperature is perhaps caused by the apparent conformational change within the micelle-like polymers as occurred at this case.

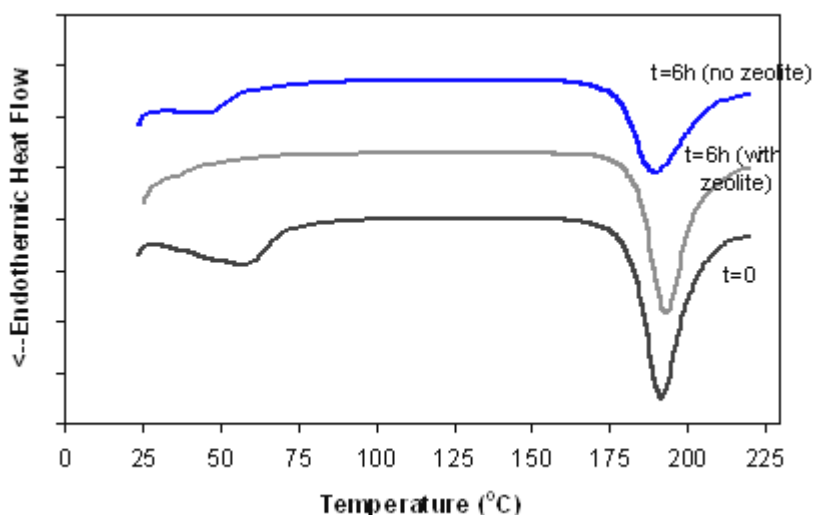


Figure 7.55. DSC thermograms of casein in SIF

The onset temperature ( $T_{\text{onset}}$ ), the peak temperature ( $T_{\text{peak}}$ ) and the enthalpy of

transition ( $\Delta H_D$ ; area under transition curve), specific  $\Delta h_d$  obtained from DSC measurements performed for the second transition region (Table 7.39).

Table 7.23. DSC Results of Samples

Sample	$T_{peak}(^{\circ}C)$	$T_{onset}(^{\circ}C)$	$T_{endset}(^{\circ}C)$
<b>t=0</b>	191.8±2	177.2±3.9	207.5±3.1
<b>t=6h (no zeolite)</b>	189.6±1	176.7±3	29.3±2.3
<b>t=6h (with zeolite)</b>	193.3±1	179.7±2	208.14±2.6

Using only casein sample at the beginning;  $T_{onset}$  decreased 1°C after 6h incubation in SIF and with zeolite a 2.5°C increase in  $T_{onset}$  was observed after 6h in SIF (Table 7.39 but they could be statistically considered same. Denaturation temperatures of proteins were in strong relation with environmental affects, such as pH and salts (deWit et al., 1984). It was interesting to note that although thermal stability of casein slightly reduced by incubation for 6h, when zeolite was added to the media, at the end of 6h peak temperature increased from 189 to 193°C. Therefore it was possible to say that zeolite slightly effected thermostability of the protein. But those slight effects were not observed in denaturation enthalpies. The enthalpy itself represented an endothermic final sum of affects that are effective in the conformational changes such as contribution mainly because of the disruption of internal hydrogen bonds in protein (Paulsson and Dejmek, 1990). During incubation in SIF, conformational changes might have happened in the nature of casein when it was incubated with zeolite. Denaturation enthalpies in DSC analyses found to be -177.02 and -151.9 j/g for casein samples incubated with and without zeolite, respectively and at time zero casein showed highest stability with highest denaturation enthalpy of -261.57. Previous results about the effect of zeolite on elementary composition of SIF media (Chapter 7) showed that  $Ca^{2+}$  ion was exchanged. This ion has primary importance on casein structure. It was reported that the  $\alpha$  and  $\beta$ -caseins were designated as calcium-sensitive: they precipitate in the presence of moderate concentrations of  $Ca^{2+}$  ions (Guo et al., 2003).  $\kappa$ -Casein, however, remained soluble in the presence of calcium. In the presence of  $\kappa$ -casein the other caseins form stable colloidal suspensions in the presence of calcium ions; in such systems  $\kappa$ -casein acts as a protective colloid. The phosphoserine residues of the caseins are responsible for their specific interaction with calcium ions and calcium phosphate, which is a key factor in the micelle formation. These residues are also responsible for the ability of

caseins to bind a broad range of metal ions (Zhang et al., 2004). Therefore  $\text{Ca}^{2+}$  ion might play a key role for the shifts in that  $T_{\text{peak}}$ .

#### 7.4.7. Effect of Zeolite on FTIR Spectra of Casein

FTIR studies were performed to determine the mechanism of interaction between zeolite and casein at adsorption studies in SIF. The first class of the infrared spectrum of the zeolites of vibrations was due to internal vibrations of the  $\text{TO}_4$  tetrahedron which is the primary unit of the structure and the second class was related to the external linkages between tetrahedral (Breck, 1974). For the zeolite framework, the internal vibrations T-O were sensitive to the Si/Al ratio of the framework. As it was seen in Figure 7.56, in all samples characteristic peaks of zeolite were observed. Internal T-O bonding was observed at  $470 \text{ cm}^{-1}$ . The  $470 \text{ cm}^{-1}$  and  $613 \text{ cm}^{-1}$  peaks were assigned to the internal and external Si (or Al)-O double ring respectively. The strong symmetric and asymmetric stretch vibrations were present at  $1070 \text{ cm}^{-1}$ . The water vibrations of zeolite were also observed after  $3450 \text{ cm}^{-1}$ . When IR-spectra of Zo (zeolite untreated) and Z6h (zeolite incubated in SIF for 6h, without casein) With respect to incubation for 6h in SIF conditions, there were no changes in characteristic peaks.

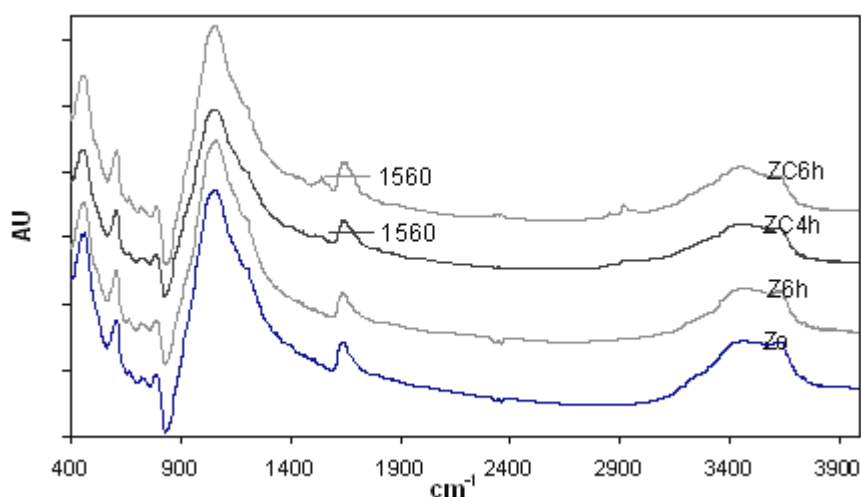


Figure 7.56. IR spectra of zeolite (Zo: untreated, Z6h:6h incubated in SIF, ZC4h:4h incubated in SIF with casein, ZC6h:6h incubated in SIF with casein )

When zeolite sample was incubated with casein according to adsorption conditions for 4h and for 6h, a foreign peak was observed at  $1560 \text{ cm}^{-1}$  indicating the

adsorption of casein on to the zeolite surface. Also it was important to note that intensity of the peak was changed with respect to time where higher intensities were determined after 6h treatment in contrary to 4h treatment which suggested higher amount of casein was adsorbed. To understand the detailed information behind the protein adsorption, first of all, characteristic IR bands of protein should be presented. Hence, FTIR analyses of treated and untreated casein were performed.

The peptide group which was the structural repeat unit of proteins, gave up to 9 characteristic bands named amide A, B, I, II ... VII given in Figure 7.57. Amide I and amide II bands were two major bands of the protein infrared spectrum and the peak positions of Amide I and II were sensitive to the protein secondary structure ( $\alpha$ -helix,  $\beta$ -sheet, random coils, etc.)

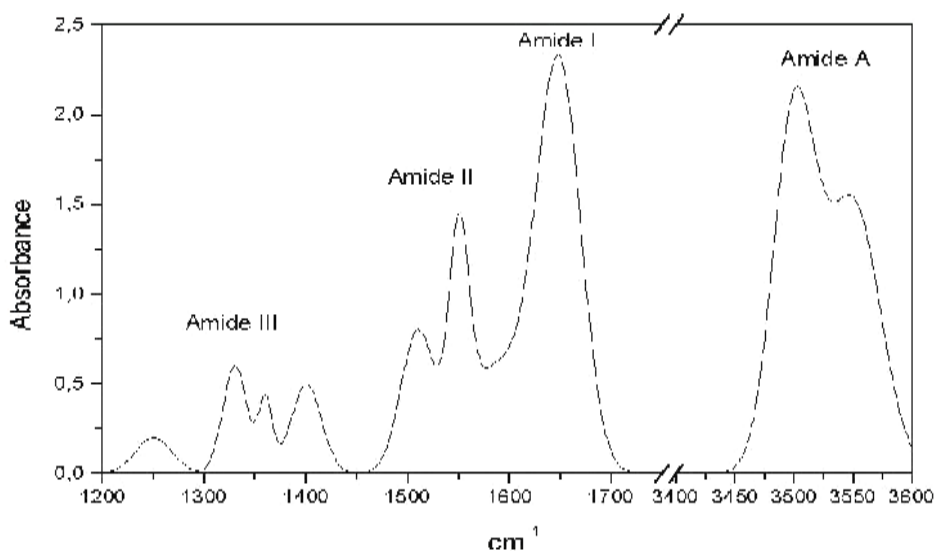


Figure 7.57. Standard protein FTIR spectra (Source: Image Library, n.d)

Results of Figure 7.58 and 7.59 for the nontreated and treated and casein samples showed characteristics peaks for the protein of Amide I and Amide II regions and regions indicated that effect of incubation in SIF and lyophilization of casein did not cause strong effects for characteristic regions of Amide I and II.

Amide I was the most intense absorption band in proteins. It was primarily governed by the stretching vibration of the C=O (70-85%) and C-N groups (10-20%). Its frequency was found in the range between 1600 and 1700  $\text{cm}^{-1}$  for proteins and in Figure 9.30 and 9.31; 1650-1690  $\text{cm}^{-1}$  spectral region was dominated by Amide I of the polypeptide backbone for the casein which were also confirmed by literature (Kong and

Yu, 2007). Amide II was found in the 1510 and 1580  $\text{cm}^{-1}$  region and it was more complex than amide I and it was conformational sensitive. Amide II derived mainly from in-plane N-H bending (40-60% of the potential energy). The rest of the potential energy arises from the C-N (18-40%) and the C-C (about 10%) stretching vibrations.

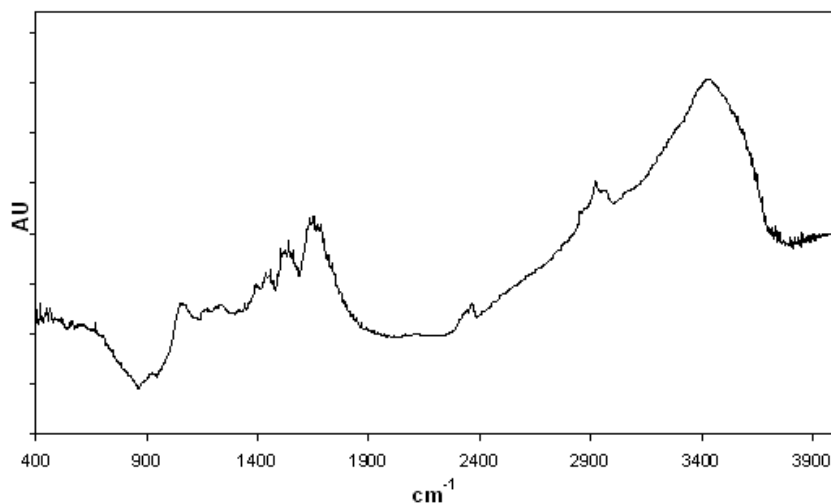


Figure 7.58. IR spectrum of casein powder (untreated).

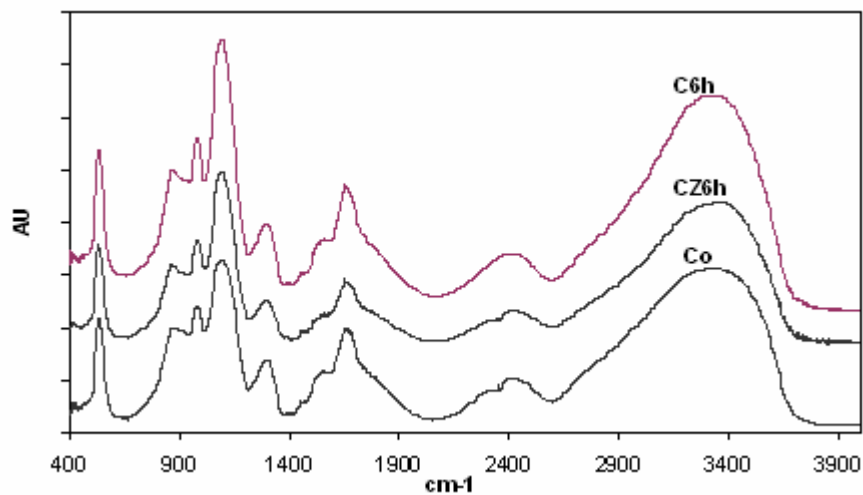


Figure 7.59. IR spectrum of casein ( $C_0$ :at time=0, CZ6h:casein incubated with zeolite for 6h in SIF, C6h:casein incubated for 6h without zeolite in SIF).

As the samples were prepared by lyophilization after incubation conditions, effect of incubation in SIF and lyophilization caused minor changes for characteristic regions of Amide I and II as explained. On contrary, different peaks were observed in Amide III region for untreated casein and treated caseins where Amide III region was

very complex bands resulting from a mixture of several coordinate displacements and complexity of bands dependent on the details of the force field, the nature of side chains and hydrogen bonding.

Considering the information given above about FTIR spectra of proteins and FTIR results of the casein samples, new peak on the zeolite surface after adsorption in Figure 9.28 was assessed. The peak indicating the adsorption of casein to the zeolite in Figure 9.28 at  $1560\text{ cm}^{-1}$  was in Amide II band region and it was corresponded to  $\text{NH}_2$  bending and due to Glutamine ( $\text{pH}:6.8 > \text{pK}: \sim 4.4$ ) for  $-\text{COO}$  stretching vibration (asymmetrical) and this result was also mentioned by Venyaminov and Kalnin (1990). Also this result was confirmed by adsorption studies performed by Ismail et al. (2005) for zeolite and protein adsorption where hydrogen bonded NH was represented in the same band region.

#### 7.4.8. Effect of Zeolite on Surface Morphology of Casein

To determine the differences in surface morphologies, SEM images prepared after adsorption studies were analyzed for both casein and zeolite. First of all, to observe the differences in raw (untreated) casein and lyophilized casein obtained after adsorption from the solution, SEM images were taken and results were given in Figure 7.60 a and b.

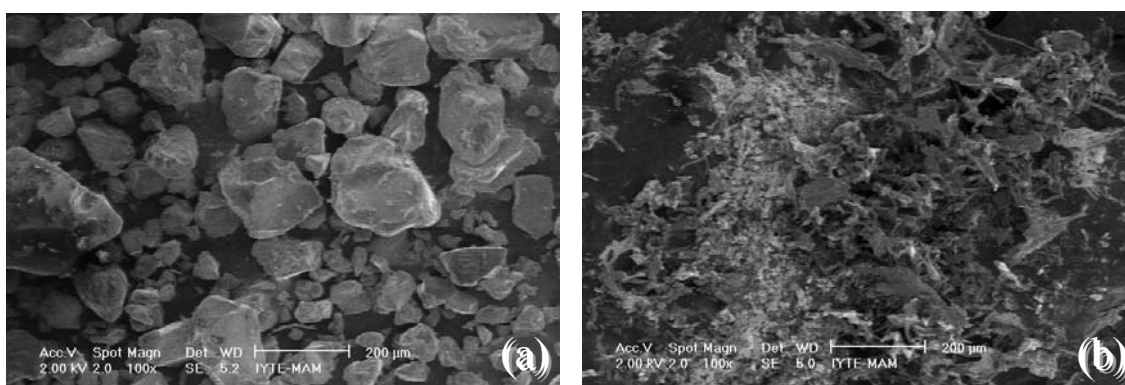


Figure 7.60. SEM images of casein samples. a) Casein powder (Untreated); b) Solubilized casein in SIF at initial.

It was found that untreated (raw) casein was in individual form and differentiate in size. As proteins flashes in SEM analyzes, gold coating was applied to the samples as

a part of sample preparation step therefore it was hard to view individual micelles. Thus no information about the fine details of the micelle surface could be obtained. Imaging of whole sample using SEM also provided no information about the structure of the interior of the micelles. But morphological difference due to solubilization, treatment of casein and sample preparation of lyophilization was exactly observed in Figure 7.60 b where irregular shapes were obtained.

During surface scanning some regions on samples were found to be easily observed for the protein-like structures (Figure 7.61). Although there were differences in micrographs of casein samples (incubated with or without zeolite), it was hard to discriminate the results based on zeolite effect. Those differences were observed as some irregularities in some regions, possibly due to hydrophobicity/hydrophilicity change of open sided peptide backbones due to presence of zeolite in SIF.

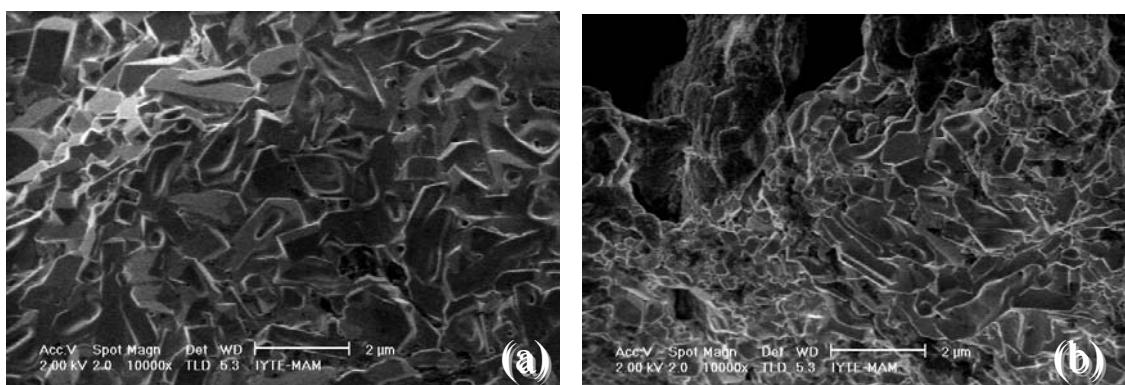


Figure 7.61. Casein after 4h incubation in SIF (without zeolite) b) Casein after 4h incubation in SIF with zeolite

When the effect of incubation was investigated in solid phase, adsorbed casein was easily observed on the zeolite's surface compared to control sample (Figure 7.62 a and b, respectively). Observation of adsorbed casein on zeolite's surface confirmed the studies of adsorption, interaction and FTIR analyzes which were presented previously.

Also SEM images were viewed to determine if there were differences at the beginning of adsorption and after 6h (Figure 7.63 a-f). It was found that surface morphology of casein was different. Solution conditions could be considered as perturbations on the protein structure and properties that might alter the adsorption dynamics. The sample in Figure 7.63-d (initial) was not as hydrated as two other treatments. Adsorption period was 6h therefore samples Figure 7.55 e and Figure 7.55.f were continuously in contact with the solution for that time period. When the casein

adsorption was conducted using zeolite for 6h, structure of casein incubated with zeolite wasn't significantly changed compared to casein control study.

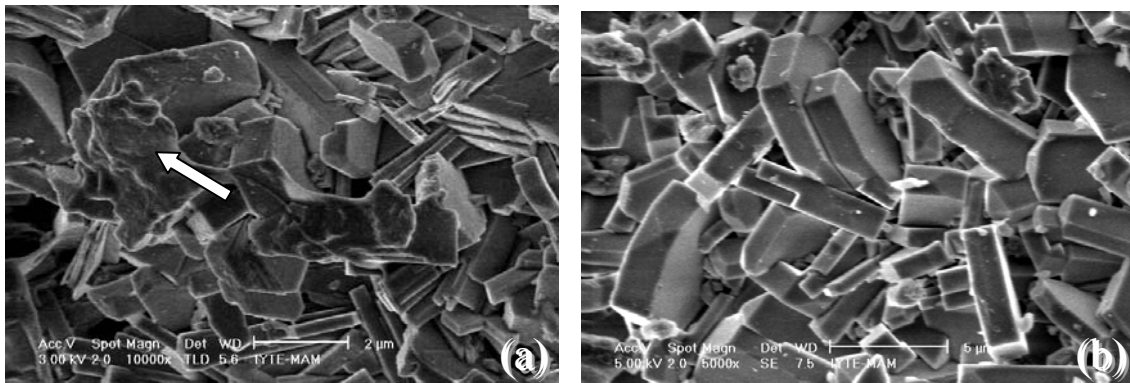


Figure 7.62. SEM images of zeolite samples. a) Zeolite after incubated 4h in SIF with casein b) Zeolite (casein free;control).

It was interesting to observe with 100x magnification that casein powders tend to form aggregates (Figure 7.63; a,b,c). When casein was incubated with zeolite for 6h, SEM images of protein powders tend to form aggregates compared to control (without zeolite) treatments. Similar case was also observed in simulated digestion treatments (See Chapter 7, SEM results) where digestion fluid powder was in larger size and formed aggregates when zeolite was used in experiments. That case was not happened in only casein samples after 6h treatment. Therefore possible interactions were due to protein structures and zeolite in aqueous media. Also those results suggest that zeolite might have caused some conformational changes. In recent studies zeolites were used in protein refolding (Ishibashi et al., 2006). Chiku et al. (2006) suggested that amine groups were required in protein refolding when they used  $\beta$ -zeolite as a tool for refolding. Nara et al. (2009) studied refolding of proteins containing disulfide bonds using hen egg lysozyme having four disulfide bonds as the model protein. Using zeolite beta they demonstrate that lysozyme was efficiently refolded, and that active lysozyme was obtained at high concentrations.



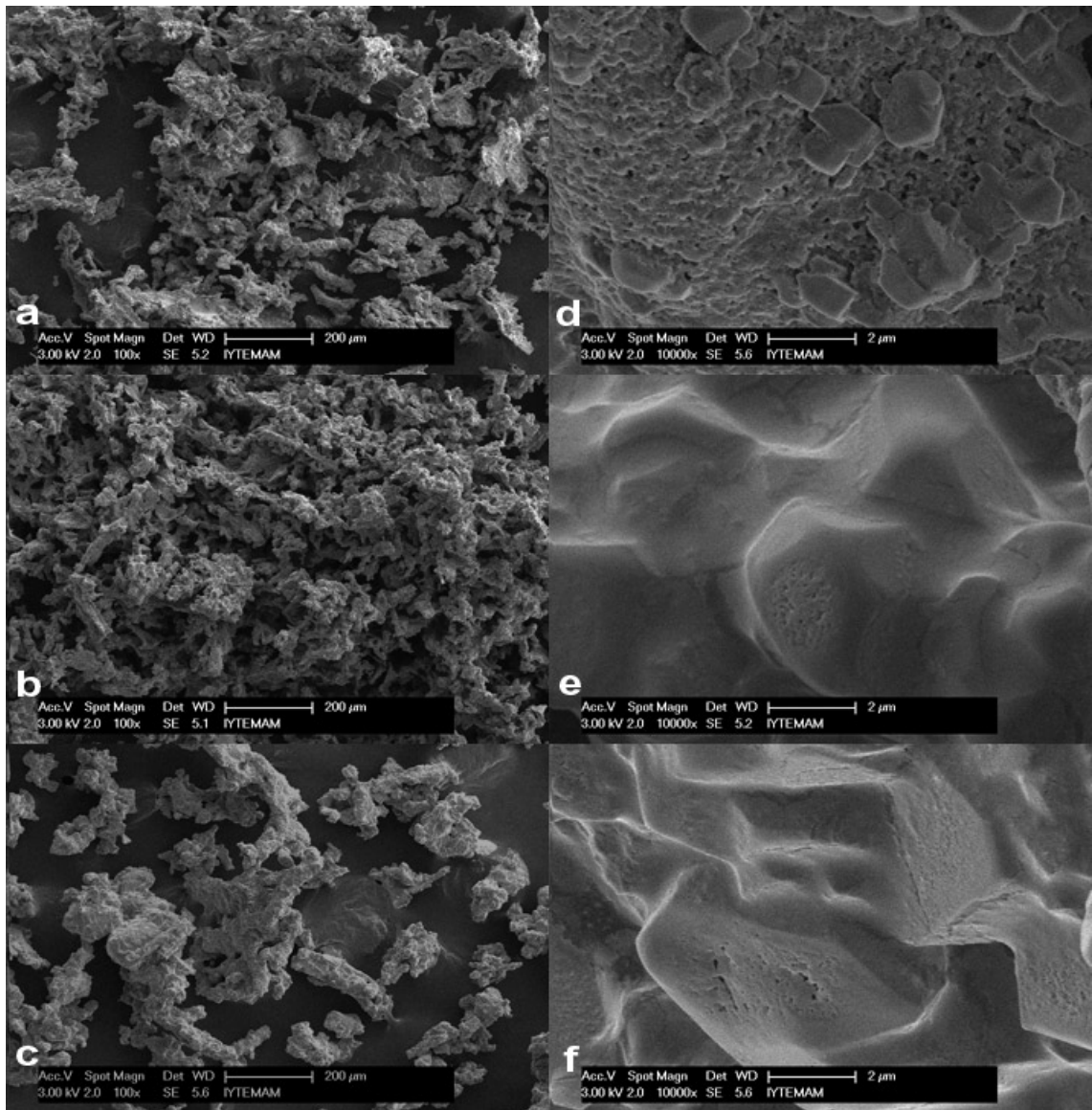


Figure 7.63. SEM images of casein powder a,b,c (100x), c,d,e(10000x) magnification. a-d: initial before adsorption, b-e: after 6h in adsorption solution without zeolite, c-d: after 6h in adsorption solution including zeolite.

Charges of the proteins form electrostatic interactions between themselves. In previous studies it was found that the amount of zeolite added to the adsorption media did not change the pH for 6 hours. But based on the pH of the media, complex structure of the casein might change. Guo (2008) reported that in the pH range of 5.5–12.0, the deprotonation of the carboxylic groups of aspartic acid (Asp) and glutamic acid (Glu) residues occurred in casein. That deprotonation gave rise to many changes in casein micelle formation, including electrostatic repulsions, the destruction of salt bridges and the formation of buried isolated charges, eventually leading to the loose structure of the casein micelle with increasing pH. Therefore the key point here was the charge of

casein in adsorption media.

In adsorption study, pH was higher than the pI of the casein. Thus more carboxylic groups would be ionized. That negative charges would result repulsion among the carboxylic groups which leads to some loosening of the hydrophobic nanodomains and the radius of casein micelles would be increased. The zeta potentials of the casein were previously found as; -18,57mV at initial, -14,87 mV after 6h and -17,67 mV after 6h with zeolite.

It is important to note that when proteins are highly charged with identical signs there should be repulsive interactions between proteins that stabilize protein solution colloidal and in that case aggregation would be energetically unfavorable (Chi et al., 2003). But in this zeolite-casein interaction treatment, it was different. Although the negative charge of the casein was high at initial measurements, the SEM images were similar to the images of casein incubated for 6h. Reason might be the long time of exposure to adsorption solution. Adsorption solution caused hydration of casein micelles (they include hydrophilic and hydrophobic subdomains as mentioned before) which gave rise to increase in size compared to initial measurements where casein was not enough hydrated.

At the end of 6h incubation with zeolite, casein was more negatively charged than sample without zeolite. Therefore, agglomeration in larger sizes might be due to highly ionized carboxylic groups where individual casein molecules become more negatively charged and were separated further from each other due to a stronger electrostatic repulsion. But, as casein was hydrophobic protein, tendency of casein to form aggregate was always active. Therefore this competition should have stronger influence on aggregation rate. Thus, possibly, molecules were together due to high hydrophobicity, but they were larger in size due to deprotonation. This leads to loosening of structure of casein micelles and increase in size of the casein structures with respect to zeolite incubations. Additionally it was possible for the protein to form complexation with the metals released to the solution from the zeolite which might lead agglomeration.

## 7.5. Interactions of Inhibitors with *E.coli*

*E.coli* was a part of our natural intestinal habitat. Besides it was an important microorganism according to its glucuronidase enzyme synthesis which was responsible for carcinogen formation (Zenser et al., 1999; Dabe et al., 2008). Therefore it was important to investigate possible interactions between *E.coli* and zeolite/casein.

*E.coli* culture (ATTC 8739) was tested for its glucuronidase enzyme production to confirm that it was GUS positive. To observe the fluorescence, enzyme extraction technique was performed using different concentrations of substrate (MUG) and different enzyme substrate incubation periods. Then enzyme was extracted by means of a non-ionic surfactant (TritonX-100). Reaction of substrate and released enzyme will give fluorescent compound which was indicator of enzyme activity after extraction.

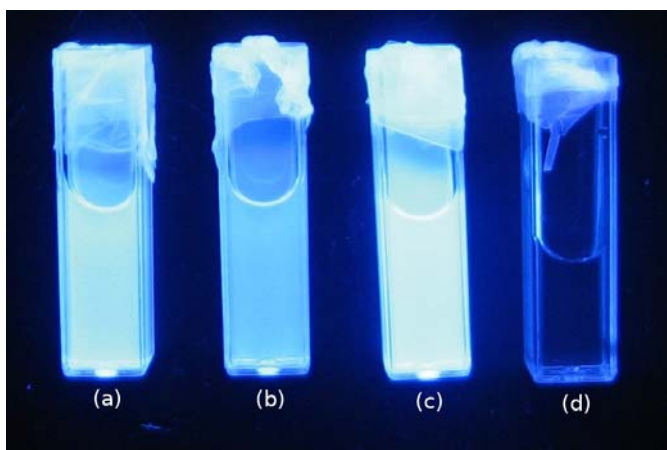


Figure 7.64. Fluorescent luminescence under UV light (a)4mg/ml 4-MU,5min ; (b)2mg/ml 4-MU,10min, (c)4mg/ml 4-MU,10min, (d)control.

In Figure 7.56, results showed that all treatments for 2 or 4mg/ml and incubation periods for 5 or 10 min; *E.coli* cell extract including GUS enzyme performed fluorescent luminescence due to enzyme substrate reaction. Therefore results indicated that *E.coli* was GUS positive and this result was also confirmed by different studies in literature (Fujisawa and Mori , 1997; Zenser et al., 1999).

### 7.5.1. Effect of Zeolite on *E.coli* Growth

To check if there was an antimicrobial effect of zeolite on *E.coli* or not, zeolite was used with different concentrations for antimicrobial tests. Results were given in

Table 7.24.

Table 7.24. Effect of different zeolite concentrations on growth of *E.coli*

	Control Samples		Zeolite Concentrations in Culture Media (g/ml)		
	(-)Control	(+)Control	0.01	0.03	0.05
cfu/ml	nc*	1.28x10 <sup>8</sup>	1.26 x10 <sup>8</sup>	1.23 x10 <sup>8</sup>	1.28 x10 <sup>8</sup>
Log(cfu/ml)	-	8.9±0.02 <sup>a</sup>	8.10±0.05	8.09±0.02	8.9±0.02

nc\*:not countable, <sup>a</sup>:standard deviation

As the zeolites have ion exchange properties, some zeolites might gain antimicrobial property via exchange of ions having antimicrobial effect such as Ag<sup>+</sup>, Zn<sup>2+</sup>, etc. This property might be achieved in laboratory conditions by modifications such as Ayben and Ülkü (2004) found that silver exchanged zeolite showed antimicrobial activity due to its silver load and it might be used in many applications.

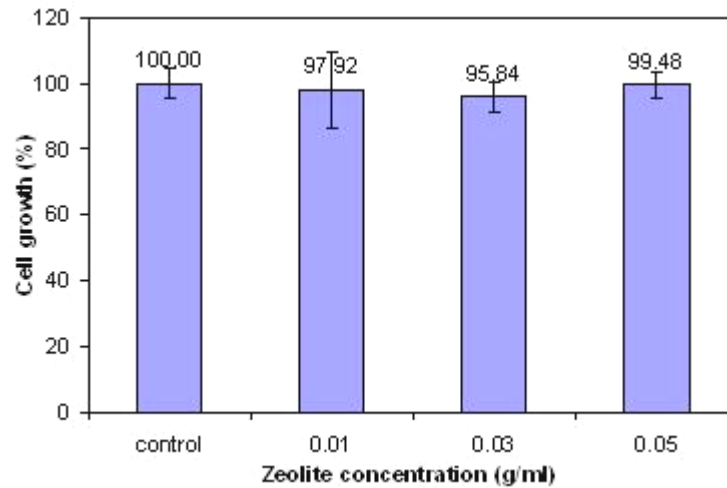


Figure 7.65. Effect of different zeolite concentrations on growth (%) of *E.coli* (*E.coli*  $t=0$ : 10<sup>8</sup> cfu/ml- McFarland 0.5 in Mueller Hinton Broth, 37°C, 24h incubation)

In this study, it was observed that there was not a difference between control samples and treatments which indicated there was no antimicrobial effect of natural zeolite on *E.coli* (Figure 7.65)

This result was also confirmed by literature studies performed by Rodriguez-Fuentes et al. (1997). They studied the microbicide effect of natural zeolite on different microorganisms such as *E.coli*, *Klebsiella pneumoniae*, *Bacillus cereus*, *Shigella flexneri*, *Staphylococcus aureus*..etc and found no microbicide effect for natural zeolite.

## 7.5.2. Effect of Casein on *E.coli* Growth

Casein has a micellar structure and it might be as a growth inhibiting agent against enteric *E.coli* such as acting as barrier for the nutrient transport in microorganisms by covering their membrane surfaces or showing antimicrobial activity. As the casein was found to inhibit the GUS enzyme, casein addition to the growth media was investigated. As *E.coli* was one of the major GUS producing bacteria, finding any overgrowth inhibitory effect for *E.coli* would be helpful for regulating intestinal microflora. Growth curves were performed using different concentrations of casein by measuring the optical density at 620 nm during 24h and results were given in Figure 7.66.

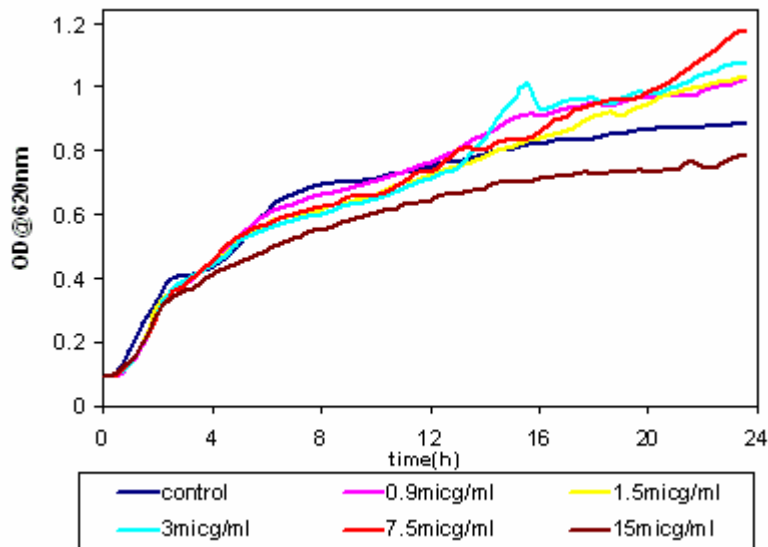


Figure 7.66. Changes of OD of *E.coli* with respect to time at various casein concentrations added to growth media ( $E.coli_{t=0}$ :OD:0.1@620nm in Mueller Hinton Broth, 37°C, 24h incubation).

It was found that at exponential phase growth in control sample (without casein) was higher where it indicated that addition of casein reduced the growth rate of *E.coli*. After the incubation time reached to 10h (OD was 0.79), it was interesting to indicate that control values were lower than the casein added samples. This result might be due to the nutritive property of casein. Initial times where OD was lower than 0.7, number of microorganisms were not high enough to utilize casein as a nutritive source. Amount of casein was high for that limited number of organisms. This high amount of casein

might have served as inhibitory factor as casein has a known ability to bind microorganism or other nutrients in the media due to its micellar structure. Besides, it might have acted growth rate reducing agent where in literature, it was reported that bioactive peptides of casein exhibited antimicrobial activity against *E.coli* (Hayes et al., 2006). After the critic value of OD was reached at 0.79, the number of microorganisms was high enough to utilize all concentrations of casein (except 15 $\mu\text{g/ml}$ ) therefore casein acted as a nutritive source. Therefore it was found that time and the concentrations of casein were effective factors during microbial growth of *E.coli*.

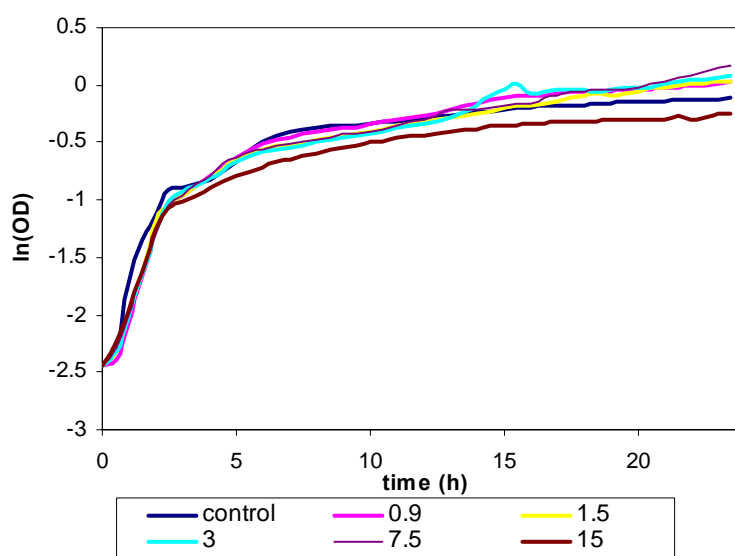


Figure 7.67. Logarithmic growth rate of *E.coli* at various concentration of the casein

Table 7.25. Specific growth rates and generation times of *E.coli* at various casein concentrations

Casein Conc. ( $\mu\text{g/ml}$ )	Specific Growth Rate ( $\text{h}^{-1}$ )	Generation Time (h)
0	0.78	0.39
0.9	0.70	0.43
1.5	0.68	0.44
3	0.67	0.45
7.5	0.64	0.47
15	0.61	0.50

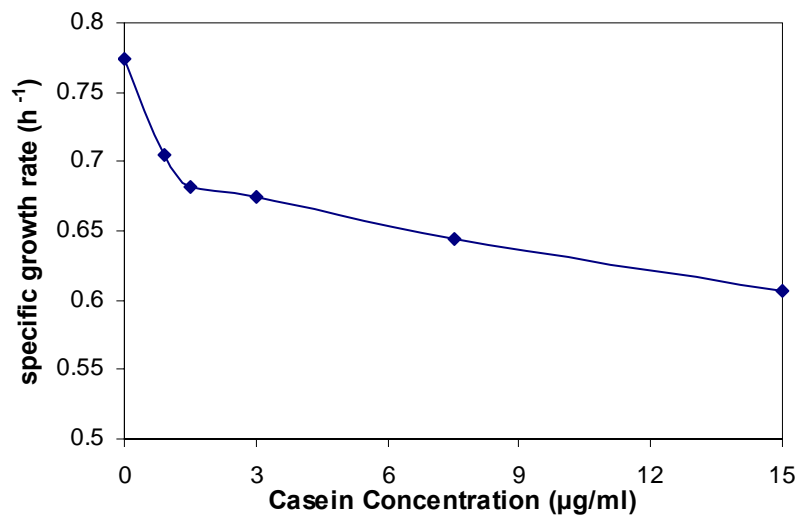


Figure 7.68. Specific growth rate curve as a function of casein concentration

The natural logarithmic increase of biomass for *E.coli* over the time is shown in Figure 7.67. The specific growth rates were reported to depend on the concentration of the limiting nutrient, which could be a carbon source or other factors needed by the microorganisms for growth (Kayombo et al., 2003). Hence the casein was the limiting nutrient, specific growth rates and generation times for different casein concentrations were calculated from the Fig. 7.14 and were given in Table 7.41.

It was found that specific growth rate decreased and generation times were increased with the increasing casein concentrations. When the specific growth rate was plotted against the initial casein concentration (Figure 7.68), the experimental data revealed that casein had a growth reducing effect. Up to 1.5 µg/ml casein, there was a sharp decrease in specific growth rates. But where casein concentrations were 1.5 and 3 µg/ml, decrease in the specific growth rates were not certain and they were nearly same.

This behaviour indicates an adaptation of the organisms. But higher casein concentrations ( $> 3\mu\text{g/ml}$ ) decrease in specific growth rate was again dominant behavior and this might be due to the inhibitory effect of casein and or metabolic activity changes takes over due to casein. Similar case was also reported by Aggary et al. (2009). They used phenol as substrate and they found that higher substrate (phenol) concentrations acted like a switch reducing metabolic activity of *Pseudomonas fluorescens* considerably.

## CHAPTER 8

### RESULTS OF INTERACTION STUDIES OF ZEOLITES AND CANCER CELLS

Natural zeolite clinoptilolite, have been shown to exhibit diverse biological activities. Pavelic et al. (2001) suggested the novel use of natural zeolites as potential adjuvants in anticancer therapy. They found that zeolite effected the tumor growth in vivo and its effect was ranged from negative antitumor response, to normalization of biochemical parameters, prolongation of life span, and decrease in tumor size. Besides, there were different studies related to novel usage of natural zeolites in anticancer therapy (Colic and Pavelic. 2000; Pavelic and Hadzija. 2003). Since it was presented in previous chapters that zeolite inhibited the GUS enzyme, other biological activities denoting usage of zeolite against cancer would be important from a medical point of view. Thus in this chapter; results of antioxidant activity of natural zeolite and its possible interactions with different cancer cell lines: Caco-2 (human colon adenocarcinoma) and a rapid growing cell line of MCF-7 (human breast cancer) cell lines were presented in details. In this study, Z1 and Z2 zeolites were used which have different purities. Moreover, a comparison was made related to of their effects on cancer cell  $\beta$ -glucuronidase production. At last, results of possible effects of zeolite treatment on cancer cells at DNA level were given.

#### **8.1. Antioxidant Activity of Zeolite**

There has been an increasing awareness about the potential health benefits of antioxidant compounds. Many epidemiological studies have suggested that regular consumption of antioxidant compounds may lead to decreased incidence of various forms of cancer and heart diseases. Therefore it was important to study on antioxidant behavior of zeolite to investigate its health benefits.



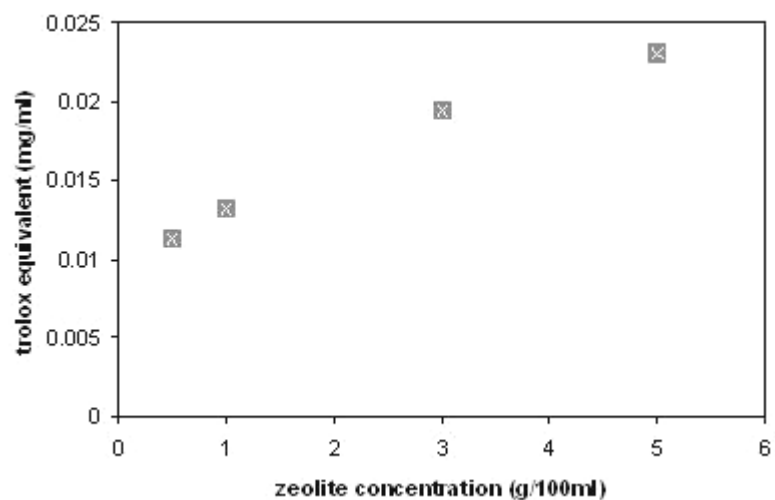


Figure 8.1. Effect of zeolite concentration on antioxidant activity.

To measure antioxidant activity, zeolite at concentrations of 0.5; 1; 3; and 5g/100ml were used in ABTS radical cation (ABTS<sup>+</sup>) decolorization assay. Results were given in Figures 8.1 and 8.2.. It was found that zeolite had high antioxidative capacity. TEAC values were 0.013 for 1g/100ml, and got a value of 0.023 for 5g/100ml zeolite. TEAC values showed linearity with the increasing zeolite concentrations.

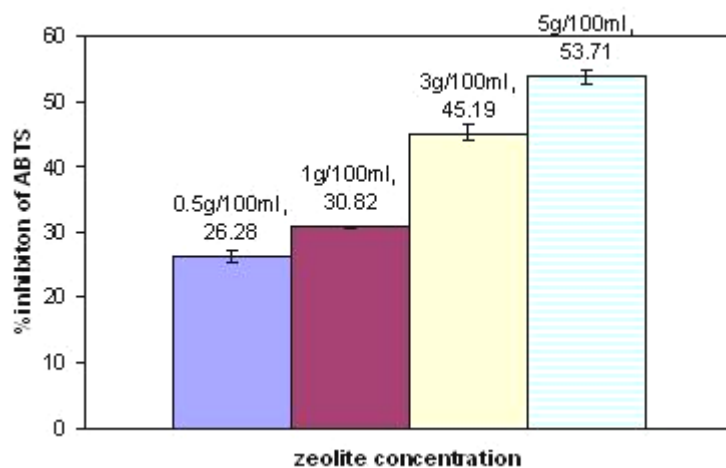


Figure 8.2. Effect of zeolite concentration on inhibition % of ABTS<sup>+</sup>.

Additionally, these results showed that highest % inhibition was obtained with the 5g/100ml zeolite. Half of the radical activity (53 %) was successfully inhibited by the zeolite. Similar results were also reported in literature that zeolites could be used as antioxidant materials. Sverko et al. (2004) reported that natural micronized clinoptilolites (TMAZ) could have an important influence on the immunological

parameters and inflammatory processes through the action on the superoxide anions and nitric oxide. They investigated antioxidant properties of TMAZ containing plant extract (*Urtica dioica L.*) against lipid peroxidation and they found synergistic action between TMAZ and *Urtica dioica L.* extract.

These results indicated that zeolite with its high antioxidant capacity, might take a role in cancer prevention or reduce risks of some diseases caused by free radicals. According to this point of view, zeolite has beneficial effects natural dietetic compound/food supplement.

## 8.2. Zeolite and Caco-2 Cell (Human Epithelial Colorectal Adenocarcinoma Cell) Interactions

Caco-2 cells were important to understand the interaction of zeolite with cancer cell lines related to intestinal system. Caco-2 cells were colorectal epithelial cells therefore digested compounds directly interacted with those cells. Therefore it was possible to understand the behavior of zeolite (in vitro) and investigate if there were positive effects of zeolite on cancer cells.

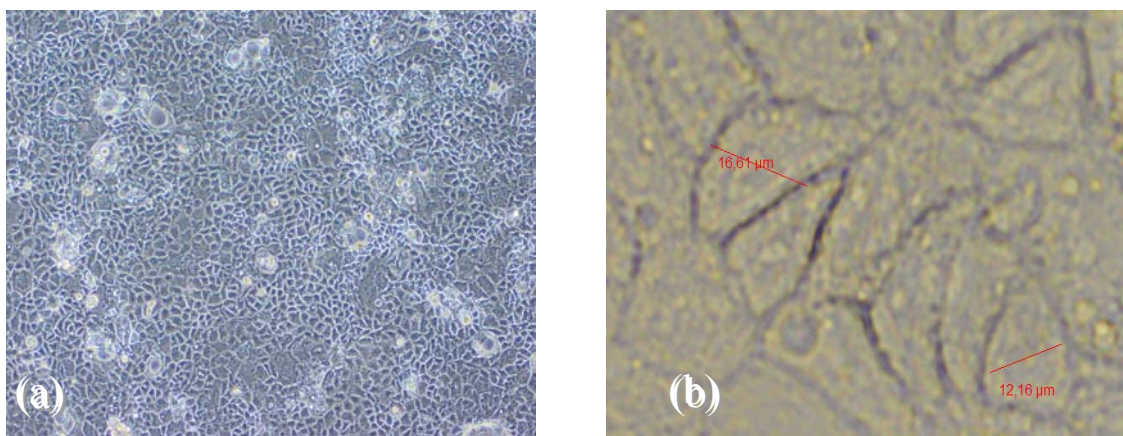


Figure 8.3. Images of Caco-2 cell under microscope.(a)View of Caco-2 cells on an optical microscope at 100% confluency, (b) Size of the cells.

Cell culture studies were performed and optimum growth conditions were determined. Time to reach the >80 % confluency was found as 10-15 days for culture studies. In Figure 8.3, confluency of cells was observed in images obtained by inverted

microscope (Olympus CKX41).

Dahm and Eriksson (2004) used synthetic zeolite-Y particles as a carrier of bioactive molecule N-nitro-L arginin methyl ester (L-NAME) to inhibit the cellular NO production in peripheral monocytes. This research was important because it represents that internalization of zeolites by phagocytosis. Therefore to give an idea about the size of the Caco-2 cell; magnitude of the cell size was measured during the obtaining images under the microscope by the digital camera (Olympus DP25) with the aid of the software program (Olympus DP2-BSW) and approximate cell size was calculated as 10-25  $\mu\text{m}$  for cells where particle size of zeolite (Z1) ranged from 0-45  $\mu\text{m}$ . Therefore large particles of zeolite could not be taken inside the cells and action of zeolite on Caco-2 colon cancer cell line would probably be by interacting with media surrounding the cells, and by direct contact with cell membrane (such as adsorption), not by internalization.

To investigate the possible internalization for small zeolite particles, detailed investigation was performed by confocal microscopy. Cells were incubated with different doses of zeolite in their culture media. High viability was desired to investigate the cell behaviour. It was interesting to note that cells were in high interaction with the fine zeolite particles. Zeolite particles were accumulated around the cell wall but their size was too high to be internalized. Instead, they tend to be cummulated around the cell membrane and seemed like to be attached on the membrane.

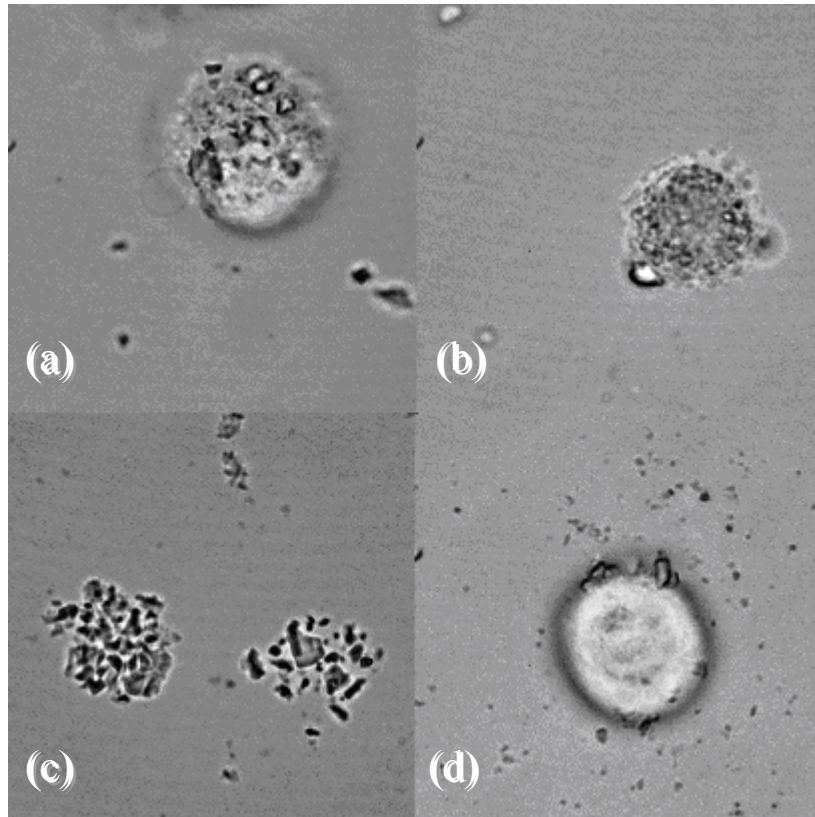


Figure 8.4. Confocal microscopy images of fine zeolite particles with the Caco-2.

Results of the interactions investigated under the confocal microscopy were given in Figure 8.4. In 8.4 (a), accumulation of zeolite particles (like flashing particles with darker frame) on the cell membrane of viable Caco-2 cell was easily seen. In (b), zeolite particle (larger size, flashing one) seemed to be attached on the cell membrane. During the treatments some cells did not preserve their viability with respect to zeolite treatment. In figure 8.4 (d), place of the dead cells were represented. Dead cells/organelles were mostly removed from the surface however, accumulation of zeolites could be easily seen on the place of cell. The last sample (d), size of the zeolites were decreased with agate mortar and same treatment procedure was applied. Measured size of the zeolite particles on the surface of the cells were around 2-3  $\mu\text{m}$  for sample a,b,c and  $<2 \mu\text{m}$  for sample (d). Zeolites with very small particle size could be easily seen as dark dots around the cell. Additionally, in the same image, the larger particles can easily be seen as in contact with the cell membrane. However, size of the cells were also measured and they were around 10-20 $\mu\text{m}$ . Therefore those results suggest that zeolite particles were highly interacted with Caco-2 cells, however, their size was too large to be internalized.

### 8.2.1. Effect of Zeolite Treatment Time on Caco-2 Cell Growth

To determine effect of zeolite treatment time on cancer cells, cells were incubated with media that was treated with 75mg/ml of zeolite for 24, 48 and 72h. In Figure 8.5, cytotoxicity tests (XTT) results for were given using 75mg/ml zeolite.

Results of the cytotoxicity test showed that zeolite had a high cytotoxic effect against Caco-2 cells. Even in 1 day treatment, there was a considerable decrease in cell viability. Results showed that when incubation time was increased to 72h, growth of cancer cells decreased considerably. As it was shown in Figure 8.5 that values for cell growth % were 40,4 to 9,7 for one day treated media and 38,1 to 6 % for 3 days treated media.

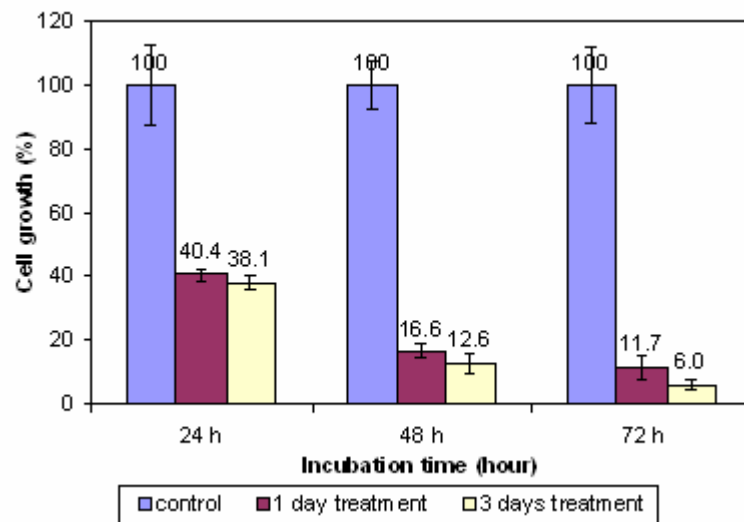


Figure 8.5. Effect of the medium pretreated with 75mg/ml zeolite on the growth of Caco-2 cell line.

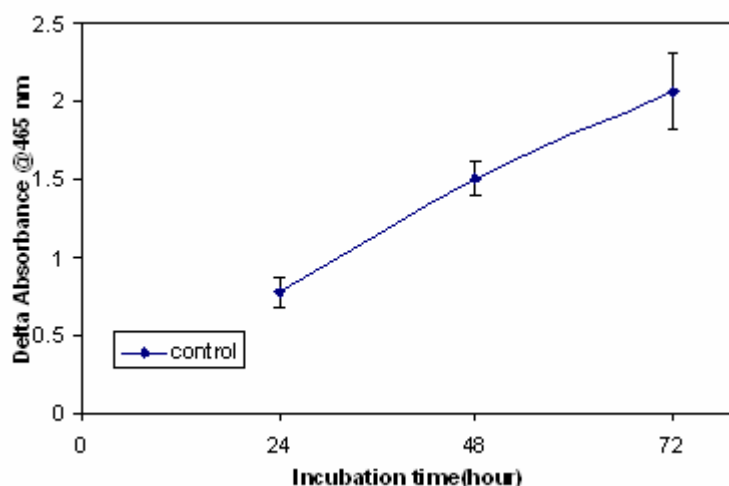


Figure 8.6. Change in absorbance values in XTT assay for the samples including non-treated (control) growth media.

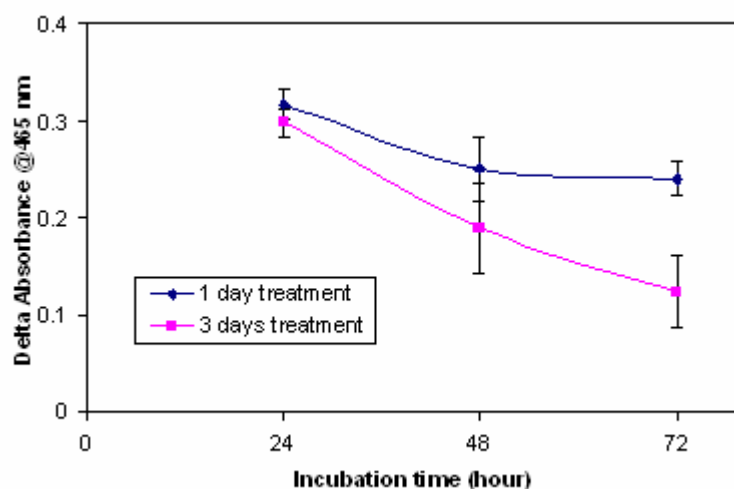


Figure 8.7. Change in absorbance values in XTT assay for the samples including 75mg/ml zeolite treated growth media.

To confirm the growth of untreated (control) cells and to compare with the treated ones, absorbance values which were proportional to cell growth, were given in Figure 8.6. and 8.7 for treated and non treated (control) samples respectively. In the Figure 8.7, there was an expected increase in number of cancer cells where higher absorbance values indicate higher cell viability and cell growth since their media were

not exposed any zeolite treatment. On the contrary, absorbance values were considerably decreased by time which corresponds to cell viability of Caco-2 cells grown in treated media (Figure 8.7). Moreover, effect of treatment time was easily observed where higher growth inhibitions were achieved as decrease in absorbance.

### **8.2.2. Effect of Zeolite Concentrations on Caco-2 Cell Growth**

As it was observed in previous results, during three days cell growth was highly effected by 75mg/ml zeolite treatments. Therefore it would be important to study with different and lower doses of zeolite and shorter time treatments to check if there still exists an inhibitory effect of zeolite on cell growth or not. By this varying concentrations, IC<sub>50</sub> value for zeolite could be determined (characteristic value for definition of the concentration of substance that provides 50% inhibition to certain reaction which is most commonly used to represent the inhibitory effect of an agent).

Therefore instead of 1 and 3 days treatment; treatment time was decreased and 18 h and 24 h treatments were used. Concentrations for zeolite treatments were 25; 50 and again 75mg/ml to check cell growth. Results were given in Figure 8.8.

It was found that IC<sub>50</sub> value for the 24h treatment was approximately 50mg/ml. Although lower doses of zeolite were used, there still exist (28,8%) considerable cell growth inhibition even in 25mg/ml zeolite for 18h where cell growth percentage was 72%. In literature Pavelic et al. (2001) studied the effect of zeolite on different cancer cell lines. They found that in lower concentrations (0.5 and 5 mg zeolite/ml), cell growth for Caco-2 cells inhibited approximately 10%. But when 50mg/ml was used, they obtained approximately 40% inhibition for cell growth which was confirmed with the results in Figure 8.8.

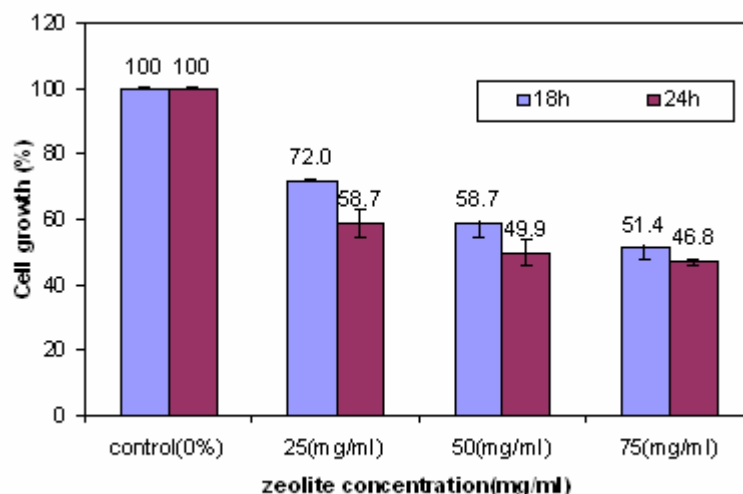


Figure 8.8. Change in cell growth (%) using 18h and 24h zeolite treated growth media.

### 8.3. Interactions of Zeolite with Cell Growth Media

Since zeolite treatments effect cell growth media, different analyzes were performed to investigate the interactions between the media and zeolite. Results for the detailed analyzes such as pH, conductivity measurement, elementary composition and FTIR analyzes of treated media were given below.

#### 8.3.1. Effect of Zeolite Treatment on pH and Conductivity of Cell Media

The pH of the normal cell media (DMEM) was about 7.4. It was clearly found that incubation of non-treated media at 37°C caused media to become alkaline. On the other hand, there was not a significant difference between pH values for the 18h and 24h incubations. On the other hand, when cell media was treated with zeolite, zeolite showed a neutralizing tendency and results suggested that increase was directly proportional with zeolite's concentration. In Table 8.1, results for pH and conductivity values for treatments for 18h and 24h with zeolite were given.



Table 8.1. pH and conductivity values of zeolite treated media.

	18h treatment				24h treatment			
<b>Concentrations of zeolite in media (mg/ml)</b>	control	25	50	75	control	25	50	75
<b>pH</b>	8.3	7.8	7.2	7.1	8.2	7.9	7.1	6.9
<b>conductivity(mV)</b>	94.3	85.2	47.7	43.3	91.6	92.5	42.8	36.1

Moreover, it was better to indicate that, when the zeolite concentrations were increased from 25 to 50 and 75 mg/ml, pH of the cell media varied between 6.9 and 7.1 for both 18h and 24h treatments. According to that result, 50mg/ml zeolite was enough to neutralize the media. The optimum growth conditions for Caco-2 cells were slightly basic and were at around pH 7.4. Decrease in cell viability may be due to reduced pH values because deviations from optimum conditions cause cells to be under stress. Reduction in pH with treatment of Z1 might be related to the responses of Caco-2 cells to the changes in the pH of the media. It was reported that the proton pumps in the cells do not rapidly reverse the effect on pH, and the buffering capacity of the cytoplasm was not strong enough to prevent the pH change (Liang et al., 2007). An increasing result for pH reduction compared to the control can therefore attain and sustain intracellular acidification, and thus might have caused reduction in cell proliferation

With respect to conductivity results, it was found that zeolite treatments caused decrease in conductivity values. The conductivity of solutions depends on the concentration of ions in solution, their ability to dissociate, their charges and their speed of diffusion. Decrease of conductivity in that treatments were parallel to decrease in pH of fluid.

To better investigate the long term effect of zeolite treatments on cell media, treated media samples were stored at +4°C for 21 days and samples were analyzed according to pH and conductivity at the end of storage. Results were given in Table 8.2.

Table 8.2. pH and conductivity values of zeolite treated media after storage at +4°C for 21 days.

	18h treatment			24h treatment		
<b>Concentrations of zeolite in media (mg/ml)</b>	25	50	75	25	50	75
<b>pH</b>	8.3	8.1	7.7	6.9	6.7	6.7
<b>conductivity(mV)</b>	107.2	94.7	72.8	26.3	17.4	15.3

Results in Table 8.2 showed that zeolite treatment displayed strong interactions during treatment periods for 18h and 24 hour. Thus, considerable changes in pH values were achieved. Similar case was also found for conductivity measurements. Conductivity values decreased with the decrease in pH values. In Table 8.1 results indicated that main difference in pH was due to the dose of zeolite but in Table 8.2, when samples were stored for three weeks, it was surprising to see that main difference between pH values were due to zeolite treatment periods. All pH values were turned in to alkaline for 18h treatments, on the contrary, they turned into acidic for 24h treatment.

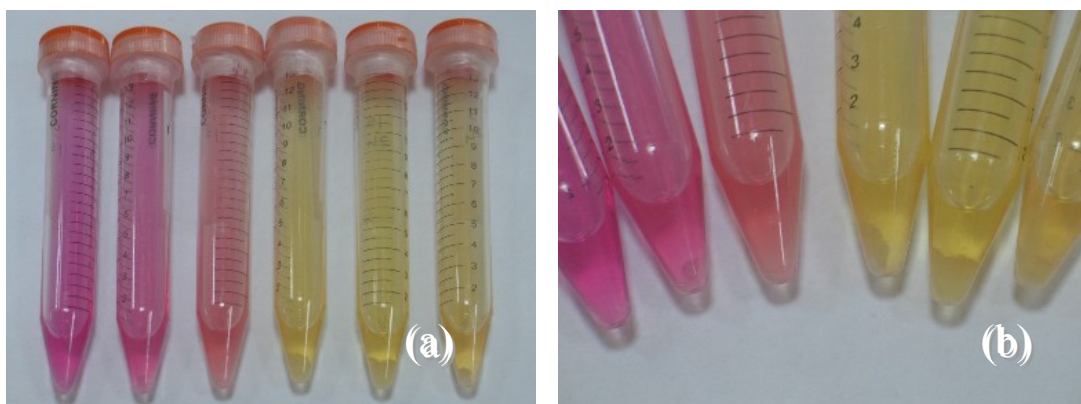


Figure 8.9. Color change in zeolite treated media after storage at +4°C for 21 days in the sample order of 25, 50, 75 (mg/ml) zeolite and 18h(pink)-24h(yellow) treatment respectively.(a): General overview, (b): precipitated proteins.

Results of pH measurements were also confirmed by the change in colors of the media. Original phenol red color which was sensitive to pH, turned into yellow in 24h treatments where all pH values were below pH 7. Therefore it was possible to say that interactions of zeolite and media treatments resulted in ongoing changes to media. Although zeolite itself was removed from the media with centrifugation its ongoing effect was more observable after a period of storage. It was clearly seen that the main affected ones were the proteins in media where they were precipitated at pH below 7 and those precipitates can be easily seen as white-like color compounds at the bottom of the falcon tubes (Figure 8.9-b).

### 8.3.2. Effect of Zeolite Treatment on Elementary Concentrations in Cell Culture Media

Even if cell was a cancer cell or healthy cell, change in ionic concentrations in cell media would alter the optimum growth conditions. Concentrations of some ions in cell growth media were essential and had a vital or immortal importance on cell growth. Therefore to obtain more information about effect of zeolite on culture media, elementary composition of culture media was investigated by ICP-MS. Media samples were treated 18h and 24h with different doses of zeolite where zeolite concentrations were 25; 50 and 75mg/ml. results were given in Table 8.3.

Media provided appropriate conditions for the cell growth due to its nature and ICP-MS results showed that it was reach in trace element compositions (control results). There were slight fluctuations in elements concentration by time. It was important to note that Zn, Cu, Pb, Ni Cd, Cr may show cytotoxic effects to the cells. Therefore investigation of the cytotoxicities of those elements was of importance.

Based on the results, a considerable increase was found in  $Zn^+$  element compared with control treatments in both 18 and 24 h treatments.  $Zn^+$  concentration decreased with increase in zeolite concentration. Another important result was found for  $Ca^{2+}$ . Increase in zeolite concentration caused an increase in  $Ca^{2+}$  concentrations in media for 18 h treatment. Additionally, for both 18 h to 24 h treatments; its concentration increased with an increase in treatment time and zeolite concentration. Besides, levels of Cu and Ag also showed slight increases with zeolite treatments. Since those elements Cu, Ag, Zn might show cytotoxicity, cytotoxicity tests were performed for MCF-7 human breast carcinoma cells using their salts ( $AgNO_3$ ,  $ZnCl_2$ ,  $CuCl_2$ ). Experiments were performed by treating cell growth media for 18h and 24h with those salts. Results for the IC-20-50 values were given in Table 8.4 and 5 for 18h and 24 h treatments, respectively.

Table 8.3. Analysis of zeolite treatments by ICP-MS.

Element	18h Treatment				24h Treatment		
	Zeolite Conc. in Media (mg/ml)						
	Control	25	50	75	25	50	75
Li	0.44	3.62	2.48	0.96	0.69	0.62	0.98
Cu	7.8	10.63	9.25	8.09	8.5	8.18	8.34
Ag	1.86	5.31	3.92	2.14	2.06	1.8	2.1
Cd	0.06	2.93	1.78	0.25	0.18	nd	0.25
Bi	0.22	3.57	2.31	0.49	0.44	0.2	0.45
Fe	nd	nd	nd	nd	nd	nd	nd
Ba	nd	3.12	1.75	0.08	0.28	nd	0.22
Pb	0.01	0.59	2.15	nd	nd	0.87	nd
Mg	23.88	31.99	28.84	24.16	26.07	27.49	28.33
Al	nd	nd	nd	nd	nd	nd	nd
K	263.8	256.9	256.3	246.4	240.5	268.1	259.2
Ca	nd	56.77	62.05	68.76	33.89	70.96	127.2
Cr	nd	2.46	1.14	nd	nd	nd	nd
Mn	nd	3.72	2.37	0.67	0.88	0.78	1.97
Ni	nd	2.62	1.29	nd	nd	nd	nd
Co	0.1	3.52	1.87	0.28	0.38	0.9	0.36
Zn	3.14	26.25	7.82	1.82	22.16	2.87	6.43

nd\* : not detected

Table 8.4. Results of cytotoxicity tests for MCF-7 cells treated 18 h with metal salts ( $\mu\text{M}$ ).

Metal	IC20	IC50	IC80
Ag <sup>+</sup>	2.53	4.53	8.02
Cu <sup>2+</sup>	70.65	84.99	101.07
Zn <sup>2+</sup>	10.96	15.91	22.78

Table 8.5. Results of cytotoxicity tests for MCF-7 cells treated 24 h with metal salts ( $\mu\text{M}$ ).

Metal	IC20	IC50	IC80
Ag <sup>+</sup>	1.58	3.20	6.23
Cu <sup>2+</sup>	39.30	58.24	84.97
Zn <sup>2+</sup>	1.00	5.33	21.40

Under the circumstances where there were slight increases in some elements having cytotoxic effects, it would be expected that, those change in elementary levels might have alter the growth of the cancer cells. But, despite high variations in pH with zeolite treatments, elementary composition changes were in minority level to reach high cytotoxicity levels obtained in Section 8.2.2.

It was important to note that as well as minor elementary concentration variations with the zeolite treatment, changes in the levels of Ca<sup>2+</sup> in the growth media

should be considered. Results showed that concentration of the calcium in the growth media increased with the treatment time and concentration. Decrease in cell proliferation might be due to the role of  $\text{Ca}^{2+}$  in the cell growth. Herbert et al. (2004) reported that colon had the capacity to respond to changes in extracellular  $\text{Ca}^{2+}$ .  $\text{Ca}^{2+}$  sensing receptor in colon epithelial cell modulates colonic fluid transport, cell proliferation, differentiation and development where this receptor was activated by  $\text{Ca}^{2+}$ . Those implications were also in good agreement with the reports of Stenhagen and Allen (2001) who reported the relation  $\text{Ca}^{2+}$  and growth inhibition. They suggested that of increase in  $\text{Ca}^{2+}$  levels in growth media caused inhibition of Caco-2 growth rates.

### **8.3.3. FTIR Results of Cell Culture Media Treated Zeolite**

Cell growth media was rich in aminoacids (ala, arg, leu, cys...etc.). To investigate any possible adsorption of the media components on zeolite during treatment, FTIR spectra of the zeolite samples were determined. Results were given in Figure 8.10 below.

FTIR spectra of samples showed that components in culture growth media were not adsorbed on zeolite. There were no additional peaks observed other than characteristic zeolite peaks. It was possible to conclude that zeolite could not interact with growth components in adsorptive way thus allowing all components available for cancer cell growth. Reason behind the inhibition of cancer cell proliferation with zeolite treatment might not be due to such kind of strong interactions like chemical bonding. However, it was important to note that some weak interactions such as van-der Waals, hydrogen bonding, electrostatic interactions between some protein like structures in media (ie. aminoacids, or ie. growth hormones secreted by the cells) which requires further detailed experiments in molecular level. Similar case was suggested by Pavelic et al. (2001) that decrease in the viability of cancer cells and increase in the apoptosis of the tumor cells with the zeolite treatment might be due to adsorption of some serum components such as EGF to clinoptilolite.

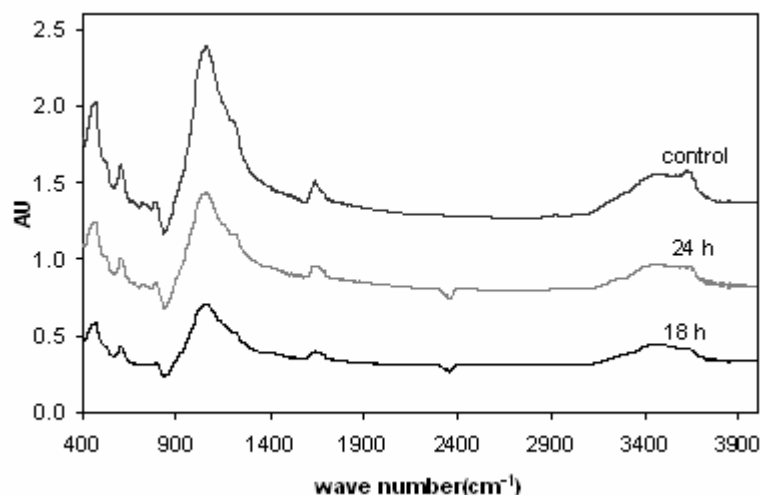


Figure 8.10. FTIR spectra of cell growth media treated with zeolite: 18h treated; 24h treated; untreated (control).

#### 8.4. Effect of Zeolite on GUS Activities of Caco-2 and MCF-7 Cancer Cells

$\beta$ -Glucuronidase is found in cancer cells and some types of cancer cells have high levels of  $\beta$ -glucuronidase activity. In some cases, glucuronide containing drugs (prodrugs; such as doxorubicin) were potentially used as a selective anti-cancer drug in cancer cells having high levels of GUS activity (Ünak et al., 1997). This enzyme is able to deglucuronidate a variety of glucuronide derivatives on the cell membrane, thus those compounds gain toxicity in situ. Therefore it was important to investigate effect of zeolite incubation on cancer cells GUS activity. Changes in the levels of enzyme activity with zeolite treatment might be a novel application for the zeolite in cancer treatment. Thus, in this Section, effect of zeolite treatment on GUS activity in Caco-2 (adenocarcinoma) Cancer cells was investigated. As Caco-2 cells are as enterocytes (absorbative cells) and epithelial cell, to compare the effect of treatment, a new cancer cell line: MCF-7 (human breast cancer cells) was introduced to the experiments. MCF-7 was reported to be a standard cell line model (Latorre-Esteves et al., 2009) in various cancer cell studies due to its high proliferation rate (especially compared to Caco-2).

Most of the cancer cells are able to produce  $\beta$ -glucuronidase. To investigate their GUS production in presence of zeolite cell viability should be checked whether their viability was affected by zeolite treatment or not. As the active cells have capability to produce enzyme, Caco-2 and MCF-7 cells viability should be preserved in experiments,

thus GUS activity can be measured. Zeolite concentration and treatment time was found as 25mg/ml and 60 min, respectively, in order to achieve high viability (>90%). Viability tests results were given below in Figure 8.11 and at Table 8.6 below.

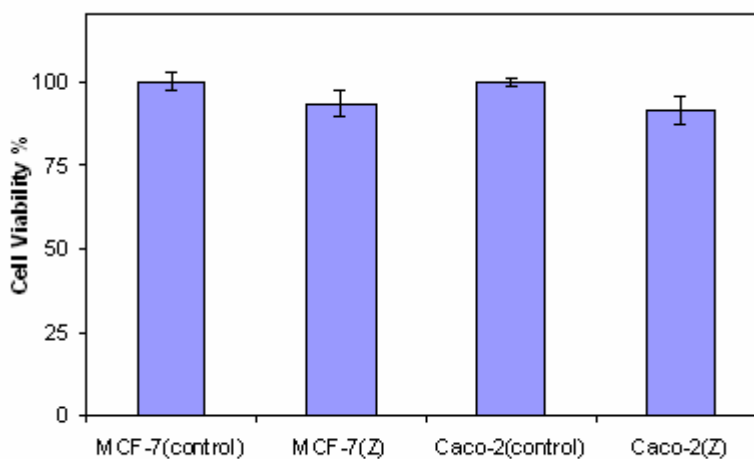


Figure 8.11. Viability histograms of two types of cancer cell lines after zeolite treatment (Z: 25 mg/ml zeolite treated; 60 min).

Results showed that desired viability value with zeolite treatment was achieved in order to analyze GUS activity in treated cells for further analyses. It was found that for that conditions of treatments, resistance of cells to zeolite were approximately same.

Table 8.6. Percentage viability of two types of cancer cell lines after zeolite treatment (Z),

	<b>MCF-7(control)</b>	<b>MCF-7(Z)</b>	<b>Caco-2(control)</b>	<b>Caco-2(Z)</b>
Cell Viability (%)	100.0±2.8	93.3±3.7	100.0±1.1	91.5±4.4

It was possible to investigate the GUS production capabilities of two types of cancer cell lines. It was found that produced GUS activity was considerable high in Caco-2 cell compared to the MCF-7 cells (Table 8.7).

Despite the low cell numbers achieved for Caco-2 cells ( $\sim 8 \times 10^4$  cell/ml for Caco-2 and  $5 \times 10^6$  cell/ml for MCF-7) ; produced GUS activity per protein was almost 4 times higher compared to MCF-7 cells.

Table 8.7. Comparison of GUS activities for two cancer cell lines.

	Cell Line	
	MCF-7	Caco-2
RFU	405.8	379.8
$\mu\text{g}$ protein (total protein of cell lysates)	908.4	29.2
RFU/ $\mu\text{g}$ protein	0.447 <sup>b</sup>	1.798 <sup>a</sup>
Ratio of GUS production ( <sup>a/b</sup> )	4.03	

To investigate the affect of zeolite treatment on GUS production in cancer cell lines, GUS activities were immediately measured after cell disruption. Results (Figure 8.12 and Table 8.8) of GUS activity were given per  $\mu\text{g}$  total protein analyzed for each cell lysates.

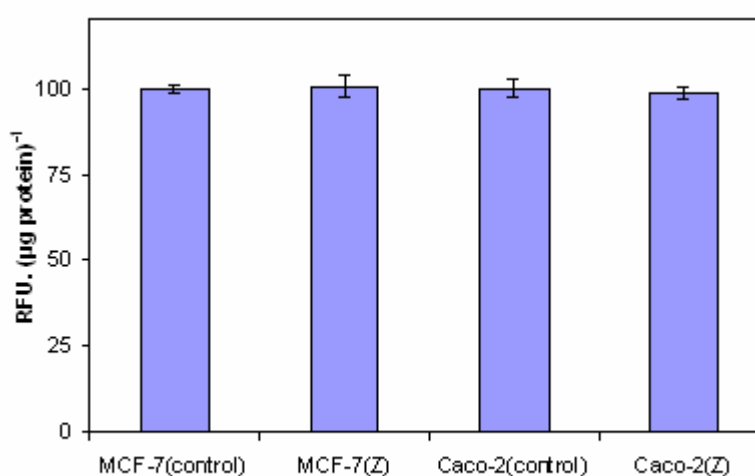


Figure 8.12. GUS activity histograms of cancer cells in terms of relative fluorescence unit (RFU) per  $\mu\text{g}$  total protein of cell lysates (Z: 25 mg/ml zeolite treated; 60 min).

Results of GUS activity implied that zeolite treatment could not alter the GUS activity in each cell. Compared to control samples, percentage of enzyme activity remained almost the same. Therefore, zeolite treatment was at a non-effective a level for preserving cell viability and resulting same GUS producing activity. Considering GUS enzyme properties (deconjugation of some toxic compounds) and considering high levels of GUS production was an important characteristic indicator in cancer cell lines, it would be suggested that to find a non-altered GUS activity or production at cellular level might be better for the experimental results. On the contrary, increased activity might be important for cancer treatments where in the future, zeolite might be supposed to be used as a pro-drug carrier in prodrug therapy for glucuronide conjugates.



Table 8.8. GUS activity of cancer cells in terms of relative fluorescence unit (RFU) per  $\mu\text{g}$  total protein of cell lysates (Z:zeolite treated).

	MCF-7 (control)	MCF-7(Z)	Caco-2 (control)	Caco-2(Z)
RFUx( $\mu\text{g protein}^{-1}$ )	100.0 $\pm$ 1.0	100.6 $\pm$ 3.1	100.0 $\pm$ 2.8	98.8 $\pm$ 1.8

## 8.5. Effect of Digested and Undigested Zeolite Samples on Cancer Cell Lines

In simulated digestion experiment, results indicated that there were not significant structural differences when two zeolites in different purity were compared. Moreover, similar results were obtained for their control (untreated) samples. As it was reported in Section 8.2 that zeolite had an important cytotoxic effect on Caco-2 cell proliferation, it was important to investigate the cytotoxic properties of digested and undigested zeolite samples with different purities on two cancer cell line: Caco-2 and MCF-7.

### 8.5.1. Changes in pH, Conductivity Values and Color of Cancer Cell Culture Media

As it was discussed in Section 8.3.1, pH of the normal cell media was about 7.4. Results showed that incubation of non-treated media at 37°C caused media to become alkaline and when cell media was treated with zeolite, zeolite showed a neutralizing tendency with the increase in its concentration. When the concentrations of zeolite were increased from 25 to 50 and 75 mg/ml, pH of the cell media varied between 6.8 and 7.9 for both of both digested and non-digested zeolite treatments (Table 8.9 and 8.10).

Despite some minor variations regarding the Z2 sample, results were in good agreement with the results given Section 8.3.1. It was observed that after treatment with second zeolite sample (Z2), pH values of growth media were a little higher than the sample Z1 at same doses of zeolite. But there was not a considerable difference between digested and non-digested samples.

Table 8.9. pH and conductivity changes in cancer cell growth media treated (24h) with digested (Z1D) and non-digested (Z1)zeolite samples with different doses (control: no zeolite).

<b>Zeolite concentrations (mg/ml)</b>	<b>Control</b>	<b>Z1</b>			<b>Z1D</b>		
		25	50	75	25	50	75
<b>pH</b>	8.2	7.9	7.2	7	7.9	6.9	6.8
<b>Conductivity (-mV)</b>	90.1	93	45	41	90	28	25

Table 8.10. pH and conductivity changes in cancer cell growth media treated (24h) with digested (Z2D)and non-digested zeolite (Z2) samples with different doses (control: no zeolite).

<b>Zeolite concentrations (mg/ml)</b>	<b>Control</b>	<b>Z2</b>			<b>Z2D</b>		
		25	50	75	25	50	75
<b>pH</b>	8.2	8.0	8.0	7.8	8.0	7.9	6.9
<b>Conductivity (-mV)</b>	90.1	97	94	88	97	94	35

The optimum growth conditions for cells were slightly basic and were at around pH 7.4. After zeolite treatments, reduction in cell proliferation observed cytotoxicity test may be due to reduced pH values because deviations from optimum conditions cause cells to be under stress.

Results indicated that zeolite treatments caused decrease in conductivity values in all zeolite samples. Conductivity values for digested samples were almost same as non-digested samples and results implied that decrease of conductivity in that treatments were parallel to decrease in pH of the fluid.

Changes in pH of the samples were also parallel by the change in colors of the media (Figure 8.13). As phenol red was a pH indicator in media, original phenol red color turned into yellow in 24h treatments were the all pH values reduced below ph7.



Figure 8.13. Color of cancer cell growth media treated with digested and non-digested zeolite samples with different doses. Left to right: each 3 tubes grouped as : a, b, c, d and they were Z1, Z1D, Z2, Z2D respectively and their concentrations in each group were (left to right) 25-50 and 75 mg/ml zeolite, last sample is untreated one as control sample.

### **8.5.2. Cytotoxicity Tests for Caco-2 Cells Using Digested and Non-digested Zeolite Samples with Different Doses**

Effect of two different zeolite samples and their simulated digested and non-digested forms were compared according to their affects on Caco-2 cell proliferation. Results were given in Figures 8.14-17. It was observed that undigested sample of Z1 inhibited cell proliferation more than the digested Z1-D sample at all doses of zeolite (Figure 8.14 and 8.17).

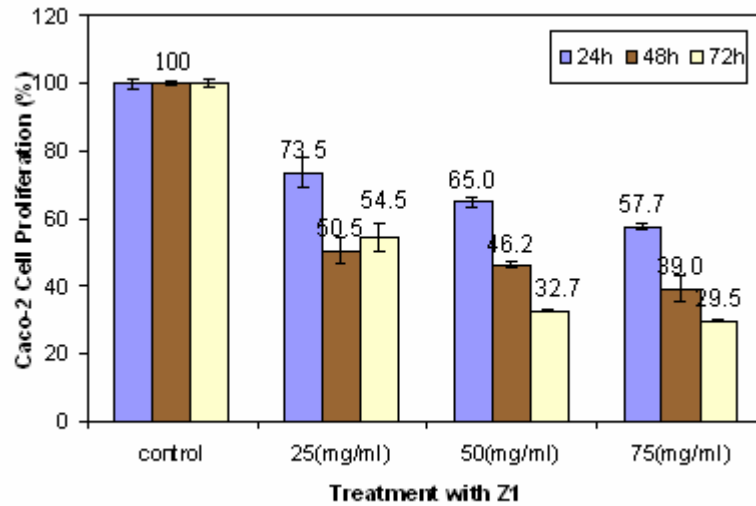


Figure 8.14. Cell proliferation % for Caco-2 cell treated with Zeolite 1

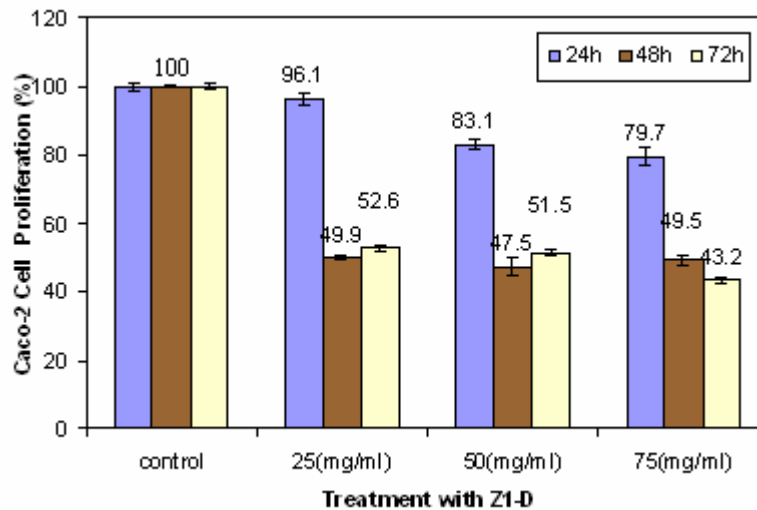


Figure 8.15. Cell proliferation % for Caco-2 cell treated with digested Zeolite 1

When the sample Z2 compared with its digested form (Figure 8.16 and 8.17), cell proliferation inhibition was more stable and showed almost same inhibition at both forms at different zeolite concentrations. This might be due to its structural homogeneity which resulted from its higher purity compared to Z1 sample (67 and 87% for Z1 and Z2, respectively).

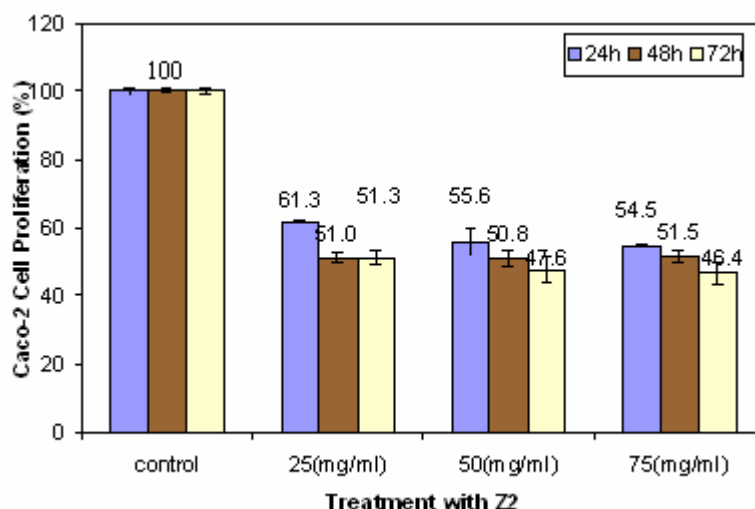


Figure 8.16. Cell proliferation % for Caco-2 cell treated with Zeolite 2

When the Z1 and Z2 samples were compared; Z2 samples (high purity) performed nearly same inhibition in cancer cell proliferation except zeolite concentration of 25mg/ml. At that dose, inhibition of Z1 sample was more effective compared to Z2 sample in both digested and undigested samples.

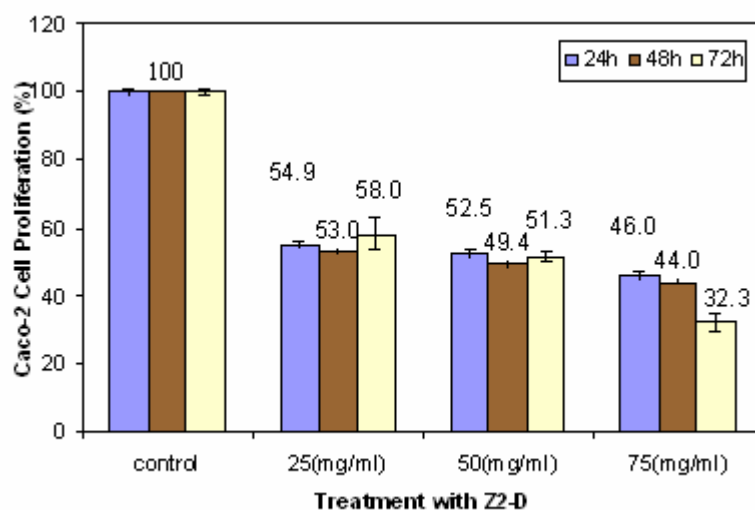


Figure 8.17. Cell proliferation % for Caco-2 cell treated with digested Zeolite 2

### 8.5.3. Cytotoxicity Tests for MCF-7 Cells Using Digested and Non-digested Zeolite Samples with Different Doses

Effect of two different zeolite samples and their simulated digested and non-digested forms were compared according to their effects on MCF-7 cells which have

high proliferation rate compared to Caco-2 cells. Results were given in Figures 8.18-21. For the sample Z1 it was observed that non-digested sample of Z1 performed slightly higher inhibition in cell proliferation compared to its digested form (Fig. 8.18-8.19).

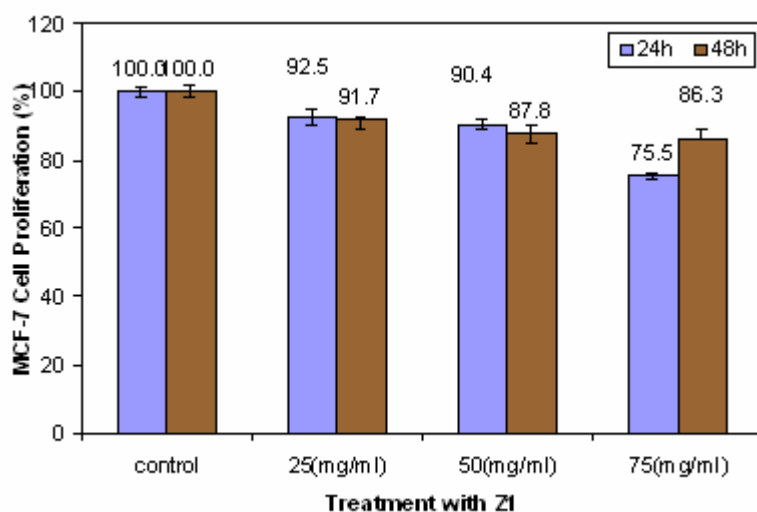


Figure 8.18. Cell proliferation % for MCF-7 cell treated with Zeolite

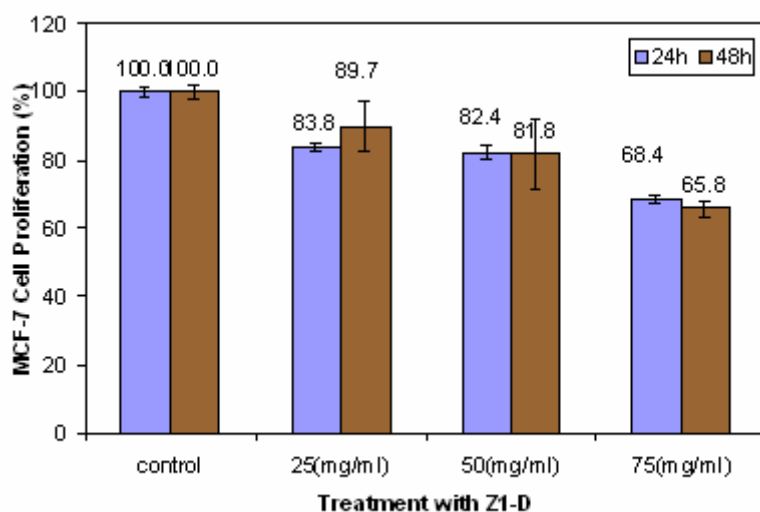


Figure 8.19. Cell proliferation % for MCF-7 cell treated with digested Zeolite 1

For the sample Z2, similar results were found as Caco-2 cells presented previously where non-digested form (see Figures 8.14 and 8.15), and digested form of sample showed almost same cell proliferation inhibition at different zeolite concentrations. This might be due to its structural homogeneity which resulted from its purity.

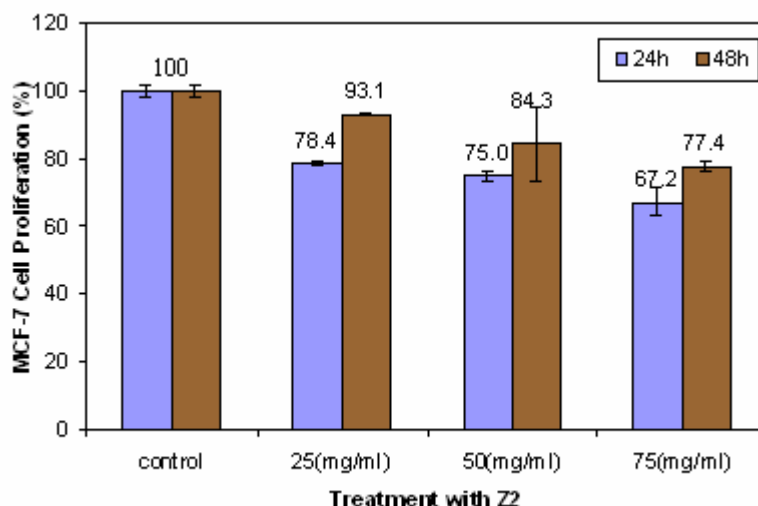


Figure 8.20. Cell proliferation % for MCF-7 cell treated with Zeolite 2

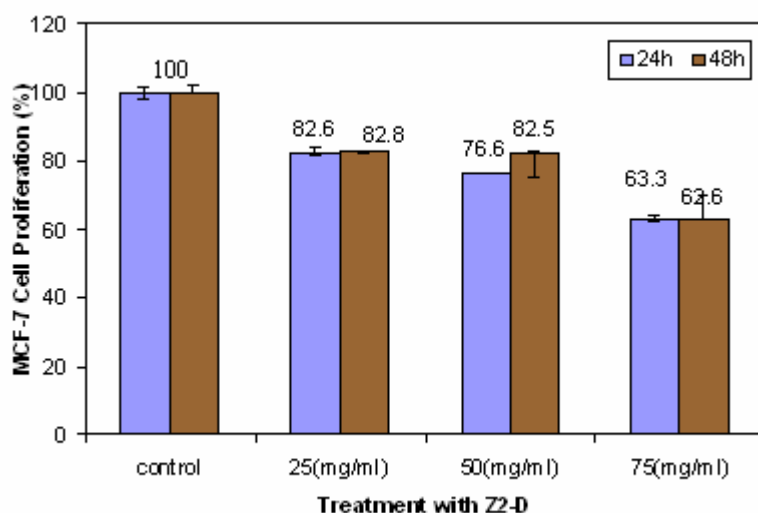


Figure 8.21. Cell proliferation % for MCF-7 cell treated with digested Zeolite 2

But it was interesting to note that time of incubations for the cells (24h and 48h) was not so effective in cell proliferation of MCF-7 cells. Results showed that inhibitions were almost same which might be due to structural differences in both cells. Caco-2 cells are more sensitive. The reason behind this might first of all be their lower proliferation rate compared to MCF-7. Second possible reason behind the high cytotoxic effect of zeolite against Caco-2 might be their structural differences compared to MCF-7 cells. Different than MCF-7, they account for majority of the absorption in the small intestine since they are enterocytes (absorbative cells) which are most abundant cells (80-90% of the total number of epithelial cells) (Shah et al., 2006). Therefore they are highly sensitive to the changes in their microenvironment. Because of this, Caco-2

cell monolayers have been widely accepted as a potent in vitro model membrane for the rapid screening of the intestinal drug absorption. Although Caco-2 cells are originated from the human colon carcinoma, they have characteristics of absorptive intestinal cells during culture, such as microvillous structure, hydrolysis enzymes and carrier mediated transport systems for sugars, amino acids and several drugs (Yamashita et al., 2000). Results implied that zeolite might be more effective at early periods of MCF-7 cell proliferation but those cells might have gathered strength due to their nature and due to their resistance to stimulants around growth media. Therefore, since Caco-2 cells were more sensitive to absorption of compounds in media, they might be more stressed with the presence of zeolite and showed lower percentages of cell proliferation with respect to zeolite treatments.

## **8.6. Cell Cycle Analysis and Apoptosis Results**

Quantitative analysis of stages in the cell cycle was performed since zeolite could modulate the cell cycle of model cancer cell line: MCF-7. MCF-7 was chosen due to its high proliferation rate. Thus possible effects of zeolite treatments were investigated. In normal apoptosis for a cell, DNA was fragmented into small fragments (base pairs). This situation should be reflected to the results of cell cycle analyses. If apoptosis was detected, DNA fragmentation should be observed in cell cycle analyses.

Results for cell cycle analyses were given in Table 8.11. Overall results indicated that mitosis of the cancer cells were not restrained by zeolite treatment. If the mitosis was restrained by the zeolite treatments, it was possible to observe a very low intensity peak for G<sub>2</sub>/M phase. However no additional peaks were observed before G<sub>0</sub>/G<sub>1</sub> phase in all samples which indicated less DNA content as fragmented DNA. Representative plots of the trials were given below (Figure 7.22-24). When two different zeolites were compared according to their population distribution for AnG<sub>2</sub> (aneuploid cells in G<sub>2</sub> phase), it was found that there were no considerable difference in percentages, also no significant difference with control sample possibly indicating treatment was not so effective in DNA level/mitosis (See Appendix C, for all cell cycle results).



Table 8.11. Summary of cell cycle analyses results for zeolite treated MCF-7 cells

Sample	AnG1 %	AnG2 %
Z1 treated	29.16	31.83
Z2 treated	24.90	25.96
Untreated (control)	19.99	25.42

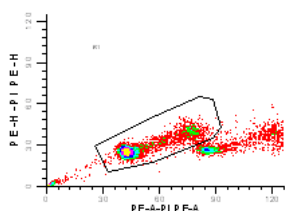
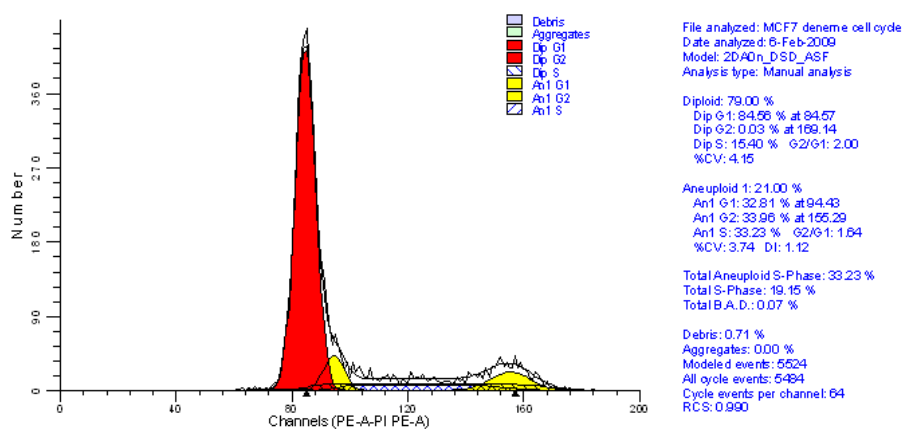
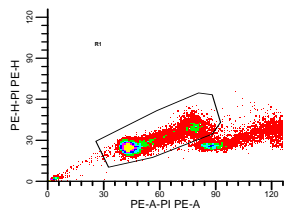
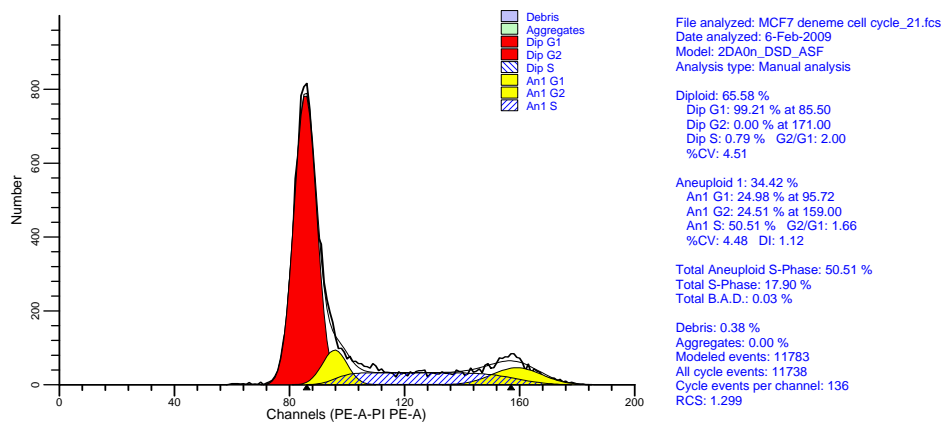
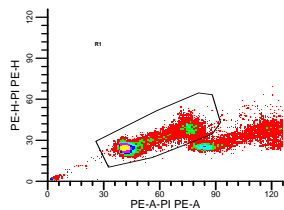
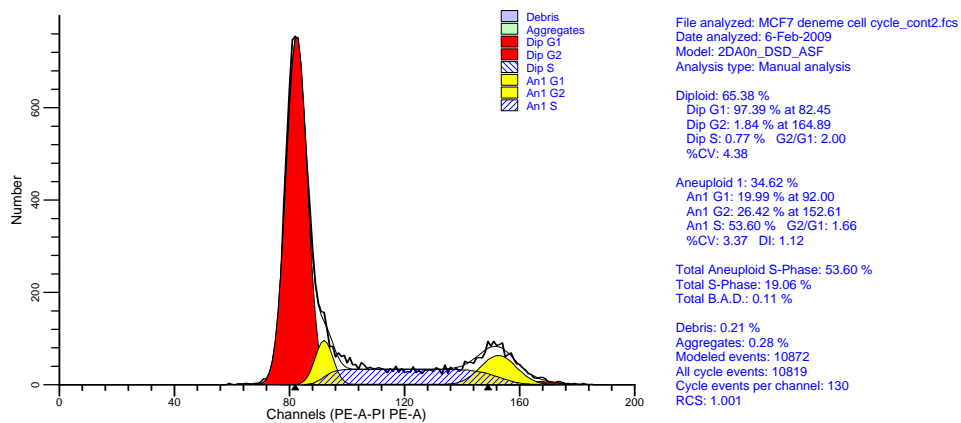


Figure 8.22. A Representative plot of cell cycle analyses results for MCF-7 cells treated with Z1.



ModFitLT V3.0(Win32)

Figure 8.23. A Representative plot of cell cycle analyses results for MCF-7 cells treated with Z2.



ModFitLT V3.0(Win32)

Figure 8.24. A representative plot for cell cycle analyses results for MCF-7 cells untreated(control).

Flow-cytometric apoptosis measurements were also performed for MCF-7 and Caco-2 cells to investigate the apoptotic effect of two different zeolites. Distribution of the cells for each population (Q3 living cells; Q4 early apoptotic; Q2 late apoptotic and Q1 necrotic cells) were given in representative plots in Figure 8.25 (see Appendix C2 and C3 for all dot plots for MCF-7 and Caco-2, respectively) and population histograms were given in Figure 8.26.

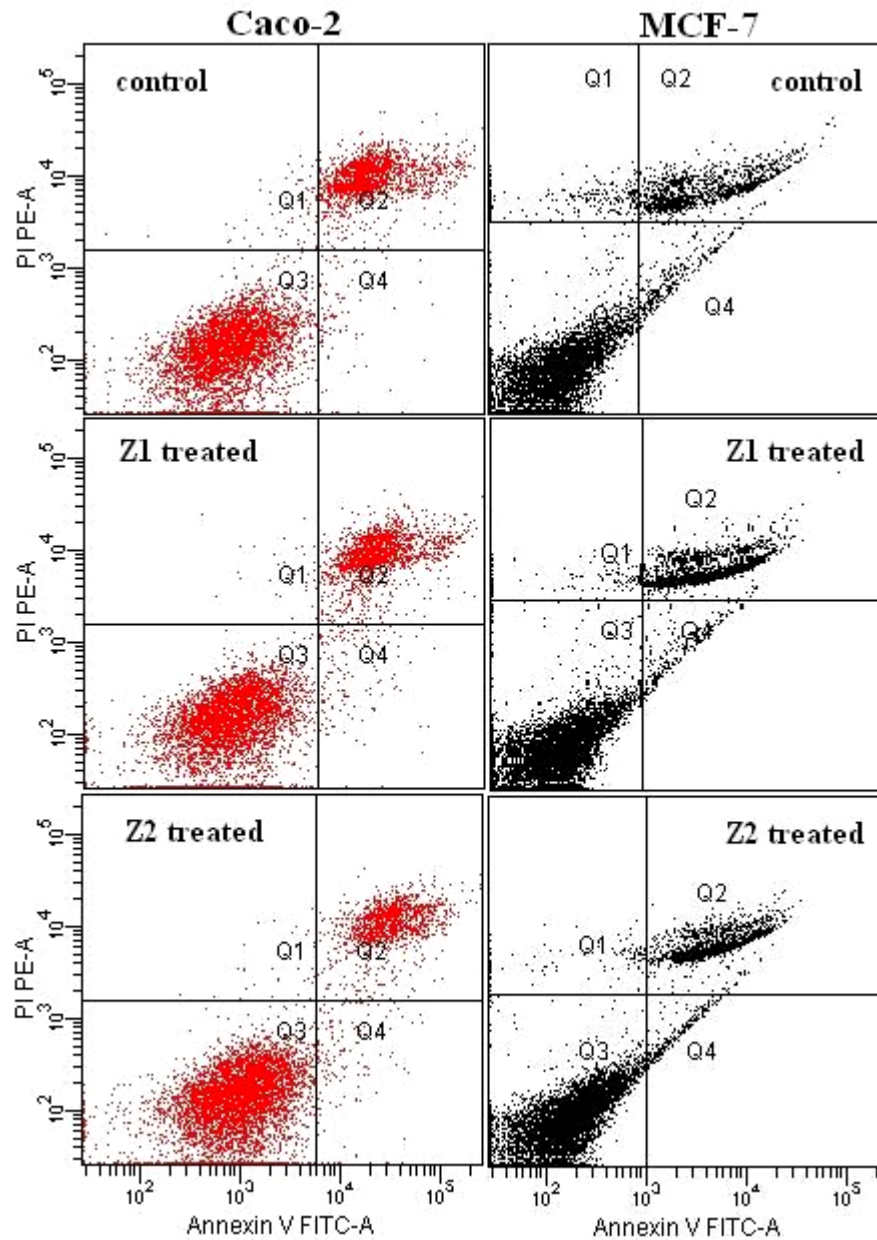


Figure 8.25. Representative dot plots for the apoptosis analyzes for Caco-2 and MCF-7 cells using Z1 and Z2.

The number of cells in the different cell populations were counted and then divided by the total number of cells analyzed; i.e. percentage of cells in each population was presented in Table 8.12.

Table 8.12. Summary of apoptosis results in percentages of populations

Sample	P1%	Q2%	Q4%
<b>MCF-7 Cells</b>			
Z1 treated	20.5	18.3	2.2
Z2 treated	18.6	16.3	2.3
Untreated (control)	15.8	13.0	2.8
<b>Caco-2 Cells</b>			
Z1 treated	57.8	24.1	3.2
Z2 treated	61	21.7	2.3
Untreated (control)	60.5	26.4	1.6

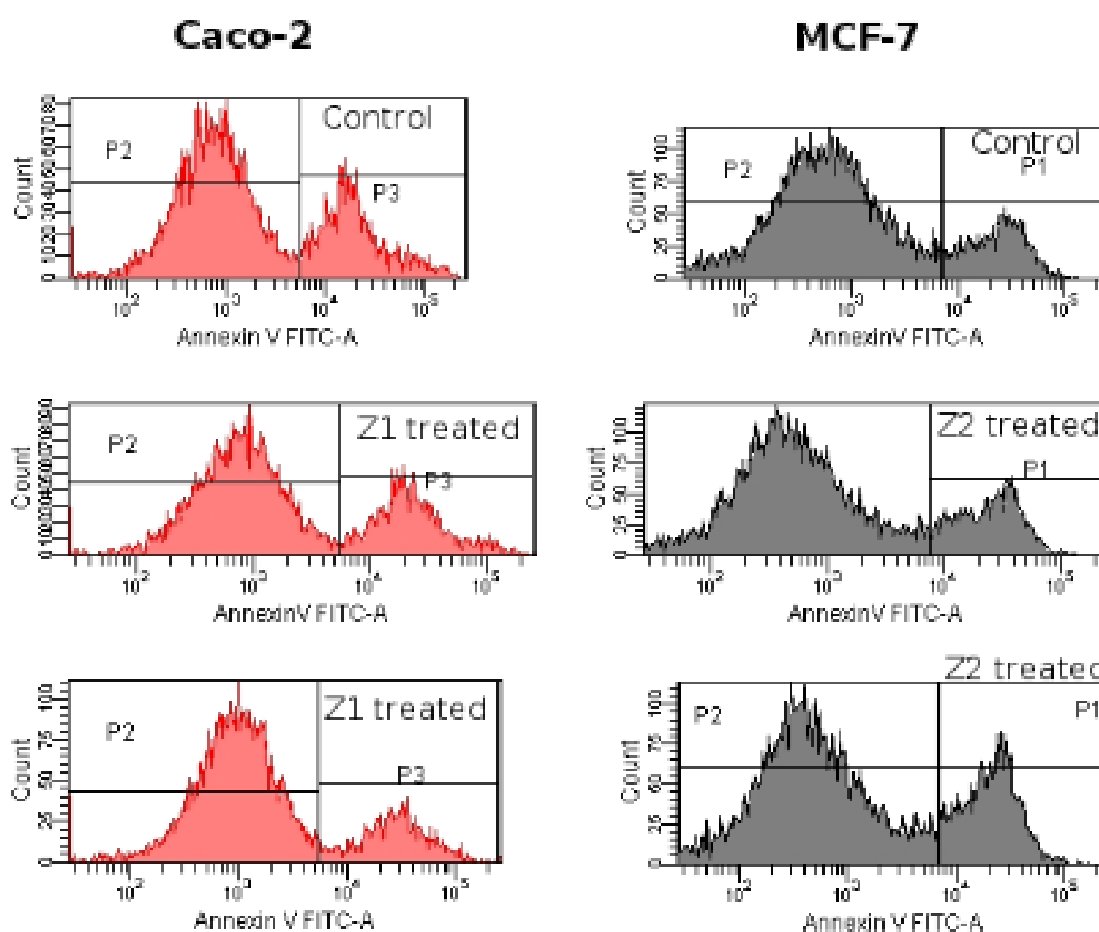


Figure 8.26. Representative population histograms for the apoptosis analyzes for Caco-2 and MCF-7 cells using Z1 and Z2

Apoptosis results were found to be parallel with cell cycle analyses. Results indicated that population of early apoptotic cells were very low (Q4%) and nearly same in both zeolite 1 and 2 treatments and at around 2-3 % for both cells. Considering the MCF-7 cells, when zeolite 1 and 2 were compared there was a slight reduction in P1 population indicating total of early apoptotic and late apoptotic cells were increased

after zeolite treatments. However, higher reductions in percentages of P1 population were found for Caco-2 cells after zeolite treatments considering the early and late apoptotic cells. Similar case was obtained for Q2 population in both zeolites and cells. Control cells % (P1) of MCF-7 and Caco-2 cells was around 16 and 60% and they were close to zeolite 1 and 2 treated populations. Therefore overall results indicated that treatment with both zeolites at the dose of 50 mg/ml did not show an important apoptotic effect on MCF-7 and Caco-2 cells.

## CHAPTER 9

### CONCLUSION

It is important to understand the basic mechanisms in intestinal system to evaluate beneficial effects of different therapeutic compounds. These therapeutic compounds may change the activity of exogenous carcinogens through stimulating intestinal conditions and modulating metabolic activation and/or detoxification.

The use of natural zeolites in different pharmaceutical forms for the treatment of several pathologies in animals and humans has received considerable attention in recent years. In this study, clinoptilolite rich mineral-natural zeolite was proposed to be a potential inhibitor/adsorbent material against bacterial  $\beta$ -glucuronidase (GUS) enzyme. Bacterial GUS enzyme was responsible for hydrolysis of glucuronides and production of number of carcinogens in the intestine by bacterial activities. Therefore in this study, inhibitory and adsorptive potential of local clinoptilolite rich mineral against *E.coli* GUS was investigated and interactions of zeolites with colon cancer (Caco-2) cells were determined. Besides, inhibitory potential of casein which is an antioxidant nutritive compound, was investigated as an alternative inhibitor towards GUS. Based on the experimental results, concluding remarks of this study are given below:

1. Results of the simulated digestion and characterization studies showed that there were no significant differences in zeolites structures during digestion. Additionally, no significant interactions between digestive enzymes and zeolite were observed.

2. Enzyme inhibition results showed that both zeolite and casein had inhibitory activity towards GUS enzyme. Inhibitory potential of 25 mg/ml zeolite was found to be 35% and for 0.125 mg/ml casein, it was found to be 15 %. Kinetic results indicated that they both acted as mixed type inhibitor where zeolite had superiority in inhibition compared to casein. Thus, proposed positive role of zeolite in health could be based on its inhibitory role on microbial  $\beta$ -glucuronidase (GUS) enzyme activity where this enzyme has a role in carcinogen formation in intestinal system.

3. It was important to find that GUS enzyme was adsorbed by zeolite. Additionally, in inhibition studies where casein and zeolite inhibitors were used together, it was found that casein was also adsorbed by zeolite. Therefore to have an

idea about interactions and dominant controlling mechanism in adsorption equilibrium studies and kinetic modeling were performed. Results showed that removal percentage of proteins was depended on their initial concentration in solution and removal was found to be in the range of 9.4-54.4% and 36.5-77.3% for GUS and casein, respectively. Activation energies and enthalpy changes for GUS were found as -34.1 and -46,9 kJ/mol where for casein adsorption they were around -6.5 and -8.9 kJ/mol, respectively. Thus various kinetic experiments and thermodynamic studies revealed that interactions between zeolite and the two proteins were exothermic and adsorption was physical adsorption. Since casein was an antioxidant and nutritive compound, adsorption phenomena for casein should also be considered carefully. Contact of this antioxidant molecule with other molecules (molecules such as having oxidation capacity) could be restricted with adsorption. But on the other hand, as zeolite increases transit time in digestive system, bioavailability of those adsorbed dietary compounds could also be increased by adsorption. Those considerations should be investigated in further analyzes to have an idea about interaction of zeolite intake with other nutrients in diet and with their bioavailability.

4. In recent studies, zeolite was used in protein refolding (Chiku et al., 2006), therefore zeolite might have caused conformational changes in casein structure where it was highly interacted with casein and acted as an adsorbent. Casein has a micellar structure and its conformation was highly effected with pH, temperature and ionic strength. As fluorescence spectrum of protein was sensitive to the microenvironment, fluorescence spectrum data were collected with respect to Trp residues where they were mainly located in a primarily hydrophobic portion of casein molecules, and could provide important information about the self-assembly of the casein molecules (Guo, 2008). But no considerable fluorescence spectrum shifts was observed during incubation of casein with zeolite.

5. Results for antioxidant analyzes showed that zeolite have high antioxidant activity, even in lower concentrations. For 1g/100ml zeolite, radical inhibition was 30 % and when dose was increased to 5 g/100ml; inhibition capacity was more than 50 %. Thus another health promoting role against carcinogen formation of zeolite could be based on its high antioxidant capacity where it will protect the cells against free radical damage.

6. It was found that zeolite had important affects on cancer cell growth. When the cytotoxicity tests were performed it was found that zeolite inhibited cell



proliferation for different cancer cell lines. Especially Caco-2 cells (human colon adenocarcinoma cells) were important in this study because digested zeolite had chance to directly interact with that cells in situ. Microscopic observations revealed that zeolite particles were not internalized by the cancer cells. However, they tend to accumulate around the cell membrane implying interactions with cell membrane and zeolite particles. Interaction of the zeolite with the media was important for the cancer cell proliferation rate. Results showed that zeolite inhibited approximately 50% of cell proliferation for 25mg/ml zeolite after 48h of caco-2 cells. This high inhibition was not observed for MCF-7 cells where proliferation was around 70-80%. Proliferation inhibition percentages didn't change considerably with zeolite type and their digested or non-digested forms. Results implied that changes in the pH and in some element composition of the culture media (ie.,  $\text{Ca}^{2+}$ ,  $\text{Zn}^{2+}$ ) with zeolite treatment might trigger the changes in the cell proliferation rates. Besides, to understand possible affects at DNA level with zeolite treatment, flow cytometric analyses for apoptosis and cell cycle measurements were performed. Apoptosis results showed that early apoptosis percentages for both Caco-2 and MCF-7 cells were low (around 2-3%) and total apoptosis percentage in overall population was also low compared to control sample. This result was confirmed by cell cycle analyses.

In conclusion, it was found that natural clinoptilolite rich mineral-natural zeolite has potential to inhibit and adsorb GUS enzyme and it preserved its structural stability during simulated digestion. Both inhibitors (zeolite and casein) had high antioxidant activity which was important against free radical damage and zeolite showed cytotoxicity against cancer cells. Those are all important findings to understand the therapeutic role of zeolite and its health promoting effects.

It was important to note that experiments given in this study were in vitro experiments therefore for the future, experiments using different animal models will be beneficial to predict if there are any side effects or not. As it was mentioned previously, investigation of the interactions of zeolite with other nutritive compounds would also be useful to decide further uses of the natural zeolites.

In the future, our natural source “zeolites” with their rich mineral content, structural stability and with their antioxidant and cytotoxic activity may be used for some health treatments based on their inhibitory effect on GUS enzyme which is a cancer risk biomarker. Also casein, as a good nutrient with blood pressure regulating, immune-modulatory and antioxidant role in body, can be an alternative inhibitor.

## REFERENCES

- Adrouny, A. R. (2002). *Understanding Colon Cancer*. U.S: University Press of Mississippi.
- Agarry, S. E., Audu, T. O. K. & Solomon, B. O. (2009). Substrate inhibition kinetics of phenol degradation by *Pseudomonas fluorescens* from steady state and wash-out data. *International Journal of Environmental Science and Technology*, 6 (3), 443-450.
- Akdeniz, Y. (1999). *Cation exchange in zeolites structure modification by using a microwave*. (Master dissertation, Izmir Institute of Technology, 1999).
- Akdeniz, Y. (2009). *Effect of microwaves on ionexchange in zeolites*. (Doctoral dissertation, Izmir Institute of Technology, 2009).
- Akkaya, G., Özer, A. (2005). Biosorption of Acid Red 274 (AR 274) on *Dicranella varia*: Determination of equilibrium and kinetic model parameters. *Process Biochemistry*, 40, 3559–3568.
- Al-Degs, Y. S., El-Barghouti, M. I., El-Sheikh, A. H. & Walker, G. M. (2008). Effect of solution pH, ionic strength, and temperature on adsorption behaviour of reactive dyes on activated carbon. *Dyes and Pigments*, 77, 16-23.
- Al-Ghouti, M., Khraisheh, M. A. M., Ahmad, M. N. M. & Allen, S. (2009). Adsorption behaviour of methylene blue onto Jordanian diatomite: A kinetic study. *Journal of Hazardous Materials*, 165, 589–598.
- Al-Ghouti, M., Khraisheh, M. A. M., Ahmad, M. N. M. & Allen, S. (2005). Thermodynamic behaviour and the effect of temperature on the removal of dyes from aqueous solution using modified diatomite: A kinetic study. *Journal of Colloid and Interface Science*, 28, 6–13.
- Arcoya, A., Gonzalez, J. A., Travieso, N. & Seoane, X. L. (1994). Physicochemical and catalytic properties of a modified natural clinoptilolite. *Clay Minerals*, 29, 123-131.

- Almajano, M. P., Delgado, M. E. & Gordon M. H. (2007). Changes in the antioxidant properties of protein solutions in the presence of epigallocatechin gallate. *Food Chemistry*, 101, 126-130.
- Aspartate. (2007). Retrieved February 10, 2009 from, <http://en.wikipedia.org/wiki/Aspartate>
- Barltop, D. & Brueton, M. J. (1990). *The Gastrointestinal Tract and Short-term Toxicity Tests*. In P. Bourdeau (Ed.), *Short-term Toxicity Tests for Non-genotoxic Effects* (99-110). U.S: John Wiley & Sons Ltd.
- Beaud, D., Tailliez, P. & Anba-Mondoloni, J. (2005). Genetic characterization of the  $\beta$ -glucuronidase enzyme from a human intestinal bacterium *Ruminococcus gnavus*. *Microbiology*, 151, 2323-2330.
- Beratis, N. G., Eliopoulou, M. I. & Syrogiannopoulos, G. A. (2003).  $\beta$ -Glucuronidase in the diagnosis of bacterial meningitis and response to treatment. *Acta Paediatr*, 92, 1272-1276.
- Bradford, M. M. (1976). A Rapid and Sensitive Method for the Quantitation of Microgram Quantities of Protein Utilizing the Principle of Protein-Dye Binding. *Anal. Biochem*, 72, 248-254.
- Bramanti, E., Ferri, F., Raspi, G., Lampugnani, L., Spinetti, M. C., Miller, K. E. & Synovec R. E. (2001). New method for separation and determination of denatured caseins by hydrophobic interaction chromatography. *Talanta*, 54, 343-349.
- Breck, D. W. (1974). *Zeolite Molecular Sieves Structure, Chemistry and Use*. New York: Wiley-Interscience.
- Brenda Enzyme Database. Retrieved March 29 2008 from, <http://www.brenda-enzymes.org>
- Bzducha, A. & Wolosiak R. (2006). Synergistic effect of antioxidant activity of casein and its enzymatic hydrolysate in combination with ascorbic acid and  $\beta$ -carotene in model oxidation systems. *ACTA Scientiarum Polonorum - Technologia Alimentaria*, 5(1), 113-133.

- Charles, W. S. (1976). Review: Casein Micelle Structure; An Examination of Models. *Journal of Dairy Science*, 59-9, 1547-1556.
- Cakicioglu-Ozkan, F. & Ulku, S. (2005). The effect of HCl treatment on water vapor adsorption characteristics of clinoptilolite rich natural zeolite. *Microporous and Mesoporous Materials*, 77, 47-53.
- Caldini, G., Cenci, G. & Strappini, C. (1999). Influence of amylose, amylopectin and pullulan on  $\beta$ -glucuronidase activity of starch-degrading *Escherichia coli*. *World Journal of Microbiology & Biotechnology*, 15, 497-499.
- Cardona, M. E., Norin, E. & Midtvedt, T. (2006).  $\beta$ -Glucuronidase activity in germ-free, monoassociated and conventional mice. *Microbial Ecology in Health and Disease*, 18, 38-41.
- Catanzaro, J. A. & Gren, L. (1997). Microbial ecology and dysbiosis in human medicine. *Alternative Medicine Review*, 2(3), 202-209.
- Chang, Y., Chu, L., Tsai, J. & Chiu, S. (2006). Kinetic study of immobilized lysozyme on the extrudate-shaped NaY zeolite. *Process Biochemistry* 41, 1864–1874.
- Chen, D. Z., Zhang, J. X. & Chen J. M. (2010). Adsorption of methyl tert-butyl ether using granular activated carbon: Equilibrium and kinetic analysis. *International Journal of Environmental Science and Technology* 7 (2), 235-242.
- Claire, L. V., Rabiou, B. A. & Gibson G. R. (2006). Human Colonic Microbiology and the Role of Dietary Intervention: Introduction to Prebiotics. In: G. R Gibson. & R. A. Rastall (Ed.), *Prebiotics: Development and Application* ( pp.1-28). John Wiley & Sons, Ltd.
- Cerri, G., Gennaro, M., Bonferonc, M. C. & Caramella, C. A. (2004). Zeolites in biomedical application: Zn-exchanged clinoptilolite-rich rock as active carrier for antibiotics in anti-acne topical therapy. *Applied Clay Science* 27, 141-150.
- Cervato, G., Cazzola, R. & Cestaro, B. (1999). Studies on the antioxidant activity of milk caseins. *International Journal of Food Sciences and Nutrition*, 50, 291-296.

- Chi, E. Y., Krishnan, S., Randolph, T. W. & Carpenter, J. F. (2003). Physical Stability of Proteins in Aqueous Solution: Mechanism and Driving Forces in Nonnative Protein Aggregation, Review. *Pharmaceutical Research*, 20, No. 9, 1325-1336.
- Chiku, H., Kawai, A., Ishibashi, T., Takehara, M., Yanai, T., Mizukami, F. & Sakaguchi, K. (2006). A novel protein refolding method using a zeolite. *Analytical Biochemistry*, 348, 307-314.
- Chiku, H., Matsui, M., Murakami, S., Kiyozumi, Y., Mizukami, F. & Sakaguchia, K. (2003). Zeolites as new chromatographic carriers for proteins-easy recovery of proteins adsorbed on zeolites by polyethylene glycol. *Analytical Biochemistry*, 318, 80-85.
- Colic, M. & Pavelic, K. (2000). Molecular mechanisms of anticancer activity of natural dietetic products. *Journal of Molecular Medicine*, 78, 333-336.
- Copeland, R. A. (2005). *Evaluations of Enzyme Inhibitors in Drug Discovery*. New Jersey: Wiley Interscience.
- Dabbrowski, A. (2001). Adsorption-from theory to practice. *Advances in Colloid and Interface Science*, 93, 135-224.
- Dabek, M., McCrae, S. I., Stevens, V. J., Duncan, S. H. & Louis, P. (2008). Distribution of  $\beta$ -glucosidase and  $\beta$ -glucuronidase activity and of  $\beta$ -glucuronidase gene gusin human colonic bacteria. *FEMS Microbiol Ecol* 66, 487-495.
- Dahm, A. & Eriksson, H. (2004). Ultra-stable zeolites—a tool for in-cell chemistry. *Journal of Biotechnology* 111, 279–290.
- De Moreno De Leblanc, A. & Perdigon G. (2001). Reduction of  $\beta$ -glucuronidase and nitroreductase activity by yoghurt in a murine colon cancer model. *Biocell*, 29(1), 15-24.
- Devasena, T. & Menon, V. P. (2003). Fenugreek Affects the Activity of  $\beta$ -glucuronidase and Mucinase in the Colon. *Phytother. Res.*, 17, 1088-1091.
- Dimirkoua, A. & Doula, M. K. (2008). Use of clinoptilolite and an Fe-overexchanged clinoptilolite in  $Zn^{2+}$  and  $Mn^{2+}$  removal from drinking water. *Desalination*, 224,

280–292.

- Doula, M., Ioannou, A. & Dimirkou, A. (2002). Copper Adsorption and Si, Al, Ca, Mg, and Na Release from Clinoptilolite. *Journal of Colloid and Interface Science*, 245, 237-250.
- Dunne, C. (2001). Basic Science Review, Inflammatory Bowel Diseases Adaptation of Bacteria to the Intestinal Niche. *Probiotics and Gut Disorder* 7(2), 136-145.
- Ersoy B. & Çelik M. S. (2002). Electrokinetic properties of clinoptilolite with mono- and multivalent electrolytes. *Microporous and Mesoporous Materials*, 55, 305-312.
- Farias, T., Ruiz-Salvador, A. R. & Rivera, A. (2003). Interaction studies between drugs and a purified natural clinoptilolite. *Microporous and Mesoporous Materials*, 61, 117–125.
- Field, K. L., Kimball, B. A., Mennella, J. A., Beauchamp, G. K. & Bachmanov, A. A. (2008). Avoidance of hydrolyzed casein by mice. *Physiology & Behavior*, 93, 189-199.
- Fishman, W. H. & Bernfeld, P. (1955). *Methods in Enzymology, Volume I*, 262-269.
- Fontes, N., Partridge, J., Halling, P., J. & Barreiros, S. (2002). Acid Base effects of Zeolite on nonaqueous biocatalysis. *Biotechnology and Bioengineering*, 77(3),296-305.
- Fujisawa, T., Aikawa, K., Takahashi, T., Yamai, S., Watanabe, K., Kubota, Y. & Miyaoka, M. (2001). Influence of butyric and lactic acids on the b-glucuronidase activity of Clostridium perfringens. *Letters in Applied Microbiology*, 32, 123-125.
- Fujisawa, T. & Mori, M. (1997). Influence of various bile salts on  $\beta$ -glucuronidase activity of intestinal bacteria. *Letters in Applied Microbiology*, 25, 95-97.
- Frost, D. & Hainsen, J., (1945). Determination of the degree of hydrolysis of partial acid hydrolysates of casein and fibrin. *The Journal of Biological Chemistry*. 517-521.

- Gacche, R. N., Gond, D.S., Dhole, N.A. & Dawane, B. S. (2006). Coumarin Schiff-bases: As Antioxidant and Possibly Anti-inflammatory Agents. *Journal of Enzyme Inhibition and Medicinal Chemistry*, April, 21(2), 157–161.
- Gilmore, M. S. & Ferretti, J. J. (2002). The thin line between gut commensal and pathogen. *Science*, 299, 1999-2002.
- Goldin, B. & Gorbach, S. L. (1977). Alterations In Fecal Microflora Enzymes Related To Diet, Age, Lactobacillus Supplements, And Dimethylhydrazine. *Cancer*, 40, 2421-2426.
- Gomez-Ruiz, J. A., Lopez-Exposito, Pihlanto, A., Ramos, M. & Recio I. (2008). Antioxidant activity of ovine casein hydrolysates: identification of active peptides by HPLC–MS/MS. *European Food Research Technology*, 227, 1061–1067.
- Gourley, G. R., Kreamer, B. L., *Aspartic and malic acid inhibition of  $\beta$ -glucuronidase*. United States Patent No:6416783
- Gourley, G. R., Kreamer, B. L. & Cohnen, M. (1997). Inhibition of beta-glucuronidase by casein hydrolysate formula. *J Pediatr Gastroenterol Nutr.*, 25(3), 267-72.
- Guo, C., Campbell, B. E., Chen, K., Lenhoff, A. M. & Velev O. D. (2003). Casein precipitation equilibria in the presence of calcium ions and phosphates. *Colloids and Surfaces B: Biointerfaces*, 29, 297-307.
- Guo, R. & Liu Y. (2008). pH-dependent structures and properties of casein micelles. *Biophysical Chemistry*, 136, 67-73.
- Han, H. K. & Amidon, G. L. (2000). Targeted prodrug design to optimize drug delivery. *AAPS Pharmsci*, 2, 1-6.
- Hashimoto, K., Saito, H. & Ohsawa, R. (2006). GlycopolymERIC Inhibitors of  $\beta$ -Glucuronidase. III. Configurational Effects of Hydroxy Groups in Pendant Glyco-Units in Polymers upon Inhibition of  $\beta$ -Glucuronidase. *Journal of Polymer Science: Part A: Polymer Chemistry*, 44, 4895–4903.
- Hayes, M., Ross, R. P., Fitzgerald, G. F., Hill, C. & Stanton, C. (2006). Casein-Derived Antimicrobial Peptides Generated by Lactobacillus acidophilus DPC6026.

*Applied and Environmental Microbiology*, March, 2260–2264.

- Hebert, S. C, Cheng, S. & Geibel, J. (2004). Functions and roles of the extracellular  $\text{Ca}^{2+}$ -sensing receptor in the gastrointestinal tract. *Cell Calcium*, 35, 239–247.
- Ho, Y. S. & McKay, G. (1999). Pseudo-second order model for sorption processes *Process Biochemistry*, 34, 451-465.
- Ho, Y. S., Ng, J. C. Y. & McKay, G. (2000). Kinetics of pollutant sorption by biosorbents: Review. *Separation and Purification Methods*, 29(2), 189-232.
- Horne, D. S. (2002). Casein structure, self-assembly and gelation. *Current Opinion in Colloid and Interface Science*, 7, 456–461.
- Huang, P. S. & Oliff, A. (2001). Drug-targeting strategies in cancer therapy. *Current Opinion in Genetics & Development*, 11, 104-110.
- Huang, Y. L., Yen, G. C., Sheu, F., Lin, J. Y. & Chau, C. F. (2007). Dose effects of the food spice cardamom on aspects of hamster gut physiology. *Mol. Nutr. Food Res.*, 51, 602-608.
- Hughes, R. & Rowland, I. R. (2000). Metabolic activities of the gut microflora in relation to cancer. *Microbial Ecology in Health and Disease, Suppl 2*, 179-185.
- Indira, M., Vijayammal, P. L., Menon P. V. G., & Kurup, P.A. (1980). Effect of Dietary Fiber on Intestinal Bacterial B-Glucuronidase Activity in Chicks Fed a Cholesterol Containing Diet. *Cancer*, 46, 2430-2432.
- Inglezakis, V. J. (2005). The concept of “capacity” in zeolite ion-exchange systems. *Journal of Colloid and Interface Science*, 281, 68–79.
- Image Library. (n.d). Image Library of Biological Molecules. Retrieved March 10, 2008 from,  
[http://www.imbjena.de/ImgLibDoc/ftir/IMAGE\\_FTIR.html.html#Amide%20vibrations](http://www.imbjena.de/ImgLibDoc/ftir/IMAGE_FTIR.html.html#Amide%20vibrations)
- Ishibashi, T., Takehara, M., Yanai, T., Mizukami, F., Sakaguchi, K., Chiku, H. & Kawai A. (2006). A novel protein refolding method using a zeolite. *Analytical*



*Biochemistry*, 348, 307-314.

- Ismail, N. M., Fei, L. Y., Cheng, L. L., Ching, Y. Y., Kamarudin, K. & Mat, H. (2005). *Adsorption of Protein on H-Beta Zeolite*. Proceeding of International Conference of Chemical and Bioprocess Engineering. Malasia.
- Jama, M. A. & Yücel, H. (1990). Equilibrium Studies of Sodium-ammonium, Potassium-ammonium, and Calcium-ammonium Exchanges on Clinoptilolite Zeolite. *Sep. Sci. Technol.*, 24, 1393-1416.
- Janer, C., Pelaez, C. & Requena, T. (2004). Caseinomacropeptide and whey protein concentrate enhance *Bifidobacterium lactis* growth in milk. *Food Chemistry* 86, 263-267.
- Jefferson, R. A., Burgess, S. M. & Hirsh D. (1986).  $\beta$ -Glucuronidase from *Escherichia coli* as a gene-fusion marker. *Proc. Natl. Acad. Sci., USA*, 83, 8447-8451.
- Kaduk, J. A. & Faber, J. (1995). Crystal structure of zeolite Y as function of ion exchange. *The Rigaku Journal*, 12, No.2.
- Kang, Q., Wu, X., Xue, Y., Liu, X. & Shen D. (1999). Maximum separation-distance for a separated-electrode piezoelectric sensor in non-electrolyte liquids. Application to determination of the adsorption human immunoglobulin G onto quartz surface. *Sensors and Actuators, B*, 61, 68-74.
- Karlsson, A.O., Ipsen, R. & Ardo, Y., (2000). *Observations of casein micelles in skim milk concentrate by transmission electron microscopy*. Research Note Dairy Technology, Department of Food Science, The Royal Veterinary and Agricultural University. Denmark.
- Kauf, A. C. W. & Kensinger, R. S. (2002). Purification of porcine  $\beta$ -casein, N-terminal sequence, quantification in mastitic milk. *Anim. Sci.*, 80, 1863-1870.
- Kaushik, R., Levine, B. & LaCourse, W. R. (2006). A brief review: HPLC methods to directly detect drug glucuronides in biological matrices (Part I). *Analytica Chimica Acta*, 556, 255-266.

- Kavak, D. D., Altıok, E., Bayraktar, O. & Ülkü, S. (2010). *Pistacia terebinthus* extract: As a potential antioxidant, antimicrobial and possible  $\beta$ -glucuronidase inhibitor. *Journal of Molecular Catalysis B: Enzymatic*, 64, 167–171.
- Kayombo, S., Mbwetee, T. S. A., Katimaa, J. H. Y. & Jorgensen, S. E. (2003). Effects of substrate concentrations on the growth of heterotrophic bacteria and algae in secondary facultative ponds. *Water Research*, 37, 2937–2943.
- Kazlauskaitė, J., Biziulevičius, G. A., Zukaite, V., Biziulevičienė, G., Miliukiene, V. & Siaurys, A. (2005). Oral tryptic casein hydrolysate enhances phagocytosis by mouse peritoneal and blood phagocytic cells but fails to prevent induced inflammation. *International Immunopharmacology*, 5, 1936-1944.
- Kim, K. H. & Lee, E. K. (2007). Biothermodynamic analyzes of BSA adsorption to alum gel using isothermal titration calorimetry. *Biotechnology and Bioprocess Engineering*, 12, 366-371.
- Kitts, D. D. (2005). Antioxidant properties of caseinphosphopeptides. *Trends in Food Science & Technology*, 16, 549–554.
- Klint, D. & Eriksson H. (1997). Conditions for the Adsorption of Proteins on Ultrastable Zeolite Y and Its Use in Protein Purification. *Protein Expression and Purification*, 10, 247-255.
- Knezevic, Z., Mojovic, L. & Adnadjevic B. (1998). Palm oil hydrolysis by lipase from *Candida cyhdracea* immobilized on zeolite type Y. *Enzyme and Microbial Technology*, 22, 275-280.
- Kong, J. & Yu S. (2007). Fourier Transform Infrared Spectroscopic Analysis of Protein Secondary Structures. *Acta Biochimica et Biophysica Sinica*, 39(8), 549-559.
- Kreamer, B. L., Siegel, F. L. & Gourley, G. R. (2001). A novel inhibitor of beta-glucuronidase: L-aspartic acid. *Pediatr Res.*, 50(4), 460-466.
- Kyriakis, S. C., Papaioannou, D. S., Alexopoulos, C., Polizopoulou, Z., Tzika, E.D. & Kyriakis, C.S. (2002). Experimental studies in safety and efficacy of the dietary use of a clinoptilolite-rich tuff in sows: a review of recent research in Greece. *Microporous and Mesoporous Materials*, 51, 65-74.

- Lampe, J. W., Li, S. S., Potter, J. D. & King, I. B. (2002). Serum B-Glucuronidase Activity Is Inversely Associated with Plant-Food Intakes in Humans. *Journal of Nutrition*, 132, 1341–1344.
- Lataye, D. H., Mishra, I. M. & Mall I. D. (2006). Removal of pyridine from aqueous solution by adsorption on bagasse fly ash. *Ind. Eng. Chem.Res.*, 45, 3934-3943.
- Latorre-Esteves, M., Cortes, A., Torres-Lugo, M. & Rinaldi C. (2009). Synthesis and characterization of carboxymethyl dextran-coated Mn/Zn ferrite for biomedical applications *Journal of Magnetism and Magnetic Materials*, 321, 3061–3066.
- Lee, H. W., Choo, M. K., Bae, E. A. & Kim, D. H. (2003).  $\beta$ -Glucuronidase inhibitor tectorigenin isolated from the flower of *Pueraria thunbergiana* protects carbon tetrachloride-induced liver injury. *Liver International*, 23, 221–226.
- Len, A., Rosell, C. M. & de Barber, C. B. (2003). A differential scanning calorimetry study of wheat proteins. *European Food Research and Technology*, 217, 13-16.
- Leopold, C. S. (1999). Coated dosage forms for colon-specific drug delivery. *PSTT*, 2(5), 197-204.
- Lescovac, V. (2003). *Comprehensive Enzyme Kinetics*. New York: Kluwer Academic Publishers.
- Liang, E., Liu, P. & Dinh, S. (2007). Use of a pH-sensitive fluorescent probe for measuring intracellular pH of Caco-2 cells. *International Journal of Pharmaceutics*, 338, 104–109.
- Li, Z. Y., Sun, X., Xiao, Q. & Xiang, S. H. (2005). Effect of Alkali Treatment on the Structure and Catalytic Properties of ZSM-5 Zeolite. *Chinese Chemical Letters*, 16, No. 1, 115-118.
- Lim, C. C., Ferguson, L. R. & Tannock, G. W. (2005). Review: Dietary fibres as “prebiotics”: Implications for colorectal cancer. *Mol. Nutr. Food Res.*, 49, 609-619.
- Logar, N. Z., Siljeg, M., Arcon, I., Meden, A. Tusar, N. N., Stefanovic, S., Kovac, J. & Kaucic, V. (2006). Sorption of  $\text{Cr}^{3+}$  on clinoptilolite tuff: A structural

- investigation. *Microporous and Mesoporous Materials*, 93, 275–284.
- Loritsch, K. B. & James, R. D. (1991). *Purified quartz and process for purifying quartz*. United States Patent No: 5037625.
- Maiti, A., Sharma, H., Basu J. K. & De, S. (2009). Modeling of Arsenic Adsorption Kinetics of Synthetic and Contaminated Groundwater on Natural Laterite. *Journal of Hazardous Materials.*, 172, 928-934.
- Mao, X. Y., Ni, J. R., Sun, W. L, Hao, P. P. & Fan L. (2007). Value-added utilization of yak milk casein for the production of angiotensin-I-converting enzyme inhibitory peptides. *Food Chemistry*, 103, 1282-1287.
- Marangoni, A. D. (2003). *Enzyme Kinetics A Modern Approach*. New Jersey: Wiley Interscience Publication.
- Martin-Kleiner, I., Flegar-Mestric, Z., Zadro, R., Breljak, D., Janda, S. S., Stockovic, et al. (2001). The effect of zeolite clinoptilolite on serum chemistry and hematopoiesis in mice. *Food and Chemical Toxicology*, 39, 717-727.
- McMahon, D. J. & Brown, R. J. (1984). Composition, Structure, and Integrity of Casein Micelles: A Review. *Journal of Dairy Science*, 67, No.3, 499-512.
- Miliauskas, G., Venskutonis, P. R. & Beek, T. A. (2004). Screening of radical scavenging activity of some medicinal and aromatic plant extracts. *Food Chemistry*, 85, 231-237.
- Montgomery, J. M. (1985). *Water Treatment Principles and Design*. USA: Consulting Engineers Inc.
- Mumpton, F. (1999). La roca magica: Uses of natural zeolites in agriculture and industry. *Colloquium Paper, Proc. Natl. Acad. Sci.*, 96, 3463-3470.
- Mück-Seler, D. & Pivac, N. (2003). The effect of natural clinoptilolite on the serotonergic receptors in the brain of mice with mammary carcinoma. *Life Sciences*, 73, 2059–2069.

- Nassar, M. M., Magdy, Y. H., Daifullah, A. H. & Kelany, H. (2008). Mass Transfer and Adsorption Kinetics of Phenolic Compounds onto Activated Carbon Prepared from Rice Husk. *Adsorption Science & Technology*, 26, No.3, 157-167.
- Nakamura, T., Ishikawa, M., Hiraiwa, T. & Sato J. (1992). X-ray diffractometric determination of clinoptilolite in zeolite tuff using multiple analytical lines. *Analytical Sciences August (8)*.
- Nalini, N., Sabitha, K., Viswanathan, P. & Menon, V. P. (1998). Influence of spices on the bacterial (enzyme) activity in experimental colon cancer. *Journal of Ethnopharmacology*, 62, 15-24.
- Nara, T. Y., Togashia, H., Sekikawa, C., Kawakami, M., Yaginuma, N., Sakaguchi K. et al. (2009). Use of zeolite to refold a disulfide-bonded protein *Colloids and Surfaces B: Biointerfaces* 68: 68–73.
- Narin, G. (2009). *Nitrogen Monoxide Storage and Release Properties of Local Natural Zeolite for Biological Applications*. (Doctoral Dissertation, Izmir Institute of Technology, 2007).
- O’Connell, J. E., Steinle, S., Reiter, F., Auty, M.A. E., Kelly, A. L, Patrick F. et al. (2003). Properties of casein micelles reformed from heated mixtures of milk and ethanol. *Colloids and Surfaces A: Physicochem. Eng. Aspects*, 213, 265-273.
- Oberg, K. A. & Fink, A. L. (1998). A New Attenuated Total Reflectance Fourier Transform Infrared Spectroscopy Method for the Study of Proteins in Solution. *Analytical Biochemistry*, 256, 92–106.
- Ogura, M., Shinomiya, S., Tateno, J., Nara, Y., Nomura, M., Kikuchi, E. et al. (2001). Alkali-treatment technique – new method for modification of structural and acid – catalytic properties of ZSM-5 zeolites. *Applied Catalysis A: General*, 219, 33-43.
- Ortatlı, M. & Oğuz, H. (2001). Ameliorative effects of dietary clinoptilolite on pathological changes in broiler chickens during aflatoxicosis. *Research in Veterinary Science*, 71, 59-66.
- Pan, X., Yu, S., Yao, P. & Shao, Z. (2007). Self-assembly of  $\beta$ -casein and lysozyme. *Journal of Colloid and Interface Science*, 316, 405-412.

- Pandya, P. H., Jasra, R. V., Newalkar, B. L. & Bhatt, P. N. (2005). Studies on the activity and stability of immobilized  $\alpha$ -amylase in ordered mesoporous silicas *Microporous and Mesoporous Materials*, 77, 67–77.
- Papaioannou, D. S., Katsoulos, P. D., Panousis, N. & Karatzias, H. (2005). The role of natural and synthetic zeolites as feed additives on the prevention and/or the treatment of certain farm animal diseases: A review. *Microporous and Mesoporous Materials*, 84, 161-170.
- Papaioannou, D. S., Kyriakis, C. S., Alexopoulos, C., Tzika, E. D., Polizopoulou, Z. S. & Kyriakis, S.C. (2004). A field study on the effect of the dietary use of a clinoptilolite-rich tuff, alone or in combination with certain antimicrobials, on the health status and performance of weaned, growing and finishing pigs. *Research in Veterinary Science*, 76, 19–29.
- Papaioannou, D. S., Kyriakis, S. C., Papasteriadis, A., Roubies, N., Yannakopoulos, A. & Alexopoulos, C. (2002). A field study on the effect of in-feed inclusion of a natural zeolite (clinoptilolite) on health status and performance of sows/gilts and their litters. *Research in Veterinary Science*, 72, 51-59.
- Papot, S., Combaud, D., Bosslet, K., Gerken, M., Czech, J. & Gesson J. P. (2000). Synthesis and cytotoxic activity of a glucuronylated prodrug of nornitrogen mustard. *Bioorganic & Medicinal Chemistry Letters*, 10, 1835-1837.
- Paulsson, M. & Dejmek, P. (1990) Thermal Denaturation of Whey Proteins in Mixtures with Caseins Studied by Differential Scanning Calorimetry. *Journal of Dairy Science*, 73, 590-600.
- Pavelic, K., Hadzija, M., Bedrica, L., Pavelic', J., Dikic', I., Katic', M. et al. (2001). Natural zeolite clinoptilolite: new adjuvant in anticancer therapy. *Journal of Molecular Medicine*, 78: 708-720.
- Pavelic, K. & Hadzija, M. (2003). Medical Applications of Zeolites. In S. M. Auerbach, K. A., Carrado, P. K Duuta (Ed.), *Handbook of Zeolite Science and Technology* (pp. 143; 1174). C.R: Taylor & Francis CRC Press.
- Pavelic, K., Katic, M., Sverko, V., Marotti, T., Bosnjak, B., Balog, T. et al. (2002). Immunostimulatory effect of natural clinoptilolite as a possible mechanism of its

- antimetastatic ability. *Journal of Cancer Research and Clinical Oncology*, 128, 37-44.
- Pehlivan, H. (2001). *Preparation and Characterization of Polypropylene Based Composite Films*. (Master dissertation, Izmir Institute of Technology, 2001).
- Phadtare, S., Vinod, V. P., Mukhopadhyay, K., Kumar, A., Rao, M., Chaudhari, R. V. et al. (2004). Immobilization and Biocatalytic Activity of Fungal Protease on Gold Nanoparticle- Loaded Zeolite Microspheres. *Biotechnology and Bioengineering*, 6(85), 629-637.
- Phadungath, C. (2005). Casein micelle structure: a concise review. *Songklanakarin Journal of Science and Technology*, 27(1), 201-212.
- Philippe, M., Le Graet, Y. & Gaucheron, F. (2005). The effects of different cations on the physicochemical characteristics of casein micelles. *Food Chemistry*, 90, 673-683.
- Polatoğlu, I. (2005). *Chemical behaviour of clinoptilolite rich natural zeolite in aqueous medium*. (Master dissertation, İzmir Institute of Technology, 2005).
- Prvulovic, D., Jovanovic-Galovic, A., Stanic, B., Popovic, M. & Grubor-Lajsic, G. (2007). Effects of a clinoptilolite supplement in pig diets on performance and serum parameters. *Czech Journal of Animal Science*, 52 (6), 159–164.
- Qiu, H., Lv, L., Pan, B., Zhang, Q., Zhang, W. & Zhang, Q. (2009). Critical review in adsorption kinetic models. *Journal of Zhejiang University Science A*, 10(5), 716-724.
- Rachwalik, R., Olejniczak, Z. a& Sulikowski, B. (2006). Catalytic properties of dealuminated ferrierite type zeolite studied in transformations of m-xylene Part 2. *Catalysis Today*, 114, 211-216.
- Rafter, J., Govers, M., Martel, P, Pannemans, D., Pool-Zobel, B., Rechkemmer, G. et al. (2004). Diet-related cancer. *European Journal of Nutrition*, Suppl 2, 47-84.
- Rivera, A. & Farias, T. (2005). Clinoptilolite–surfactant composites as drug support: A new potential application. *Microporous and Mesoporous Materials*, 80, 337-346.

- Rivera, A., Farias, T., Ruiz-Salvador, A. R. & de Menorval, L.C. (2003). Preliminary characterization of drug support systems based on natural clinoptilolite. *Microporous and Mesoporous Materials*, 61, 249-259.
- Rivera, A., Rodriguez-Fuentes, G. & Altshuler E. (1998). Characterization and neutralizing properties of a natural zeolite/Na<sub>2</sub>CO<sub>3</sub> composite material. *Microporous and Mesoporous Materials*, 24, 51-58.
- Rivera, A., Rodriguez-Fuentes, G. & Altshuler, E. (2000). Time evolution of a natural clinoptilolite in aqueous medium: conductivity and pH experiments. *Microporous and Mesoporous Materials*, 40, 173–179.
- Rodriguez-Fuentes, G., Barrios, M.A., Iraizoz, A., Perdoma, I. & Cedre, B. (1997). Enterex: Anti-Diarrheic drug based on purified natural zeolite clinoptilolite. *Zeolites*, 19, 441-448.
- Rodriguez-Fuentes, G., Denis, A. R., Alvarez, M. A. B. & Colarte, A. I. (2006). Antacid drug based on purified natural clinoptilolite. *Microporous and Mesoporous Materials*, 94, 200–207.
- Rovira-Bru, M., Giralt, F. & Coheny, Y. (2001). Protein Adsorption onto Zirconia modified with Terminally Grafted Polyvinylpyrrolidone. *Journal of Colloid and Interface Science*, 235, 70-79
- Rozic, M., Stefanovic, S. J. & Curkovic, L. (2002). Evaluation of Croation Clinoptilolite- and Montmorillonite-rich Tuffs for Ammonium Removal. *Croatica Chemica Acta*, 75, 255-269.
- Ruthven, D. M. (1989). The statistical thermodynamic approach to the correlation of equilibrium data. In A. E. Rodriguez, M. D. LeVan, D. Tondeur (Ed.), *Adsorption: Science and Technology*. U.S: Kluwer Academic Publishers.
- Sağ, Y. & Aktay, Y. (2000). Mass transfer and equilibrium studies for the sorption of chromium ions onto chitin. *Process Biochemistry*, 36, 157-173.
- Sakaguchi, K., Matsui, M. & Mizukami, F. (2005). Applications of zeolite inorganic composites in biotechnology: current state and perspectives *Applied Microbiology and Biotechnology*, 67, 306–311.



- Sarkar, M., Acharya, P. K. & Bhattacharya, B. (2003). Modeling the adsorption kinetics of some priority organic pollutants in water from diffusion and activation energy parameters. *Journal of Colloid and Interface Science*, 266, 28–32.
- Saier, M. H. & Mansour, Jr. N. M. (2005). Probiotics and prebiotics in human health. *Journal of Molecular Microbiology and Biotechnology*, 10, 22-25.
- Segel, I. H. (1993). *Segel Enzyme Kinetics: Behavior analysis and Rapid Equilibrium and Steady State Systems*. New York : Wiley Interscience Publication.
- Semo, E., Kesselman, E., Danino D. & Livney, Y. D. (2006). Casein micelle as a natural nano-capsular vehicle for nutraceuticals., *Food Hydrocolloids*.
- Serralha, F. N., Lopes, J. M., Lemos F., Prazeres D. M. F., Aires-Barros, M. R., Cabral J. M. S. et al. (1998). Zeolites as supports for an enzymatic alcoholysis reaction. *Journal of Molecular Catalysis B: Enzymatic*, 4, 303–311.
- Serres, R., McCown, B., & Zeldin, E. (1997). Detectable B-glucuronidase activity in transgenic cranberry is affected by endogenous inhibitors and plant development. *Plant Cell Reports*, 16, 641–646.
- Shah, P., Jogani, V., Bagchi, T. & Misra, A. (2006). Role of Caco-2 Cell Monolayers in Prediction of Intestinal Drug Absorption. *Biotechnology Progress*, 22, 186-198.
- Shipkova, M. & Wieland, E. (2005). Glucuronidation in therapeutic drug monitoring. *Clinica Chimica Acta*, 358, 2-23.
- Silva, S. V. & Malcata, F. X. (2005). Caseins as source of bioactive peptides. *International Dairy Journal*, 15, 1-15.
- Slattery, C. W. (1976). Review: Casein Micelle Structure; An Examination of Models *Journal of Dairy Science* Vol. 59, No. 9 :1547-1556.
- Spelzini, D., Peleteiro, J., Picó, G. & Farruggia, B. (2008). Polyethyleneglycol–pepsin interaction and its relationship with protein partitioning in aqueous two-phase systems. *Colloids and Surfaces B: Biointerfaces*, 67, 151–156.

- Stemhagen, L. G. & Allen, J. C. (2001). Human colon adenocarcinoma growth rates and  $\alpha$ -lactalbumin. In N. Newburg (Ed.), *Bioactive components of human milk* (pp.114-119). New York: Kluwer Academic Press.
- Suzuki, M., (1990). *Adsorption Engineering*. Elsevier , Tokyo. Sverko V., Soboanec S., Balog T., Colic M., Marotti T., 2004. Natural Micronised Clinoptilolite and Clinoptilolite Mixtures with *Urtica dioica L.* Extract as Possible Antioxidants. *Food Technology and Biotechnology* 42: (3) 189–192.
- Swanson, K. C., Matthews, J. C., Woods, C. A. & Harmon, D. L. (2002). Postprandial Administration of Partially Hydrolyzed Starch and Casein Influences Pancreatic  $\alpha$ -Amylase Expression in Calves. *Journal of Nutrition, March 1*, 376-381.
- Tavolaro, A., Tavolaro, P. & Drioli, E. (2007). Zeolite inorganic supports for BSA immobilization: Comparative study of several zeolite crystals and composite membranes. *Colloids and Surfaces B: Biointerfaces*, 55, 67-76.
- Top, A. & Ülkü, S. (2004). Silver, zinc, and copper exchange in a Na-clinoptilolite and resulting effect on antibacterial activity. *Applied Clay Science, Volume 27, Issues 1-2*, 13-19.
- Trckova, M., Matlova, L., Dvorska, L. & Pavlic I. (2004). Kaolin, bentonite, and zeolites as feed supplements for animals: health advantages and risks. *Veterinary Medicine – Czech*, 49-10, 389-399.
- Trgo, M, Peric, J. & Medvidovic N. V. (2006). A comparative study of ion exchange kinetics in zinc/lead-modified zeolite-clinoptilolite systems. *Journal of Hazardous Materials*, 136(5), 938-945.
- Tsitsishvili, G. V., Andronikashvili, T. G., Kirov, T. G. & Filizova, L. D. (1992). *Natural Zeolites*. New York: Ellis Horwood,.
- Tu, M., Pan, X. & Saddler, J. N. (2009). Adsorption of cellulose on cellulolytic enzyme lignin from lodgepole pine. *Journal of Agricultural and Food Chemistry*, 57, 7771-7778.
- Ülkü, S. (1991). Heat and Mass Transfer in Adsorbent Beds. In S. Kakaç, , B. Kilkış, F. A. Kulakci, F. Arınç (Ed.), *Convective Heat and Mass Transfer in Porous Media*

(pp.695- 725). DordrechtNATO Series: Kluwer Academic Publishers.

- Ünak, T., Avcibasi, U. & Yildirim, Y. (2005). A radioanalytical technique for measurement of beta-glucuronidase activities. *Journal of Radioanalytical and Nuclear Chemistry, Vol. 266(3)*, 503-506.
- Ünak, T., Ünak, P. & Ongun, B. (1997). Synthesis and Iodine-125 Labelling of Glucuronide Compounds for Combined Chemo- and Radiotherapy of Cancer. *Applied Radiation and Isotopes, 48, 6*, 777-783.
- Vadivelan, V. & Kumar, V. K. (2005). Equilibrium, kinetics, mechanism, and process design for the sorption of methylene blue onto rice husk. *Journal of Colloid and Interface Science, 286*, 90–100.
- Venyaminov, S. & Kalnin, N. N. (1990) Quantitative IR spectrophotometry of peptide compounds in water (H<sub>2</sub>O) solutions. I. Spectral parameters of amino acid residue absorption bands. *Biopolymers, 30(13-14)*: 1243-1257.
- Vernazza, C. L., Rabiou, B. A. & Gibson, G. R. (2006). Human colonic microbiology and the role of dietary intervention: Introduction to prebiotics. In G.R. Gibson and R.A. Rastall (Ed.), *Prebiotics: Development and application* (pp. 1-29).England: John Wiley and Sons Ltd.
- Wang, H., Fei, Z., Chen, J., Zhang, Q. & Xu, Y. (2007). Adsorption thermodynamics and kinetic investigation of aromatic amphoteric compounds onto different polymeric adsorbents. *Journal of Environmental Sciences, 19*, 1298–1304.
- Wang, H., Ye, X. & Ng, T. B. (2000). First demonstration of an inhibitory activity of milk proteins against human immunodeficiency virus-1 reverse transcriptase and the effect of succinylation. *Life Sciences, 67*, 2745-2752.
- Wei, G., Loktionova, N. A., Pegg, A. E. & Moschel, R. C. (2005). B-Glucuronidase-cleavable prodrugs of O6-Benzylguanine and O6-Benzyl-2'-deoxyguanosine. *Journal of Medicinal Chemistry, 48*, 256-261.
- de Wit, J. N & Klarenbeek, G. (1984). Effects of Various Heat Treatments on Structure and Solubility of Whey Proteins. *Journal of Dairy Science, 67*, 2701-2710.

- Worringer, J. T., Sørensen, J. & Lopez-Fandin, R. (2006). Health effects and technological features of caseinomacropptide. *International Dairy Journal*, 16, 1324-1333.
- Xia, M. S., Hu, C. H. & Xu, Z. R. (2005). Effects of copper bearing montmorillonite on the growth performance, intestinal microflora and morphology of weanling pigs. *Animal Feed Science and Technology*, 118, 307-317.
- Xie, Y., Liu, H. & Hu, N. (2007). Layer-by-layer films of hemoglobin or myoglobin assembled with zeolite particles. *Electrochemistry and electrocatalysis Bioelectrochemistry*, 70, 311-319.
- Yamashita, S., Furubayashi, T., Kataoka, M., Sakane, T., Sezaki, H. & Tokuda, H. (2000). Optimized conditions for prediction of intestinal drug permeability using Caco-2 cells. *European Journal of Pharmaceutical Sciences*, 10, 195–204
- Yang R.T. (2003). *Adsorbents: Fundamentals and Applications*. USA: John Wiley & Sons Inc.
- Yang, R. T. (1999). *Gas Separation by Adsorption Processes*. USA: Imperial College Press.
- Zarkovic, N., Zarkovic, K., Kralj, M., Borovic, S., Sabovlovic, S., Blazi M. P. et al. (2003). Anticancer and antioxidative effects of micronized zeolite clinoptilolite. *Anticancer Research*, 23, 1589-1596.
- Zhang, Z., Dalgleish, D. G. & Goff, H. D. (2004). Effect of pH and ionic strength on competitive protein adsorption to air/water interfaces in aqueous foams made with mixed milk proteins. *Colloids and Surfaces B: Biointerfaces*, 34, 113-121.
- Zenser, T. V., Lakshmi V. M. & Davis, B. B. (1999). Human and Escherichia coli  $\beta$ -glucuronidase hydrolysis of glucuronide conjugates of benzidine and 4-aminobiphenyl, and their hydroxy metabolites. *Drug metabolism and Disposition*, 27(9), 1064-1067.

## APPENDIX A

### COMPLEMENTARY ANALYZES

#### A.1. $\beta$ -Glucuronidase Activity Measurement

To perform activity measurements, enzyme  $\beta$ -glucuronidase (GUS) and substrate 4-Methylumbelliferyl  $\beta$ -D-glucuronide hydrate (4-MUG) were used. 5 min incubation was performed for enzyme and substrate solutions and reaction was terminated by carbonate stop buffer and enzyme activities in samples solutions were analyzed triplicate for GUS activities by microplate reader (Varioskan, Thermo) using 96-wells at  $360 \lambda_{ex}/ 450 \lambda_{em}$  (Figure A1a below).

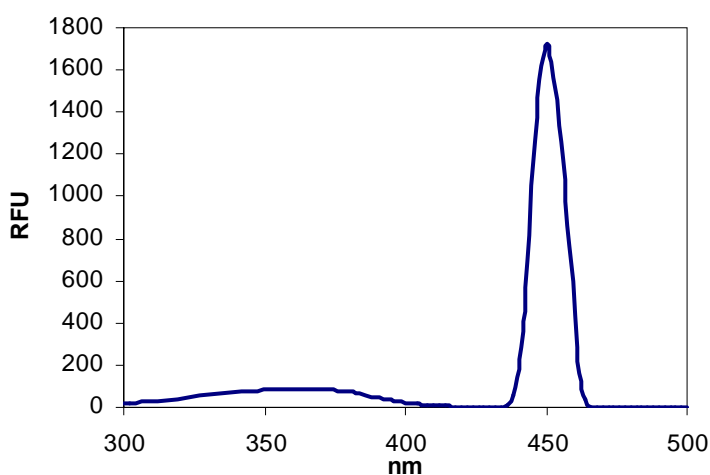


Figure A.1. Excitation and emission wavelengths :  $360 \lambda_{ex}/ 450 \lambda_{em}$

Activities were determined from the standard curve given below where 4-methylumbelliferone sodium salt (4-MU) was used as standard. Standard curve was given in Figure A.2 below. Chemical formulas of the substrate and standard were given below in Figure A.3 and A.4, respectively. Velocity change for different initial substrate concentrations were given in Figure A.5.

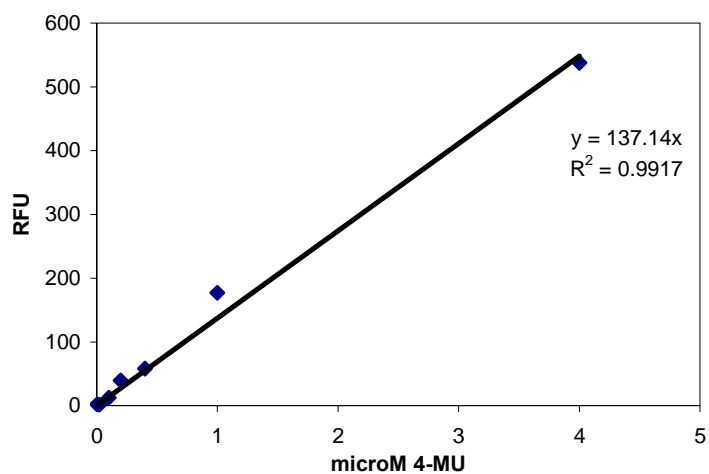


Figure A.2. Standard curve for  $\beta$ -Galacturonidase Activity Measurement using 4-methylumbelliferone sodium salt (4-MU) as fluorescent standard

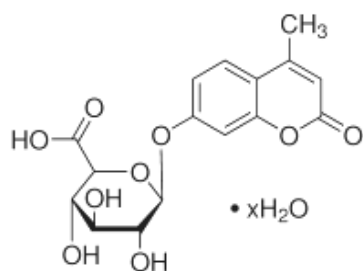


Figure A.3. 4-Methylumbelliferyl  $\beta$ -D-glucuronide hydrate

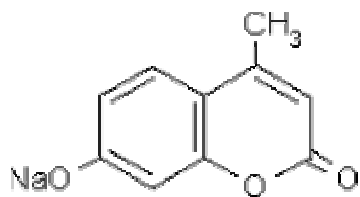
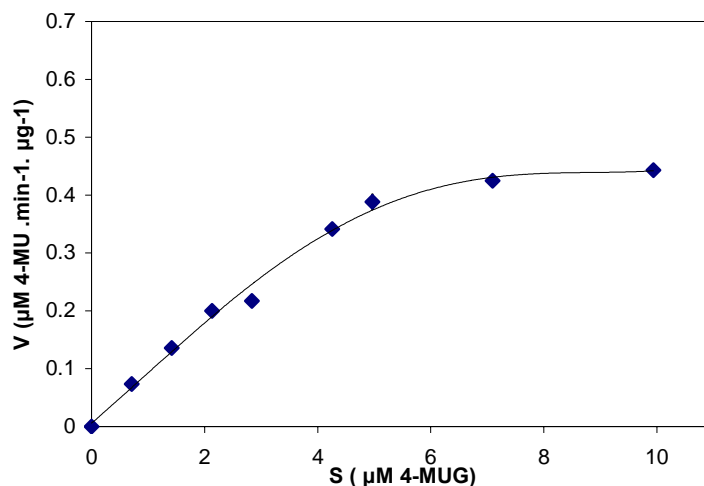


Figure A.4. 4-Methylumbelliferone sodium salt



A.5. Velocity change for different initial substrate (4-MUG) concentrations

## A.2. Double reciprocal plots in enzyme inhibition experiments

The double-reciprocal form of the Michaelis-Menten equation is useful for calculating  $K_m$  and  $V_{max}$ . Double reciprocal form of the Michaelis Menten equation is:

$$\frac{1}{V} = \left( \frac{K_m}{V_{max}} \right) \frac{1}{[S]} + \frac{1}{V_{max}} \quad (\text{A.1})$$

Plotting  $1/v$  (reciprocal of rate) vs.  $1/[S]$  (reciprocal of substrate concentration) yields a straight line. One can then use this equation to calculate  $V_{max}$  and  $K_m$ . from intercept and slope of this plot.

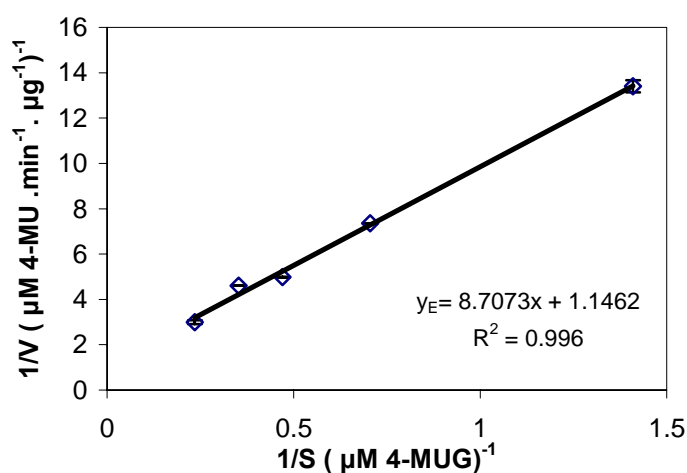


Figure A.6. Double reciprocal plot for GUS enzyme

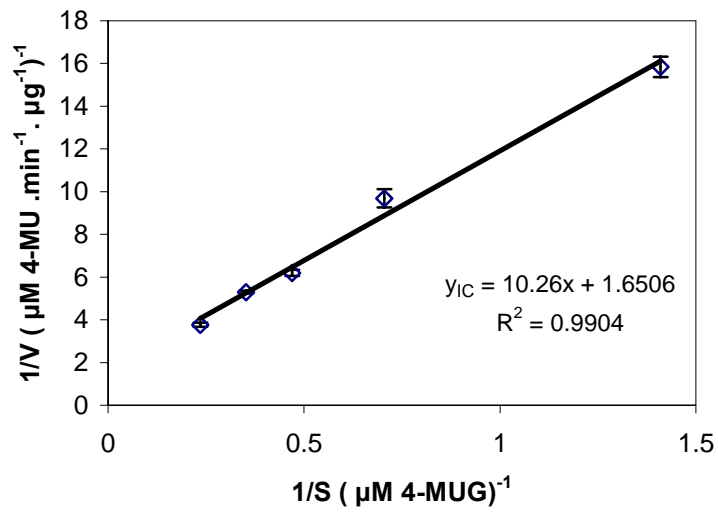


Figure A.7. Double reciprocal plot for GUS enzyme with casein inhibitor

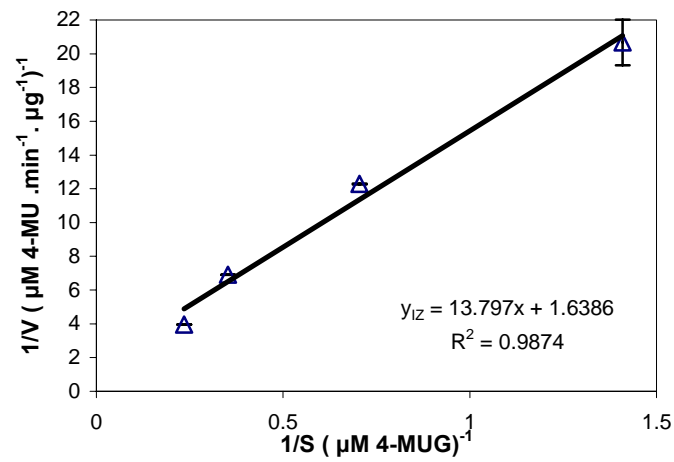


Figure A.8. Double reciprocal plot for GUS enzyme with zeolite inhibitor



### A.3. Sample calculation for remaining enzyme activity

Table A3. Sample data for inhibition experiments in RFU (relative fluorescence units)

# of Measurements	Control	[I <sub>C</sub> ]=0.125mg/ml	[I <sub>Z1</sub> ]=25mg/ml
1	248.2	212.1	191.9
2	249.7	201.1	167.7
3	238	209.4	173.8
<b>Ave:</b>	<b>245.3</b>	<b>207.53</b>	<b>177.8</b>

As control sample was inhibitor free, percentage (%) activity of this sample was 100 %. Then, samples containing inhibitors % activity were calculated as follow:

% activity for [I<sub>C</sub>]=0.125mg/ml;

$$= \frac{207.53}{245.3} * 100$$

=86.61 %

### A.4. Determination of the growth rates and specific time for the MIC experiments

Specific growth rate “μ” (slope of the logarithmic growth curve) in the exponential phase for five different casein concentrations were calculated by the following formula:

$$\mu = \frac{\ln(OD_2 / OD_1)}{t_2 - t_1} \quad (A.2)$$

where OD<sub>1</sub> is the cell’s optical density at time t<sub>1</sub> (start of the exponential phase), OD<sub>2</sub> is the optical density at time t<sub>2</sub> (end of the exponential phase). Generation time which is defined as time required for cell number to double was calculated by following equation:

$$t = \frac{0.301}{\mu} \quad (A.3)$$

where 0.301 represents the log(2N)-log(N)

### A.5. Protein Analyzes

Amount of protein in the liquid and zeolite phases was calculated by using the mass balance with the following equation:

$$q_t = \frac{v(C_o - C_t)}{w} \quad (\text{A.4})$$

where  $C_o$  and  $C_t$  ( $\mu\text{g}$  protein /ml solution) are the liquid phase concentrations of casein initially and at time  $t$ , respectively.  $q_t$  ( $\mu\text{g}$  protein/mg zeolite) is the zeolite phase concentration of casein at time  $t$ ,  $v$  the volume of aqueous phase (ml) and  $w$  is the weight of zeolite (g).

#### a ) Protein analyzes for casein

Protein in the samples was determined by Bradford method (Bradford 1976) based on the proportional binding of the dye Coomassie to proteins which was colorimetric method. Absorbances were measured by Perkin Elmer UV-spectrophotometer at 595 and 634 nm. Bovine Serum Albumin (BSA, Sigma) was used as the Standard.

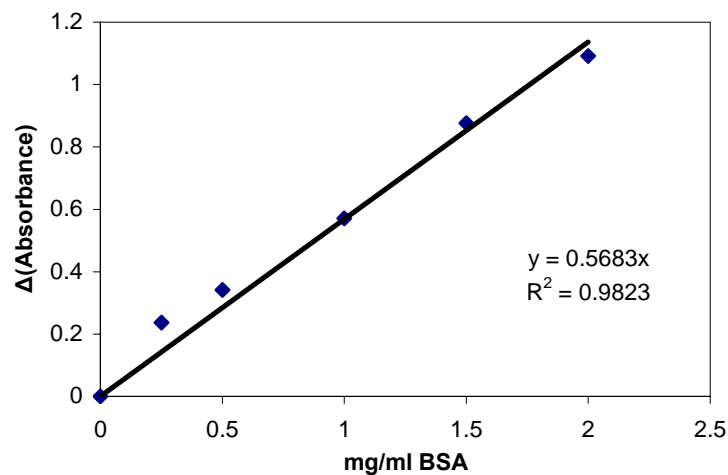


Figure A.9. BSA Standard Curve (cuvette) used in protein analyzes

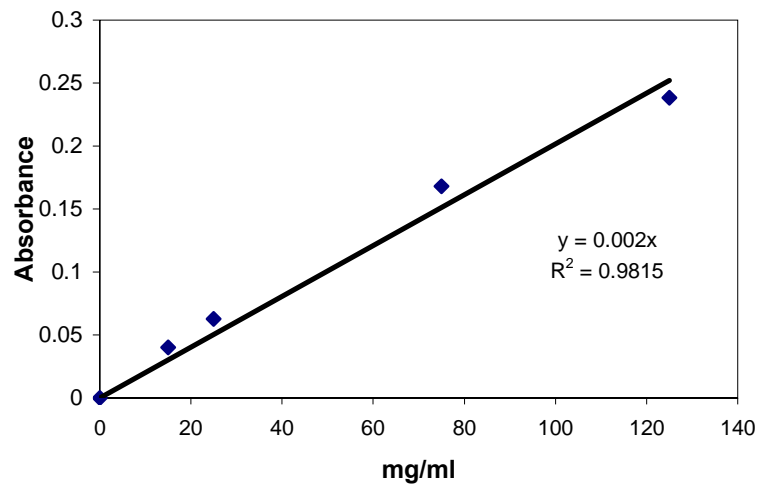


Figure A.10. Standard curve for protein determination using BSA as protein standard for microplate readings at 634 nm.

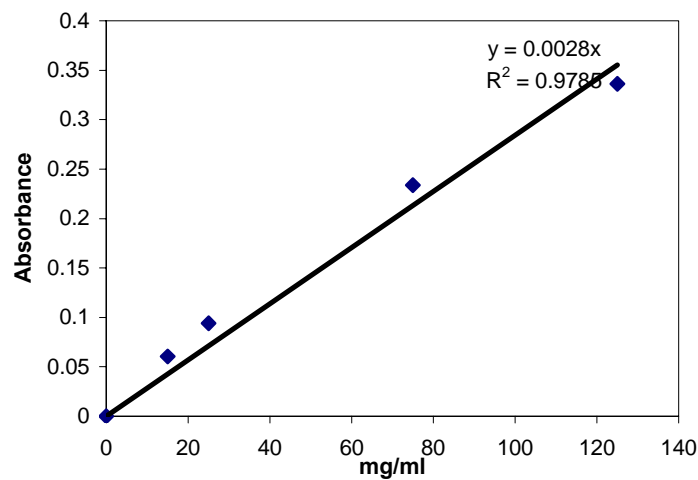


Figure A.11. Standard curve for protein determination using BSA as protein standard for microplate readings at 595 nm.

***b) Protein analyzes for GUS***

Protein concentrations in samples were determined spectrophotometrically. First of all, wavelength for the maximum absorbance was determined in UV region between 200 and 380 nm. A representative graph was given in Figure A.12. Maximum absorbance was determined at 255 nm. Calibration curve obtained by scanning at the

same wavelength interval was given in Figure A.13 for varying GUS concentrations in the range of 0-500 µg/ml.

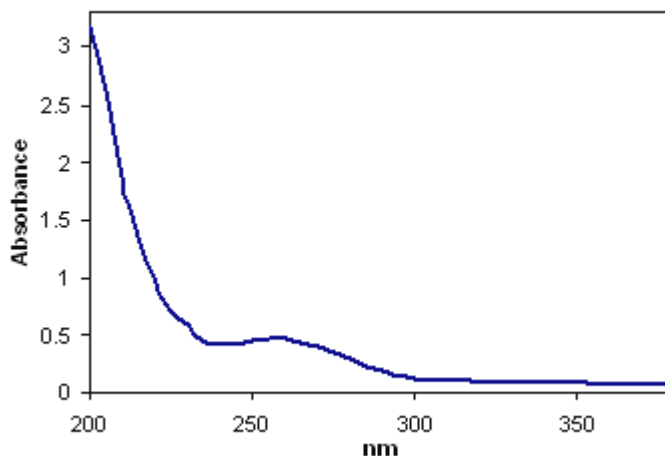


Figure A.12. A representative graph for the UV scanning for 200-380 nm.

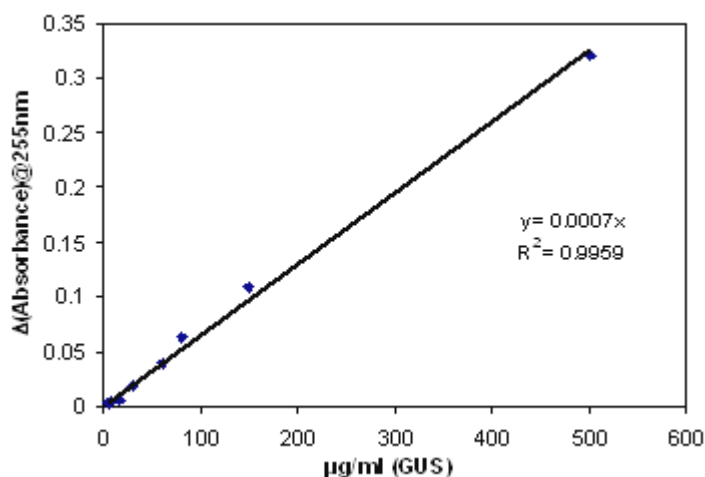


Figure A.13. Standard curve for GUS

## A.6. Antioxidant Activity Measurement

ABTS, 2,2'-azinobis (3-ethylbenzothiazoline-6-sulfonic acid) diammonium salt radical cation decolourisation assay was used for the assessment of antioxidant activity of samples according to procedure given by Miliauskas et al, 2004. Scavenging ability of samples for ABTS radical cation ( $ABTS^{\bullet+}$ ) at different concentrations were measured using UV-visible spectrophotometer (Perkin Elmer) at 734 nm and results

were compared with Trolox standard absorbance curve given below.

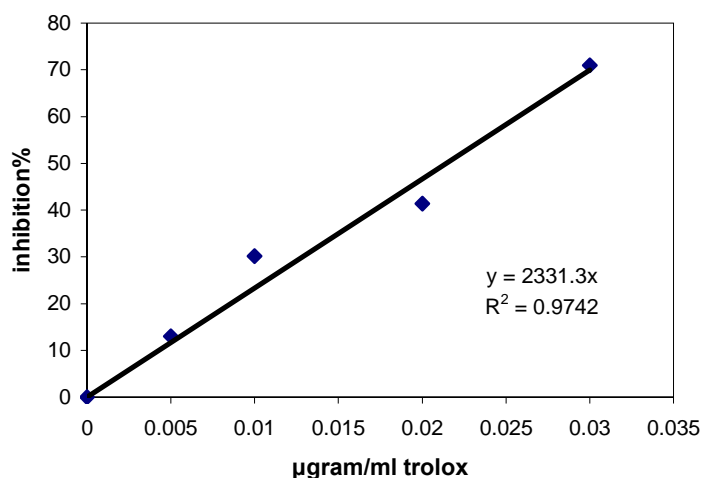


Figure A.14. Trolox standard curve for antioxidant activity experiments

The antioxidant activity results were reported as the micromolar Trolox equivalent antioxidant capacity ( $\mu\text{mole TEAC}$ ) and also % inhibition which was calculated as follows:

$$\% \text{ inhibition} = 100 * [(\text{reading at } t_0 / \text{reading at } t_{6\text{min}}) / \text{reading at } t_0] \quad (\text{A.5})$$

### A.7. MTT Cell Proliferation Assay

The yellow tetrazolium MTT (3-(4,5-dimethylthiazolyl-2)-2,5-diphenyl tetrazolium bromide) was reduced by metabolically active cells, in part by the action of dehydrogenase enzymes, to generate reducing equivalents such as NADH and NADPH. The resulting intracellular purple formazan was solubilized and quantified by spectrophotometric means. 20 $\mu\text{l}$  MTT solution was added to each well and shaken to thoroughly mix the MTT into the media. Cells were incubated under an atmosphere of 95% humidified air and 5%  $\text{CO}_2$  at 37°C. for 4 hours to allow the MTT to be metabolized. Cell media was dumped off the media and formazan dye was resuspended in dimethyl sulfoxide (DMSO) and well was shaken to thoroughly mix the formazan into the solvent. Optical density was measured at 540 nm by Multiskan Spectrum (Thermo) which was directly correlated with cell quantity.

### **A.8. XTT Cell Proliferation Assay**

XTT Cell Proliferation Kit (B.I) was used to study cell death mediated by possible cytotoxic zeolite. The assay was based on the ability of metabolic active cells to reduce the tetrazolium salt XTT to orange colored compounds of formazan. During incubation period, XTT was converted into a colored, soluble formazan salt by the metabolic activity of viable cells. XTT reagent was added to culture media and cells were incubated with the reagent for 4h. After incubation the dye intensity was read by Multiskan Spectrum (Thermo) at a wavelength of 450 nm. The intensity of the color produced was directly proportional to the number of viable cells. Relative cell viability (in percentage) was expressed as:

$$\text{Cell viability \%} = (\text{Abs}_{465} \text{ treated cells} / \text{Abs}_{465} \text{ control cells}) \times 100 \quad (\text{A.6})$$

## APPENDIX B

### ANALYZES OF ADSORPTION DATA

#### B.1. Analyzes with Equilibrium Data

Equilibrium data plots of GUS and casein adsorption for calculation of Langmuir and Freundlich model parameters were given below.

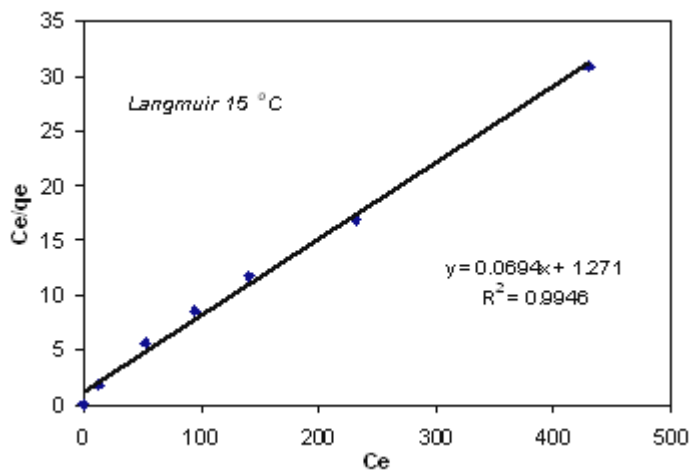


Figure B.1. Langmuir Model plot for GUS adsorption onto zeolite at 15°C

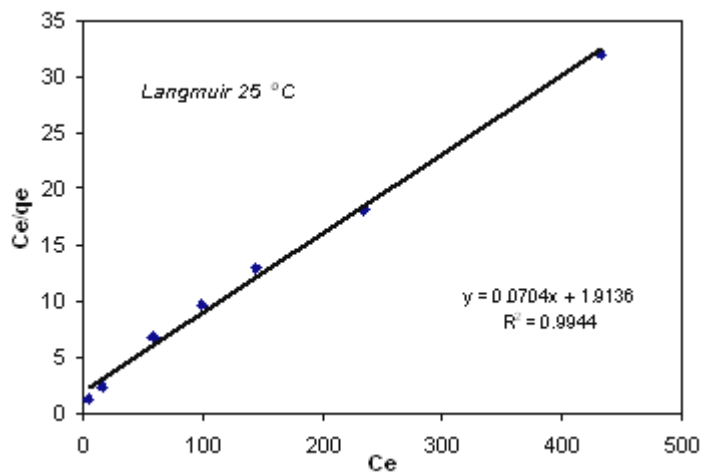


Figure B.2. Langmuir Model plot for GUS adsorption onto zeolite at 25°C

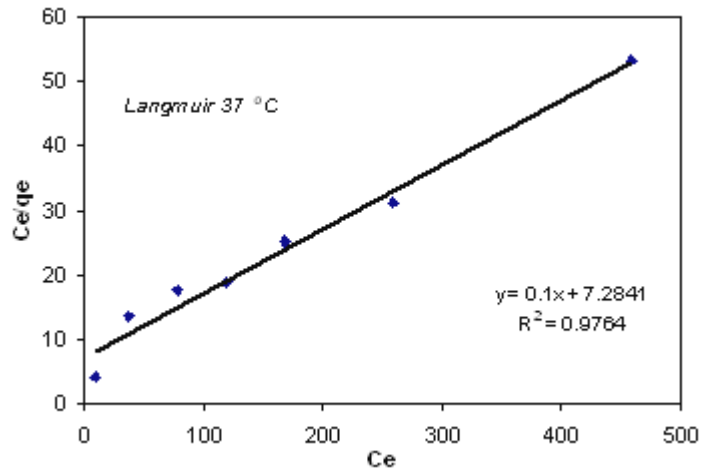


Figure B.3. Langmuir Model plot for GUS adsorption onto zeolite at 37°C

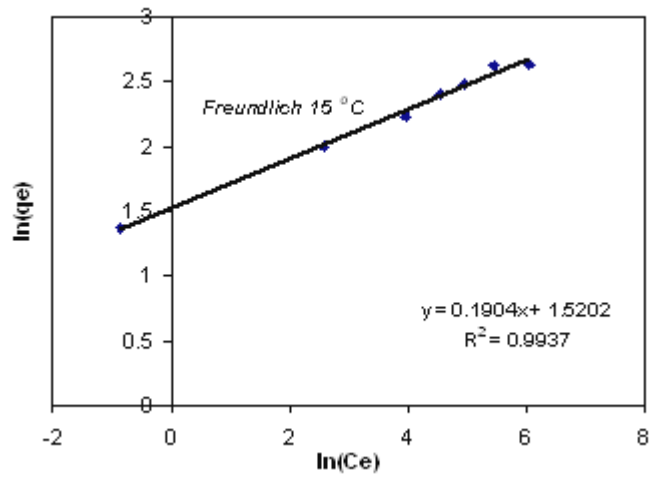


Figure B.4. Freundlich Model plot for GUS adsorption onto zeolite at 15°C

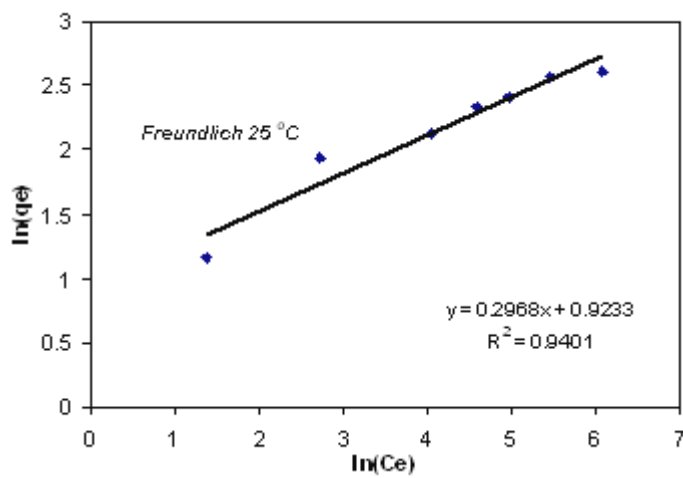


Figure B.5. Freundlich Model plot for GUS adsorption onto zeolite at 25°C



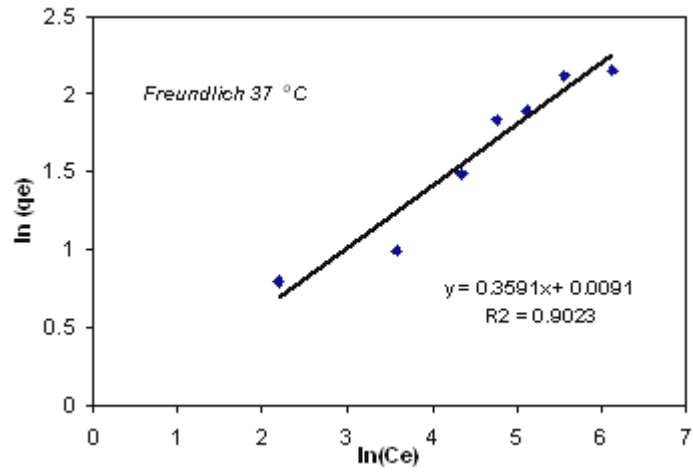


Figure B.6. Freundlich Model plot for GUS adsorption onto zeolite at 37°C

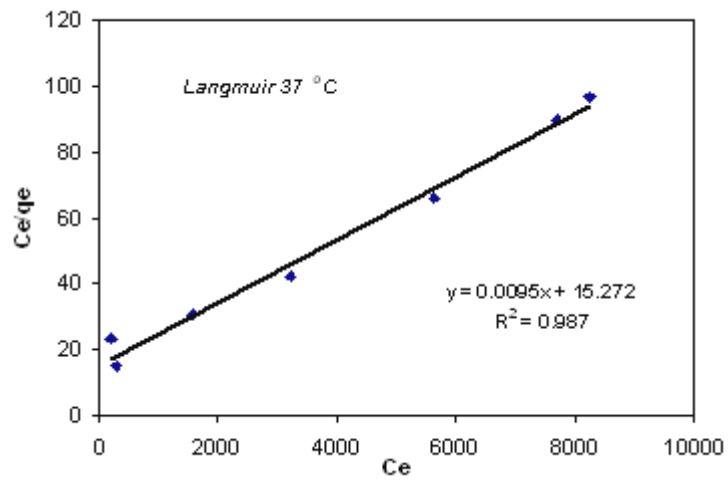


Figure B.7. Langmuir Model plot for casein adsorption onto zeolite at 37°C

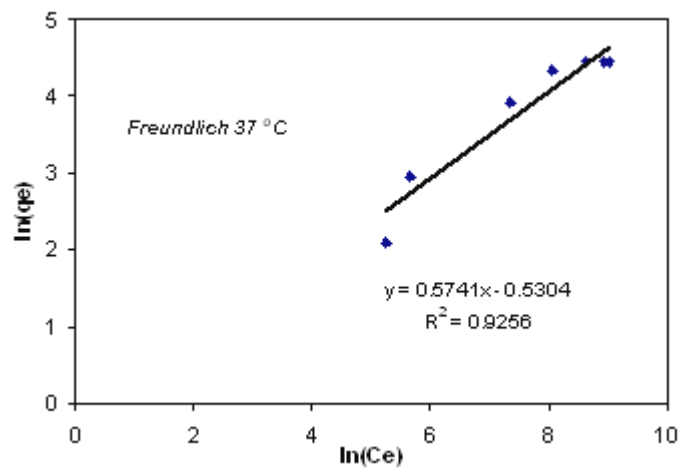
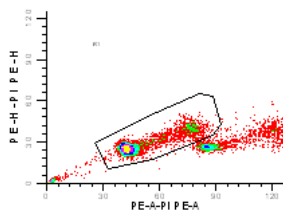
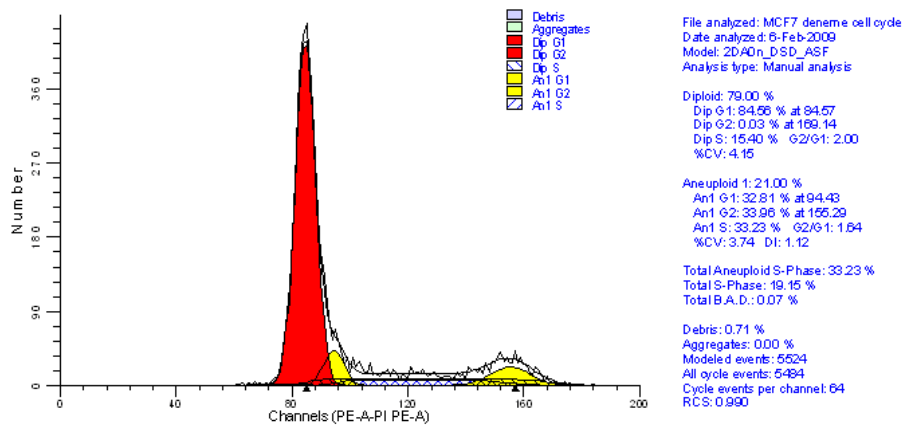


Figure B.8. Freundlich Model plot for casein adsorption onto zeolite at 37°C

# APPENDIX C

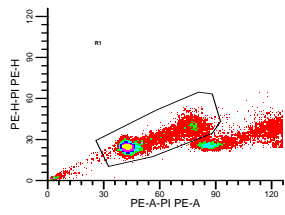
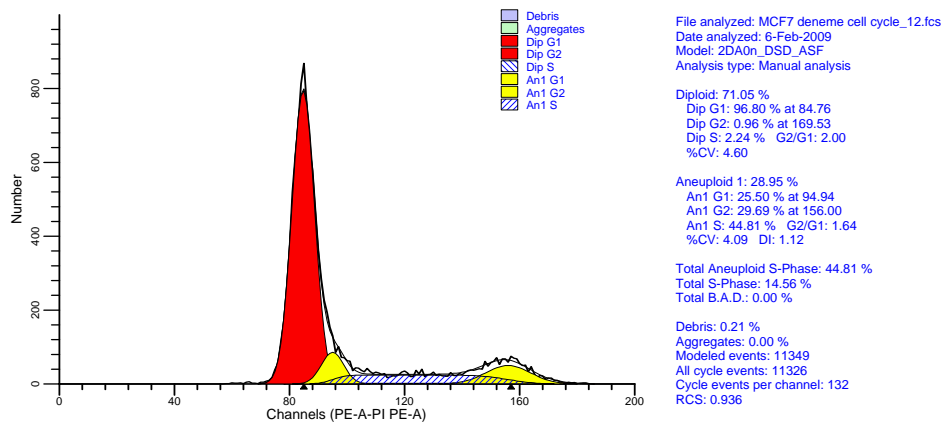
## ANALYZES WITH FLOW CYTOMETRY

### C.1. Cell Cycle Analyzes



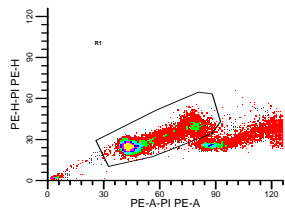
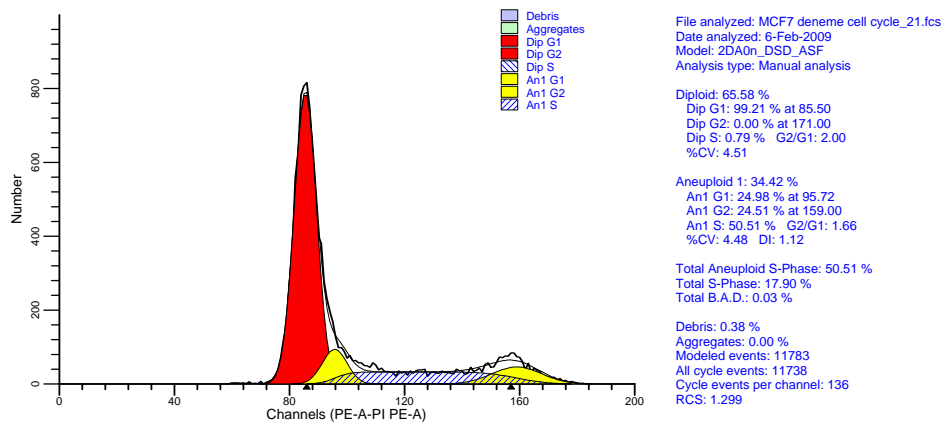
Model: 2DA0n\_DSD\_ASF

Figure C.1. Cell cycle analyses results for MCF-7 cells treated with Z1 (trial 1)



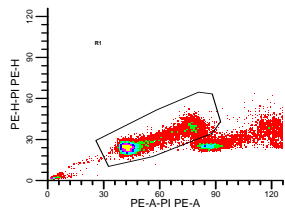
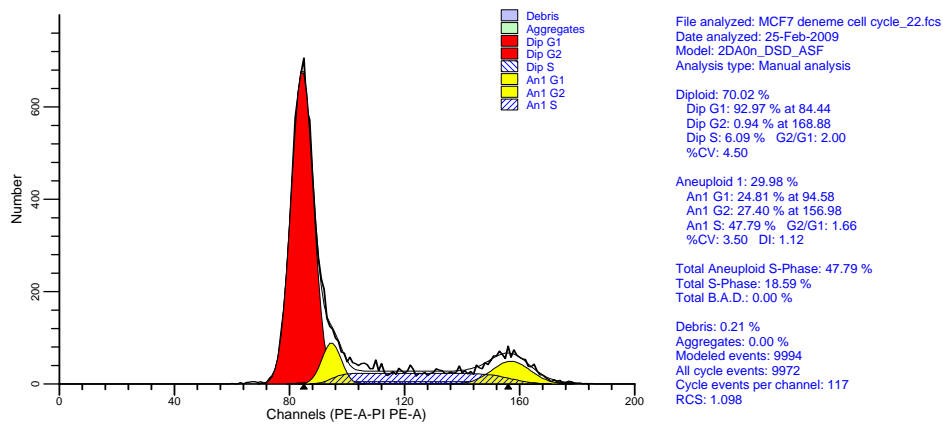
ModFitLT V3.0(Mv32)

Figure C.2. Cell cycle analyses results for MCF-7 cells treated with Z1 (trial 2)



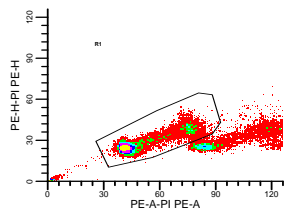
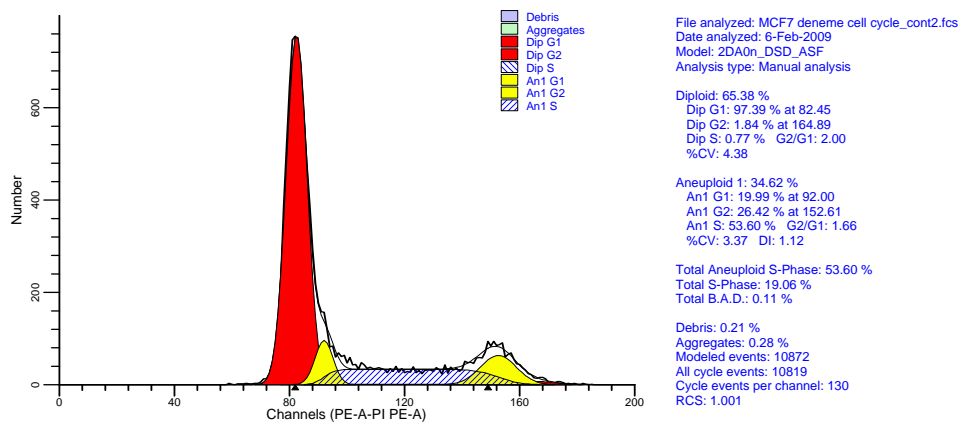
ModFitLT V3.0(Win32)

Figure C.3. Cell cycle analyses results for MCF-7 cells treated with Z2 (trial 1)



ModFitLT V3.0(Win32)

Figure C.4. Cell cycle analyses results for MCF-7 cells treated with Z2 (trial 2)



ModFitLT V3.0(Win32)

Figure C.5. Cell cycle analyses results for MCF-7 cells untreated (control)

## C.2. Apoptosis Analyzes for MCF-7

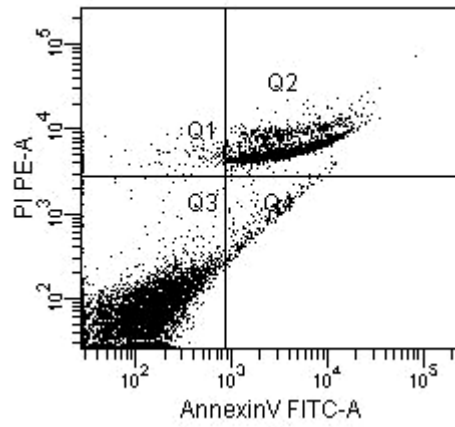


Figure C.6. Dot plot for MCF-7 cells treated with Z1 (trial 1)

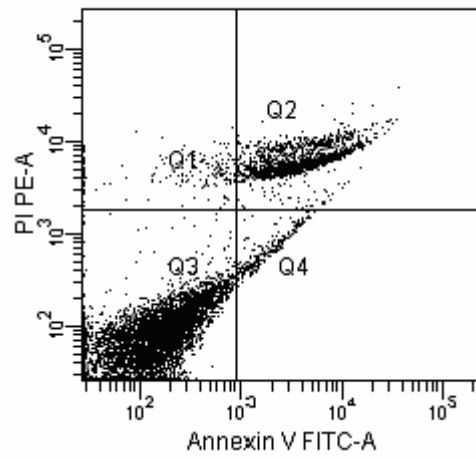


Figure C.7. Dot plot for MCF-7 cells treated with Z1 (trial 2)

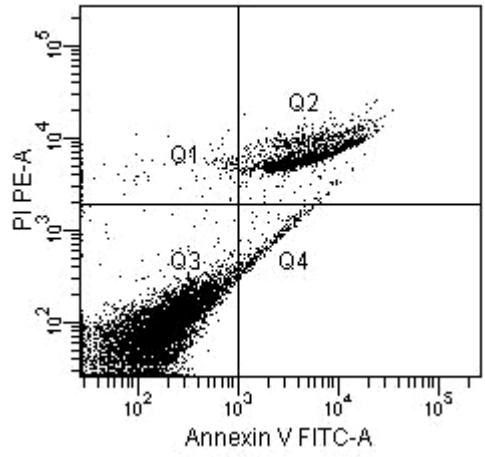


Figure C.8. Dot plot for MCF-7 cells treated with Z2 (trial 1)

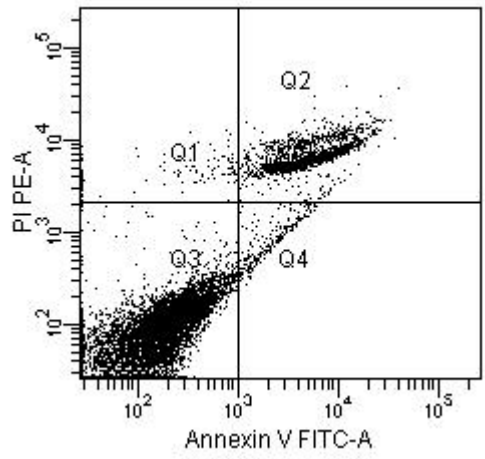


Figure C.9. Dot plot for MCF-7 cells treated with Z2 (trial 2)

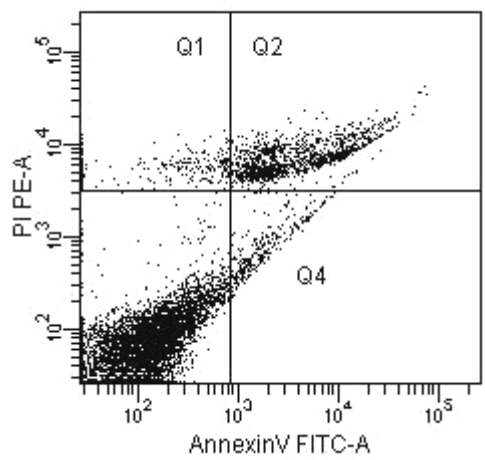


Figure C.10. Dot plot for MCF-7 cells untreated (control)



Table C.1. Statistics of MCF-7 cell populations treated with Z1 (trial 1)

Tube: 11			
Population	#Events	%Parent	%Total
■ All Events	10,000		100.0
☒ P1	2,146	21.5	21.5
☒ P2	2,055	20.5	20.5
☒ Q1	129	1.3	1.3
☒ Q2	1,926	19.3	19.3
☒ Q3	7,728	77.3	77.3
☒ Q4	217	2.2	2.2
☒ Q1-1	115	1.2	1.2
☒ Q2-1	1,945	19.4	19.4
☒ Q3-1	7,709	77.1	77.1
☒ Q4-1	231	2.3	2.3
☒ P3	7,854	78.5	78.5
☒ P4	7,942	79.4	79.4

Table C.2. Statistics of MCF-7 cell populations treated with Z1 (trial 2)

Tube: 12			
Population	#Events	%Parent	%Total
■ All Events	10,000		100.0
☒ P1	1,937	19.4	19.4
☒ P2	8,063	80.6	80.6
☒ P3	1,924	19.2	19.2
☒ P4	8,076	80.8	80.8
☒ Q1	191	1.9	1.9
☒ Q2	1,728	17.3	17.3
☒ Q3	7,868	78.7	78.7
☒ Q4	213	2.1	2.1
☒ Q1-1	167	1.7	1.7
☒ Q2-1	1,726	17.3	17.3
☒ Q3-1	7,840	78.4	78.4
☒ Q4-1	267	2.7	2.7

Table C.3. Statistics of MCF-7 cell populations treated with Z2 (trial 1)

Tube: 21			
Population	#Events	%Parent	%Total
■ All Events	10,000		100.0
☒ P1	1,768	17.7	17.7
☒ P2	8,232	82.3	82.3
☒ P3	1,666	16.7	16.7
☒ P4	8,329	83.3	83.3
☒ Q1	119	1.2	1.2
☒ Q2	1,547	15.5	15.5
☒ Q3	8,113	81.1	81.1
☒ Q4	221	2.2	2.2

Table C.4. Statistics of MCF-7 cell populations treated with Z2 (trial 2)

Tube: 22			
Population	#Events	%Parent	%Total
■ All Events	10,000		100.0
☒ P1	1,944	19.4	19.4
☒ P2	8,056	80.6	80.6
☒ P3	1,843	18.4	18.4
☒ P4	8,150	81.5	81.5
☒ Q1	124	1.2	1.2
☒ Q2	1,707	17.1	17.1
☒ Q3	7,927	79.3	79.3
☒ Q4	242	2.4	2.4

Table C.5. Statistics of MCF-7 cell populations untreated (control)

Specimen Name: MCF7-D2				
Tube Name: control stained				
Population	#Events	%Parent	AnnexinV FI... Mean	PI PE-A Mean
■ All Events	10,000	###	929	1,201
☒ P1	342	3.4	15,134	10,502
☒ P2	9,638	96.4	413	861
☒ P3	649	6.5	8,780	10,085
☒ P4	9,303	93.0	368	553
☒ Q1	241	2.4	313	6,143
☒ Q2	1,302	13.0	5,852	7,461
☒ Q3	8,178	81.8	121	67
☒ Q4	279	2.8	2,190	952

### C.3. Apoptosis Analyzes for Caco-2

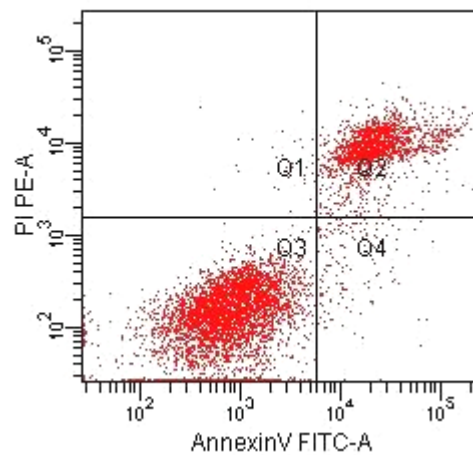


Figure C.11. Dot plot for Caco-2 cells treated with Z1 (trial 1)

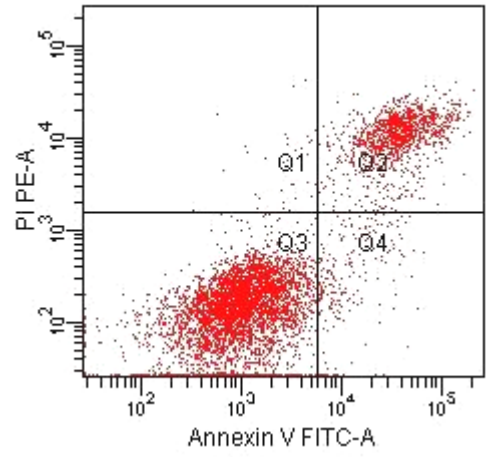


Figure C.12. Dot plot for Caco-2 cells treated with Z1 (trial 2)

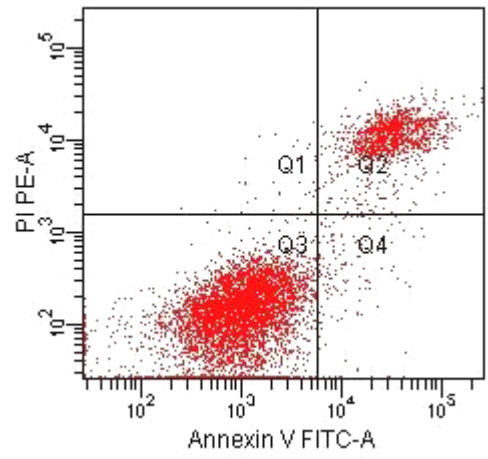


Figure C.13. Dot plot for Caco-2 cells treated with Z2 (trial 1)

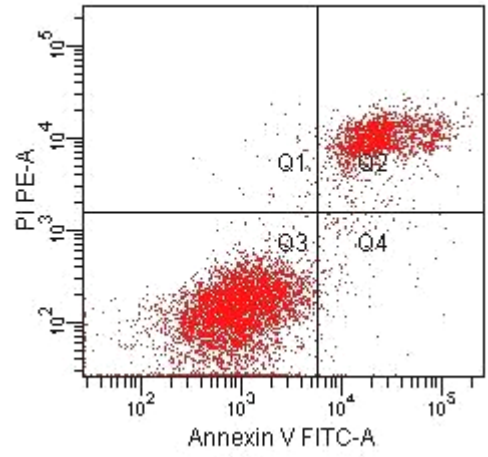


Figure C.14. Dot plot for Caco-2 cells treated with Z2 (trial 2)

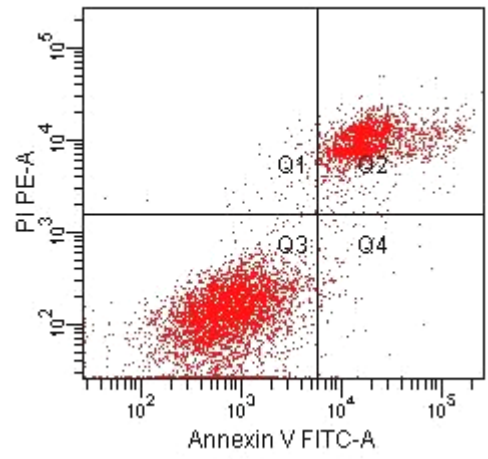


Figure C.15. Dot plot for Caco-2 cells untreated (control, trial 1)

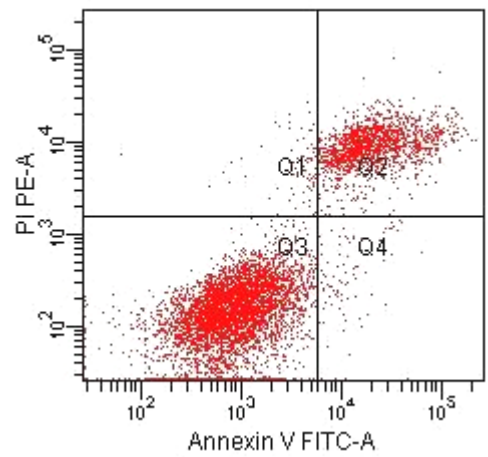


Figure C.16. Dot plot for Caco-2 cells untreated (control, trial 2)

Table C.6. Statistics of Caco-2 cell populations treated with Z1 (trial 1)

Tube: 1A 1			
Population	#Events	%Parent	%Total
■ All Events	10,000		100.0
■ P1	5,862	58.6	58.6
☒ Q1	40	0.7	0.4
☒ Q2	1,568	26.7	15.7
☒ Q3	4,106	70.0	41.1
☒ Q4	148	2.5	1.5
☒ P2	4,139	70.6	41.4
☒ P3	1,722	29.4	17.2
☒ P4	4,256	72.6	42.6
☒ P5	1,606	27.4	16.1

Table C.7. Statistics of Caco-2 cell populations treated with Z1 (trial 2)

Tube: 1A 2			
Population	#Events	%Parent	%Total
■ All Events	10,000		100.0
■ P1	5,749	57.5	57.5
☒ Q1	35	0.6	0.4
☒ Q2	1,236	21.5	12.4
☒ Q3	4,261	74.1	42.6
☒ Q4	217	3.8	2.2
☒ P2	4,281	74.5	42.8
☒ P3	1,468	25.5	14.7
☒ P4	4,482	78.0	44.8
☒ P5	1,267	22.0	12.7

Table C.8. Statistics of Caco-2 cell populations treated with Z2 (trial 1)

Tube: 2B 1			
Population	#Events	%Parent	%Total
■ All Events	10,000		100.0
■ P1	6,530	65.3	65.3
☒ Q1	33	0.5	0.3
☒ Q2	1,184	18.1	11.8
☒ Q3	5,167	79.1	51.7
☒ Q4	146	2.2	1.5
☒ P2	5,187	79.4	51.9
☒ P3	1,340	20.5	13.4
☒ P4	5,317	81.4	53.2
☒ P5	1,213	18.6	12.1

Table C.9. Statistics of Caco-2 cell populations treated with Z2 (trial 2)

Tube: 2B 2			
Population	#Events	%Parent	%Total
■ All Events	10,000		100.0
■ P1	6,309	63.1	63.1
☒ Q1	44	0.7	0.4
☒ Q2	1,587	25.2	15.9
☒ Q3	4,541	72.0	45.4
☒ Q4	137	2.2	1.4
☒ P2	4,570	72.4	45.7
☒ P3	1,738	27.5	17.4
☒ P4	4,679	74.2	46.8
☒ P5	1,630	25.8	16.3

Table C.10. Statistics of Caco-2 cell populations untreated (control trial 1)

Tube: Control 2			
Population	#Events	%Parent	%Total
■ All Events	10,000		100.0
■ P1	6,100	61.0	61.0
☒ Q1	82	1.3	0.8
☒ Q2	1,475	24.2	14.8
☒ Q3	4,449	72.9	44.5
☒ Q4	94	1.5	0.9
☒ P2	4,513	74.0	45.1
☒ P3	1,587	26.0	15.9
☒ P4	4,548	74.6	45.5
☒ P5	1,552	25.4	15.5

Table C.11. Statistics of Caco-2 cell populations untreated (control trial 2)

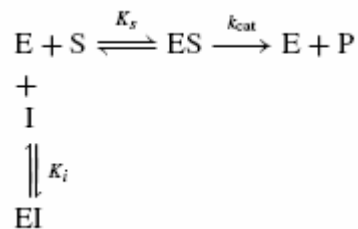
Tube: Control 1			
Population	#Events	%Parent	%Total
■ All Events	10,000		100.0
■ P1	5,824	58.2	58.2
☒ Q1	73	1.3	0.7
☒ Q2	1,656	28.4	16.6
☒ Q3	4,003	68.7	40.0
☒ Q4	92	1.6	0.9
☒ P2	4,061	69.7	40.6
☒ P3	1,762	30.3	17.6
☒ P4	4,097	70.3	41.0
☒ P5	1,727	29.7	17.3

## APPENDIX D

### GOVERNING EQUATIONS FOR ENZYME INHIBITION MODELS

#### D.1. Competitive Inhibition

A competitive inhibitor is a substance that combines with free enzyme in a manner that prevents substrate binding (Segel 1993). In competitive inhibition inhibitor have an affinity towards enzyme. Thus the substrate and inhibitor cannot bind to the enzyme at the same time. In competitive inhibition this binding results from the inhibitor having an affinity for the active site of an enzyme where the substrate also binds; the substrate and inhibitor compete for access to the enzyme's active site. The equilibrium describing competitive inhibition is given below:



In this case, the enzyme's maximum velocity is unchanged. The apparent affinity of the substrate to the binding site is decreased which means: the enzyme-substrate dissociation constant is apparently increased. The rate equation with the presence of a competitive inhibitor, the dissociation constants for enzyme-substrate (ES) and enzyme-inhibitor (EI) complexes, and the enzyme mass balance are given in Eq.18-21 respectively:

$$v = k_{cat}[ES] \quad (D.1)$$

$$K_s = \frac{[E][S]}{[ES]} \quad (D.2)$$

$$K_i = \frac{[E][I]}{[EI]} \quad (D.3)$$

$$[E_T] = [E] + [ES] + [EI] = [E] + \frac{[E][S]}{K_s} + \frac{[E][I]}{K_i} \text{ mass balance} \quad (\text{D.4})$$

If the rate equation was normalized by total enzyme concentration ( $v/[E_T]$ ) and rearranged the following expression for the velocity of an enzymatic reaction in the presence of a competitive inhibitor was obtained:

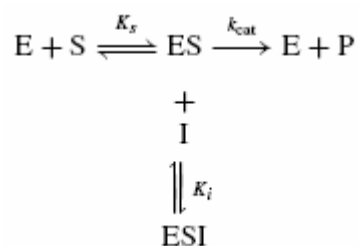
$$V = \frac{V_{\max}[S]}{K_s^* + [S]} = \frac{V_{\max}[S]}{\alpha K_s + [S]} \quad (\text{D.5})$$

where  $K_s^*$  is the apparent enzyme–substrate dissociation constant in the presence of an inhibitor and  $K_s^* = \alpha K_s$  where:

$$\alpha = 1 + \frac{[I]}{K_i} \quad (\text{D.6})$$

## D.2. Uncompetitive Inhibition

In this type of reversible inhibition, uncompetitive inhibitors are believed to form a complex with the enzyme substrate complex. Therefore inhibitor compound interacts with the enzyme–substrate complex at a site other than the active site:



The remaining substrate in ESI complex is unable to react and form its normal product which affects the rate of the reaction catalysed by the enzyme. Uncompetitive inhibition results in an apparent decrease in both  $V_{\max}$  and  $K_s$ . Therefore apparent increase in affinity of enzyme for substrate (i.e., a decrease in  $K_s$ ) is because of unproductive substrate binding, resulting in a decrease in free enzyme concentration. The rate equation for the formation of product, the dissociation constants for enzyme–substrate (ES) and ES–inhibitor (ESI) complexes and the enzyme mass balance are given in Eq. 23-26 respectively:



$$v = k_{cat}[ES] \quad (D.7)$$

$$K_s = \frac{[E][S]}{[ES]} \quad (D.8)$$

$$K_i = \frac{[ES][I]}{[ESI]} \quad (D.9)$$

$$[E_T] = [E] + [ES] + [ESI] = [E] + \frac{[E][S]}{K_s} + \frac{[E][S][I]}{K_s K_i} \quad \text{mass balance} \quad (D.10)$$

If the rate equation was normalized by total enzyme concentration ( $v/[E_T]$ ) and rearranged the following expression for the velocity of an enzymatic reaction in the presence of a uncompetitive inhibitor was obtained:

$$V = \frac{V_{max}^*[S]}{K_s^* + [S]} = \frac{(V_{max}/\alpha)[S]}{(K_s/\alpha) + [S]} \quad (D.11)$$

where  $V_{max}^*$  and  $K_s^*$  are the apparent enzyme maximum velocity and apparent enzyme–substrate dissociation constant in the presence of an inhibitor respectively where

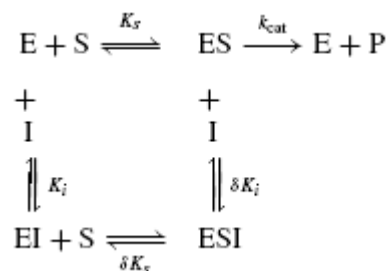
$$V_{max}^* = V_{max} / \alpha \quad (D.12)$$

$$K_s^* = K_s / \alpha \quad (D.13)$$

$$\alpha = 1 + \frac{[I]}{K_i} \quad (D.14)$$

### D.3. Linear Mixed Inhibition

In linear mixed inhibition, inhibitor compound can act either as competitive or uncompetitive inhibitor therefore it can interact with both the free enzyme and the enzyme–substrate complex at a site other than the active site:



Due to this kind of interactions, a mixed type inhibitor affects both  $V_{max}$  and  $K_m$  values of enzyme catalyzed reaction. In the linear mixed inhibition the rate equation, the dissociation constants for enzyme–substrate (ES and ESI) and enzyme–inhibitor (EI and ESI) complexes, and the enzyme mass balance are given below in Eq. 31-36, respectively:

$$v = k_{cat}[ES] \quad (D.15)$$

$$K_s = \frac{[E][S]}{[ES]} \quad (D.16)$$

$$\delta K_s = \frac{[EI][S]}{[ESI]} \quad (D.17)$$

$$K_i = \frac{[E][I]}{[EI]} \quad (D.18)$$

$$\delta K_i = \frac{[ES][I]}{[ESI]} \quad (D.19)$$

$$[E_T] = [E] + [ES] + [EI] + [ESI] = [E] + \frac{[E][S]}{K_s} + \frac{[E][I]}{K_i} + \frac{[E][S][I]}{K_s \delta K_i} \quad \text{mass balance (D.20)}$$

If the rate equation was normalized by total enzyme concentration ( $v/[E_T]$ ) and rearranged the following expression for the velocity of an enzymatic reaction in the presence of a linear mixed type competitive inhibitor was obtained:

$$V = \frac{V_{max}^*[S]}{K_s^* + [S]} = \frac{(V_{max}/\beta)[S]}{(\alpha/\beta)K_s + [S]} \quad (D.21)$$

where  $V_{max}^*$  and  $K_s^*$  are the apparent enzyme maximum velocity and apparent enzyme–substrate dissociation constant in the presence of an inhibitor, respectively where:

$$V_{max}^* = V_{max} / \beta \quad (D.22)$$

$$K_s^* = (\alpha / \beta) K_s \quad (D.23)$$

$$\alpha = 1 + \frac{[I]}{K_i} \quad (D.24)$$

$$\beta = 1 + \frac{[I]}{\delta K_i} \quad (\text{D.25})$$

#### D.4. Noncompetitive Inhibition

Noncompetitive inhibition is a special case of linear mixed inhibition where  $\delta = 1$  and  $\alpha = \beta$  and differs from competitive inhibitors where there is no competition between the inhibitor and the substrate. The expression for the velocity of an enzymatic reaction in the presence of a noncompetitive inhibitor becomes

$$V = \frac{V_{\max}^* [S]}{K_s + [S]} = \frac{(V_{\max} / \alpha) [S]}{K_s + [S]} \quad (\text{D.26})$$

where  $V_{\max}^*$  corresponds to the apparent enzyme maximum velocity in the presence of an inhibitor. Also  $V_{\max}^*$  can be written as:

$$V_{\max}^* = V_{\max} / \alpha, \quad (\text{D.27})$$

$$\text{where } \alpha = 1 + \frac{[I]}{K_i} \quad (\text{D.28})$$

In noncompetitive inhibition, an apparent decrease in  $V_{\max}$  is observed while  $K_s$  is remained unaffected.

## **DİLEK DEMİRBÜKER KAVAK**

**Date of Birth:** 05.08.1978

**Place of Birth:** Manisa

**Citizenship:** Turkish

### **EDUCATION**

#### **[1996-2000] B.Sc. (Food Engineering)**

Ege University

Department of Food Engineering, Izmir, Turkey

Dissertation: Production of Ethanol by Immobilized Cells

#### **[2000-2003] M.Sc. (Food Engineering)**

İzmir Institute of Technology

Department of Food Engineering, İzmir, Turkey

Dissertation: Control of Microbial and Enzymatic Changes in Intermediate Moisture Sun-Dried Figs by Mild Heating and Hydrogen Peroxide Disinfection

#### **[2003-2010] Ph.D. (Chemical Engineering)**

İzmir Institute of Technology

Department of Chemical Engineering, İzmir, Turkey

Dissertation: Inhibition of Microbial  $\beta$ -Glucuronidase by Natural Zeolites and Their Effects on Cancer Prevention in Human Intestinal System

### **PUBLICATIONS**

Kaya Y. E., Kavak D. D., (Submitted Manuscript). Application of Factorial Design for the  $\text{Ca}^{2+}$  Exchanged NaX Zeolite. *Powder Technology*, Manuscript Number: POWTEC-D-10-00762.

Kavak, D.D.; ALTIOK, E.; Bayraktar, O.; Ülkü, S. (2010). Pistacia terebinthus extract: As a potential antioxidant, antimicrobial and possible  $\beta$ -glucuronidase inhibitor, *Journal of Molecular Catalysis B: Enzymatic*, 64, 167-171.

Demirbucker D., Arcan I., Tokatlı F., Yemenicioğlu A. (2005). The effects of hot rehydration in the presence of hydrogen peroxide on microbial quality, texture, color and antioxidant activity of cold stored intermediate moisture sun-dried figs. *Journal of Food Science*, 70(3), 153-159.

Demirbucker D., Simsek S., Yemenicioğlu A. (2004). Potential application of hot rehydration alone or in combination with hydrogen peroxide to control pectinmethylesterase activity and microbial load in cold stored intermediate moisture sun-dried figs. *Journal of Food Science*, 69(3), 170-178.